รายงานวิจัยฉบับสมบูรณ์

การหาลักษณะเฉพาะของโลหะซัลไฟด์ ทังสเตท และโมลิบเดต ที่สังเคราะห์โดยวิธีต่าง ๆ

Characterization of metal sulfides, tungstates and molybdates synthesized by different methods

ศาสตราจารย์ ดร. สมชาย ทองเต็ม มหาวิทยาลัยเชียงใหม่
รองศาสตราจารย์ ธิติพันธุ์ ทองเต็ม มหาวิทยาลัยเชียงใหม่
อาจารย์วัลย์ชัย พรมโนภาศ มหาวิทยาลัยเชียงใหม่
ดร. สุลาวัลย์ ขาวผ่อง มหาวิทยาลัยเชียงใหม่
นายอนุกร ภู่เรืองรัตน์ มหาวิทยาลัยเชียงใหม่

สนับสนุนโดยสำนักงานกองทุนสนับสนุนการวิจัย

กิตติกรรมประกาศ

คณะผู้วิจัยฯ ขอขอบคุณ สำนักงานกองทุนสนับสนุนการวิจัย (ส.ก.ว.) กรุงเทพ 10400 ที่ได้สนับสนุนทุนวิจัยองค์ความรู้ใหม่ที่เป็นพื้นฐานต่อการพัฒนา เป็นระยะเวลา 2 ปี

พร้อมกันนี้คณะผู้วิจัยขอขอบคุณ คณะวิทยาศาสตร์ และสถาบันวิจัยวิทยาศาสตร์และเทคโนโลยี มหาวิทยาลัยเชียงใหม่ ที่ให้บริการและอำนวยความสะดวกต่าง ๆ ทำให้งานวิจัยนี้สำเร็จลุล่วงไปด้วยดี

(นายสมชาย ทองเต็ม)

หัวหน้าโครงการวิจัยฯ

บทคัดย่อ

ในงานวิจัยนี้ได้เตรียม nano- และ micro-crystallines ของ $BaMoO_4$, $SrMoO_4$, $CaMoO_4$, $SrWO_4$, $PbWO_4$, CuS, CdS และ PbS ที่มี morphologies ต่าง ๆ กันได้สำเร็จด้วยวิธีต่าง ๆ กันคือ microwave radiation, sonochemical process, และ solvothermal/hydrothermal reactions ได้ตรวจสอบหา phases ต่าง ๆ และ phase transformation โดยใช้ XRD และ SAED พบว่ามีความสอดคล้องกับการ simulations และ elemental analysis โดยใช้ EDX จากการใช้ SEM และ TEM แสดงให้เห็นว่ามี nano- and micro-sized particles ที่มี morphologies ต่าง ๆ กัน ที่ถูกควบคุมโดย prepared conditions และ methods ในการเตรียมสารตัวอย่าง ส่วน Raman และ FTIR spectra ได้แสดงถึงการมี stretching และ bending modes ของ atoms ที่ประกอบเป็น products นอกจากนี้ยังได้ตรวจพบ PL emissions ที่ wavelengths ต่าง ๆ กัน ที่เกิดจากการ transitions ของ electrons ใน products ต่าง ๆ และมีความสอดคล้องกับที่ตรวจพบโดยนักวิจัยท่านอื่น ๆ

Abstract

Nano- and micro-crystallines of $BaMoO_4$, $SrMoO_4$, $CaMoO_4$, $SrWO_4$, $PbWO_4$, CuS, CdS and PbS with different morphologies were successfully prepared using a variety of methods: microwave radiation, sonochemical process, and solvothermal and hydrothermal reactions. The corresponding phases and phase transformation were detected using XRD and SAED, corresponding to their simulations and elemental analysis using EDX. SEM and TEM analyses revealed the presence of nano- and micro-sized particles with different morphologies, controlled by the prepared conditions and methods. Raman and FTIR spectra provide the evidence of stretching and bending modes of atoms, composing the products. Their PL emissions were also detected at different wavelengths, caused by the electronic transitions of different products, and are in accordance with those obtained by other researchers.

สารบาญ

กิตติกรรมประกาศ 2

บทคัดย่อ 3

Abstract 4

บทนำ 6

Characterization of $MMoO_4$ (M = Ba, Sr and Ca) with different morphologies prepared using a cyclic microwave radiation 7

Preparation and characterization of nanocrystalline $SrWO_4$ using cyclic microwave radiation 15

Sonochemical preparation of $PbWO_4$ crystals with different morphologies 42

Synthesis and analysis of CuS with different morphologies using cyclic microwave irradiation 53

Free surfactant synthesis of microcrystalline CdS by solvothermal reaction 73

Phase transformation of nanocrystalline CdS synthesized by solvothermal reaction 86

Preparation of flower-like PbS nano-structures using cyclic microwave radiation 94

Biomolecule- and surfactant- assisted hydrothermal synthesis of PbS crystals 102

Output ที่ได้จากโครงการวิจัย ฯ 111

ผลงานวิจัยที่เผยแพร่ในวารสารต่าง ๆ 117

บทนำ

ปัจจุบัน วัสดุที่มีโครงสร้างในระดับนาโนและไมโครเมตร กำลังเป็นที่สนใจกันมากเนื่องจากมีประโยชน์ในการนำไปประยุกต์ใช้ในอุตสาหกรรมต่าง ๆ ได้อย่างกว้างขวาง สำหรับในประเทศไทยได้มีการนำเข้าจากต่างประเทศทั้งในลักษณะที่เป็นวัตถุดิบและสำเร็จรูปเป็นจำนวนมาก ซัลไฟด์ ทังสเตท และโมลิบเดตจำนวนมาก เป็นสารที่มีสมบัติเรืองแสงที่น่าสนใจทั้งในทางการค้า และอุตสาหกรรมเป็นอย่างมาก สามารถนำไปประยุกต์ใช้ทางด้านที่เกี่ยวกับ flat panel display, luminescent device, infrared window, solar cell, lasers, microwave, optical fiber, catalyst ใช้ใน Raman scattering behavior และอื่น ๆ ในปัจจุบันนี้ได้มีการทำวิจัยกันอย่างกว้างขวางเพื่อสังเคราะห์สารดังกล่าวให้มีรูปร่างต่าง ๆ กัน ซึ่งจะทำให้สารมีสมบัติที่แตกต่างกันด้วย ทั้งนี้ขึ้นอยู่กับกระบวนการและสภาวะที่ใช้สังเคราะห์ และอื่น ๆ

สำหรับการวิจัยนี้ได้สังเคราะห์ nano- และ micro-crystallines ของ $BaMoO_4$, $SrMoO_4$, $CaMoO_4$, $SrWO_4$, $PbWO_4$, CuS, CdS และ PbS ที่มี morphologies ต่าง ๆ กันได้สำเร็จด้วยวิธีต่าง ๆ กันคือ microwave radiation, sonochemical process, และ solvothermal/hydrothermal reactions จากนั้น ได้ตรวจสอบหา phases และ phase transformation, morphologies, vibrational modes ตลอดจนการเรืองแสงและอื่น ๆ ดังต่อไปนี้

Characterization of $MMoO_4$ (M = Ba, Sr and Ca) with different morphologies prepared using a cyclic microwave radiation

Abstract

Scheelite molybdates ($MMoO_4$, M = Ba, Sr and Ca) were successfully prepared by the reactions of $M(NO_3)_2.2H_2O$ and $Na_2MoO_4.2H_2O$ in propylene glycol and NaOH using a microwave radiation. The phases were detected using XRD and SAED. TEM analysis revealed the presence of microsized bi-pyramids with a square base, nano-sized particles in clusters, and dispersed nano-sized particles for $BaMoO_4$, $SrMoO_4$ and $CaMoO_4$, respectively. Diffraction patterns of the bi-pyramids were simulated, and are in accordance with the experimental results. Raman and FTIR spectra provide the evidence of scheelite structure with Mo-O stretching vibration in MoO_4^{2-} tetrahedrons at 742-901 cm^{-1}.

Keywords : Cyclic microwave radiation, Bi-pyramidal $BaMoO_4$, Nano-sized $SrMoO_4$ and $CaMoO_4$

1. Introduction

The scheelite molybdates ($MMoO_4$, M = Ba, Sr and Ca) have C_{4h} point group with two formula units per primitive cell [1-3]. They have attracted particular interest in a variety of applications such as hosts for lanthanide activated lasers [4], luminescence materials [5,6], microwave applications [7] and catalysts [6,8]. The materials were prepared by different methods, such as mechanochemical process [9], solvothermal reaction [10] and microwave radiation with further calcination [4]. A conventional solvothermal process is a method used for growing crystalline materials in a solvent containing in a tightly closed autoclave (system) at high temperatures. Heat, generated from an electrical heater, is supplied to the system to raise its temperature. For a microwave-solvothermal process, the system is heated using a microwave radiation. It becomes hot by the vibration of charged particles with electric field intensity. The purpose of the research is to prepare $MMoO_4$ with different morphologies in basic solutions using a cyclic (on and off over a period of time, and happen in the same order) microwave radiation without the requirement of any further calcination. The reaction proceeded in an open system at atmospheric pressure. No other additives were used. The process is very simple, attractive and

novel by focusing large amount of microwave radiation into the solutions to produce pure products.

2. Experiment

Each of 0.005 mol $M(NO_3)_2.2H_2O$ (M = Ba, Sr and Ca) and $Na_2MoO_4.2H_2O$ was dissolved in 20 ml propylene glycol containing 10 ml 3 M NaOH. The reactions cyclically proceeded using 600 W microwave for 20 min (10 cycles). One cycle is 2 min long and composes of irradiation and non-irradiation for 1 min each. Current temperatures of different solutions are shown in Fig 1. They are increased with the increasing of the prolonged times within about the first 9 min and show very little oscillation around a constant value afterwards. The final products were washed with water and 95 % ethanol, dried at 80 °C for 24 h, and intensively characterized.

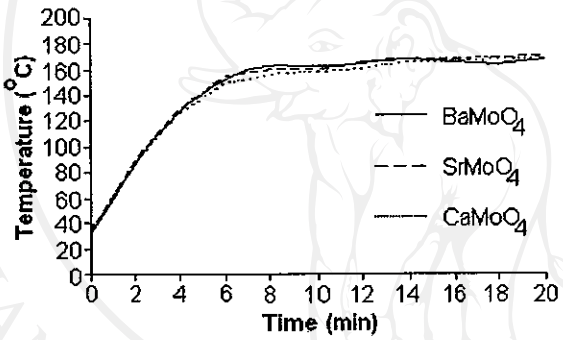

Fig 1. Current temperatures of the system during processing.

3. Results and Discussion

3.1 XRD

XRD spectra (Fig 2) were compared with those of the JCPDS software (reference codes : 29-0193, 08-0482 and 85-0585) [2], and specified as $MMoO_4$ (M = Ba, Sr and Ca). They have scheelite structure with tetragonal crystal system and have I41/a space-group symmetry [2,3,9,11]. Calculated lattice parameters [12] for $BaMoO_4$ (a = b = 0.5573 and c = 1.2786 nm), $SrMoO_4$ (a = b = 0.5406 and c = 1.1988 nm) and $CaMoO_4$ (a = b = 0.5212 and c = 1.1438 nm) are very close to those of the corresponding JCPDS software, and have the influence on their interplanar spaces. No other characteristic peaks of impurities were detected showing that the products are pure phase. Their strongest intensity peaks are at 2θ = 26.53, 27.66 and 28.75

deg for $BaMoO_4$, $SrMoO_4$ and $CaMoO_4$, respectively. They diffracted from the same plane indexed by (112).

To produce $MMoO_4$, $M(NO_3)_2.2H_2O$ reacted with $Na_2MoO_4.2H_2O$ in propylene glycol under basic condition using a microwave radiation.

$$M(NO_3)_2.2H_2O + Na_2MoO_4.2H_2O \xrightarrow[\text{microwave radiation}]{\text{propylene glycol}} MMoO_4 + 2NaNO_3 + 4H_2O$$

During the synthesis, vibrating electric field of a microwave applied a force on electric charged particles. They vibrated with the electric field strength. Vibrations of the reactants have the influence on the reaction to effectively proceed. Subsequently, pure product was produced.

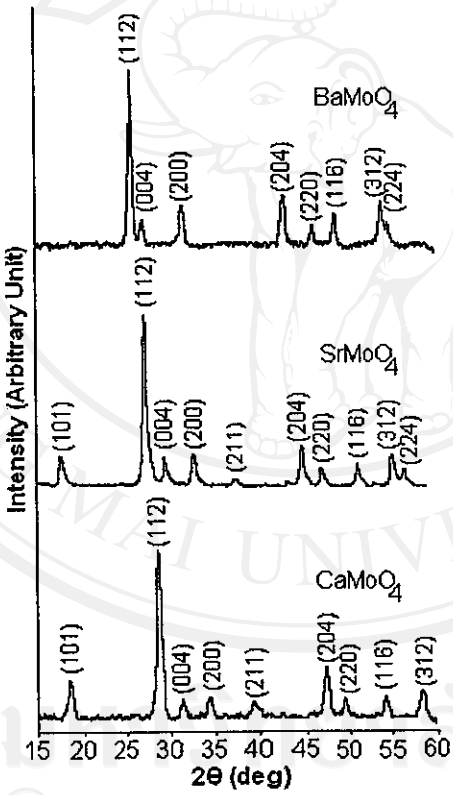

Fig 2. XRD spectra of the products.

3.2 Vibration Spectra

Vibrations of $MMoO_4$ are classified into two types, the internal and external modes [13]. The first belongs to the vibration inside $[MoO_4]^{2-}$ molecular units of which the centers of mass are stationary. The second is called lattice phonon which

corresponds to the motion of M^{2+} cations and the rigid molecular units. In free space, $[MoO_4]^{2-}$ tetrahedrons have T_d-symmetry [1,13]. Their vibrations compose of four internal modes ($v_1(A_1)$, $v_2(E)$, $v_3(F_2)$ and $v_4(F_2)$), one free rotation mode ($v_{f.r.}(F_1)$), and one translation mode (F_2) [13]. In lattice space, the symmetry is reduced to S_4. All degenerative vibrations are split [1,13] due to the crystal field effect and Davydov splitting [13]. For tetragonal scheelite primitive cell (wavevector, k = 0) [13,14], there are 26 different vibrations ($\Gamma = 3A_g + 5A_u + 5B_g + 3B_u + 5E_g + 5E_u$) determined by group-theory calculation [1,13]. Among them, $3A_g$, $5B_g$ and $5E_g$ vibrations are Raman-active. Only $4A_u$ and $4E_u$ of the $5A_u$ and $5E_u$ vibrations are active in IR frequencies, and their remains ($1A_u$ and $1E_u$) are acoustic vibrations. The $3B_u$ vibrations are silent modes [1,13].

For the present research, six different vibrations were detected on Raman spectra (Fig 3a). Among them, $v_1(A_g)$, $v_3(B_g)$, $v_3(E_g)$, $v_4(B_g)$, $v_2(A_g)$ and $v_{f.r.}(A_g)$ are at 872, 818, 776, 355, 320 and 188 cm^{-1} for $BaMoO_4$, 871, 829, 780, 362, 325 and 184 cm^{-1} for $SrMoO_4$, and 875, 843, 793, 391, 324 and 205 cm^{-1} for $CaMoO_4$, respectively. Each vibration mode is in accord with Raman vibrations analyzed by other researchers [1,13]. The spectra provide the evidence of scheelite structure for the three products [1,13].

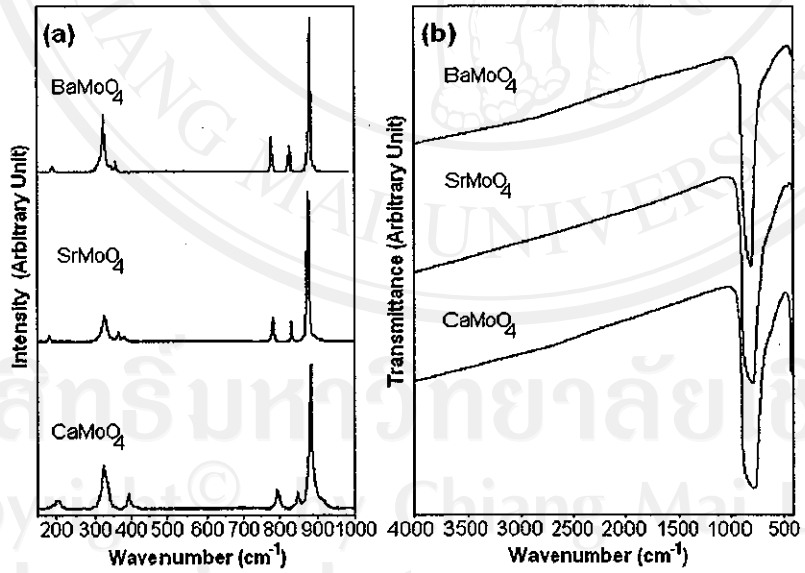

Fig 3. (a) Raman and (b) FTIR spectra of the products.

In addition, FTIR spectra (Fig 3b) were analyzed using a transmittance mode. For T_d-symmetry, $v_3(F_2)$ and $v_4(F_2)$ are IR active and correspond to stretching and bending modes, respectively [3]. The spectra show a band of Mo-O stretching vibration in MoO_4^{2-} tetrahedrons [3] at 742-901 cm^{-1}. It is one of the internal modes specified as $v_3(F_2)$ antisymmetric stretching vibrations [3].

3.3 TEM and SAED

TEM images (Figs 4a, 4d and 5) show different morphologies for different products although they were prepared using the same conditions. They consist of microsized bi-pyramids with a square base and their apexes of 651 nm apart for $BaMoO_4$, nano-sized particles in clusters for $SrMoO_4$, and dispersed nano-sized particles for $CaMoO_4$. A diffraction pattern (Fig 4b) of $BaMoO_4$ at a circle in Fig 4a was interpreted [12]. It appears as a periodic array of bright spots due to the diffraction of electron through crystallographic planes of the product. It shows that each of bi-pyramidal particles is single crystal. Both of the calculated angles between any pair of the directions belonging to these planes, and interplanar spaces determined from (hkl) are in accord with those of the diffraction pattern on the film. The pattern compose of a number of spots corresponding to $(\bar{1}12)$, $(1\bar{1}2)$, (004) and $(1\bar{1}6)$ planes of the crystalline particles, and was specified as $BaMoO_4$ [2]. The incident beam of electron might not be exactly perpendicular to the planes leading to the asymmetric diffraction pattern. Calculated zone axis [12] is in the $[\bar{1}\bar{1}0]$ direction which is parallel or nearly parallel to the electron beam. By using $[\bar{1}\bar{1}0]$ direction as zone axis, a diffraction pattern (Fig 4c) for $BaMoO_4$ was simulated [15]. The pattern is symmetric and systematic. It is in good accord with the experimental result. Another diffraction pattern (Fig 4e) at a square in Fig 4d was also interpreted [12]. It corresponds to $(0\bar{2}0)$, $(2\bar{2}0)$ and (200) planes of the product which was specified as $BaMoO_4$ [2] with single crystal. Its zone axis is in the $[001]$ direction. It is in good accord with the simulated pattern (Fig 4f). In case of $SrMoO_4$ and $CaMoO_4$, the diffraction patterns (Fig 5) show several concentric rings characterized as polycrystals. Each of them composes of a number of nano-sized crystals. They are so tiny that the analysis of a single crystal is not possible. Interplanar spaces were calculated [16,17] using diameters of the diffraction rings, and compared with those

of the JCPDS software [2]. Both patterns correspond to (101), (112), (004), (200), (114), (204), (116) and (312) planes. Additional (224) plane was detected in Fig 5b. The patterns were specified as $SrMoO_4$ and $CaMoO_4$.

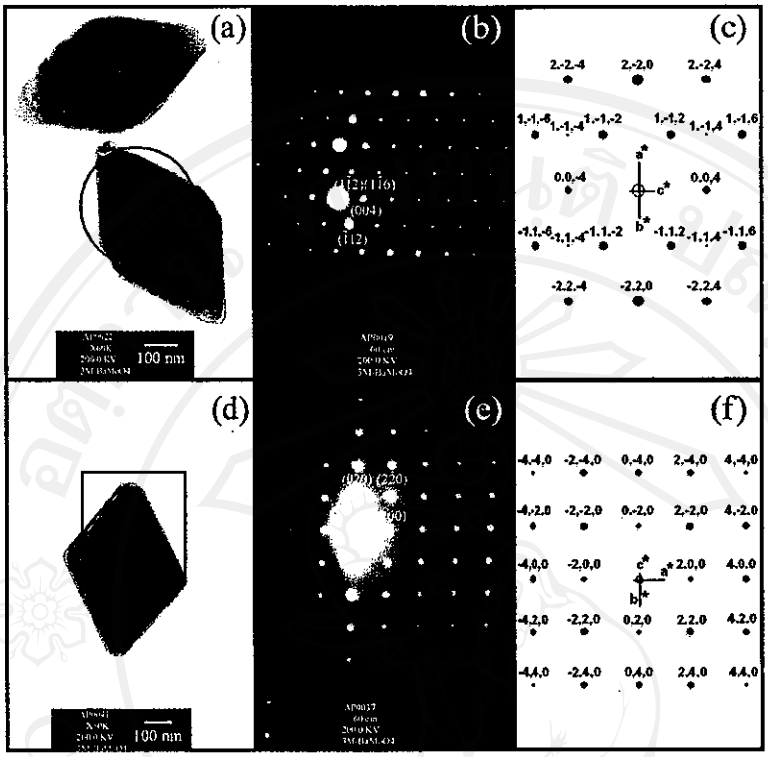

Fig 4. TEM images, SAED and simulated patterns of $BaMoO_4$. [(b, c) and (e, f) are for a circle in (a) and a square in (d), respectively.]

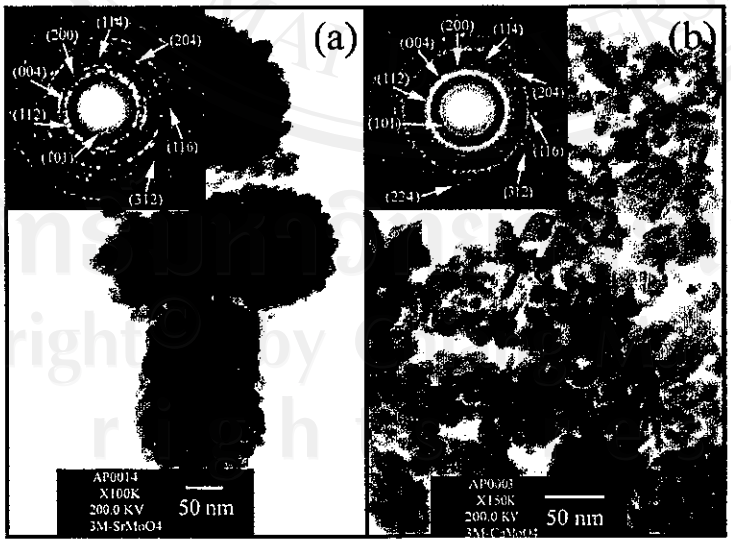

Fig 5. TEM images and SAED patterns of (a) $SrMoO_4$ and (b) $CaMoO_4$.

4. Conclusions

$MMoO_4$ (M = Ba, Sr and Ca) were successfully synthesized using a cyclic microwave radiation. Each of them is pure phase, and composes of microsized bi-pyramids with a square base for $BaMoO_4$, nano-sized particles in clusters for $SrMoO_4$, and dispersed nano-sized particles for $CaMoO_4$. The products provide the evidence of scheelite structure with Mo-O stretching vibration in MoO_4^{2-} tetrahedrons at 742-901 cm^{-1}.

References

1. S.P.S. Porto, J.F. Scott, Phys. Rev. 157 (1967) 716.
2. Powder Diffract. File, JCPDS Internat. Centre Diffract. Data, PA 19073-3273, U.S.A., (2001).
3. A.P. de Azevedo Marques, D.M.A. de Melo, C.A. Paskocimas, P. S. Pizani, M.R. Joya, E.R. Leite, E. Longo, J. Solid State Chem. 179 (2006) 671.
4. J.H. Ryu, J.W. Yoon, C.S. Lim, K.B. Shim, Mater. Res. Bull. 40 (2005) 1468.
5. Y. Wang, J. Ma, J. Tao, X. Zhu, J. Zhou, Z. Zhao, L. Xie, H. Tian, Ceram. Internat. 33 (2007) 693.
6. Y. Zhang, F. Yang, J. Yang, Y. Tang, P. Yuan, Solid State Comm. 133 (2005) 759.
7. J.H. Ryu, J.W. Yoon, C.S. Lim, W.C. Oh, K.W. Shim, J. Alloys Comp. 390 (2005) 245.
8. A. Sen, P. Pramanik, Mater. Lett. 50 (2001) 287.
9. P. Parhi, S.S. Singh, A.R. Ray, A. Ramanan, Bull. Mater. Sci. 29 (2006) 115.
10. C. Zhang, E. Shen, E. Wang, Z. Kang, L. Gao, C. Hu, L. Xu, Mater. Chem. Phys. 96 (2006) 240.
11. V. Thangadurai, C. Knittlmayer, W. Weppner, Mater. Sci. Engin. B 106 (2004) 228.
12. T. Thongtem, A. Phuruangrat, S. Thongtem, Mater. Lett. 61 (2007) 3235.
13. T.T. Basiev, A.A. Sobol, Y.K. Voronko, P.G. Zverev, Optic. Mater. 15 (2000) 205.
14. A. Golubović, R. Gajić, Z. Dohčević-Mitrović, S. Nikolić, J. Alloys Comp. 415 (2006) 16.
15. C. Boudias, D. Monceau, CaRIne Crystallography 3.1, 17 rue du Moulin du Roy, F-60300 Senlis, France, (1989-1998).
16. T. Thongtem, A. Phuruangrat, S. Thongtem, Mater. Lett. 60 (2006) 3776.

17. T. Thongtem, S. Kaowphong, S. Thongtem, J. Mater. Sci., 42 (2007) 3923.

Preparation and characterization of nanocrystalline $SrWO_4$ using cyclic microwave radiation

Abstract

Nanocrystalline $SrWO_4$ was successfully prepared using $SrCl_2$ and Na_2WO_4 in ethylene glycol at different pH values, microwave powers and prolonged times. The phase was detected using XRD and SAED. TEM, HRTEM, SEM and particle size distribution revealed the presence of nano-sized crystals with their crystallographic planes aligning in systematic order. Raman and FTIR spectra provide the evidence of scheelite structure with W-O stretching vibration in WO_4^{2-} tetrahedrons at 781-912 cm^{-1}. PL emission of the products is considered to be from the $^1T_2 \rightarrow {}^1A_1$ transition of electrons within $[WO_4]^{2-}$ tetrahedrons at 420-428 nm (2.901-2.956 eV).

Keywords : Cyclic microwave radiation, Nanocrystalline, $SrWO_4$

1. Introduction

Scheelite structured tungstates are specified as cubic close-packed array of M^{2+} cations and WO_4^{2-} anions. They belong to a body-centered tetragonal system and have C_{4h} point group with two formula units per primitive cell [1,2]. Typical scheelite structured tungstates are $CaWO_4$, $SrWO_4$, $BaWO_4$ and $PbWO_4$ [2-5]. They have attracted interest in a wide variety of applications such as laser host materials in quantum electronics and scintillators in medical devices [6], microwave applications [7], stimulated Raman scattering technique [8], humidity sensors [7] and catalysts [7]. They have luminescent property due to the electronic transition between oxygen and tungsten within tetrahedral WO_4^{2-} units [9]. $SrWO_4$ with different shapes and sizes was prepared by different methods, such as nanoparticles, nanopeanuts, and nanorods with rough surface by a solvothermal - mediated microemulsion method [10], nanofilm on glass substrates by a reverse micelle system combined with dip-coating [11], hollow spheres by a precipitation reaction [12], and thin film on glass substrates by spray pyrolysis [2]. Other luminescent materials were $BaWO_4$ with olive-like, flake-like and whisker-like structures by hydrothermal process [3], nanocrystalline MWO_4 (M = Ca, Co, Ni, Cu and Zn) powders by evaporation of a polymer based metal-complex precursor solution [5], and nanocrystalline MWO_4 (M =

Ca and Ni) by microwave-assisted synthesis with further calcination [7]. Sometimes, templates, surfactants and other additives were used to control the product morphologies.

Microwave radiation has very attractive attention used for preparing materials. It is able to reduce time scales of the reactions, and can rapidly lead to very high temperatures which have the influence to accelerate the reaction process. When microwave radiation is supplied to chemical solutions, one or more of the components dissolving in the solutions is capable of coupling with the radiation. It can lead to higher heating rate than that achieved by conventional method. Microwave radiation can solve the problems of temperature and concentration gradients. By focusing large amount of microwave radiation into the solutions, vibrating electric field applied a force on charged particles which vibrated accordingly. Vibrations of the reactants have the influence on the reaction to proceed with efficiency (shorter time and lower power). Subsequently, pure products were produced [13].

A polar solvent, which has permanent dipole moment, has relaxation process in microwave region. It is very good candidacy using in the process. Compounds with large permanent dipole moments also have large dielectric constants or relative permittivities [13], and are rapidly heated up by a microwave radiation [14]. When water (dielectric constants at 25 °C = 78.4 [15]) was used as a solvent, its temperature was about 110 °C by a microwave radiation within 1 min [14]. Ethylene glycol (dielectric constant at 25 °C = 40.3 [15] and T_b = 197 °C [16]) was heated up to about 120 °C within 3 min [16]. When relaxation time is one or two orders of magnitude different from that corresponding to the microwave frequency, the solvent is still to be an effective medium due to its large loss tanδ. The 90 – δ is phase difference between electric field strength and current in the materials in which the loss energy develops as heat. For water (relaxation time = 9.04 ps) at 2.45 GHz microwave, tanδ is only 0.1 [13]. It is good enough for using in the microwave process [13,17]. High boiling point solvents can prevent chemicals from overflowing. Therefore, solvents with tanδ > 0.1, such as ethylene glycol (tanδ = 1.35, relaxation time = 112.87 ps and T_b = 197 °C) is good choice for using in the microwave process [13,16].

For the present research, nanocrystalline $SrWO_4$ was prepared in ethylene glycol using different pH values, microwave powers and prolonged times without the

requirement of any further calcination. No surfactants, complexing agents or other additives were used. The process is very simple, attractive and novel.

2. Experiment

Each of 0.005 mol $SrCl_2$ and Na_2WO_4 was dissolved in 30 ml ethylene glycol. The solution has a pH of 9.6 which was adjusted to the range of 3 – 13 using HCl or NaOH. The reactions cyclically proceeded at 180-600 W microwave powers for 20-80 min (10-40 cycles). One cycle is 2 min long and composes of irradiation and non-irradiation for 1 min each. Current temperatures at different microwave powers and prolonged times are shown in Fig 1. At constant microwave power, the temperatures were increased with the increasing of the prolonged times. They tend to be constant after the first 10 min for 600, 450 and 300 W, and 20 min for 180 W.

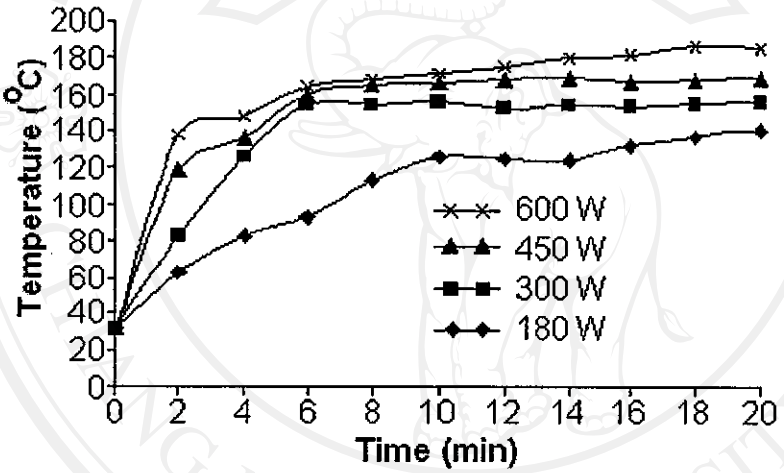

Fig 1. Current temperatures at different microwave powers and prolonged times used for the present process.

To produce $SrWO_4$, $SrCl_2$ reacted with Na_2WO_4 dissolving in ethylene glycol by the use of a microwave radiation.

$$SrCl_2 + Na_2WO_4 \xrightarrow[\text{microwave radiation}]{\text{ethylene glycol}} SrWO_4 + 2NaCl$$

The final products (precipitates) were washed with water and 95 % ethanol, dried at 80 °C for 24 h, and characterized using XRD (SIEMENS D500) operated at 20 kV, 15 mA and using the Kα line from a Cu target, TEM (JEOL JEM-2010) and high

resolution transmission electron microscopy (HRTEM) as well as the use of selected area electron diffraction (SAED) operated at 200 kV, SEM (JEOL JSM-6335F) operated at 15 kV, Raman spectrometer (HORIBA JOBIN YVON T64000) using 50 mW Ar laser with λ = 514.5 nm, FTIR (BRUKER TENSOR27) with KBr as a diluting agent and operated in the range 400-4,000 cm^{-1} and photoluminescence (PL) spectrometer (PERKIN-ELMER LS50B) using a 270 nm exciting wavelength at room temperature.

3. Results and Discussion

3.1 XRD

Comparing XRD spectra (Fig 2) of the powdered products to that of the JCPDS software (reference code : 85-0587) [18]. They were specified as $SrWO_4$ with tetragonal crystal system and $I4_1/a$ space group. They have scheelite structure [2]. No other characteristic peaks of impurities were detected showing that the products prepared using a microwave radiation are pure phase. At 180 W for 20 min, no any product was produced using a solution with a pH of 3. The acidity seems to have the influence on the precipitation process. For the solutions with the pH of 5 and 7, broad spectra were detected showing that the products composed of very fine particles. The degree of crystalline products is low. The XRD peaks become sharper at higher pH values. At a pH of 9.6 for higher microwave powers and longer times, the spectra are very sharp showing that the products are very good crystals. Their strongest intensity peaks are at 2θ = 27.6 deg and diffracted from (112) crystallographic planes.

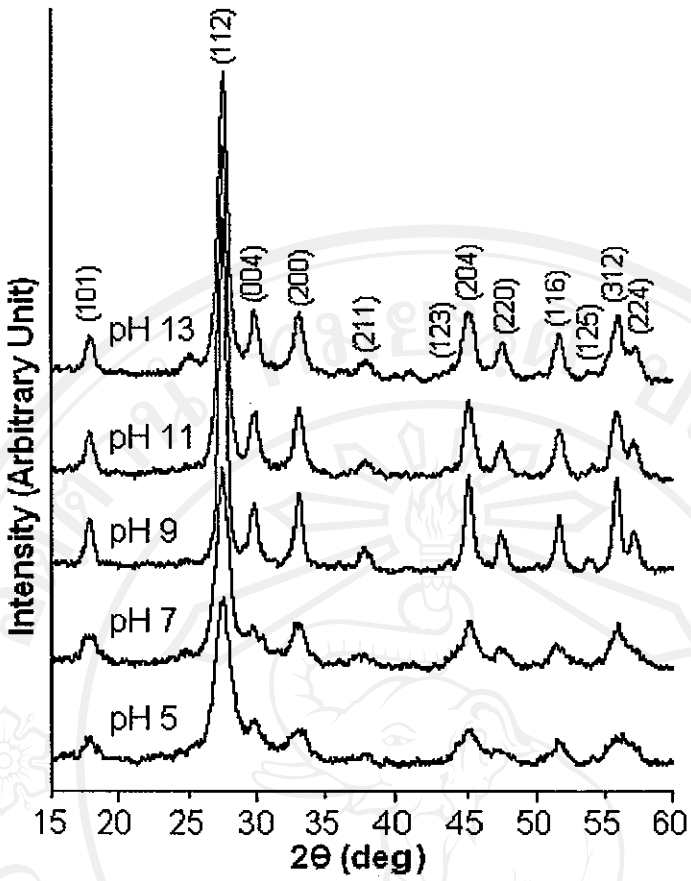

(a)

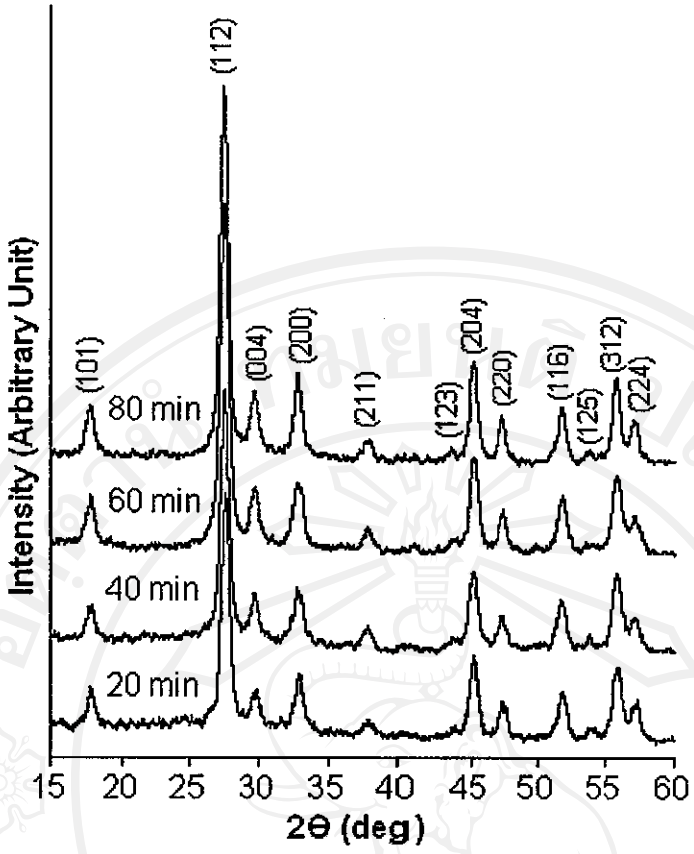

(b)

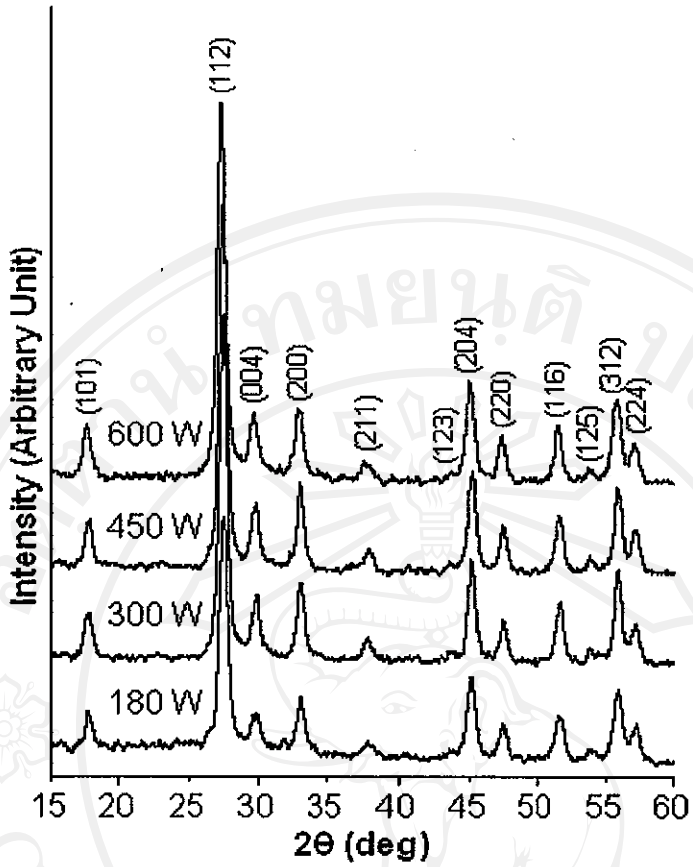

(c)

Fig 2. XRD spectra of the products prepared using (a) 180 W for 20 min at different pH values, (b) 180 W at a pH of 9.6 for 20-80 min, and (c) a pH of 9.6 for 20 min at different microwave powers.

3.2 TEM, HRTEM, SEM and SAED

TEM images (Fig 3) show nano-particles with different morphologies influenced by the microwave powers, prolonged times and pH values. At 180 W 20 min and pH 5, the product composes of < 10 nm particles in clusters. Moiré fringes (e.g. marked with a square) were detected. They are the interference patterns between two crystallographic phases with slightly different lattice parameters [19]. Lattice planes (e.g. marked with a circle) were detected as well. They are crystallographic planes of the products. At 180 W 20 min and a pH of 9.6, the product composes of very fine particles in clusters. They appear as dark and grey contrast areas for the dense and less dense substances, respectively. When the pH was adjusted to 13, the product

composes of nano-sized particles with oval shape in clusters. They are 219 - 381 nm long. Clearer morphology can be seen on SEM image (Fig 4). These show that pH values play a role in the particle shapes and sizes.

In general, most polymeric anions formed in weekly acidic [20] and neutral solutions. Nucleation and growth rates of strontium tungstate particles were very low. Precipitates composing of very fine particles formed in small quantities. H^+ ions seemed to prevent the precipitation process. At higher pH values (weakly basic solutions), more precipitates were produced. The OH^- concentration was not sufficient to have the influence on growth directions. The particles became larger but were still nano-meter in size. In very strong basic solution, growth of the crystalline product was changed in such a way that different morphology formed. At the present stage, a number of OH^- ions selectively adsorbed on different crystallographic planes. The activities of the planes with sufficient OH^- ions were reduced, and growth rates in some certain directions were confined. These led to the anisotropic growth process. A number of nano-sized particles with oval shape formed. They were in clusters due to the attractive force among the different nano-sized particles.

For a pH of 9.6 and at 180 W microwave power, the particles became larger when the time was increased from 20 to 80 min. At pH 9.6 for 600 W and 20 min, the crystalline product became improved. The facets of the particles were detected. At a constant pH of 9.6, the particle sizes were measured along ten straight lines drawn in random directions. Their distributions are shown in Fig 5. Average and standard deviation were then calculated. They were 3.39 ± 0.82, 18.42 ± 5.04 and 18.48 ± 4.32 nm for the products produced using 180 W 20 min, 180 W 80 min and 600 W 20 min, respectively. Their particle sizes were increased with the increasing of the prolonged times and microwave powers.

HRTEM images of lattice planes (Fig 6) for the products produced using different conditions were characterized. The images show that the crystallographic planes are aligned in systematic order although the products are not perfect crystals. They contain some defects. The (101), (112) and (004) planes were detected. Their interplanar spaces (d) were measured and are summarized in Table 1. The spaces are a little lower than those of the JCPDS software [18]. The differences are influenced by the temperature, stress, defects and others. SAED patterns (Fig 3) show several concentric rings characterized as polycrystals. Interplanar spaces (d) were calculated [21,22] using their diffraction ring diameters, and compared with

those of the JCPDS software [18]. They correspond to (101), (112), (004), (200), (211), (204), (220), (116) and (312) crystallographic planes of the products and were specified as $SrWO_4$. At 180 W for all the prolonged times and pH values, the inner rings are diffuse and continuous showing that the products compose of a number of nano-sized crystals. The degree of crystalline products is low. At 600 W, a clearer pattern was detected and composes of a number of bright spots arranged as discontinuous rings. At the present stage, the electron beam reflects and diffracts from polycrystals which become the largest at 600 W. Their coverage by the aperture is lesser in number leading to a greater degree of discontinuity in the diffraction rings. The present analyses show that the interpretations using XRD, SAED, TEM, HRTEM and SEM are in good accord.

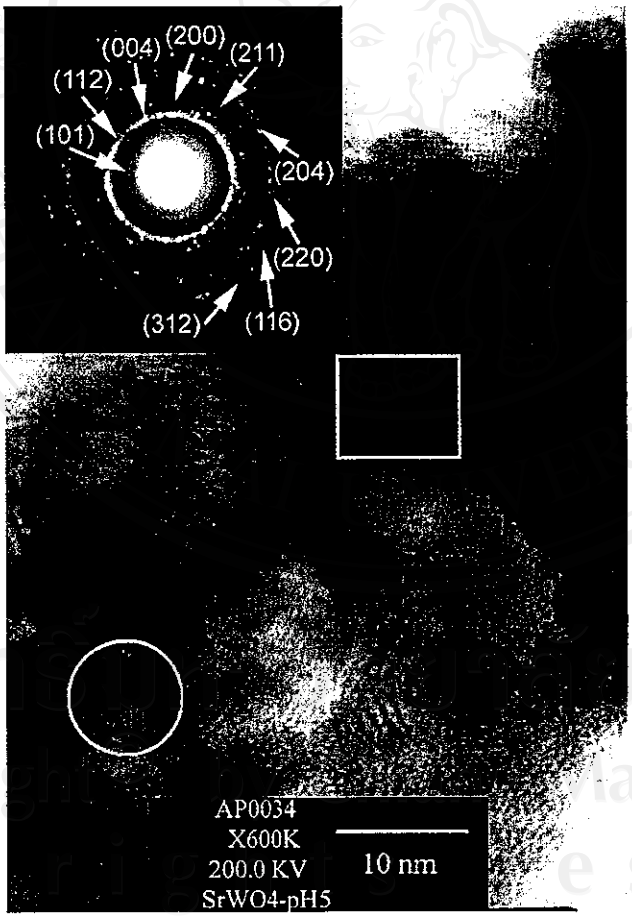

(a)

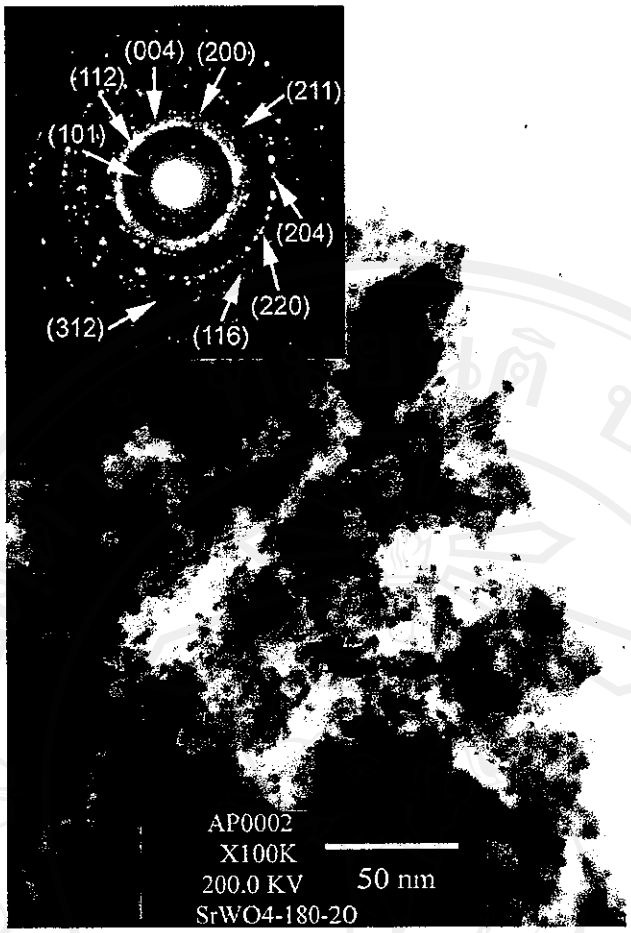

(b)

(c)

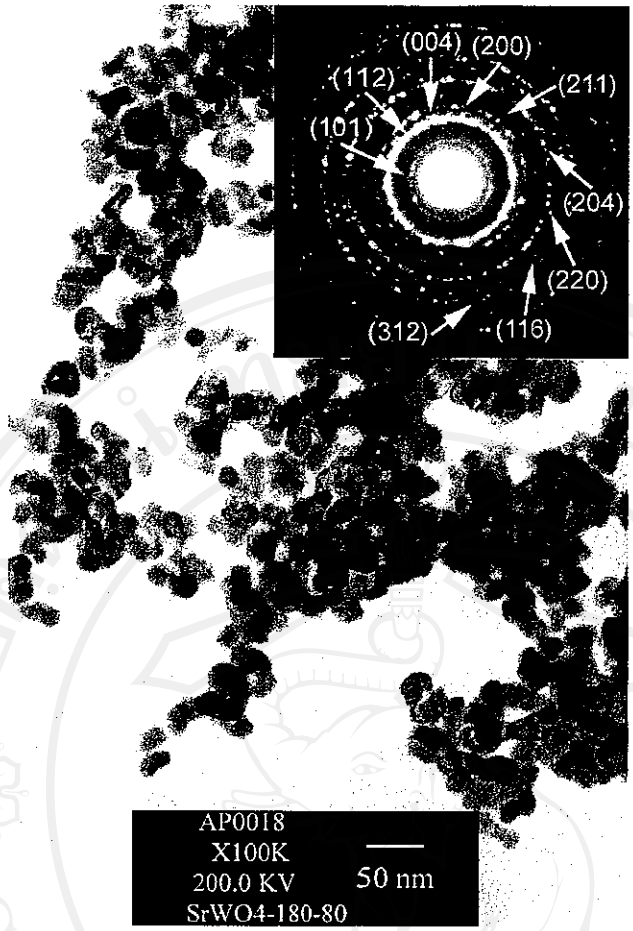

(d)

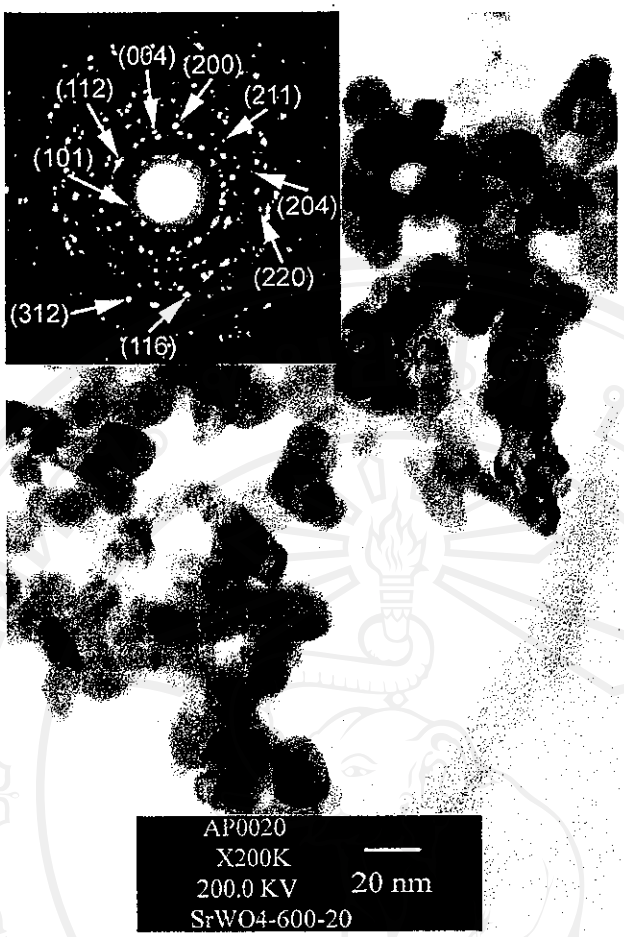

(e)

Fig 3. TEM images and SAED patterns of the products prepared using (a) a pH of 5 at 180 W for 20 min, (b) a pH of 9.6 at 180 W for 20 min, (c) a pH of 13 at 180 W for 20 min, (d) a pH of 9.6 at 180 W for 80 min, and (e) a pH of 9.6 at 600 W for 20 min.

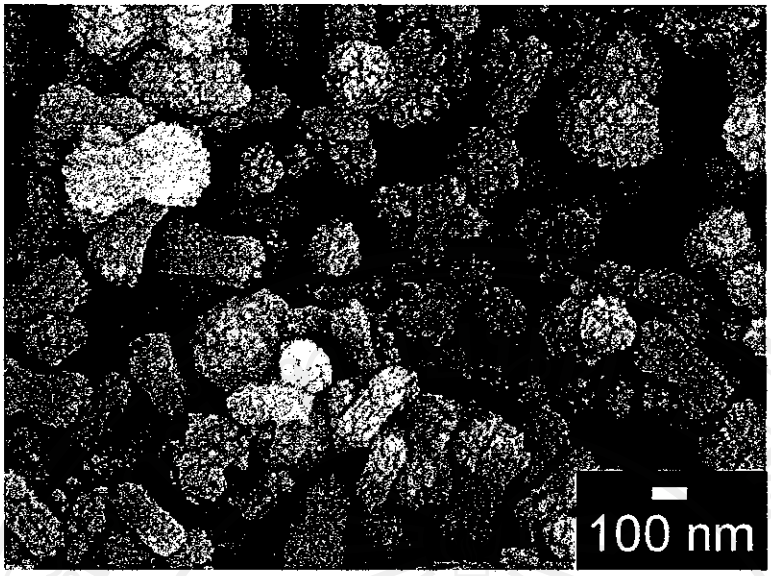

Fig 4. SEM image of the product prepared in a solution with a pH of 13 using 180 W for 20 min.

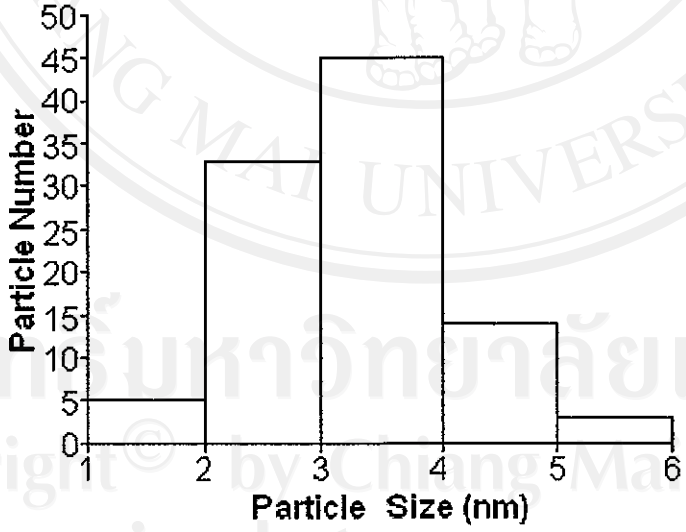

(a)

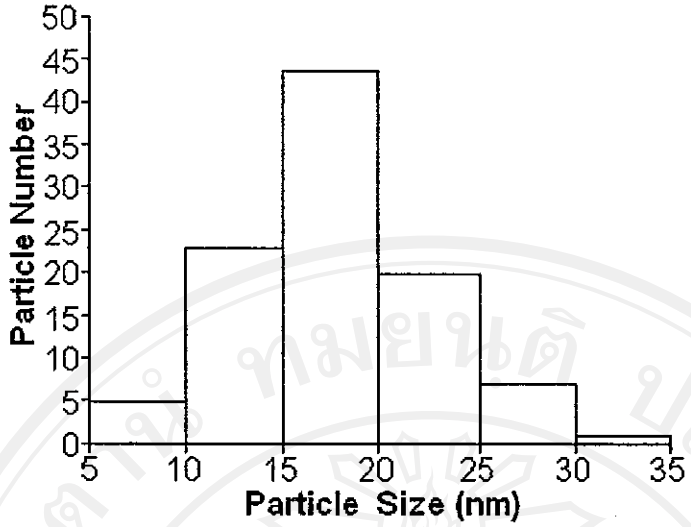

(b)

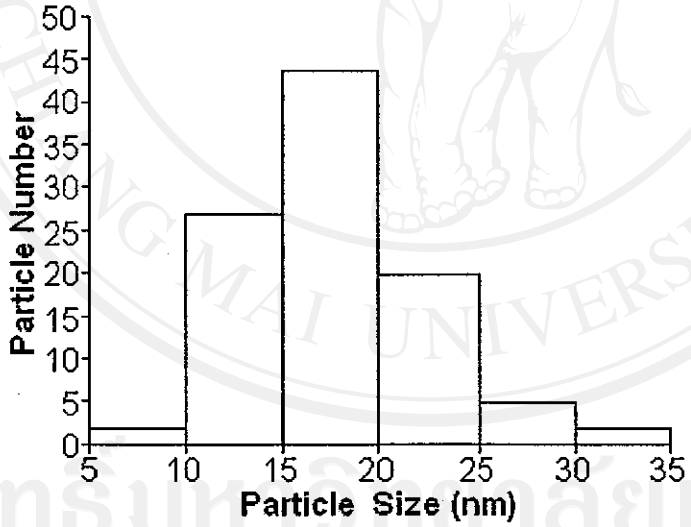

(c)

Fig. 5. Particle size distributions of the products prepared in a solution with a pH of 9.6 using (a) 180 W for 20 min, (b) 180 W for 80 min, and (c) 600 W for 20 min.

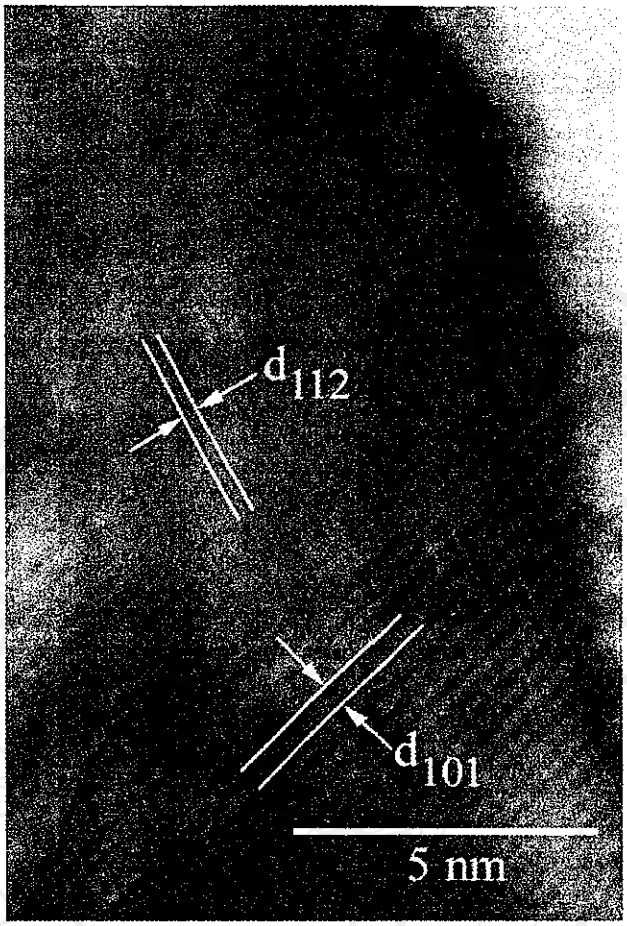

(a)

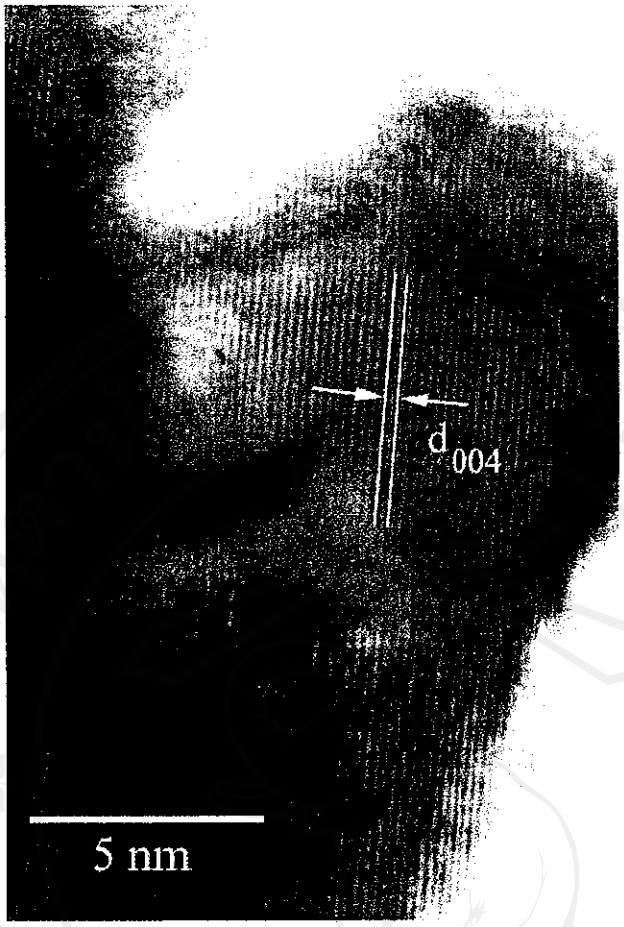

(b)

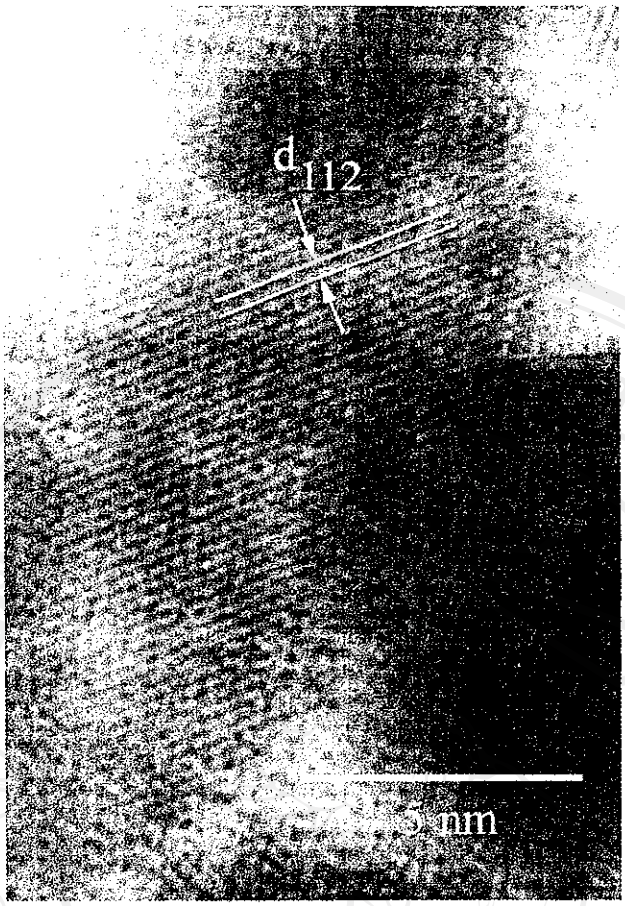

(c)

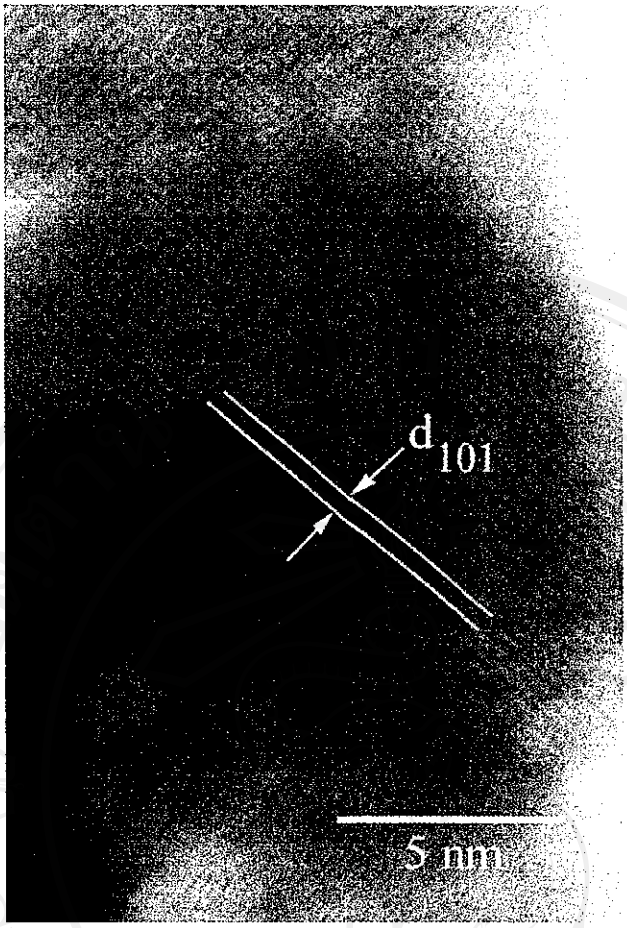

(d)

Fig 6. HRTEM images of lattice planes for the products prepared using (a and b) a pH of 9 at 180 W for 20 min, (c) a pH of 9.6 at 180 W for 80 min, and (d) a pH of 9.6 at 600 W for 20 min.

Table 1. Interplanar spaces of the products prepared using different microwave powers, prolonged times and pH values.

Preparation Condition			Crystallo-graphic Plane	Interplanar Space (nm)
Power (W)	Time (min)	pH		
600	20	9.6	101	0.4009
180	20	9	101	0.4255
	20	9	112	0.2837
	20	9	004	0.2727
	80	9.6	112	0.3030

3.3 Raman and FTIR Spectra

Vibrations of $SrWO_4$ are classified into two types, the internal and external modes [23]. The first belongs to the vibration inside $[WO_4]^{2-}$ molecular units of which the centers of mass are stationary. The second is called lattice phonons which correspond to the motion of Sr^{2+} cations and the rigid molecular units. In free space, $[WO_4]^{2-}$ tetrahedrons have T_d-symmetry [23,24]. Their vibrations compose of four internal modes ($v_1(A_1)$, $v_2(E)$, $v_3(F_2)$ and $v_4(F_2)$), one free rotation mode ($v_{f.r.}(F_1)$), and one translation mode (F_2) [23]. In lattice space, the symmetry is reduced to S_4. All degenerative vibrations are split [23,24] due to the crystal field effect and Davydov splitting [23]. For tetragonal scheelite primitive cell (wavevector, **k** = **0**) [1,23], there are 26 different vibrations ($\Gamma = 3A_g + 5A_u + 5B_g + 3B_u + 5E_g + 5E_u$) determined by group-theory calculation [23,24]. Among them, $3A_g$, $5B_g$ and $5E_g$ vibrations are Raman-active. Only $4A_u$ and $4E_u$ of the $5A_u$ and $5E_u$ vibrations are active in infrared (IR) frequencies, and their remains ($1A_u$ and $1E_u$) are acoustic vibrations. The $3B_u$ vibrations are silent modes [1,23].

For the present research, six different vibrations were detected on Raman spectra (Fig 7) of the products. Among them, $v_1(A_g)$, $v_3(B_g)$, $v_3(E_g)$, $v_4(B_g)$, $v_2(A_g)$ and $v_{f.r.}(A_g)$ are at 916.34, 832.48, 793.26, 371.01, 334.20 and 186.84 cm^{-1}, respectively. The vibration modes are very close to those for $SrWO_4$ with hollow spheres [12], $Sr_{1-x}Ca_xWO_4$ film [25] and $BaWO_4$ at 300 K [23]. The spectra provide the evidence of scheelite structure [12,23,25]. In addition, FTIR spectra (Fig 8) of the products were analyzed using a transmittance mode. For T_d-symmetry, $v_3(F_2)$ and $v_4(F_2)$ are IR

active and correspond to stretching and bending modes, respectively [26,27]. The spectra show a band of W-O stretching vibration in WO_4^{2-} tetrahedrons [27] at 781-912 cm^{-1}. It is one of the internal modes specified as $v_3(F_2)$ antisymmetric stretching vibration [26]. The result is in accord with those of MWO_4 (M = Ca, Sr and Ba) [11,28]. Generally, vibration wavenumbers are influenced by atomic masses, force constant of lattice atoms, atomic bonding and others.

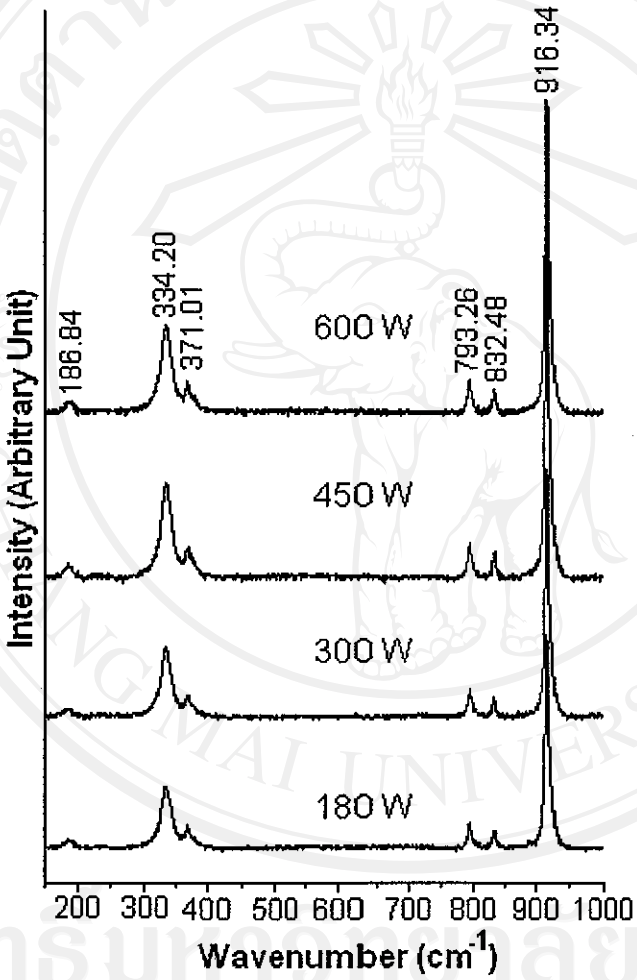

Fig 7. Raman spectra of the products prepared in a solution with a pH of 9.6 at different microwave powers for 20 min.

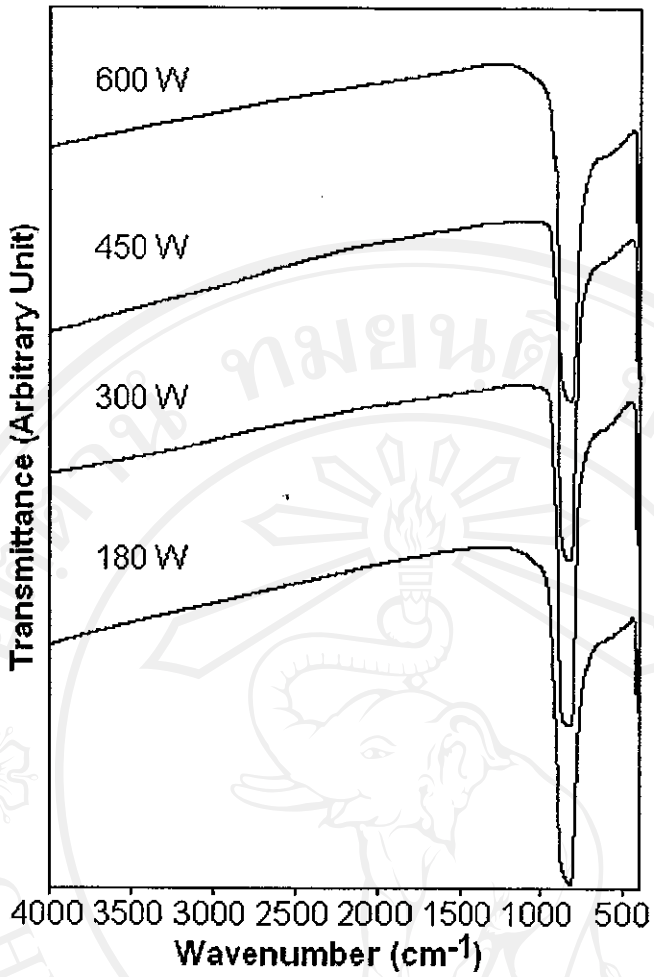

Fig 8. FTIR spectra of the products prepared in a solution with a pH of 9.6 at different microwave powers for 20 min.

3.4 PL Luminescence

The crystal-field splitting and hybridization of the molecular orbitals of $[WO_4]^{2-}$ tetrahedrons [4] are shown in Fig 9. The W 5d(t_2) and W 5d(e) orbitals are hybridized with the O 2p(σ) and O 2p(π) ligand orbitals to form $[WO_4]^{2-}$ tetrahedrons. The four ligand p(σ) orbitals are compatible with the tetrahedral representation for a_1 and t_2 symmetries and the eight ligand p(π) orbitals are for t_1, t_2 and e symmetries. The top occupied state has t_1 symmetry formed from O 2p(π) states. The lowest unoccupied state has e symmetry formed from a combination of the W 5d(e) and O 2p(π) orbitals to give antibonding (*). The hybridization between the W 5d and O 2p orbitals is specified as covalent bonding between the ions. For ground state system, all one-electron states below band gap are filled to give a many-electron $^1A_1$ state. At the lowest excited state, there are one hole in t_1 (primarily O 2p(π)) state and one

electron in e (primarily W 5d) state which give rise to many-electron $^1T_1$, $^3T_1$, $^1T_2$ and $^3T_2$ states. Among them, only $^1T_2 \rightarrow {}^1A_1$ transition is electric dipole allow [4,29].

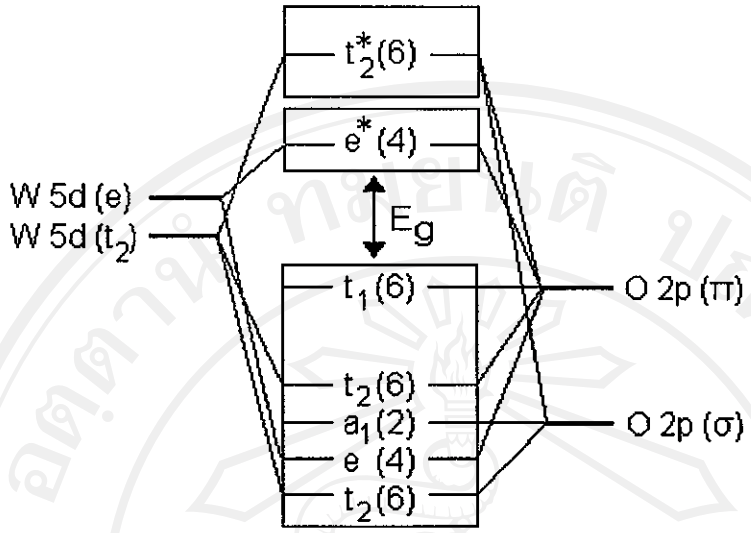

Fig 9. Schematic diagram of the crystal-field splitting and hybridization of the molecular orbitals of $[WO_4]^{2-}$ tetrahedrons. [E_g = Energy band gap, * = Antibonding (Unoccupied) states, Degeneracy of each cluster state is specified as the figures in brackets.]

By using a 270 nm exciting wavelength, PL spectra (Fig 10) of the products were characterized. They show the narrow central peaks with their surrounding shoulders. The central (intrinsic) peaks are considered to be from the $^1T_2 \rightarrow {}^1A_1$ transition of electrons within $[WO_4]^{2-}$ anions [4,29,30]. The transition can be treated as an exciton [30]. The shoulders are from some defects and/or impurities, and interpreted as extrinsic transitions [30]. PL intensity is controlled by the number of charged transfers. For the present analysis, the emission peaks are in the blue spectral region at 420-428 nm (2.901-2.956 eV). Shapes, sizes, degree of crystal and other conditions can play a role in their emission peaks as well.

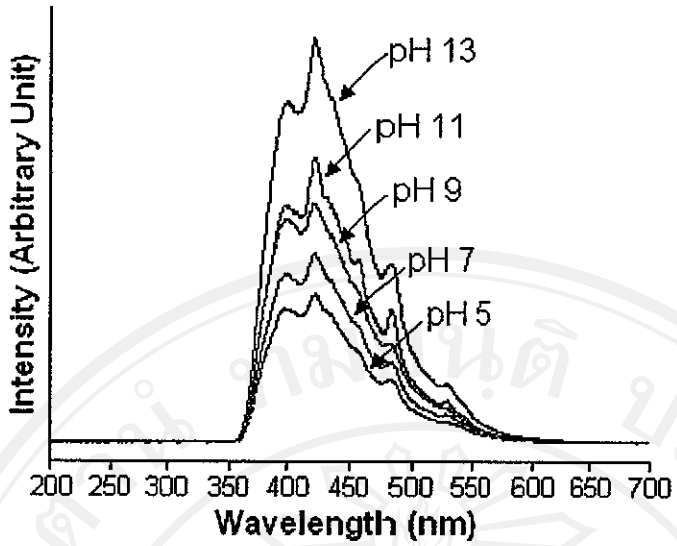

(a)

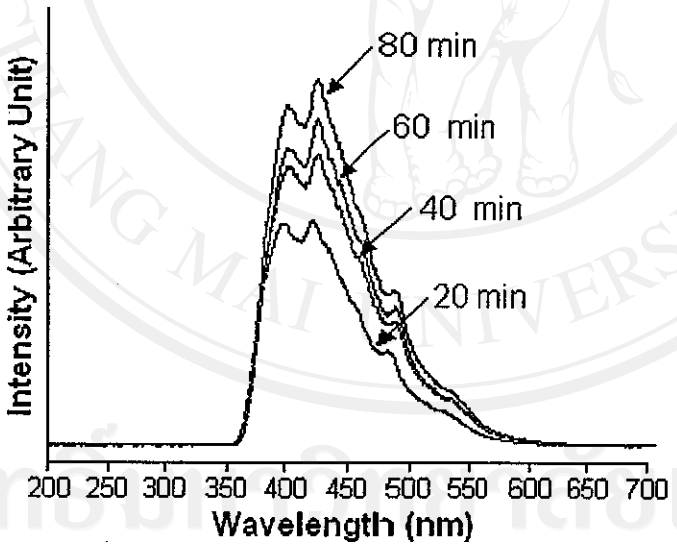

(b)

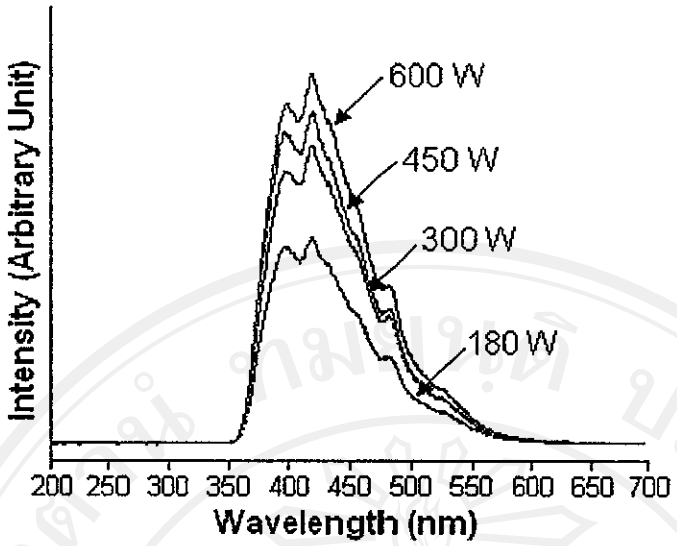

(c)

Fig 10. PL spectra of the products prepared using (a) 180 W for 20 min at different pH values, (b) a pH of 9.6 at 180 W for different prolonged times, and (c) a pH of 9.6 for 20 min at different microwave powers.

4. Conclusions

The advantages of microwave radiation are rapid, simple and efficient process used for producing nanocrystalline $SrWO_4$ in ethylene glycol at different microwave powers, prolonged times and pH values. All of the crystalline products are pure phase with scheelite structure and $I4_1/a$ space group. They compose of nano-sized particles and lattice planes in systematic array. The W-O stretching vibration in WO_4^{2-} tetrahedrons was detected at 781-912 cm^{-1}. Their emission peaks are due to the $^1T_2 \rightarrow {}^1A_1$ transition in WO_4^{2-} tetrahedrons at 420-428 nm (2.901-2.956 eV).

References

1. A. Golubović, R. Gajić, Z. Dohčević-Mitrović, S. Nikolić, J. Alloys Comp. 415 (2006) 16.

2. Z. Lou, M. Cocivera, Mater. Res. Bull. 37 (2002) 1573.

3. B. Xie, Y. Wu, Y. Jiang, F. Li, J. Wu, S. Yuan, W. Yu, Y. Qian, J. Crys. Growth 235 (2002) 283.

4. Y. Zhang, N.A.W. Holzwarth, R.T. Williams, Phys. Rev. B 57 (1998) 12 738.

5. A. Sen, P. Pramanik, J. Europ. Ceram. Soc. 21 (2001) 745.

6. B. Grobelna, B. Lipowska, A.M. Kłonkowski, J. Alloys Comp. 419 (2006) 191.

7. J.H. Ryu, J.W. Yoon, C.S. Lim, W.C. Oh, K.B. Shim, Ceram. Internat. 31 (2005) 883.

8. Z.C. Ling, H.R. Xia, D.G. Ran, F.Q. Liu, S.Q. Sun, J.D. Fan, H.J. Zhang, J.Y. Wang, L.L. Yu, Chem. Phys. Lett. 426 (2006) 85.

9. V.B. Mikhailik, H. Kraus, D. Wahl, M. Itoh, M. Koike, I.K. Bailiff, Phys. Rev. B 69 (2004) 205110-1.

10. L. Sun, Q. Guo, X. Wu, S. Luo, W. Pan, K. Huang, J. Lu, L. Ren, M. Cao, C. Hu, J. Phys. Chem. C 111 (2007) 532.

11. G. Zhang, R. Jia, Q. Wu, Mater. Sci. Eng. B 128 (2006) 254.

12. X. Zhao, T.L.Y. Cheung, X. Zhang, D.H.L. Ng, J. Yu, J. Am. Ceram. Soc. 89 (2006) 2960.

13. C. Gabriel, S. Gabriel, E.H. Grant, B.S.J. Halstead, D.M.P. Mingos, Chem. Soc. Rev. 27 (1998) 213.

14. R. He, X. Qian, J. Yin, Z. Zhu, J. Crys. Growth 252 (2003) 505.

15. S. Yin, M. Shinozaki, T. Sato, J. Luminesc. 126 (2007) 427.

16. J. Lu, Q. Han, X. Yang, L. Lu, X. Wang, Mater. Lett. 61 (2007) 2883.

17. J. Zhu, M. Zhou, J. Xu, X. Liao, Mater. Lett. 47 (2001) 25.

18. Powder Diffract. File, JCPDS Internat. Centre Diffract. Data, PA 19073-3273, U.S.A., (2001).

19. K.I. Gnanasekar, H.A. Cathrino, J.C. Jiang, A.A. Mrse, G. Nagasubrahmanian , D.H. Doughty, B. Rambabu, Solid State Ion. 148 (2002) 299.

20. F.A. Cotton, G. Wilkinson, C.A. Murillo, M. Bochmann, Adv. Inorg. Chem., 6th ed., John Wiley & Sons, New York, (1999) 925.

21. T. Thongtem, A. Phuruangrat, S. Thongtem, Mater. Lett. 60 (2006) 3776.

22. A. Phuruangrat, T. Thongtem, S. Thongtem, Mater. Lett. 61 (2007) 3805.

23. T.T. Basiev, A.A. Sobol, Y.K. Voronko, P.G. Zverev, Optic. Mater. 15 (2000) 205.

24. S.P.S. Porto, J.F. Scott, Phys. Rev. 157 (1967) 716.

25. W.S. Cho, M. Yashima, M. Kakihana, A. Kudo, T. Sakata, M. Yoshimura, Appl. Phys. Lett. 68 (1996) 137.

26. A.P. de Azevedo Marques, D.M.A. de Melo, C.A. Paskocimas, P. S. Pizani, M.R. Joya, E.R. Leite, E. Longo, J. Solid State Chem. 179 (2006) 671.

27. G.M. Clark, W.P. Doyle, Spectrochim. Acta 22 (1966) 1441.

28. J.A. Gadsden, Infrared Spectr. Miner. Relat. Inorg. Comp., Butterworths, (1975) 152.

29. M.J. Treadaway, R.C. Powell, J. Chem. Phys. 61 (1974) 4003.

30. V.B. Mikhailik, I.K. Bailiff, H. Kraus, P.A. Rodnyi, J. Ninkovic, Radiat. Measur. 38 (2004) 585.

Sonochemical preparation of $PbWO_4$ crystals with different morphologies

Abstract

$PbWO_4$ was prepared from $Na_2WO_4.2H_2O$ and $Pb(OAc)_2.3H_2O$ in a solution containing a cationic surfactant (N-cetyl pyridinium chloride) using the sonochemical process (ultrasonic irradiation). The product morphologies, characterized using scanning electron microscopy (SEM) and transmission electron microscopy (TEM), were controlled by the surfactant, pH values and ultrasonic irradiation times. X-ray diffraction (XRD) and selected area electron diffraction (SAED) studies revealed diffraction patterns in good agreement with the simulation model, along with Fourier transform infrared (FTIR) and Raman analyses showed a W-O stretching band consistent with tetragonal $PbWO_4$. Photoluminescent properties of the pine tree shaped products were also investigated.

Keywords : Lead tungstate, Sonochemical process, N-cetyl pyridinium chloride, Pine tree shape

1. Introduction

$PbWO_4$ is one of the most interesting tungstates and it has found wide use in applications such as electromagnetic calorimetry, excitonic luminescence, thermoluminescence and stimulated Raman scattering behavior [1-3]. A variety of preparation processes have been used to produce different shapes and sizes which strongly affect the material's properties. These processes include synthesis with and without using organic additives, such as microemulsion-based synthesis [4, 5], wet chemistry methods [3, 6, 7], microwave-assisted synthesis [8, 9], sonochemical processes [2] and hydrothermal reactions [10]. Surfactants have been added in some of these processes and it is believed that they function as shape directors in product formations [6]. Other parameters, such as pH, temperature, prolonged reaction time and solvent system, can play a role in the formation of different shapes and sizes as well.

Several groups have reported the preparation of $PbWO_4$ using the sonochemical process that yields a variety of shapes : polyhedra, spindle-like and dot-shaped

nanostructures [2], hollow spindle [11], and Sb(III)-doped single crystals [12]. The purpose of the present research was to sonochemically prepare $PbWO_4$ in a solution containing N-cetyl pyridinium chloride (a cationic surfactant) and classify and examine the resulting structures. The effects of pH and irradiation times on the morphologies have been investigated. An unusual pine tree shaped product, not previously reported from sonochemical studies, is a promising material that contains a number of defects having influence on the luminescent intensity [5].

2. Experiment

All chemicals were of reagent grade. Three solutions were prepared by separately dissolving 0.003 mol $Na_2WO_4.2H_2O$, 0.005 mol N-cetyl pyridinium chloride (a cationic surfactant) and 0.003 mol $Pb(OAc)_2.3H_2O$ in 20 ml de-ionized water each. The $Na_2WO_4.2H_2O$ and N-cetyl pyridinium chloride solutions were mixed for 30 min under ultrasonic irradiation (sonochemical process). Then the $Pb(OAc)_2.3H_2O$ solution was added and the pH was adjusted to be in the range of 3-11. Ultrasonic irradiation was carried out for 1-5 h, resulting in the gradual formation of white precipitates with different shapes and sizes. The crystals were washed with water and ethanol, and dried at 80 °C for 24 h for further analysis. The final products were analyzed using X-ray diffraction (XRD) operating at 20 kV, 15 mA, using the K_α line from a Cu target, transmission electron microscopy (TEM) as well as selected area electron diffraction (SAED) operated at 200 kV, scanning electron microscopy (SEM) operated at 15 kV, Fourier transform infrared (FTIR) with KBr as a diluting agent and operated in the range 400-4,000 cm^{-1}, a Raman spectrometer using 50 mW Ar Laser with λ = 514.5 nm, and a luminescence spectrometer using a 300 nm exciting wavelength. In addition, diffraction patterns were simulated using CaRIne Crystallography 3.1 software [13] and compared with those interpreted from the experimental results.

3. Results and Discussion

XRD spectra of all the products (Fig 1) correspond to $PbWO_4$ with tetragonal stolzite structure [1, 14]. Its space group is $I4_1/a$. The unit cell parameters are a = b = 0.5445 nm, c = 1.2050 nm, and $\alpha = \beta = \gamma = 90$ deg. The spectra diffracted from crystallographic planes of the products are (112), (004), (200), (121), (204), (220), (116), (312) and (224). The strongest intensity diffracted from (112) plane and is at

2θ = 27.5 deg. The spectra are very sharp showing that the product was composed of a number of crystals. No other characteristic peaks of impurities were detected showing that each product is a pure phase. By mixing $Na_2WO_4.2H_2O$ and surfactant (positively charge), $(WO_4)^{2-}$ anions were possibly coordinated the surfactant molecules to form surfactant-tungstate complexes. The addition of $Pb(OAc)_2.3H_2O$ into the solution containing the surfactant-tungstate complexes under the assistance of ultrasonic irradiation led to the substitution of the surfactant by Pb^{2+} cations. Once $PbWO_4$ nuclei (very fine particles) formed, they came together to form crystalline solids. The surfactant may have been selectively adsorbed onto the crystals [7] and possibly desorbed due to the ultrasonic irradiation, resulting in a particular shape from the anisotropic process.

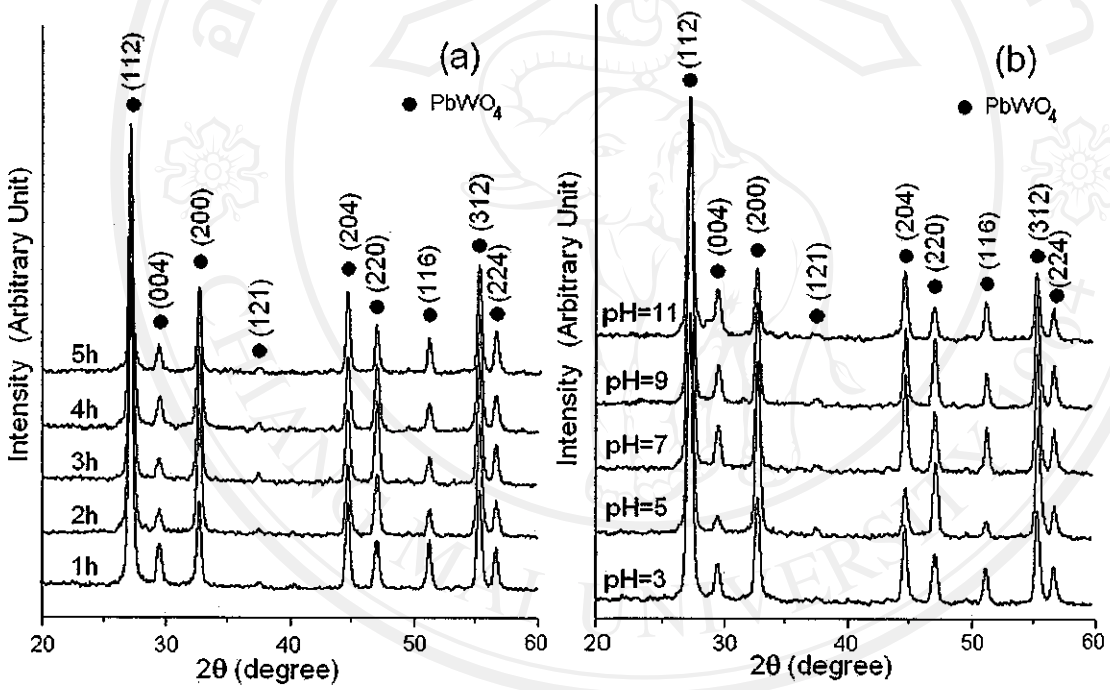

Fig 1. XRD spectra of the products prepared in the solution containing N-cetyl pyridinium chloride using (a) the pH of 6.54 for different irradiation times, and (b) the 1 h irradiation with different pH values.

SEM images of $PbWO_4$ are shown in Fig 2. These are especially well-defined, complex and highly ordered. They are structurally similar to those prepared by wet chemical methods without sonication [15] but the current structures are more highly ordered. At the pH of 6.54 and for 1 h ultrasonic irradiation (Fig 2a), the product is composed of six tree trunk like structures at right angle. Two pairs are in the same plane. One pair is shorter than the other. The third pair is at a right angle to the four-

trunk structure. One trunk is on the top and the other is at the bottom. Sometimes the trunks were released by ultrasonic irradiation. The structure is complex, uniform and systematic. The trunks are in the shape of pine trees and have arrowhead-shaped tips. When the ultrasonic irradiation was prolonged (Figs 2b-2d), the trunks became longer. Some structures were broken and some side grains were released (marked with a circle in Fig 2d). For the preparation without the use of a surfactant, the product (Fig 2e) is in the shape of seaweed and resembles those of Liu B. et al. [15].

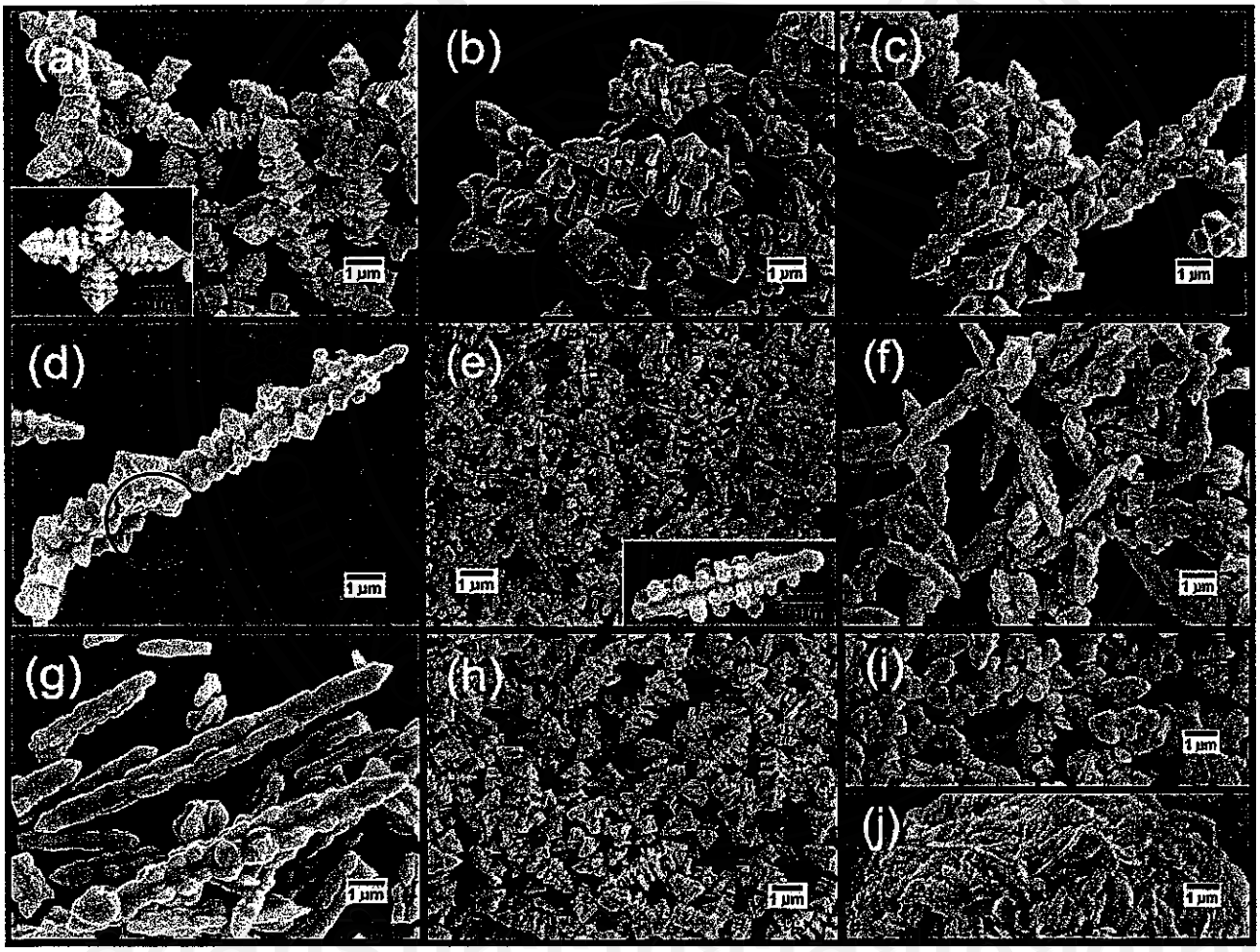

Fig 2. SEM images of $PbWO_4$ prepared in (a-d) the solution containing N-cetyl pyridinium chloride (pH = 6.54) with 1, 2, 3 and 5 h irradiations, (e) the surfactant-free solution (pH = 6.26 and 1 h irradiation), and (f-j) the solution containing N-cetyl pyridinium chloride with the pH of 3, 5, 7, 9 and 11 (1 h irradiation), respectively.

This demonstrates that N-cetyl pyridinium chloride plays the role in the product morphologies and functions as the shape director of the process. In addition, $PbWO_4$ crystals prepared using a variety of the pH values with 1 h irradiation (Figs 2f-2j) have different morphologies. They have corn-like shape for the pH of 3 and 5, pine tree structure for the pH 7, granular shape for the pH 9, and irregular shape and size particles in clusters for the pH 11. At the pH above 11, lead hydroxide complex instead of $PbWO_4$ is probably formed due to the high OH^- concentration. These results show that the pH value plays the role in the shape and size of the products as well. At 1 h irradiation, the structures for the pH 6.54 (Fig 2a) and 7 (Fig 2h) are in the shape of a pine tree and are very similar.

Close examination of the TEM image of $PbWO_4$ prepared at pH 6.54 with 1 h of irradiation (Fig 3a) shows the trunk of the product shaped like a pine tree which slopes up to a point. It has two halves that are the same in size and shape. SAED patterns (Figs 3b and 3c) at two positions marked with a square and an ellipse on the product were interpreted [16-19]. The patterns correspond to $PbWO_4$ with tetragonal crystal system [14]. For the present research, zone axes [18-20] are in the $[001]$ and $[0\bar{1}0]$ directions for the analyses at the square and ellipse, respectively. Each of them is parallel or nearly parallel to the electron beams. Diffraction patterns for $PbWO_4$ with $[001]$ and $[0\bar{1}0]$ zone axes were simulated [13] and are shown in Figs 3d and 3e. They are very symmetric and systematic. The a*, b* and c* reciprocal lattice vectors for both patterns are in the [100], [010] and [001] directions, respectively. For one crystal structure, the corresponding lattice vectors are the same although their zone axes are different. Comparisons between the SAED and simulated patterns, they are in good accordance.

FTIR and Raman spectra of $PbWO_4$ with tetragonal stolzite structure are shown in Fig 4. For the pH of 6.54 and different irradiation times (Fig 4a), very strong W-O stretching bands of WO_4 tetrahedra were detected over the range 779-787 cm^{-1} [21-24]. O-H stretching and O-H bending bands of residual water were detected over the range 3302-3642 and 1654-1656 cm^{-1}, respectively. Comparisons to FTIR spectrum of N-cetyl pyridinium chloride (result not shown) reveal very weak bands of the surfactant at 2922 and 2852 cm^{-1}. At 1 h ultrasonic irradiation and different pH values

(Fig 4b), O-H stretching, O-H bending and W-O stretching bands were detected in the same way as the above. At the pH of 3, six vibrating bands of the surfactant were detected at 2922, 2852, 1631, 1486, 1175 and 478 cm^{-1}. The surfactant intensities decreased with the increase in the pH values. They were no longer detected at pH of 9 and 11. For pH 5, asymmetric and symmetric COO stretching bands of carboxylate group [25] were also detected at 1513 and 1410 cm^{-1}.

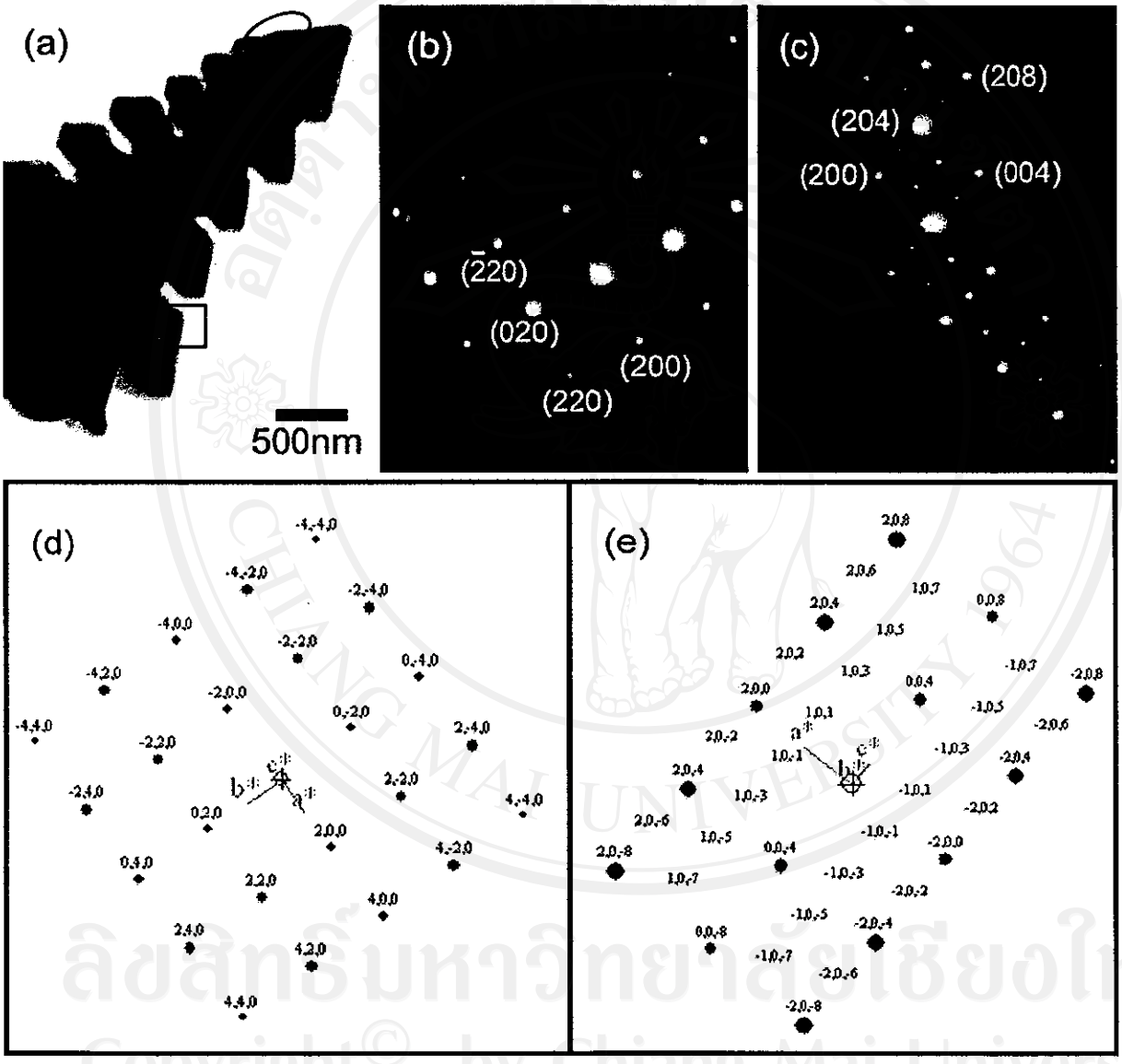

Fig 3. (a) TEM image of $PbWO_4$ prepared in the solution containing N-cetyl pyridinium chloride (pH = 6.54) with 1 h irradiation. (b-e) SAED and simulated patterns at the square and ellipse on the product, respectively.

Raman spectra (Figs 4c and 4d) revealed the presence of six vibrating bands over the range 100-1000 cm^{-1} although their morphologies are different. The $v_1(A_g)$, $v_3(B_g)$ and $v_3(E_g)$ specified as WO_4 stretching vibrations [2, 22] were detected at 907.5, 768.5 and 752.7 cm^{-1}, respectively. The $v_1(A_g)$ has the strongest intensity. The $v_2(A_g)$ was detected as a strong band at 326.8 cm^{-1} with a weak band of $v_2(B_g)$ at 358.3 cm^{-1} [1, 2]. They are the WO_4 bending vibrations [22, 26]. The 176.9 cm^{-1} wavenumber is specified as a translational band of WO_4 groups [1, 2]. There are some differences in the vibration frequencies, depending on the preparation processes and others.

The crystal-field splitting and hybridization of the molecular orbitals of $(WO_4)^{2-}$ tetrahedra [27] are shown in Fig 5. The W 5d(t_2) and W 5d(e) orbitals are hybridized with the O 2p(σ) and O 2p(π) ligand orbitals to form $(WO_4)^{2-}$ tetrahedra. The four ligand p(σ) orbitals are compatible with the tetrahedral representation for a_1 and t_2 symmetries and the eight ligand p(π) orbitals are for t_1, t_2 and e symmetries. The top occupied state has t_1 symmetry formed from O 2p(π) states. The lowest unoccupied state has e symmetry formed from a combination of the W 5d(e) and O 2p(π) orbitals to give antibonding (*). The hybridization between the W 5d and O 2p orbitals is specified as covalent bonding between the ions. For ground state system, all one-electron states below band gap are filled to give a many-electron $^1A_1$ state. At the lowest excited state, there are one hole in t_1 (primarily O 2p(π)) state and one electron in e (primarily W 5d) state which give rise to many-electron $^1T_1$, $^3T_1$, $^1T_2$ and $^3T_2$ states. Among them, only $^1T_2 \rightarrow {}^1A_1$ transition is electric dipole allow [27,28].

For the present research, luminescence of the pine tree product is the strongest. Photoluminescent (PL) spectra of $PbWO_4$, the shape of a pine tree (Fig 6), are very similar due to the similarity in the morphologies [5, 8]. The PL emission is 415.5 nm wavelength due to the $^1T_2 \rightarrow {}^1A_1$ transition [27,28] of $(WO_4)^{2-}$ anions [8, 9] in the blue range. The PL property is suitable for photoelectronic applications. Different morphologies can play the role in the difference of band gap and wavenumber. For instance, the emission wavenumbers of polyhedra, spindle-like and dot-shaped $PbWO_4$ nanostructures were detected at 493, 491 and 483 nm, respectively [2]. Dot-shaped $PbWO_4$ has the lowest wavenumber due to the smallest dimension. Crystallinity promotes PL intensity as well [2]. The polyhedral crystal is likely to contain the largest number of defects which lead to the highest PL intensity [2].

Comparing the macro- and nano-particles of $PbWO_4$, the first showed stronger blue emission than the second. The opposite is also true for the green emission [6]. The quantum sizes of particles influence their band gaps as well. For $CaWO_4$, band gap of bulk (2.95 eV, 421 nm) is smaller than that of nanofilm (3.03 eV, 409 nm) [21]. Photon energy emitted from the nanofilm is higher than that emitted from the bulk. It occurs a 12 nm blue-shift due to the quantum size effect [21].

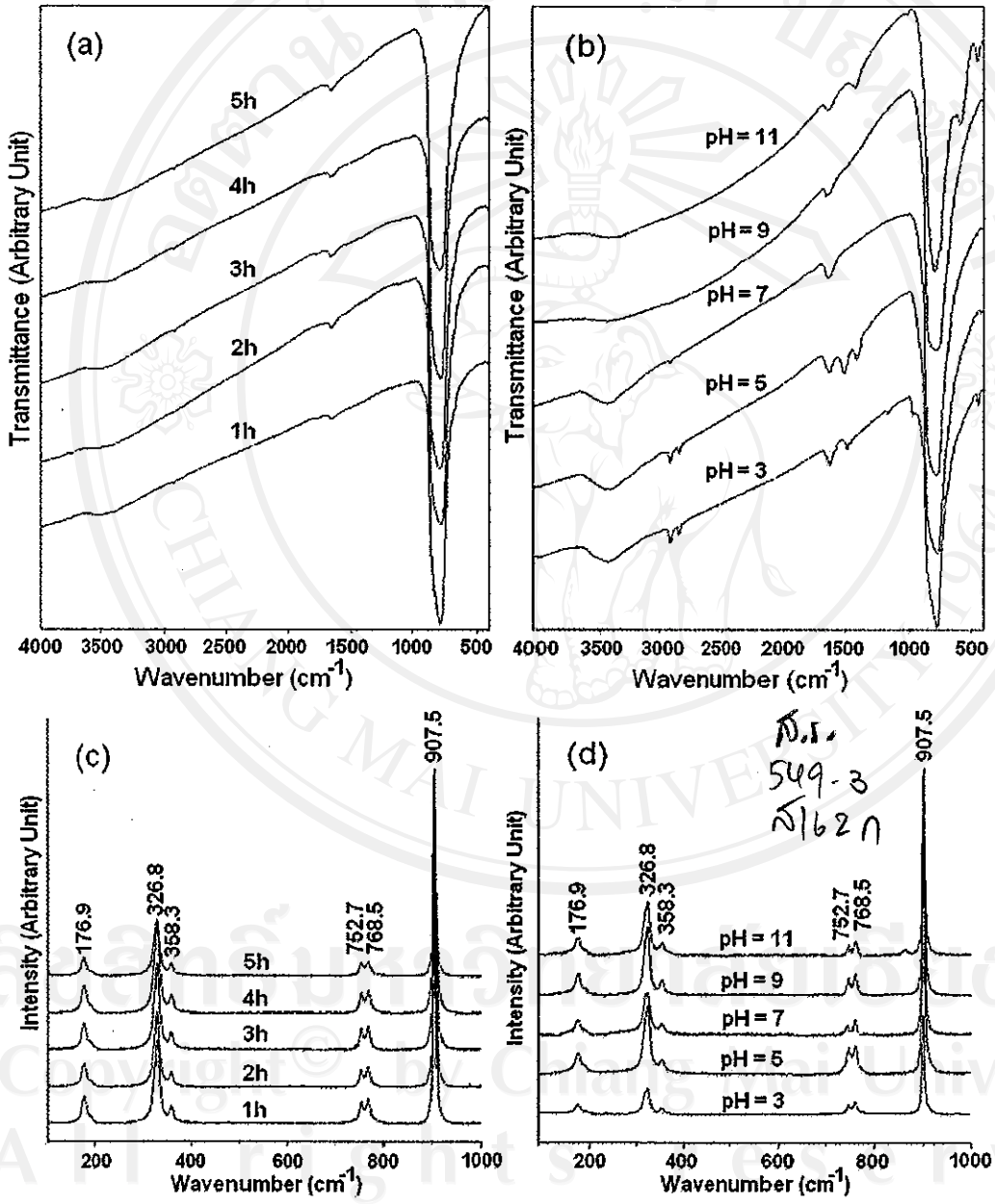

Fig 4. (a, b) FTIR and (c, d) Raman spectra of $PbWO_4$ prepared in the solution containing N-cetyl pyridinium chloride using (a, c) the pH of 6.54 with 1-5 h irradiations, and (b, d) the 1 h irradiation with the pH of 3-11.

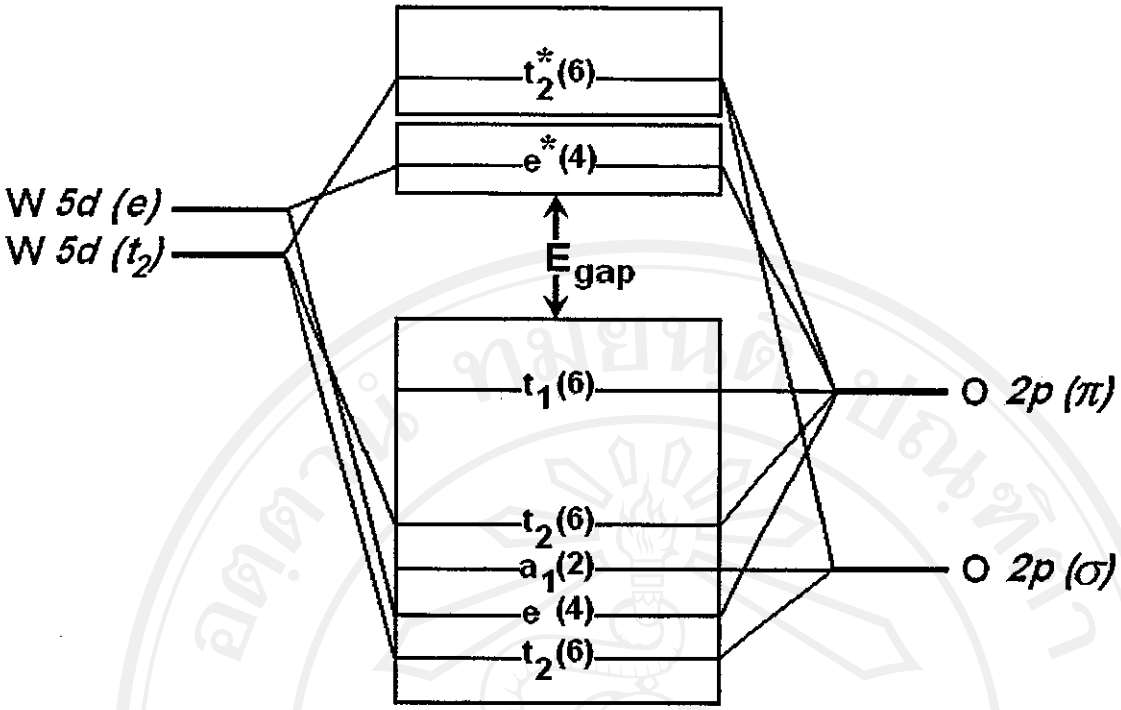

Fig 5. Schematic diagram of the crystal-field splitting and hybridization of the molecular orbitals of $(WO_4)^{2-}$ tetrahedra. E_{gap} = Energy band gap. * = Antibonding (Unoccupied) states. Degeneracy of each cluster state is specified as the figures in brackets. [27]

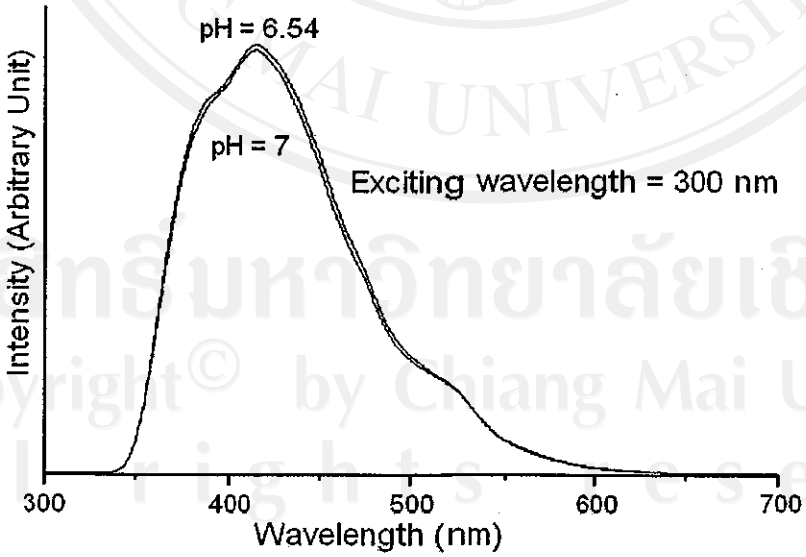

Fig 6. PL spectra of $PbWO_4$ prepared in the solution containing N-cetyl pyridinium chloride using the pH of 6.54 and 7 with 1 h irradiation.

4. Conclusions

$PbWO_4$ with different morphologies was successfully prepared from $Pb(OAc)_2.3H_2O$, $Na_2WO_4.2H_2O$ and N-cetyl pyridinium chloride by a sonochemical process. The final products, analyzed using XRD and SAED, were specified as pure $PbWO_4$ with tetragonal stolzite structure. SAED and simulated patterns are also in good agreement. The W-O stretching bands of WO_4 tetrahedra were detected by using FTIR at 779-787 cm^{-1} and Raman analysis at 907.5, 768.5 and 752.7 cm^{-1}. Their morphologies, characterized by SEM and TEM, were controlled by pH value, surfactant and irradiation times. They are corn-like, pine tree, granular and irregular in shape, depending on the reaction conditions. PL emission of the pine tree shaped products was detected at 415.5 nm due to the $^1T_2 \rightarrow {}^1A_1$ transition of $(WO_4)^{2-}$ tetrahedra.

References

1. Kloprogge J.Th., Weier M.L., Duong L.V., Frost R.L., Mater. Chem. Phys., 88 (2004) 438.

2. Geng J., Zhu J.J., Chen H.Y., Cryst. Growth Design, 6 (2006) 321.

3. Zhou G., Lü M., Gu F., Xu D., Yuan D., J. Cryst. Growth, 276 (2005) 577.

4. Huo L., Chu Y., Mater. Lett., 60 (2006) 2675.

5. Chen D., Shen G., Tang K., Liang Zh., Zheng H., J. Phys. Chem. B, 108 (2004) 11280.

6. Zhou G., Lü M., Su B., Gu F., Xiu Zh., Wang Sh., Optical Mater., 28 (2006) 1385.

7. Hu X.L., Zhu Y.J., Langmuir, 20 (2004) 1521.

8. Ryu J.H., Koo S.M., Chang D.S., Yoon J.W., Lim Ch.S., Shim Kw.B., Ceram. Internat., 32 (2006) 647.

9. Ryu J.H., Yoon J.W., Shim Kw.B., Solid State Comm., 133 (2005) 657.

10. An Ch., Tang K., Shen G., Wang Ch., Qian Y., Mater. Lett., 57 (2002) 565.

11. Geng J., Zhu J.J., Lu D.J., Chen H.Y., Inorg. Chem., 45 (2006) 8403.

12. Geng J., Lu D.J., Zhu J.J., Chen H.Y., J. Phys. Chem. B, 110 (2006) 13777.

13. Boudias C., Monceau D., CaRIne Crystallography 3.1, 17 rue du Moulin du Roy, F-60300 Senlis, France (1989-1998).

14. JCPDS software, Powder Diffract. File, JCPDS Internat. Centre Diffract. Data, PA 19073-3273, U.S.A., (2001) reference code : 85-1857

15. Liu B., Yu S.H., Li L., Zhang Q., Zhang F., Jiang K., Angew. Chem. Int. Ed., 43 (2004) 4745.

16. Andrews K.W., Dyson D.J., Keown S.R., Interpret. Electr. Diffract. Patter., 2nd ed, Plenum Press, NY (1971).

17. Fultz B., Howe J., Transmiss. Electr. Microscop. Diffract. Mater., 2nd ed., Springer (2002).

18. Thongtem T., Phuruangrat A., Thongtem S., Mater. Lett., 61 (2007) 3235.

19. Thongtem T., Phuruangrat A., Thongtem S., Mater. Lett., 62 (2008) 454.

20. Cullity B.D. Elem. X-ray Diffract., 2nd ed., Addison-Wesley Publ. Co., MA (1978).

21. Zhang G., Jia R., Wu Q., Mater. Sci. Engin. B, 128 (2006) 254.

22. Frost R.L., Duong L., Weier M., Spectrochim. Acta Part A, 60 (2004) 1853.

23. Gadsden J.A., Infrared Spectr. Miner. Relat. Inorg. Comp., Butterworths, England (1975).

24. Clark G.M., Doyle W.P., Spectrochim. Acta, 22 (1966) 1441.

25. Smith B., Infrared Spectr. Interpret., CRC Press, NY (1999).

26. Huang Y., Seo Hy.J., Feng Q., Yuan Sh., Mater. Sci. Engin. B, 121 (2005) 103.

27. Zhang Y., Holzwarth N.A.W., Williams R.T., Phys. Rev. B, 57 (1998) 12 738.

28. Treadaway M.J., Powell R.C., J. Chem. Phys. 61 (1974) 4003.

Synthesis and analysis of CuS with different morphologies using cyclic microwave irradiation

Abstract

Nano- and micro-sized CuS crystals were successfully synthesized from copper and sulfur sources ($CuCl_2.2H_2O$, CuBr, $Cu(CH_3COO)_2.H_2O$, CH_3CSNH_2, $NH_2CSNHNH_2$ and NH_2CSNH_2) in ethylene glycol assisted by the cyclic irradiation of different microwave powers and prolonged times. By using XRD and SAED, CuS (hcp) was detected. The products characterized using SEM and TEM compose of assemblies of nano-flakes, clusters of nano-particles, nano-fibers, nano-rods and sponge-like structures influenced by the synthesized conditions. Their lattice vibrations are in the same Raman wavenumber at 474 cm^{-1}. Among the different products, the emission peaks are over the range 414-435 nm (2.85 - 2.99 ev). Reaction evidences of the sources were provided using FTIR. Phase and morphology formations are also proposed on according to the analytical results.

Keywords : CuS, Cyclic microwave irradiation, Phase and morphology formations

1. Introduction

Copper sulfides are one of the IB-VIA compounds. They have a wide varieties of compositions, ranging from S-rich (CuS_2) to Cu-rich (Cu_2S). CuS is an intermediate compound. It is very interesting due to its wide range of applications in optical and electrical devices, such as catalysts, solar cells and cathode materials in lithium rechargeable batteries [1]. It has metallic conduction property, and transforms into a superconductor below the 1.6 K [2]. Recently, copper sulfides with different morphologies have been synthesized. Among them are hollow spheres [1,3], nanoparticles [4,5], nanorods [6-8], nanoflakes [9], nanoplates [10], and nanocones and nanobelts [11]. There are different methods used for the synthesis, such as solid-state reaction [7], hydrothermal fabrication [2,11], sonochemical synthesis [12], photochemical deposition [13] and microwave irradiation [4]. For the present research, nano- and micro-sized CuS crystals with different morphologies such as assemblies of nano-flakes, clusters of nano-sized particles, nano-fibers, nano-rods and sponge-like structures were successfully synthesized from different copper and

sulfur sources in ethylene glycol by the cyclic exposure to microwave irradiation. No surfactants were used in the process which is very simple and novelty.

2. Experiment

Each of 0.005 mole copper and sulfur sources was dissolved in 30 ml ethylene glycol and stirred for 30 min. The reactions cyclically proceeded using different microwave powers and prolonged times to produce products with different morphologies (Table 1). One cycle of 2 min prolonged time composes of irradiation and non-irradiation for 1 min each. Current temperatures at different microwave powers and prolonged times are shown in Fig 1. At constant microwave power, the temperatures were increased with the increasing of the prolonged times within about the first 10 min. They tend to be constant afterwards. At the conclusion of the process, the final products were washed with water and ethanol, and dried at 80 °C for 12 h. Then, they were characterized using XRD operated at 20 kV, 15 mA and using the Kα line from a Cu target, SEM operated at 15 kV, TEM as well as the use of selected area electron diffraction (SAED) operated at 200 kV, FTIR with KBr as a diluting agent and operated in the range 400-4,000 cm^{-1}, Raman spectrometry using 50 mW Ar Laser with λ = 514.5 nm, and photoluminescence (PL) spectrometry using a 202 nm exciting wavelength.

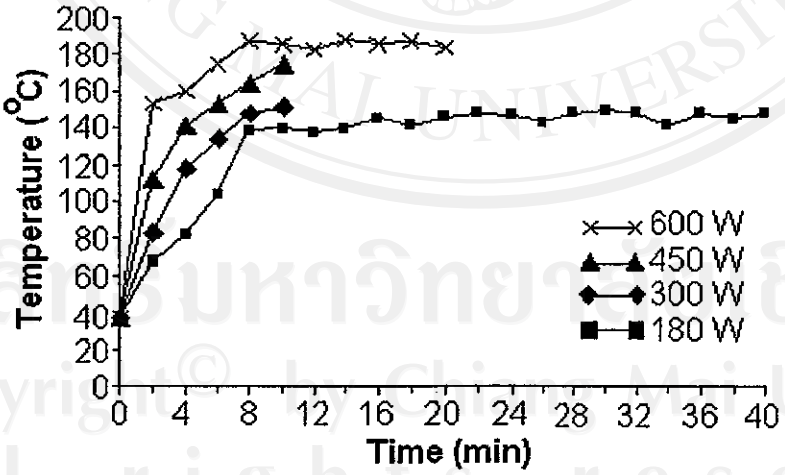

Fig 1. Current temperatures at different microwave powers and prolonged times used for the present process.

Table 1. Copper and sulfur sources, product codes and morphologies at different conditions.

Copper and sulfur sources	Power (W)	Prolonged time (min)	Product codes	Morphologies
$CuCl_2.2H_2O$ + CH_3CSNH_2	180	10	CA1	Assemblies of nano-flakes (Micro-sized flowers)
	180	20	CA2	
	180	30	CA3	
	180	40	CA4	
	300	10	CA5	
	450	10	CA6	
	600	10	CA7	
$CuCl_2.2H_2O$ + CH_3CSNH_2	600	20	CA	Assemblies of nano-flakes (Micro-sized flowers)
$CuCl_2.2H_2O$ + $NH_2CSNHNH_2$	600	20	CC	
$CuCl_2.2H_2O$ + NH_2CSNH_2	600	20	CU	
CuBr + CH_3CSNH_2	600	20	BA	Clusters of nano-sized particles
CuBr + $NH_2CSNHNH_2$	600	20	BC	Nano-rods
CuBr + NH_2CSNH_2	600	20	BU	Sponge-like structures
$Cu(CH_3COO)_2.H_2O$ + CH_3CSNH_2	600	20	AA	Assemblies of nano-flakes
$Cu(CH_3COO)_2.H_2O$ + $NH_2CSNHNH_2$	600	20	AC	Nano-fibers
$Cu(CH_3COO)_2.H_2O$ + NH_2CSNH_2	600	20	AU	Clusters of nano-sized particles

3. Results and Discussion

3.1 XRD

XRD spectra of the products (Fig 2) synthesized using different conditions were analyzed and compared with that of the JCPDS software (reference code : 78-0876) [14]. When $CuCl_2.2H_2O$ and CH_3CSNH_2 were used as the starting agents, XRD spectra of the products synthesized at different prolonged times and microwave powers revealed the presence of pure CuS (hexagonal) with P63/mmc space group. No characteristic peaks arising from impurities such as CuO and Cu_2S were detected. The XRD peaks became higher and narrower with the increase in the prolonged times and microwave powers. These show that the crystalline products were improved. The prolonged times and microwave powers have the influence on the phase formation by assisting Cu and S atoms in violent vibrating and diffusing (higher amplitude) at longer time. The atoms have the better chance to reside in their normal lattices or in the periodic array. These lead to the increase in the degree or extent of the product crystalline. When one of the copper and sulfur sources were used at constant 20 min prolonged time and 600 W microwave power, pure CuS can be synthesized as well.

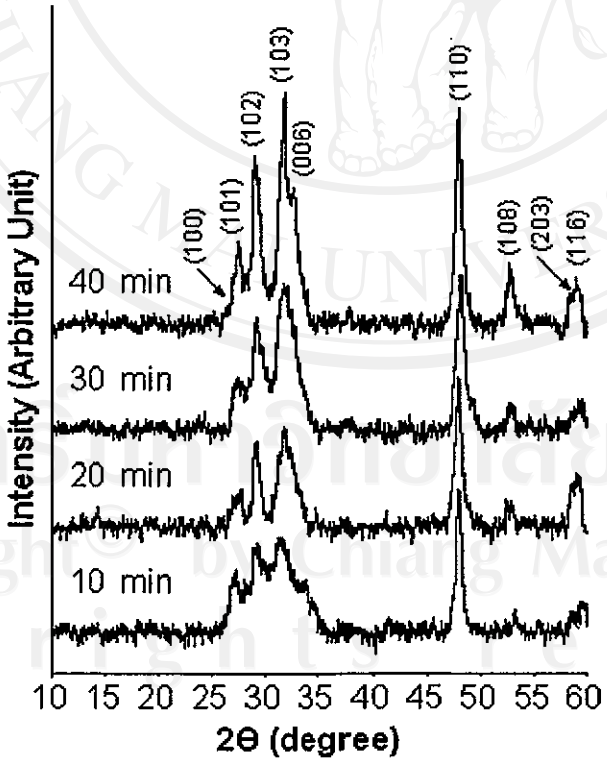

(a)

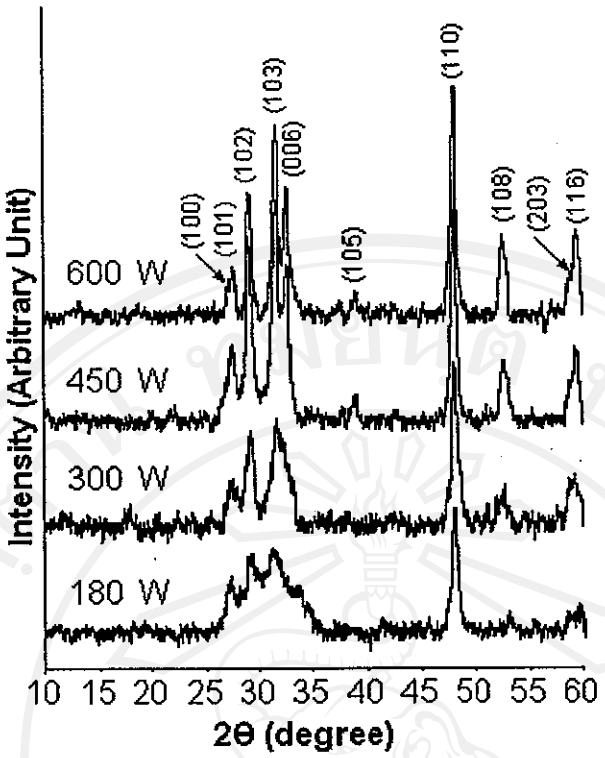

(b)

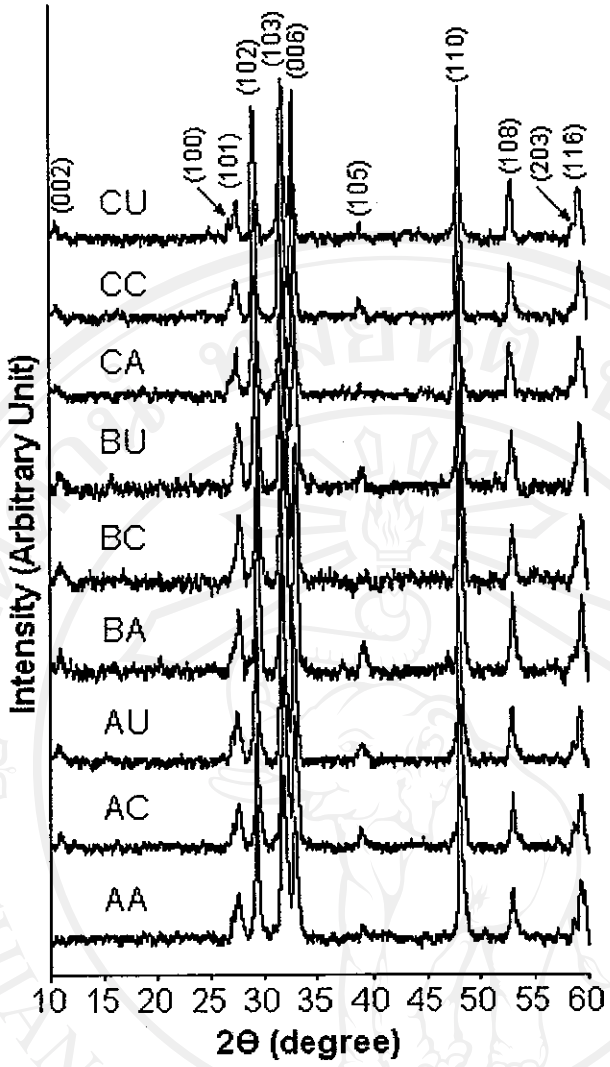

(c)

Fig 2. XRD spectra of the products synthesized using different conditions (starting agents / microwave powers / prolonged times). (a) $CuCl_2.2H_2O$ and CH_3CSNH_2 / 180 W / 10 – 40 min, (b) $CuCl_2.2H_2O$ and CH_3CSNH_2 / 180 - 600 W / 10 min, and (c) different starting agents / 600 W / 20 min.

3.2 Phase formation

During the synthesis, $CuCl_2.2H_2O$ reacted with CH_3CSNH_2 in ethylene glycol for several steps and copper complex ($[Cu(CH_3CSNH_2)_2]^{2+}$) formed. Then, the complex was decomposed by microwave irradiation to produce CuS [4]. Due to the existence of crystal water in $CuCl_2.2H_2O$ and trace water in ethylene glycol, CH_3CSNH_2 reacted with H_2O to form H_2S. Subsequently, H_2S was decomposed by the microwave irradiation [15,16]. S^{2-} generated and further reacted with Cu^{2+} to produce CuS.

The reactions were similar to the above when $CuCl_2.2H_2O$ was replaced by $Cu(CH_3COO)_2.H_2O$, and CH_3CSNH_2 by $NH_2CSNHNH_2$ or NH_2CSNH_2. In case of using CuBr as a copper source, Cu^{1+} is not stable in the solution. It can undergo disproportionation in which the oxidation state of Cu^{1+} is simultaneously raised and lowered [17].

$$2Cu^{1+} \longrightarrow Cu^{2+} + Cu^{0}$$

With the assistance of microwave irradiation, Cu^0 was further oxidized to Cu^{2+} by H_2S.

$$Cu^{0} \xrightarrow{\text{Microwave irradiation}} Cu^{2+} + 2e^{-}$$

Cu^{2+} combined with S^{2-} to produce CuS.

$$Cu^{2+} + S^{2-} \xrightarrow{\text{Microwave irradiation}} CuS$$

Reaction evidences between copper and sulfur sources were provided on according to the following. During the synthesizing process, copper and sulfur salts were separately dissolved in ethylene glycol and mixed. The precipitates (copper complexes) formed. Subsequently, they turned into black (CuS) in a microwave oven. In addition, pure thiourea (NH_2CSNH_2) and copper-thiourea complex were characterized using FTIR. Their spectra are shown in Fig 3. For thiourea spectrum, bands of C=S and C-N stretching vibrations [18,19], were detected at 735 and 1464 cm^{-1}, respectively. Corresponding bands of the complex were at 697 and 1494 cm^{-1}, respectively. Comparing to thiourea, the first vibration shows red-shift which was caused by lowering in the wavenumber. It was characterized as the reduced double bond character of carbon and sulfur in the complex. The second is blue-shift due to the greater double bond character of carbon and nitrogen in the complex. It shows the presence of sulfur-copper coordination [19]. Three bands of NH_2 stretching vibrations of thiourea and the complex [19] were the same wavenumber at 3171, 3269 and 3373 cm^{-1}. Their NH_2 bending [18] is also the same wavenumber at 1600

cm^{-1}. The NH_2 stretching and bending vibrations are stationary. In the present case, no bonding between nitrogen and copper is present [18,19]. Some difference in the intensity peak at 1104 cm^{-1} of thiourea and the complex was detected. When copper-thiourea complex was produced, the intensity peak in thiourea was diminished in the complex. It was influenced by a change in the nature of C=S and C-N bonds due to the complex formation [18].

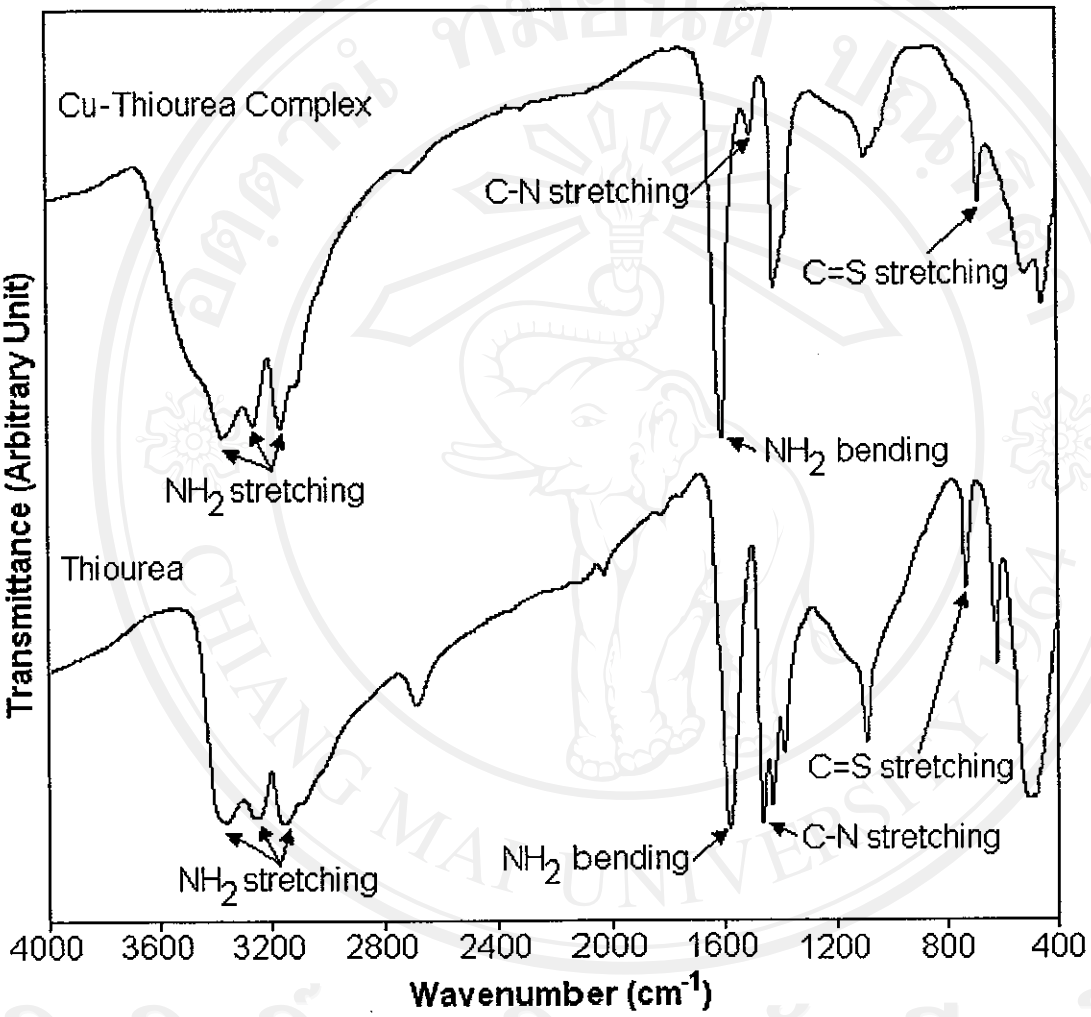

Fig 3. FTIR spectra of thiourea and copper-thiourea complex.

Microwave irradiation is at an advantage over other processes by solving the problems of concentration and temperature gradients in the solution. Its vibration frequency provides uniform condition for the nucleation and growth due to the rapid, uniform and effective heating process. It accelerates the reactions by assisting the decomposition of copper complexes and H_2S, the oxidation and reduction processes, and the formation of CuS.

3.3 SEM

Morphologies of the products synthesized using different prolonged times, microwave powers, and starting agents are summarized in Table 1, and SEM images of the selected products are shown in Fig 4. For the synthesis process using $CuCl_2.2H_2O$ and CH_3CSNH_2 as the starting agents at 180 W microwave powers for 10, 20, 30 and 40 min prolonged times, at 300, 450 and 600 W for 10 min, and at 600 W for 20 min, the products (CA1, CA2, CA3, CA4, CA5, CA6, CA7 and CA) are the assemblies of nano-flakes (micro-sized flowers). Both the flowers and flakes became larger at higher power and longer time. The flowers are 4.5 μm in diameters at 600 W and 20 min. A microwave oven supplies energy to the system which was used to decompose the complexes and accelerate copper sulfide formation. Microwave powers and prolonged times did not have so strong influence on the product shapes as on the sizes.

At constant 600 W for 20 min with the same copper source ($CuCl_2.2H_2O$) but different sulfur sources (CH_3CSNH_2, $NH_2CSNHNH_2$ and NH_2CSNH_2), the products (CA, CC and CU) are the assemblies of nano-flakes (micro-sized flowers) although the three sulfur sources are different. They compose of nano-flakes as the fundamental particles. It shows that $CuCl_2.2H_2O$ dominated the sulfur sources. Product morphology was influenced by chloride ions in the system. Anions of the copper sources have the influence on growth of the particles. But for those synthesized using CuBr or $Cu(CH_3COO)_2.H_2O$ as copper sources with different sulfur sources, the products have a variety of morphologies. They are clusters of nano-sized particles, nano-rods, sponge-like structures, assemblies of nano-flakes and nano-fibers for BA and AU, BC, BU, AA and AC, respectively. Different product morphologies were influenced by sulfur sources which have different structure formulas. Nucleation and growth of the particles can play roles in the morphology. The crystal growth of some preferred structure or planes relates to the surface energy of the planes in the specified condition. The planes with lower surface energy dominate those with higher surface energy. It is described as the shape selective surface absorption process [20]. The amount of starting agents in the solution also has the influence on different orientation of the particles which reflects nucleation and growth of the crystals. The orientation was increased with the increasing in the amount of starting agents [21]. Phase with the lowest free energy is

thermodynamically stable, and has more chance to exist in the process [22]. This can reflect the product morphologies. Apart from the above, crystal growth is influenced by the solubility of the precursors in the particular solvent and synthesized temperature which reflects the morphologies [20]. Polarities and boiling points of solvents [23], pH values of the solutions and others can play a role in the shapes and sizes due to the different rates of nucleation and growth.

Different starting agents play a significant role to produce the products with different shapes and sizes which was influenced by nucleation and growth. They had more role than the microwave irradiation did.

During the formation of CuS, round particles were formed by the assemblage of hcp unit cells. Growths in the x-, y- and z- directions are almost at the same rates. Rod-shaped particles and fibers were formed by stacking up hcp unit cells. There were some unit cells stacked aside as well. To form rods and fibers, growth rate in the z-direction is the fastest. Flake-like particles were formed by the similar process as the rod/fiber formation but growth in the z-direction is the slowest.

The products may contain some imperfect round particles, curved rods/fibers and wavy flakes, due to the microwave vibration frequency, internal stress and others. Different morphologies have the influence on the luminescent property as well.

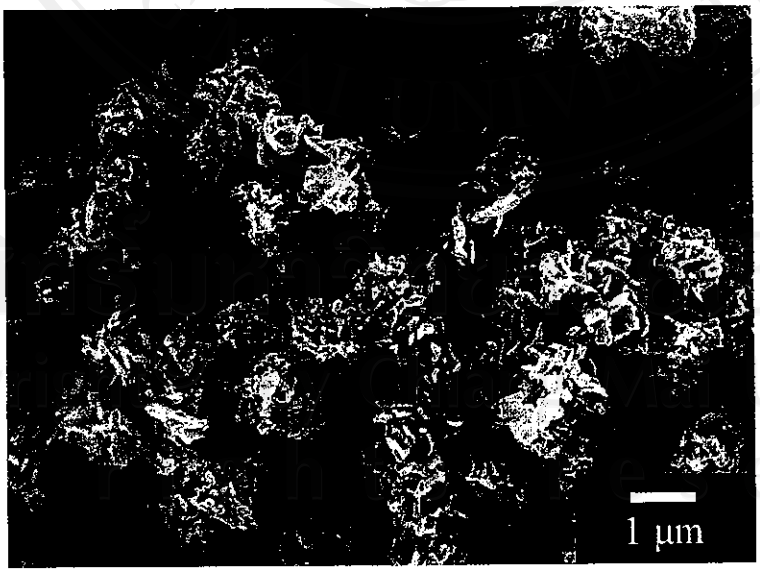

(a)

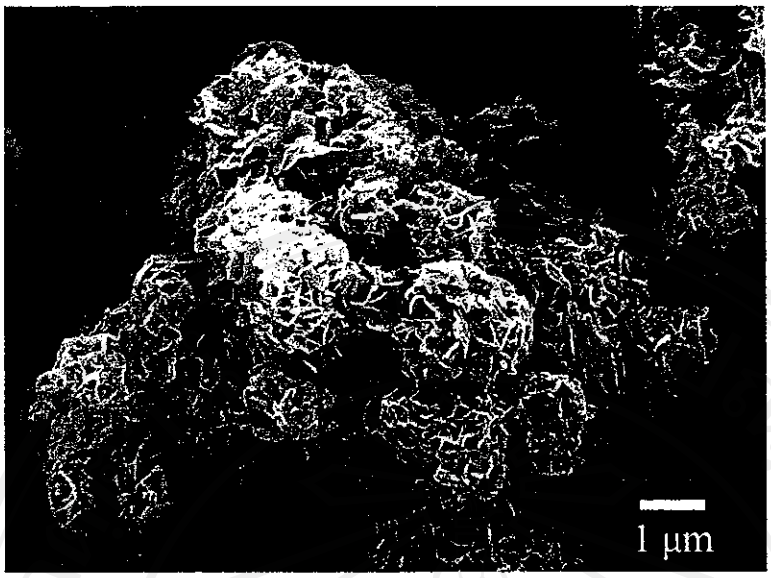

(b)

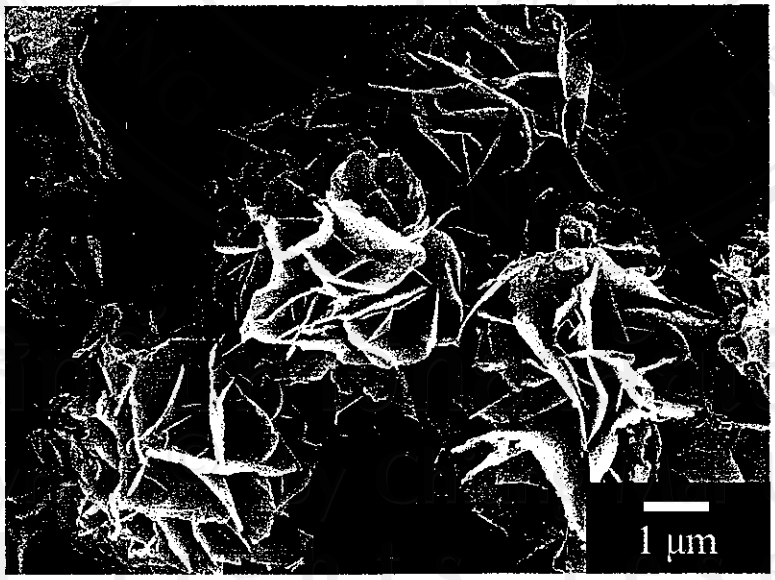

(c)

(d)

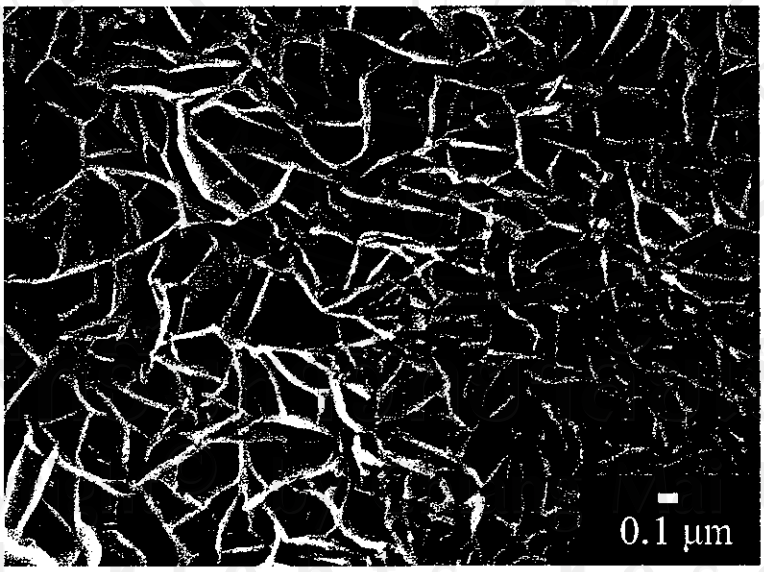

(e)

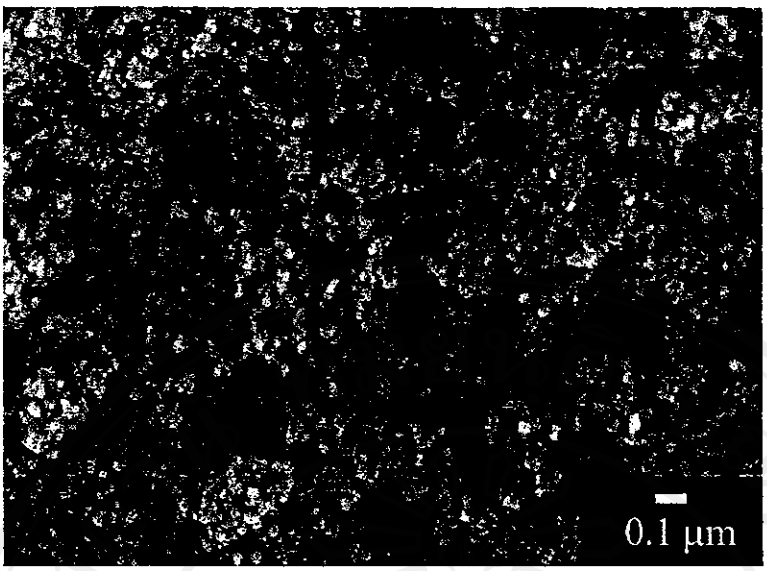

(f)

Fig 4. SEM images of the products. (a - f) are CA1, CA7, CA, BU, AA and AU, respectively.

3.4 TEM and SAED

To show more details, the synthesized products were put into a beaker containing ethanol. After ultrasonic vibration, the liquid was dropped on a copper grid and dried in ambient atmosphere. TEM images and SAED patterns (Fig 5) of the selected products were characterized and analyzed. They compose of round nano-particles with < 20 nm in diameter for BA and AU, nano-rods with < 20 nm in diameter for BC, and nano-fibers with as long as 105 nm for AC.

SAED patterns show eight concentric rings corresponding to diffraction planes of the crystalline products. Diameters of the rings were measured from the diffraction patterns on the films. The values of d-spacing of the diffraction planes were calculated [24,25] and compared with those of the JCPDS software [14]. The diffraction patterns show that the products compose of CuS with hexagonal structure. The analyses interpreted from SAED and XRD patterns are in good accord. The diffraction planes of the products are (100), (103), (006), (105), (110), (108), (203) and (116). The rings are diffuse and hollow showing that the products composed of very fine particles.

3.5 Raman analysis

Raman spectra of different products (Fig 6) are very sharp showing that lattice atoms are arranged in the periodic array. Vibration modes of the crystalline products synthesized from different starting agents are in the same wavenumber at 474 cm^{-1} corresponding to the lattice vibrations. The present results are in accord with those of CuS thin films [26,27]. Generally, vibration frequency is a parameter controlled by atomic masses, force constant of lattice atoms, atomic bonding and others.

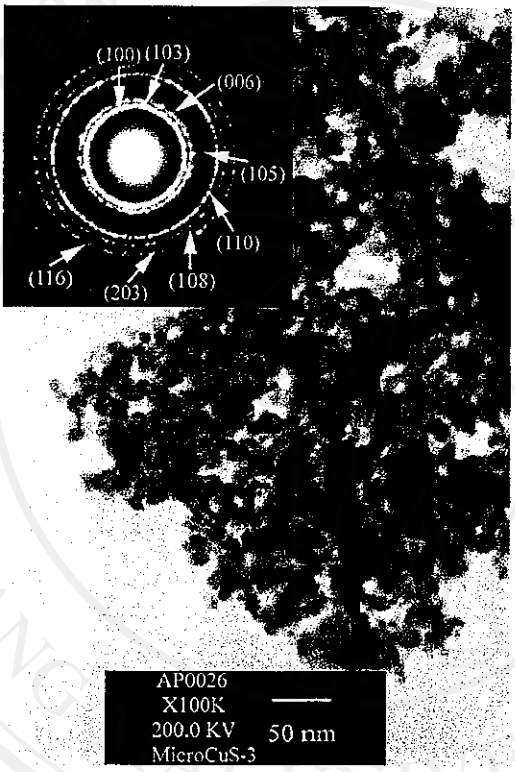

(a)

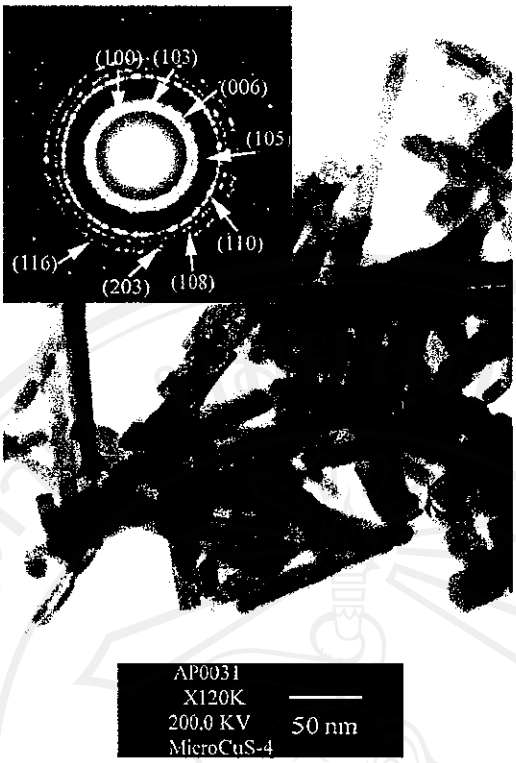

(b)

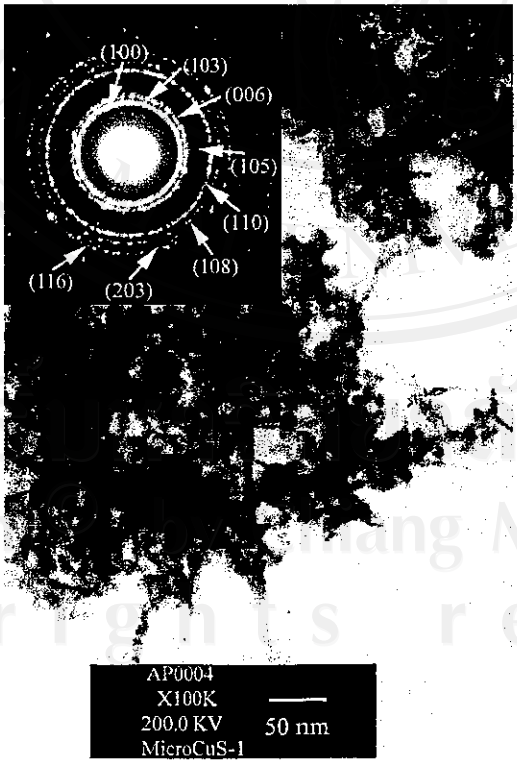

(c)

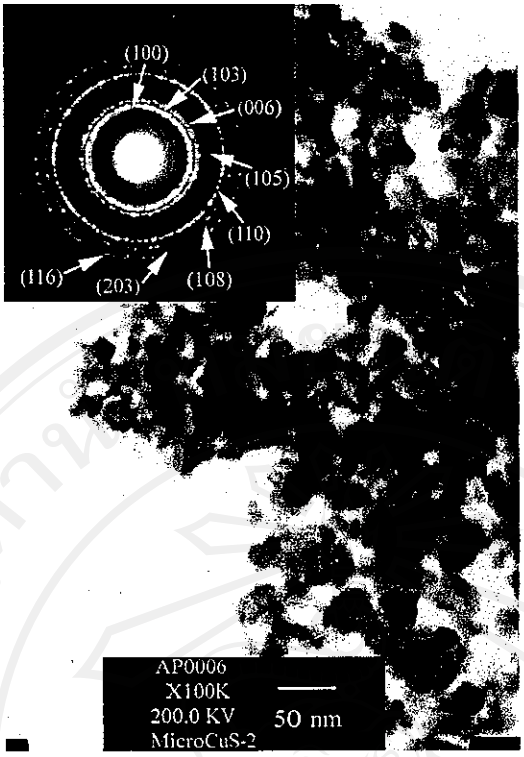

(d)

Fig 5. TEM images and SAED patterns of the products synthesized at 600 W microwave power for 20 min prolonged time. (a) – (d) are BA, BC, AC and AU, respectively.

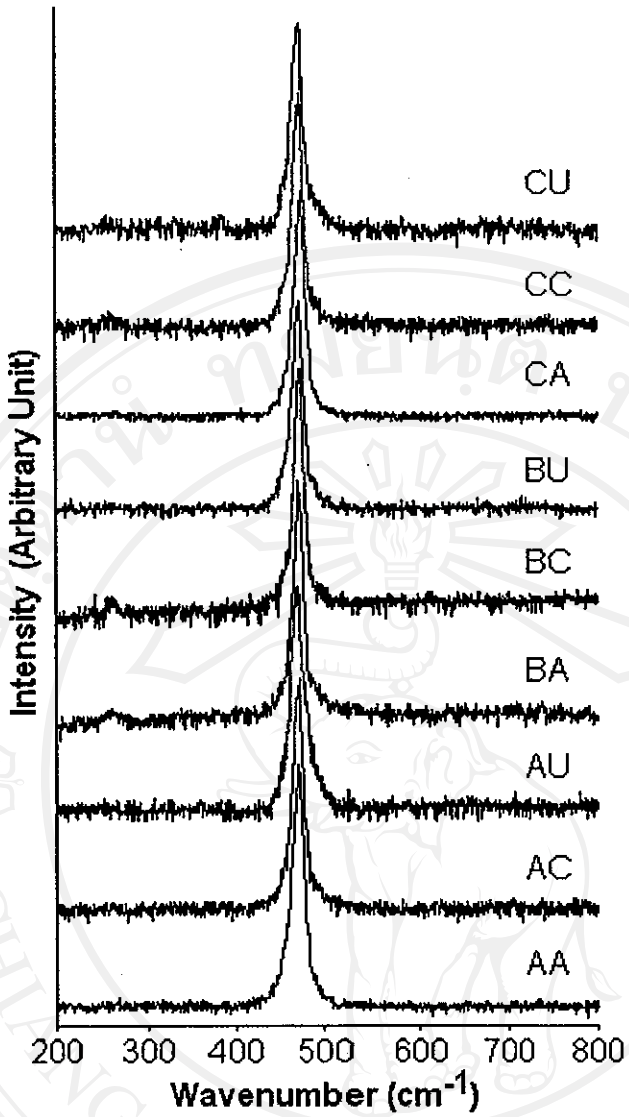

Fig 6. Raman spectra of the products synthesized using different starting agents at 600 W microwave power for 20 min prolonged time.

3.6 PL spectra

PL emission of CuS dispersed in absolute ethanol (Fig 7) was determined using a 202 nm (6.14 ev) exciting wavelength. PL spectra of all the products show the broad emission peaks in the range 414 – 435 nm (2.85 – 2.99 ev). For each of the copper sources, the spectra show the highest intensities at 414 nm (2.99 ev), 414 nm (2.99 ev) and 434 nm (2.86 ev) for the CC, BC and AC products, respectively. The results are in accord with the emission peaks of CuS at 414 nm (2.995 ev) and 437.5 nm (2.834 ev) [28].

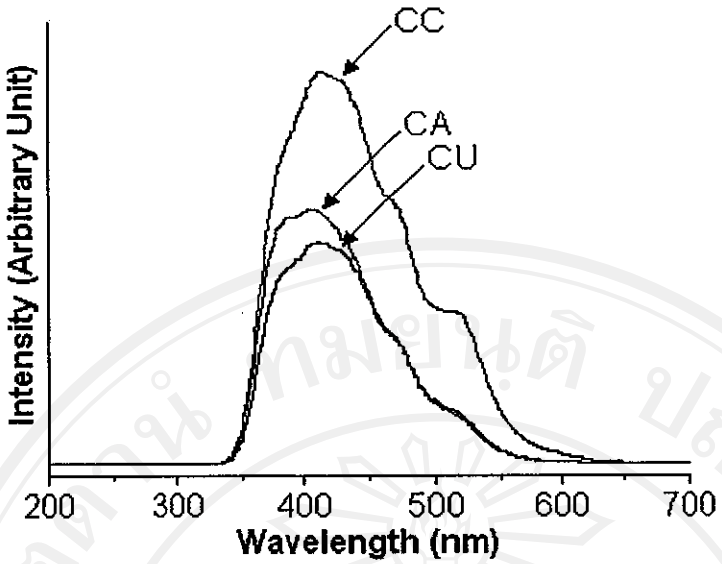

(a)

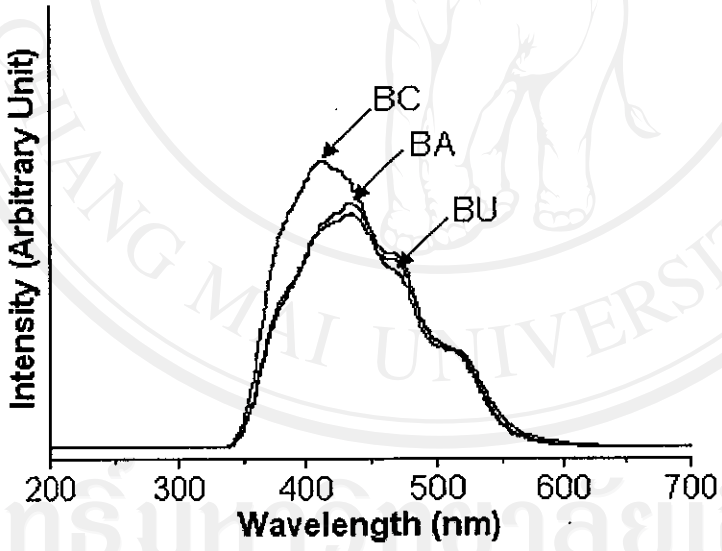

(b)

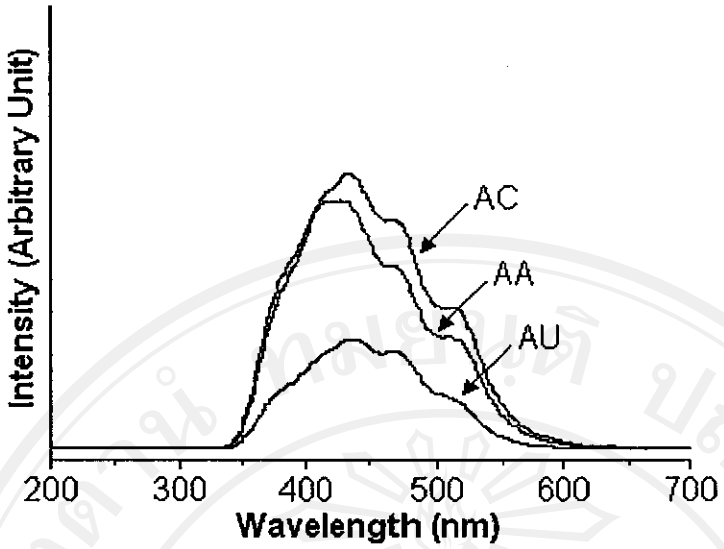

(c)

Fig 7. PL spectra of different products synthesized at 600 W microwave power for 20 min prolonged time. (a) CA, CC and CU, (b) BA, BC and BU and (c) AA, AC and AU.

4. Conclusions

Nano- and micro-sized CuS crystals with different morphologies were successfully synthesized by the reactions of different copper and sulfur sources assisted by the cyclic microwave irradiation. The detections of CuS (hcp) phase using XRD and SAED, and of 474 cm^{-1} vibration wavenumber using the Raman spectrometer are in good accord. PL emission peaks of the products are at 414 – 435 nm (2.85 – 2.99 ev). Phase and morphology formations are proposed on according to the results characterized using XRD, FTIR, SAED, SEM and TEM.

References

1. Y. He, X. Yu, X. Zhao, Mater. Lett. 61 (2007) 3014.

2. K. Tezuka, W. C. Sheets, R. Kurihara, Y.J. Shan, H. Imoto, T.J. Marks, K.R. Poeppelmeier, Solid State Sci. 9 (2007) 95.

3. X. Chen, Z. Wang, X. Wang, R. Zhang, X. Liu, W. Lin, Y. Qian, J. Cryst. Growth 263 (2004) 570.

4. D. Chen, K. Tang, G. Shen, J. Sheng, Z. Fang, X. Liu, H. Zheng, Y. Qian, Mater. Chem. Phys. 82 (2003) 206.

5. Y. Ni, H. Liu, F. Wang, G. Yin, J. Hong, X. Ma, Z. Xu, Appl. Phys. A 79 (2004) 2007.

6. X.H. Liao, N.Y. Chen, S. Xu, S.B. Yang, J.J. Zhu, J. Cryst. Growth 252 (2003) 593.

7. X. Wang, C. Xu, Z. Zhang, Mater. Lett. 60 (2006) 345.

8. Y.J. Yang, J.W. Xiang, Appl. Phys. A 81 (2005) 1351.

9. H.T. Zhang, G. Wu, X.H. Chen, Mater. Chem. Phys. 98 (2006) 298.

10. H. Xu, W. Wang, W. Zhu, Mater. Lett. 60 (2006) 2203.

11. C. Jiang, W. Zhang, G. Zou, L. Xu, W. Yu, Y. Qian, Mater. Lett. 59 (2005) 1008.

12. J.Z. Xu, S. Xu, J. Geng, G.X. Li, J.J. Zhu, Ultrason. Sonochem. 13 (2006) 451.

13. J. Podder, R. Kobayashi, M. Ichimura, Thin Solid Films 472 (2005) 71.

14. Powder Diffract. File, JCPDS Internat. Centre Diffract. Data, PA 19073-3273, U.S.A., (2001).

15. N.M. Huang, C.S. Kan, P.S. Khiew, S. Radiman, J. Mater. Sci. 39 (2004) 2411.

16. Y. Li, F. Huang, Q. Zhang, Z. Gu, J. Mater. Sci. 35 (2000) 5933.

17. D.F. Shriver, P.W. Atkins, T.L. Overton, J.P. Rourke, M.T. Weller, F.A. Armstrong, Inorg. Chem, 4th ed., (Oxford Univ. Press, 2006) p. 151.

18. K. Swaminathan, H.M.N.H. Irving, J. Inorg. Nucl. Chem. 26 (1964) 1291.

19. J. Yang, J.H. Zeng, S.H. Yu, L. Yang, Y.H. Zhang, Y.T. Qian, Chem. Mater. 12 (2000) 2924.

20. S. Biswas, S. Kar, S. Chaudhuri, J. Cryst. Growth 299 (2007) 94.

21. Y.C. Zhang, X.Y. Hu, T. Qiao, Solid State Comm. 132 (2004) 779.

22. K. Sopunna, T. Thongtem, M. McNallan, S. Thongtem, J. Mater. Sci. 41 (2006) 4654.

23. J. Lu, Q. Han, X. Yang, L. Lu, X. Wang, Mater. Lett. 61 (2007) 2883.

24. T. Thongtem, S. Kaowphong, S. Thongtem, J. Mater. Sci. 42 (2007) 3923.

25. A. Phuruangrat, T. Thongtem, S. Thongtem, Mater. Lett. 61 (2007) 3805.

26. S.Y. Wang, W. Wang, Z.H. Lu, Mater. Sci. Engin. B 103 (2003) 184.

27. B. Minceva-Sukarova, M. Najdoski, I. Grozdanov, C.J. Chunnilall, J. Molec. Struct. 410-411 (1997) 267.

28. S. Ou, Q. Xie, D. Ma, J. Liang, X. Hu, W. Yu, Y. Qian, Mater. Chem. Phys. 94 (2005) 460.

Free Surfactant Synthesis of Microcrystalline CdS by Solvothermal Reaction

Abstract

Microcrystalline CdS was solvothermally synthesized by free surfactant reaction at 200 °C in a variety of solvents [benzene (BZ), toluene (TL), p-xylene (XL), cyclohexane (CHX) and tetrahydrofuran (THF)]. An X-ray diffractometer (XRD), a selected area electron diffraction (SAED) technique and an energy dispersive X-ray (EDX) analyzer show that the products are CdS (hexagonal structure) composing of Cd and S. The SAED patterns are also in accordance with a simulation model. Strong fundamental and weak overtone modes were detected using a Raman spectrometer at 297.0 and 597.1 cm^{-1}, respectively. By using a transmission electron microscope (TEM), those synthesized in BZ, TL and XL are the mixtures of hexagonal and triangular plates. They are hexagonal and rod shapes in CHX and THF, respectively. Photoluminescent (PL) energies at the maximum intensities were detected over the range of 3.10-3.16 ev (392-400 nm).

Keywords : Free surfactant synthesis, Solvothermal reaction, Microcrystalline CdS

1. Introduction

CdS is one of the IIB-VIA compounds that have novel optical, electronic and thermoelectric properties [1]. Its band gap is 2.42 eV [2]. It has a wide variety of applications such as laser light emitting diodes, solar cells, and non-linear optical and electronic devices [3,4]. There are different methods used to synthesize nano- and micro-crystalline CdS such as microwave-solvothermal synthesis [4], metal-oleylamine complex [5], hydrothermal route [6] and surfactant-ligand co-assisting solvothermal method [7]. Most of the products have different morphologies such as dendrites [2], flakes [8], spheres [9], nanorods [7,10], nanowires [11,12], triangular and hexagonal plates [13], flower-like shape [1,14] and sea-urchinlike shape [3]. Solvothermal process is simple and inexpensive; therefore, it is very attractive for use as the chemical synthesis of a substance. Among the required morphologies, different solvents in combination with organic additives were used. Presently, there are a few reports on the free surfactant synthesis of CdS by solvothermal reaction. The purpose of the research is to solvothermally synthesize microcrystalline CdS with

different shapes and sizes by free surfactant reaction at low temperature in a variety of solvents.

2. Experiment

Each 0.005 mol of $CdCl_2.2.5H_2O$ and $(NH_2)_2CS$ was dissolved in a variety of solvents [benzene (BZ), toluene (TL), p-xylene (XL), cyclohexane (CHX) and tetrahydrofuran (THF)]. They were mixed to occupy 65 vol % of a 45 ml home-made stainless steel autoclaves. The free surfactant reaction proceeded at 200 °C for 10 h to form precipitates. By washing with water and ethanol, the precipitates were dried at 80 °C for 24 h. The final products were analyzed using an X-ray diffractometer (XRD) operated at 20 kV, 15 mA and using Cu K_α radiation in the 2θ angular range of 10-60 deg, a transmission electron microscope (TEM) as well as a selected area electron diffraction (SAED) technique operated at 200 kV, an energy dispersive X-ray (EDX) analyzer operated at 15 kV, a Raman spectrometer using 50 mW Ar Laser with λ = 514.5 nm and a luminescence spectrometer using 225 nm exciting wavelength.

3. Results and Discussion

3.1 XRD

XRD spectra (Fig 1) are very sharp showing that the products are composed of crystals. Comparing the spectra to those of the JCPDS standard (PDF # 06-0314) [15], the products were identified as CdS with hexagonal structure. Generally, the hexagonal structure is more stable than the cubic one [16]. For the present research, no impurity peaks were detected showing that the products are pure phase. Calculated lattice parameters [17] are shown in Table 1. In general, lattice parameters of crystals with the same structure are constant. For CdS synthesized using the solvents, a and c are 0.4135 ± 0.0000 nm and 0.6717 ± 0.0001 nm, respectively. They have zero and very little standard deviations, and are in accord with those of the JCPDS standard (a = 0.4136 nm, c = 0.6713 nm) [15].

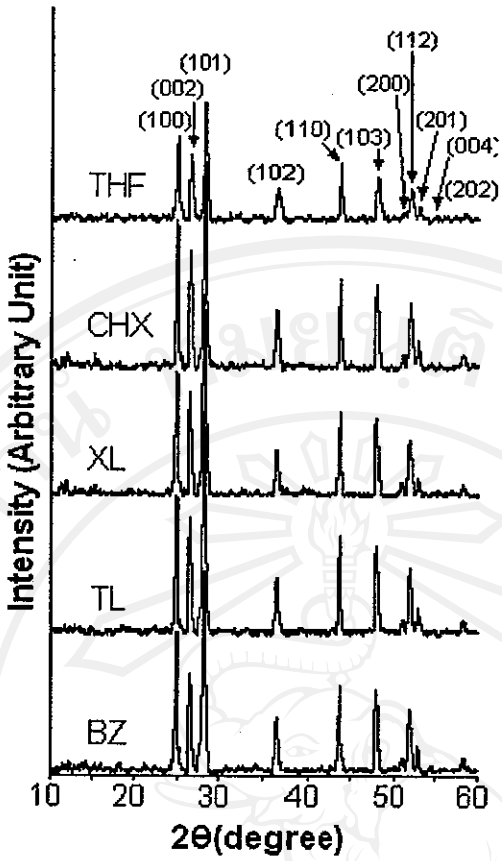

Fig 1. XRD spectra of the products synthesized using a variety of solvents.

Table 1. Calculated lattice parameters.

Solvent	a (nm)	c (nm)
Benzene	0.4135	0.6716
Toluene	0.4135	0.6716
p-Xylene	0.4135	0.6718
Cyclohexane	0.4135	0.6716
Tetrahydrofuran	0.4135	0.6718
	0.4135 ± 0.0000	0.6717 ± 0.0001

3.2 SAED

SAED patterns and a simulation model are shown in Fig 2. The diffraction patterns were interpreted [18] and identified as CdS with hexagonal structure [15]. It shows that XRD and SAED analyses are in accord. Zone axis is in the [001] direction which is parallel or nearly parallel to the electron beam [18]. The SAED patterns are not exactly symmetric due to the deviation of electron beam from the zone axis. A diffraction pattern for CdS (hexagonal structure) using [001] as zone axis was simulated [19]. The pattern is symmetric and systematic. The results shown on the SAED patterns of the powders are in accord with that shown on the simulated pattern.

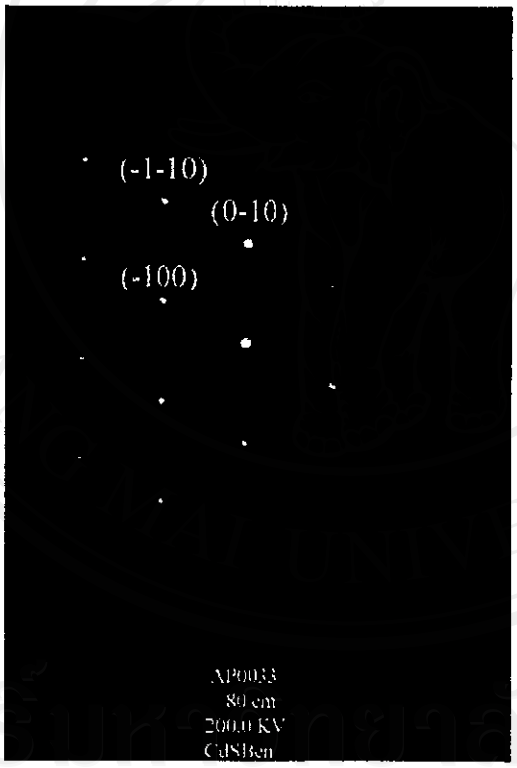

(a)

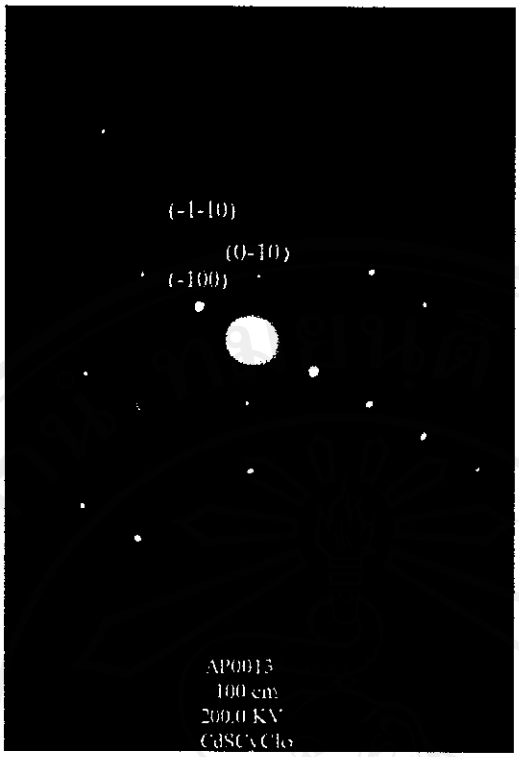

(b)

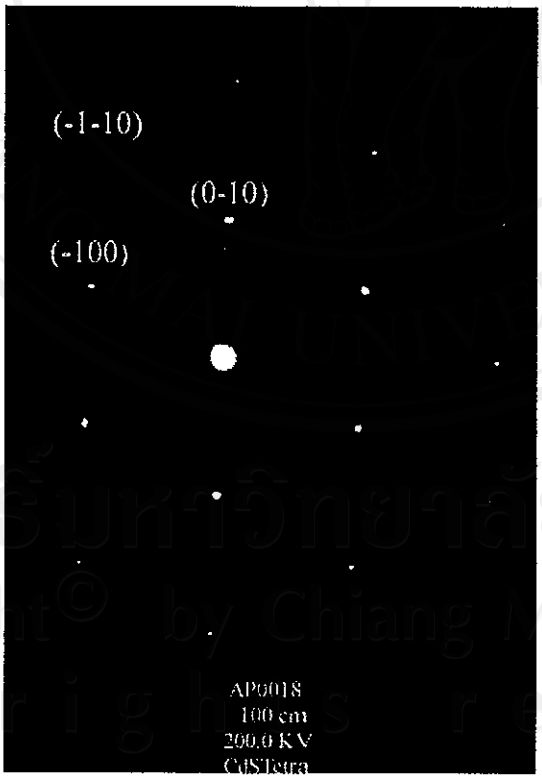

(c)

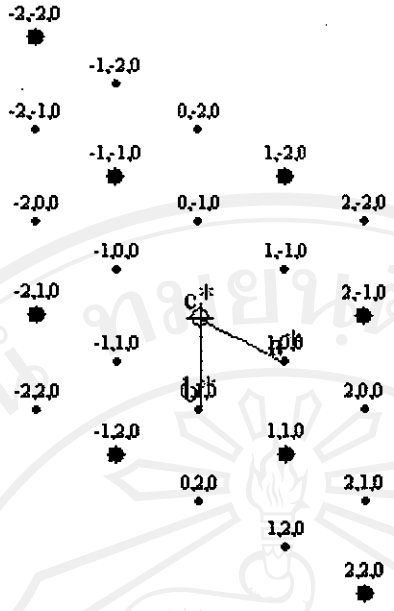

(d)

Fig 2. SAED patterns of the products synthesized using (a) BZ, (b) CHX and (c) THF. (d) A simulation model of CdS.

3.3 Raman Spectra

Raman spectra of the products are shown in Fig 3. A strong fundamental and a weak overtone modes were detected at 297.0 and 597.1 cm^{-1}, respectively. The fundamental and overtone modes correspond to the 1LO (longitudinal optical) and 2LO peaks [16]. They are the results of phonon vibration [6,16]. For the present research, the spectra are very similar to that of CdS [6]. Comparing to Ar Laser (λ = 514.5 nm), a great deal of energy was lost during the inelastic scattering process. By using a Fourier transform infrared spectrometer (FTIR) (results not shown), no solvents were left in the products.

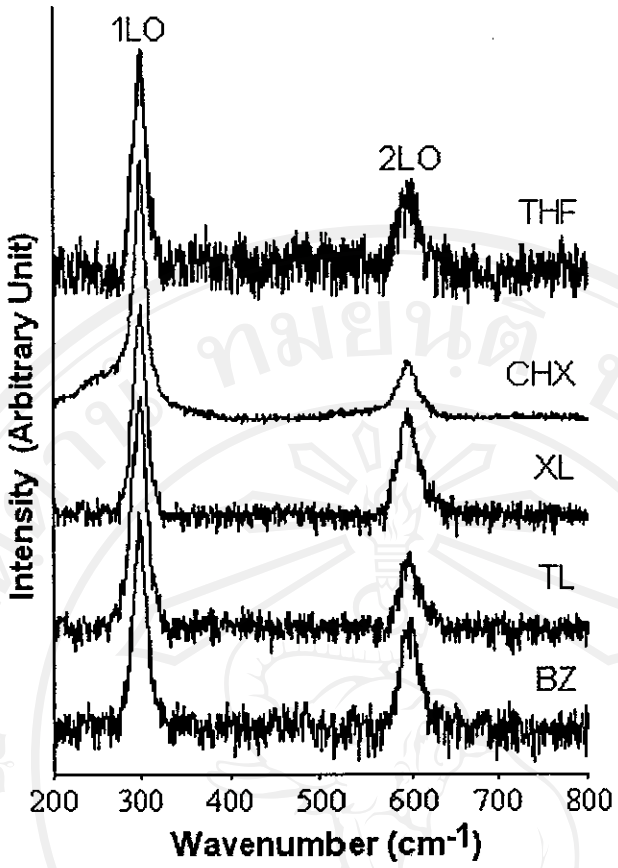

Fig 3. Raman spectra of the products synthesized using a variety of solvents.

3.4 EDX

EDX spectra (Fig 4) were interpreted [20]. They revealed the presence of three Cd peaks at 3.13, 3.32 and 3.53 keV which were identified as the L_{α}, $L_{\beta 1}$ and $L_{\beta 2}$ lines, respectively. S peak was detected at 2.31 keV identified as the $K_{\alpha 1,2}$ line. C of carbon tape was also detected at 0.28 keV ($K_{\alpha 1,2}$ line). EDX analysis shows that atomic ratio of Cd : S is 1 : 1. The detection of Cd and S using the EDX, and CdS using the XRD and SAED are in accord.

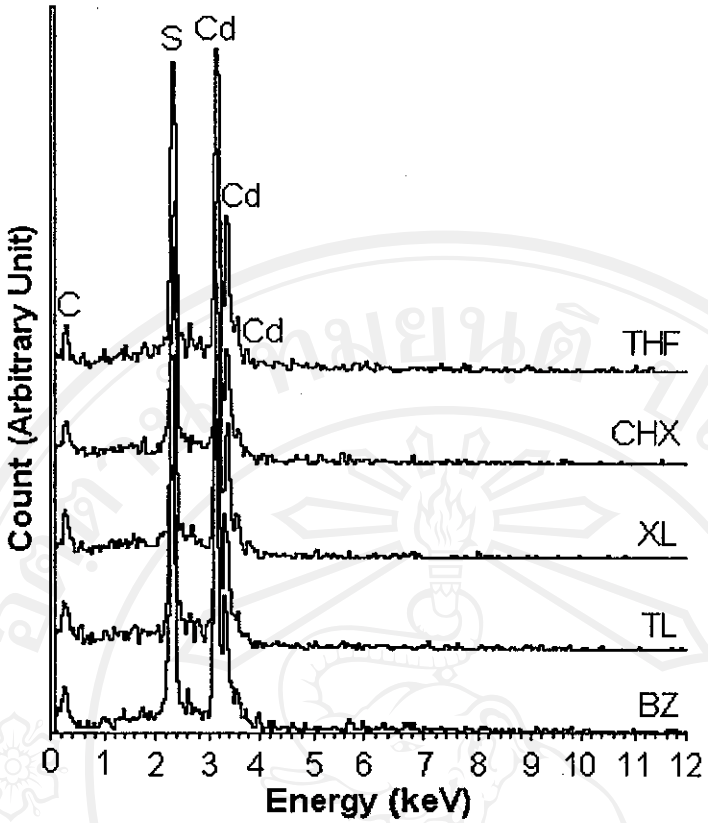

Fig 4. EDX spectra of the products synthesized using a variety of solvents.

3.5 TEM

TEM images (Fig 5) show different morphologies controlled by a variety of solvents. The products are micro-sized particles. Some physical and chemical properties of the solvents seem to play the role in the shapes and sizes of the product particles [9], and the luminescent property [21]. For the present research, no surfactants were used. Relative polarities of BZ, TL, XL, CHX and THF are 0.111, 0.099, 0.074, 0.006 and 0.207, respectively [22]. The solvents are classified into three groups due to their polarities. CHX has the lowest value and THF at the highest. BZ, TL and XL have almost the same medium values. The particles shaped like the hexagon with 122-257 nm straight sides, and the rod with 81 nm in diameter when they were synthesized in CHX and THF, respectively. Those synthesized using one of the BZ, TL and XL solvents compose of both hexagons with 100-160 nm straight sides and triangles with 145-300 nm straight sides. The particles are hexagonal, a mixture of hexagonal and triangular, and rod shapes in the solvents with low, medium and high polarities, respectively. Structure formulae of the solvents,

starting agents, temperature, time and others have the effect on their morphologies as well. Theoretically, it is possible to solvothermally synthesize nanocrystalline CdS using the present solvent at very high pressure. Under this condition, the crystallite size is then limited.

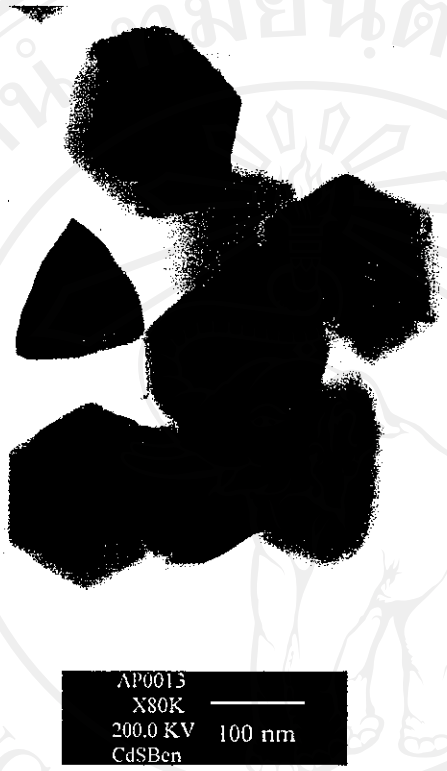

(a)

(b)

(c)

(d)

(e)

Fig 5. TEM images of the products synthesized using (a) BZ, (b) TL, (c) XL, (d) CHX and (e) THF.

3.6 Photoluminescence

Photoluminescence (PL) of the products were analyzed using 225 nm exciting wavelength and are shown in Fig 6. PL energies at the maximum intensities were detected over the range of 3.10 – 3.16 eV (392 - 400 nm). The intensity values and PL wavelengths are different and are controlled by their morphologies [23]. PL intensity of the rod-shaped crystal synthesized in THF is at the highest. Comparing to the estimated band gap of bulk CdS (2.42 eV, 512 nm) [2], the PL energies are blue shifted. However, band gap can be modified by high temperature treatment [24].

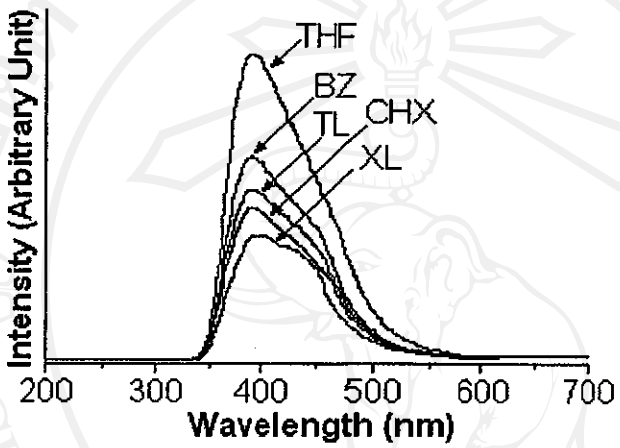

Fig 6. PL spectra of the products synthesized using different solvents.

4. Conclusions

Microcrystalline CdS (hexagonal structure) with different morphologies was successfully synthesized by free surfactant reaction of $CdCl_2.2.5H_2O$ and $(NH_2)_2CS$ in a home-made stainless steel autoclave at 200 °C. Solvent polarities seem to play the role in the shapes and sizes of the product particles. The calculated lattice parameters are very close to those of the JCPDS standard. The 1LO and 2LO peaks of CdS are at 297.0 and 597.1 cm^{-1}, respectively. PL energies of different products are blue shifted in comparison with band gap of CdS (bulk).

References

1. S.M. Zhou, Mater. Lett. 61 (2007) 119.

2. A.M. Qin, Y.P. Fang, W.X. Zhao, H.Q. Liu, C.Y. Su, J. Cryst. Growth, 283 (2005) 230.

3. X. Liu, Mater. Chem. Phys., 91 (2005) 212.

4. A.V. Murugan, R.S. Sonawane, B.B. Kale, S.K. Apte, A.V. Kulkarni, Mater. Chem. Phys., 71 (2001) 98.

5. J. Joo, H.B. Na, T. Yu, J.H. Yu, Y.W. Kim, F. Wu, J.Z. Zhang, T. Hyeon, J. Am. Chem. Soc., 125 (2003) 11100.

6. C. Li, X. Yang, B. Yang, Y. Yan, Y. Qian, J. Cryst. Growth, 291 (2006) 45.

7. C. Bao, M. Jin, R. Lu, P. Xue, Q. Zhang, D. Wang, Y. Zhao, J. Solid State Chem., 175 (2003) 322.

8. N. Gao, F. Guo, Mater. Lett., 60 (2006) 3697.

9. F.H. Zhao, Q. Su, N.S. Xu, C.R. Ding, M.M. Wu, J. Mater. Sci., 41 (2006) 1449.

10. W. Qingqing, Z. Gaoling, H. Gaorong, Mater. Lett. 59 (2005) 2625.

11. C. Cheng, G. Xu, H. Zhang, H. Wang, J. Cao, H. Ji, Mater. Chem. Phys., 97 (2006) 448.

12. X. Guo-yue, W. Han, C. Chuan-wei, Z. Hai-qian, C. Jie-ming, J. Guang-bin, Trans. Nonferrous Met. Soc. China, 16 (2006) 105.

13. M. Chen, L. Pan, J. Cao, H. Ji, G. Ji, X. Ma, Y. Zheng, Mater. Lett., 60 (2006) 3842.

14. L. Wang, L. Chen, T. Luo, Y. Qian, Mater. Lett., 60 (2006) 3627.

15. Powder Diffract. File, JCPDS Internat. Centre Diffract. Data, PA 19073-3273,U.S.A., (2001).

16. J. Lee, Thin Solid Films, 451-452 (2004) 170.

17. B.D. Cullity, (Elem. X-ray Diffract., 2nd Ed., Addison-Wesley Publ. Co., MA, 1978).

18. K.W. Andrews, D.J. Dyson, S.R. Keown, (Interpret. Electr. Diffract. Patter., 2nd ed, Plenum Press, NY, 1971).

19. C. Boudias, D. Monceau, CaRIne Crystallography 3.1, 17 rue du Moulin du Roy, F-60300 Senlis, France, (1989-1998).

20. X-ray Absorp. Emiss. Energ., Oxford Instrum. Analyt., Halifax Rd., High Wycombe Bucks HP12 3SE, U.K.

21. K. S. Babu, C. Vijayan, P. Haridoss, Mater. Lett., 60 (2006) 124.

22. http://virtual.yosemite.cc.ca.us/smurov/orgsoltab.htm (Aug. 2006).

23. G. Zhou, M. Lü, Z. Xiu, S. Wang, H. Zhang, Y. Zhou, S. Wang, J. Phys. Chem. B, 110 (2006) 6543.

24. O. de Melo, L. Hernández, O. Zelaya-Angel, R. Lozada-Morales, M. Becerril, E. Vasco, Appl. Phys. Lett. 65 (1994) 1278.

Phase Transformation of Nanocrystalline CdS Synthesized by Solvothermal Reaction

Abstract

CdS was synthesized by solvothermal reaction of $CdCl_2.2.5H_2O$ and $(NH_2)_2CS$ in ammonia solution at 200 °C for 10 h. XRD, TEM and SAED show that the products are nanocrystalline CdS. The phase is 100 % hexagonal (hcp) in pure water, gradually transformed into cubic with the increase of NH_3 concentration, and 100 % cubic in 25 % NH_3 solution. By using FTIR, no solvents were detected in the products. Raman analysis revealed the presence of 1LO (longitudinal optical) and 2LO phonon peaks at 297.0 and 597.1 cm^{-1} for CdS (hcp), and 295.9 and 596.9 cm^{-1} for CdS (cubic), respectively. Strong peaks of the photoluminescent (PL) spectra were detected at 450 nm for hcp, and 519 nm for cubic.

Keywords : Phase Transformation, Nanocrystalline CdS, Solvothermal reaction

Introduction

Among group II-VI compounds, CdS has received significant attention due to its outstanding potential applications [1] such as solar cells [2], light emitting diodes [1] and photocatalysts [1]. Recently, nanocrystallines have been increasingly important due to their novel properties controlled by the shapes and sizes [3]. Therefore, nanocrystalline has been the subject to investigate. There are a variety of methods used to synthesize the compound such as polyol route [1], hot-wall epitaxy [4] and hydrothermal [5]. For the present research, nanocrystalline CdS was synthesized using a home-made stainless steel autoclave. Phase transformation, luminescent property and morphology were then studied and explained.

Experiment

Each 0.005 mol of $CdCl_2.2.5H_2O$ and $(NH_2)_2CS$ dissolving in 0 – 25 % NH_3 solution were mixed to occupy 65 vol % of a home-made stainless steel autoclave. The reaction proceeded at 200 °C for 10 h to form precipitate. By washing with water and ethanol, the precipitate was dried at 80 °C for 24 h. The final products were analyzed to determine their characters and properties.

Results and discussion

Comparing XRD spectra (Fig 1) to those of the JCPDS standard (Reference codes : 06-0314 for CdS (hcp) and 89-0440 for CdS (cubic)) [6], the products synthesized using pure water (0 % NH_3) and 25 % NH_3 were specified as CdS (hcp) and CdS (cubic), respectively. The diffraction peaks of hcp correspond to (100), (002), (101), (102), (110), (103), (200), (112), (201), (004) and (202) planes of the product. The (101) peak is the highest. For cubic, they correspond to (111), (200), (220) and (311) planes and the first peak is the highest. All peaks of hcp were decreased with the increase of the NH_3 concentration. Those of cubic showed the opposite effect. The products are the mixture (solid solution) of hcp and cubic phases in 5, 10, 15 and 20 % NH_3 solutions. Two different calculated phases [7] using (101) hcp and (200) cubic peaks are shown (Fig 2), hcp on the left extremity and cubic on the right. Mixture of the phases is between the two ends. These show that NH_3 concentration plays the role in the phase formation. Calculated lattice parameters (a = 0.4136 and c = 0.6718 nm for hcp, and a = 0.5831 nm for cubic) [7] are very close to those of the JCPDS standard (a = 0.4136 and c = 0.6713 nm for hcp, and a = 0.5830 nm for cubic) [6].

TEM images and SAED patterns are shown (Fig 3). The products compose of rather round particles of which the sizes were measured (Fig 4). They are 62.1 ± 20.1 nm for the product synthesizing in pure water, and 37.2 ± 13.7 nm in 25 % NH_3 solution. The first composes of larger particles and size distributions than the second does. The solvent is likely to play the role in the particle sizes and size distributions. SAED patterns compose of a number of bright spots of concentric rings. The diffraction rings of the product in 25 % NH_3 are not sharp resulting from the effect of fine particles. The diameter of each ring was measured and the interplanar space (d) was calculated [8]. Comparing to the JCPDS standard [6], the products synthesized in pure water and 25 % NH_3 correspond to CdS (hcp) and CdS (cubic), respectively. SAED and XRD planes of both products are in accord.

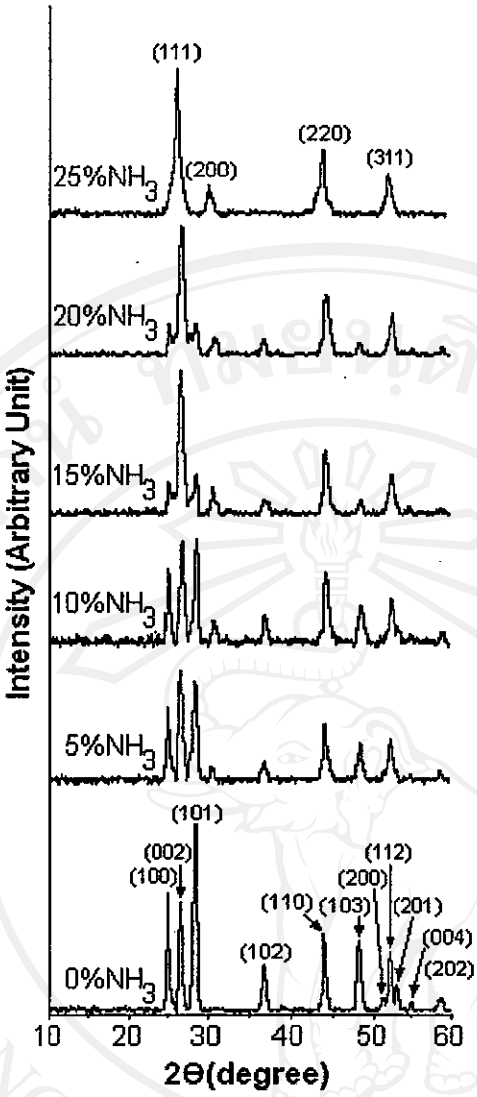

Fig 1. XRD spectra of CdS synthesized using different percentages of NH_3 solution.

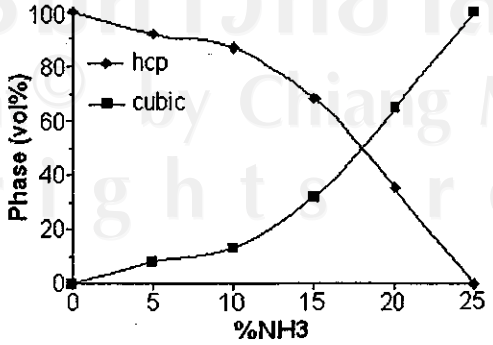

Fig 2. CdS phases synthesized using different percentages of NH_3 solution.

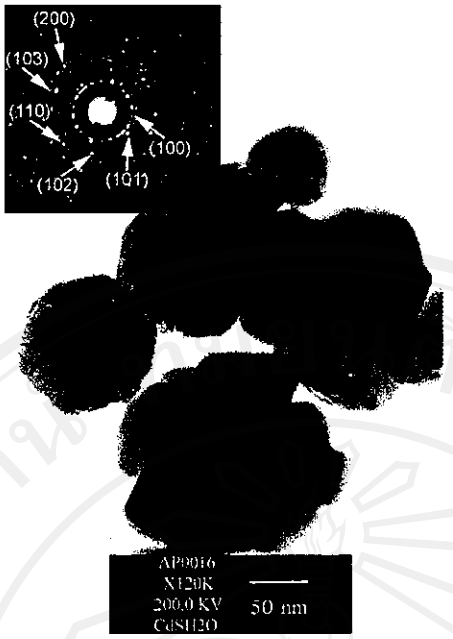

(a)

(b)

Fig 3. TEM images and SAED patterns of CdS synthesized using (a) pure water and (b) 25 % NH_3 solution.

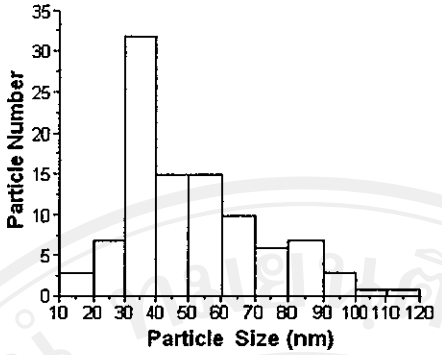

(a)

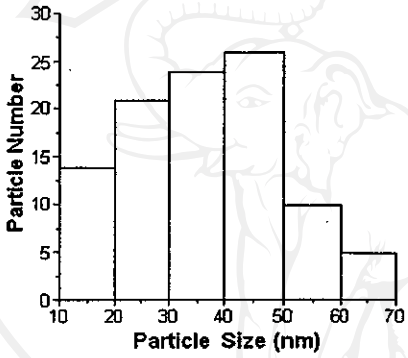

(b)

Fig 4. Particle size distributions of CdS synthesized using (a) pure water and (b) 25 % NH_3 solution.

Raman spectra of hcp and cubic phases (Fig 5) are almost identical to each other. Two peaks were detected on both spectra. The products are nanocrystalline CdS; therefore, their spectra are rather broad [9]. The strong 1LO (longitudinal optical) and weak 2LO phonon peaks corresponding to the fundamental and overtone modes [5] are at 297.0 and 597.1 cm^{-1} for CdS (hcp), and 295.9 and 596.9 cm^{-1} for CdS (cubic), respectively. The Raman shift values of CdS (hcp) and CdS (cubic) are in accord with those of the undoped CdS (hcp) [2] and CdS (mixture of hcp and cubic phases) [10] films. The explanation clearly shows that Raman shift values for both phases are very close to each other. The values of full width at half maximum (FWHM) of 1LO and 2LO peaks are 18.2 and 27.6 cm^{-1} for CdS (hcp), and

15.8 and 26.1 cm^{-1} for CdS (cubic), respectively. CdS (hcp) is the stable phase. FWHM of the dominant 1LO agrees very well with that of the undoped CdS film [2] reflecting the quality of the synthesized product. By using FTIR (results not shown), no solvents were left in the products.

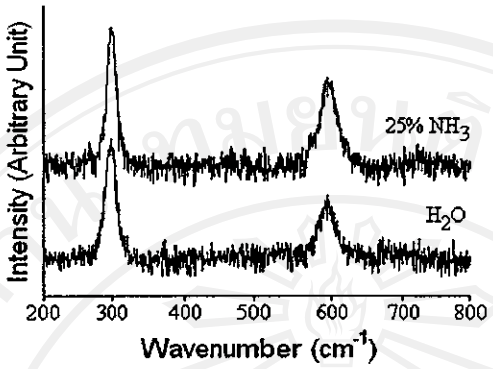

Fig 5. Raman spectra of CdS synthesized using pure water and 25 % NH_3 solution.

Photoluminescent (PL) spectra of hcp and cubic phases were analyzed using exciting wavelength (λ_{ex}) of 231 and 282 nm, respectively (Fig 6). The strong peaks were detected at 450 nm (2.755 ev) for hcp, and 519 nm (2.389 ev) for cubic. The radiation of longer wavelength than λ_{ex} was emitted due to some energy loss and others. The PL property was controlled by the crystal sizes and shapes [3]. Comparing to band gaps of 2.42 ev (512 nm) for bulk CdS (hcp) [11] and 2.366 ev (524 nm) for CdS (cubic) film [4], the strong peaks of the synthesized products are blue shift. It is the result of the quantum size effect [11] which is increasing in the extent as the particle size decreases and the surface-to-volume ratio increases. Band gap can be modified by heating the products at high temperatures [12], and the synthesized processes as well. An electron in valence band was excited into conduction band, and hole was left in the valence band. Generally, the solid has some defects introducing energy levels in the forbidden region. The excited state is not stable. The electron in conduction band recombined with the hole in valence band via the energy levels of the defects [13]. Therefore, band gaps for the synthesized products are no less than 2.755 ev for CdS (hcp) and 2.389 ev for CdS (cubic).

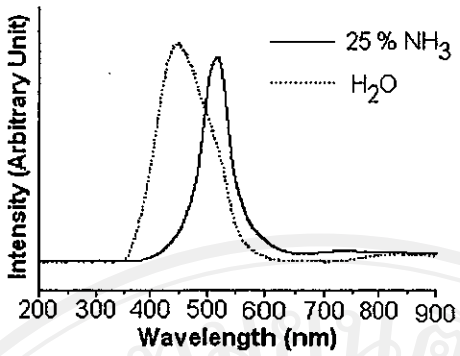

Fig 6. PL spectra of CdS synthesized using pure water and 25 % NH_3 solution.

Summary

Nanocrystalline CdS was successfully synthesized by 200 °C solvothermal reaction in 0-25 % NH_3 solution. The phase is hcp using pure water, transformed into cubic by the increase of the NH_3 concentration, and cubic in 25 % NH_3 solution. Raman spectra of hcp and cubic phases are almost identical with the presence of 1LO and 2 LO peaks. Their strong luminescent peaks were detected at 450 nm (2.755 ev) and 519 nm (2.389 ev), respectively.

References

1. Y.J. Yang, Coll. Surf. A, 276 (2006) 192.

2. J. Lee, Thin Solid Film., 451-452 (2004) 170.

3. Q. Wang, D. Pan, S. Jiang, X. Ji, L. An, B. Jiang, J. Cryst. Growth, 286 (2006) 83.

4. Y.M. Yu, K. Kim, B. O., K.S. Lee, Y.D. Choi, P.Y. Yu, J. Appl. Phys., 92 (2002) 1162.

5. C. Li, X. Yang, B. Yang, Y. Yan, Y. Qian, J. Cryst. Growth, 291 (2006) 45.

6. Powder Diffract. File, JCPDS Internat. Centre Diffract. Data, PA 19073-3273,U.S.A.,(2001).

7. B.D. Cullity, (Elem. X-ray Diffract., Addison-Wesley Publ. Co., MA, 1967).

8. K.W. Andrews, D.J. Dyson, S.R. Keown, (Interpret. Electr. Diffract. Patter., 2nd ed, Plenum Press, NY, 1971).

9. K.K. Nanda, S.N. Sahu, Appl. Surf. Sci., 119 (1997) 50.

10. O. Trujillo, R. Moss, K.D. Vuong, D.H. Lee, R. Noble, D. Finnigan, S. Orloff, E. Tenpas, C. Park, J. Fagan, X.W. Wang, Thin Solid Film., 290-291 (1996) 13.

11. X. Guo-yue, W. Han, C. Chuan-wei, Z. Hai-qian, C. Jie-ming, J. Guang-bin, Trans. Nonferrous Met. Soc. China, 16 (2006) 105.

12. O. de Melo, L. Hernández, O. Zelaya-Angel, R. Lozada-Morales, M. Becerril, E. Vasco, Appl. Phys. Lett. 65 (1994) 1278.

13. M. Alonso, E.J. Finn, (Fundamental University Phys., Vol.3, Addison-Wesley Publ. Co., MA, 1968).

Preparation of flower-like PbS nano-structures using cyclic microwave radiation

Abstract

Flower-like PbS nano-structures were successfully prepared from different mole ratios of $Pb(NO_3)_2$ to CH_5N_3S in propylene glycol, using the cyclic process of 600 W microwave power for 15 minutes. PbS (cubic) was detected using X-ray diffraction (XRD) and selected area electron diffraction (SAED). The experimental and simulated patterns are in good accordance. A Raman spectrometer revealed the presence of vibrations at 134, 275 and 431 cm^{-1}. Flower-like PbS nano-structures were also characterized using a scanning electron microscope (SEM) and a transmission electron microscope (TEM), although the products were prepared using different mole ratios of the starting agents.

Keywords : Cyclic microwave radiation, Flower-like PbS nano-structures

1. Introduction

Generally, different morphologies of luminescent materials have an influence on their properties [1]. Preparation of such materials is now increasingly important. PbS is a material which has a small band gap (0.41 eV) and large exciton Bohr radius (18 nm) [2-4]. It has novel semiconducting and optical properties [5], which are very sensitive to a quantum-size effect [2,3]. There are different nano- and micro-structures of PbS that have an influence on its properties. Among them are nanocubes [6], nanoparticles [7], dendrites [6,8], star-shapes [9], flower-like crystals [10], nanotubes [11] and nanorods [11,12]. They can be prepared by different methods, such as microwave radiation [10], a hydrothermal process [4], solvothermal synthesis [6], electroless chemical deposition [13] and a sonochemical process [11].

Microwave radiation [14] is a very attractive method used for preparing materials. It is able to reduce time scales of the reactions, and accelerate the reaction process. When microwave radiation is supplied to chemicals, one or more of them is capable of coupling with the radiation. This can lead to a high temperature faster than that achieved by a conventional method. Microwave radiation can solve the problems of temperature and concentration gradients. By focusing large amounts of microwave

radiation into solutions, the vibrating electric field applies a force on charged particles which vibrate accordingly. Vibrations of the reactants have an influence on the reaction to proceed with efficiency. Subsequently, pure product is produced.

At present, there are a few reports on the preparation of flower-like PbS using microwave radiation. For the present research, flower-like PbS nano-structures were prepared from different mole ratios of Pb and S sources, using a cyclic microwave radiation. The final products were then analyzed for further discussion.

2. Experiment

Flower-like PbS particles were prepared from 1 : 4, 1 : 1 and 4 : 1 mole ratios of $Pb(NO_3)_2$ to CH_5N_3S in propylene glycol, using 600 W microwave power for 15 minutes. The process was repeated many times and always happened in the same order. For every 100 s, microwave radiation was on for 30 s and off for 70 s. At the conclusion of the test, the products were washed with water and ethanol, and dried at 80 °C for 12 h. The final products were characterized using an X-ray diffractometer (XRD) operated at 20 kV, 15 mA and using Cu K_α radiation in the 2θ angular range of 15 - 60 degrees, a Raman spectrometer using a 50 mW Ar laser with λ = 514.5 nm at room temperature, a scanning electron microscope (SEM) operated at 15 kV and a transmission electron microscope (TEM) as well as the use of the selected area electron diffraction (SAED) technique operated at 200 kV. The electron diffraction pattern was simulated [15] and compared with that obtained experimentally [16].

3. Results and Discussion

3.1 XRD

XRD spectra (Fig 1a) were indexed using Bragg's law for X-ray diffraction and compared with that of the JCPDS software (reference code : 05-0592) [17]. They were specified that the products were cubic PbS (a = b = c, α = β = γ = 90 degrees) with the Fm-3m space group. The strongest intensity is at 2θ = 30.1 degrees and diffracted from the (200) planes of the crystalline products. The spectra are very sharp showing that well-crystallized crystals were successfully synthesized [18,19]. The products are composed of a number of atoms aligning in a periodic lattice. No characteristic peaks of impurities were detected showing that each of the products is a pure phase. Atoms were involved in violent vibration with the microwave frequency. They aligned in a systematic and symmetric order, which led to high intensities. Their

lattice parameters were calculated form the equation of plane spacing for the cubic crystal system and Bragg's law for diffraction [20]. The parameters corresponding to different crystallographic planes of the products are summarized in Table 1. The averages and standard deviations are 5.9476 ± 0.0111, 5.9473 ± 0.0096 and 5.9522 ± 0.0119 Å for the products prepared using 1 : 4, 1 : 1 and 4 : 1 mole ratios of $Pb(NO_3)_2$ to CH_5N_3S, respectively. They are very close to those of the JCPDS software [17].

To form PbS (cubic), the reaction [21] proceeded according to the following :

$$Pb(NO_3)_2 + CH_5N_3S \rightarrow PbS + CH_5N_3(NO_3)_2$$

Theoretically, 1 mol $Pb(NO_3)_2$ and 1 mol CH_5N_3S were used to produce 1 mol PbS and 1 mol $CH_5N_3(NO_3)_2$. For the present research, PbS was able to be produced even when either of the reactants was in excess.

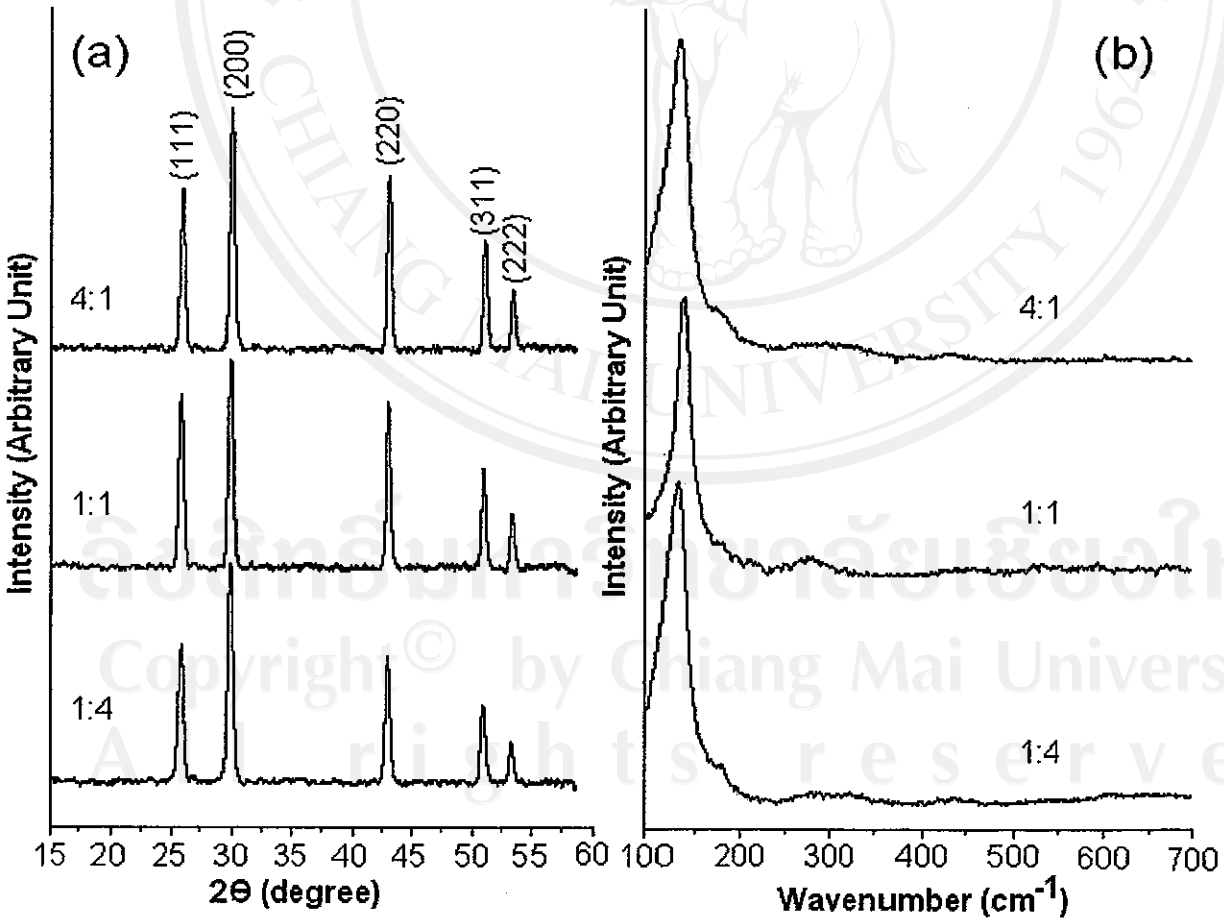

Fig 1. (a) XRD and (b) Raman spectra of the products prepared using different mole ratios of $Pb(NO_3)_2$ to CH_5N_3S.

Table 1. Calculated lattice parameters of PbS (cubic) prepared using different mole ratios of $Pb(NO_3)_2$ to CH_5N_3S.

Plane	Lattice Parameter (Å)		
	1 : 4	1 : 1	4 : 1
(111)	5.9670	5.9611	5.9675
(200)	5.9456	5.9531	5.9620
(220)	5.9447	5.9436	5.9476
(311)	5.9391	5.9380	5.9415
(222)	5.9416	5.9405	5.9422
	5.9476 ± 0.0111	5.9473 ± 0.0096	5.9522 ± 0.0119

3.2 Raman analysis

A definite existence of PbS (cubic) was analyzed using a Raman spectrometer. These test specimens are not destructed and are able to be re-used for other purposes. Their Raman spectra (Fig 1b) contain prominent bands at the same wavenumbers. They are influenced by some parameters, such as atomic masses of Pb and S, and vibration constant of bonding between Pb and S atoms residing in the lattice. Among the different spectra, their peaks are at 134, 275 and 431 cm^{-1}. The peak below 150 cm^{-1} is tentatively attributable to the so-called plasma line of the excitation laser [5,22]. The 275 cm^{-1} peak corresponds to two-phonon process [5]. The peak at 431 cm^{-1} is allowed in the rock-salt structure [23]. It is specified as the first overtone mode [22], which involves two phonons with equal but opposite wave vectors (**k**) [23]. The fundamental longitudinal optical (LO) mode of the rock-salt structure at approximately 215.5 cm^{-1} was unable to be detected due to the rising in intensity of baseline (disorder in PbS lattice) at low wavenumbers. The baseline intensity covered the fundamental LO mode, which was forbidden [22,23].

3.3 SEM

SEM images (Fig 2) show that the products are micro-sized flowers over the whole range of $Pb(NO_3)_2$ and CH_5N_3S mole ratios. Flower-like PbS nano-structures were able to be produced even when either of the reactants was in excess. The flower-like products are made up of several petals, which slope up to a point. They have two halves that are the same in size and shape. Each of the petals is composed of a number of small plates arranged in a systematic order. The distance between

two apices of the two petals across the center of the flower is 1.7 - 5.8 micrometers long. The micro-flower is the most complete at 1 : 4 mole ratio.

Fig 2. SEM images of the products prepared using (a) 1 : 4, (b) 1 : 1, and (c) 4 : 1 mole ratios of $Pb(NO_3)_2$ to CH_5N_3S, respectively.

3.4 TEM, SAED and Simulation

TEM images (Fig 3) were used to specify the morphologies of the products. They have a flat shape with four or more acute angles. The results characterized using TEM are in accord with those characterized using SEM. A SAED pattern (Fig 4a) of the product prepared using a 4 : 1 mole ratio of $Pb(NO_3)_2$ to CH_5N_3S appears as a symmetric and systematic array of bright spots showing that a number of atoms are arranged on their crystal lattices. The pattern was interpreted [16], and specified as cubic PbS [17]. The calculated electron beam used for the analysis is in the [001] direction. A diffraction pattern of the product with the electron beam in the [001] direction was simulated by respective use of a*, b* and c* lattice vectors in [100], [010] and [001] directions [15]. The simulated pattern (Fig 4b) is composed of systematic and symmetric bright spots, and is in good accord with the experimental pattern. Additional concentric rings were also detected in the experimental pattern. They were caused by the C supporting grid in the TEM chamber.

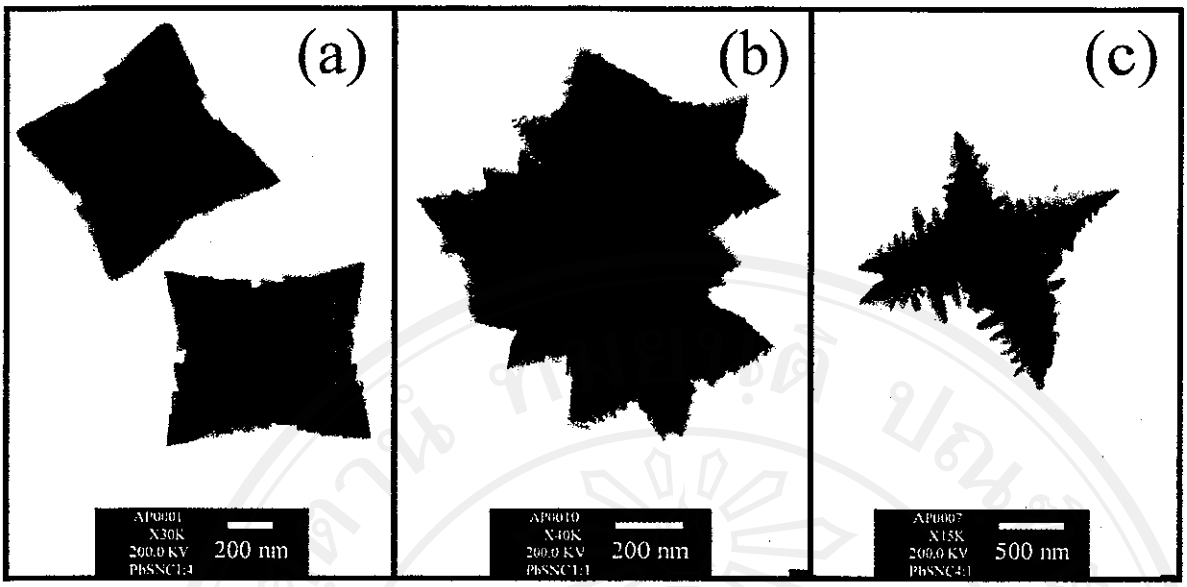

Fig 3. TEM images of the products prepared using (a) 1 : 4, (b) 1 : 1, and (c) 4 : 1 mole ratios of $Pb(NO_3)_2$ to CH_5N_3S, respectively.

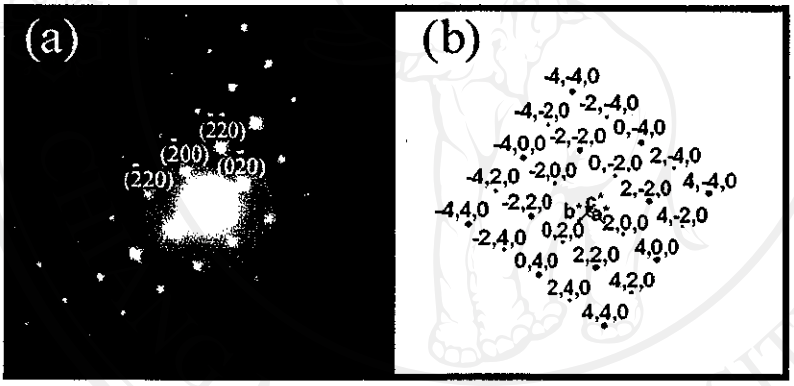

Fig 4. (a) SAED and (b) simulated patterns of the product prepared using 4 : 1 mole ratio of $Pb(NO_3)_2$ to CH_5N_3S.

4. Conclusions

Flower-like PbS nano-structures were successfully prepared from 1 : 4, 1 : 1 and 4 : 1 mole ratios of $Pb(NO_3)_2$ to CH_5N_3S in propylene glycol, using cyclic microwave radiation. XRD and SAED analyses revealed the presence of PbS with a cubic structure. For the present analysis, the experimental and simulated patterns are in good accord. Calculated lattice parameters are 5.9476 ± 0.0111, 5.9473 ± 0.0096 and 5.9522 ± 0.0119 Å for the products prepared using 1 : 4, 1 : 1 and 4 : 1 mole ratios of $Pb(NO_3)_2$ to CH_5N_3S. Both SEM and TEM analyses revealed the presence of flower-like PbS nano-structures which were prepared using different mole ratios of

Pb and S sources. The 431 cm^{-1} first overtone mode was detected using a Raman spectrometer, but the fundamental one was forbidden.

References

1. H.F. Shao, Y.B. Zhang, X.F. Qian, J. Yin, Z.K. Zhu, Mater. Lett. 59 (2005) 3507.

2. L. Xu, W. Zhang, Y. Ding, W. Yu, J. Xing, F. Li, Y. Qian, J. Cryst. Growth 273 (2004) 213.

3. Y.C. Zhang, T. Qiao, X.Y. Hu, G.Y. Wang, X. Wu, J. Cryst. Growth 277 (2005) 518.

4. S. Wang, A. Pan, H. Yin, Y. He, Y. Lei, Z. Xu, B. Zou, Mater. Lett. 60 (2006) 1242.

5. A.M. Qin, Y.P. Fang, W.X. Zhao, H.Q. Liu, C.Y. Su, J. Cryst. Growth 283 (2005) 230.

6. W. Zhang, Q. Yang, L. Xu, W. Yu, Y. Qian, Mater. Lett. 59 (2005) 3383.

7. U.K. Gautam, R. Seshadri, Mater. Res. Bull. 39 (2004) 669.

8. Z. Zhang, S.H. Lee, J.Vittal, W.S. Chin, J. Phys. Chem. B 110 (2006) 6649.

9. G. Zhou, M. Lü, Z. Xiu, S. Wang, H. Zhang, Y. Zhou, S. Wang, J. Phys. Chem. B 110 (2006) 6543.

10. Y. Ni, F. Wang, H. Liu, G. Yin, J. Hong, X. Ma, Z. Xu, J. Cryst. Growth 262 (2004) 399.

11. S.F. Wang, F. Gu, M.K. Lü, G.J. Zhou, A.Y. Zhang, J. Cryst. Growth 289 (2006) 621.

12. T. Saraidarov, R. Reisfeld, A. Sashchiuk, E. Lifshitz, Physica E 37 (2007) 173.

13. B. Minceva-Sukarova, M. Najdoski, I. Grozdanov, C.J. Chunnilall, J. Molec. Struct. 410-411 (1997) 267.

14. C. Gabriel, S. Gabriel, E.H. Grant, B.S.J. Halstead, D.M.P. Mingos, Chem. Soc. Rev. 27 (1998) 213.

15. C. Boudias, D. Monceau, CaRIne Crystallography 3.1, 17 rue du Moulin du Roy, F-60300 Senlis, France (1989-1998).

16. T. Thongtem, A. Phuruangrat, S. Thongtem, Mater. Lett. 61 (2007) 3235.

17. Powder Diffract. File, JCPDS Internat. Centre Diffract. Data, PA 19073-3273, U.S.A., (2001).

18. T. Thongtem, S. Thongtem, Ceram. Internat. 30 (2004) 1463.

19. T. Thongtem, S. Thongtem, Ceram. Internat. 31 (2005) 241.

20. C. Suryanarayana, M.G. Norton, X-ray Diffract., A Practical Approach, Plenum Press, New York, (1998).

21. L. Xu, W. Zhang, Y. Ding, W. Yu, J. Xing, F. Li, Y. Qian, J. Cryst. Growth 273 (2004) 213.

22. G.D. Smith, S. Firth, R.J.H. Clark, M. Cardona, J. Appl. Phys. 92 (2002) 4375.

23. R. Sherwin, R.J.H. Clark, R. Lauck, M. Cardona, Solid State Comm. 134 (2005) 565.

Biomolecule- and surfactant- assisted hydrothermal synthesis of PbS crystals

Abstract

PbS was hydrothermally synthesized from $Pb(NO_3)_2$, L-cysteine, and N-cetyl pyridinium chloride in the solutions with different pH values at 140 °C. Flower-like shaped, granular and truncated cubic PbS crystals which composed of Pb and S were detected by the scanning electron microscopy (SEM), transmission electron microscopy (TEM), X-ray diffraction (XRD), selected area electron diffraction (SAED), and energy dispersive X-ray (EDX) analysis. In addition, Raman and photoluminescence spectrometries revealed the presence of the first and second overtone modes at 436 and 602 cm^{-1}, and emission wavelengths at 412 nm, respectively.

Keywords : L-cysteine, N-cetyl pyridinium chloride, Hydrothermal synthesis, PbS crystals

1. Introduction

It is generally known that particle shape and size of materials have an important role in their luminescent properties [1]. Therefore, the synthesis of nano- and micro-crystals has been increasingly important. One of the materials is PbS which has small band gap (0.41 eV) and large exciton Bohr radius (18 nm) [2-4]. It has novel semiconducting and optical properties [5], and is very sensitive to quantum-size effect [2,3]. There are a variety of shapes and sizes that play the role in their properties. Among them are cross shaped [6], star-like [3,7], fish bone-like [3], flower-like [3,8], nano-cubic [7], nano-rod [9], nano-belt [9], and nano-dendrite [9]. It was reported that biomolecules were used as a sulfur source and complexing agent for the synthesis processes [10,11]. A surfactant was used as the directing molecules to control the shapes and sizes of the crystals [1,4,9]. Currently, there are no reports on the use of both bio- and surfactant-molecules in a reaction process. For the present research, nano- and micro-crystalline PbS was hydrothermally synthesized using L-cysteine and N-cetyl pyridinium chloride at different pH values and prolonged times. Then, the final products were intensively analyzed for further discussion.

2. Experiment

Different shapes and sizes of PbS were synthesized in the home-made stainless steel autoclaves using 0.003 mol $Pb(NO_3)_2$, 0.003 mol L-cysteine ($C_3H_7NO_2S$) and 0.0005 mol N-cetyl pyridinium chloride ($C_{21}H_{38}NCl$) in 40 ml deionized water at 140 °C. By washing with water and ethanol, and drying at 80 °C for 24 h, the final products were analyzed using an X-ray diffractometer (XRD) operated at 20 kV, 15 mA and using Cu K_α radiation in the 2θ angular range of 15-60 deg, a transmission electron microscope (TEM) as well as a selected area electron diffraction (SAED) technique operated at 200 kV, a scanning electron microscope (SEM) and an energy dispersive X-ray (EDX) analyzer operated at 15 kV, a Raman spectrometer using 50 mW Ar Laser with λ = 514.5 nm, and a luminescence spectrometer using 250 nm exciting wavelength.

3. Results and Discussion

3.1 XRD

XRD spectra (Fig 1) were indexed, and specified as cubic PbS with Fm-3m space group, a = b = c = 0.5936 nm, and $\alpha = \beta = \gamma = 90$ deg (reference code : 05-0592) [12]. The spectra are very sharp showing that well-crystallized PbS was successfully synthesized [13-15]. The strongest intensity is at $2\theta = 30.08$ deg and diffracted from (200) plane of the products. For the present analysis, no impurities were detected.

3.2 SEM

SEM images (Fig 2) show that the products were synthesized in a variety of shapes and sizes influenced by the pH values, cationic surfactant and hydrothermal times. At 12 h hydrothermal reaction, the products are nano-sized granules in the pH of 7 and 11, but it is micro-sized flower in the pH of 2.36. The flower-like products are made up of several petals. A distance between two apices of the two petals across the center of the flower is approximately fourteen microns long. Each of the petals composes of a number of small plates arranging in systematic order. They are very beautiful and interesting, and have never been synthesized using the biomolecule

and surfactant in the hydrothermal reaction. Therefore, the constant pH of 2.36 for a variety of the prolonged times was used. At 8 h reaction, the flower-like product is made up of three to four petals and is not complete. It contains a greater number of the petals when the hydrothermal times were prolonged. There are ten petals at 48 h reaction.

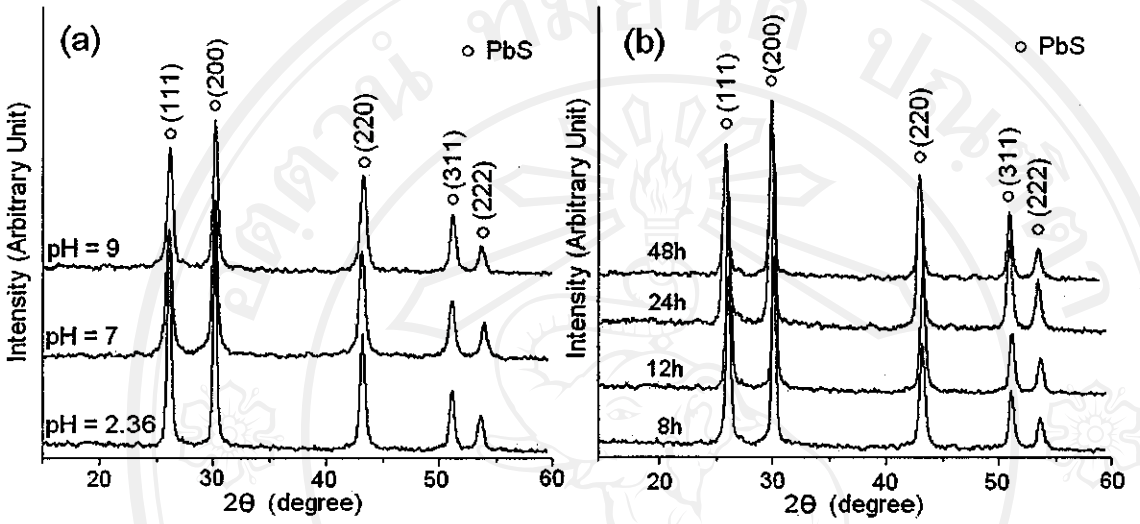

Fig 1. XRD spectra of the products synthesized in (a) the solutions with different pH values for 12 h, and (b) the solutions with the pH of 2.36 for different hydrothermal times.

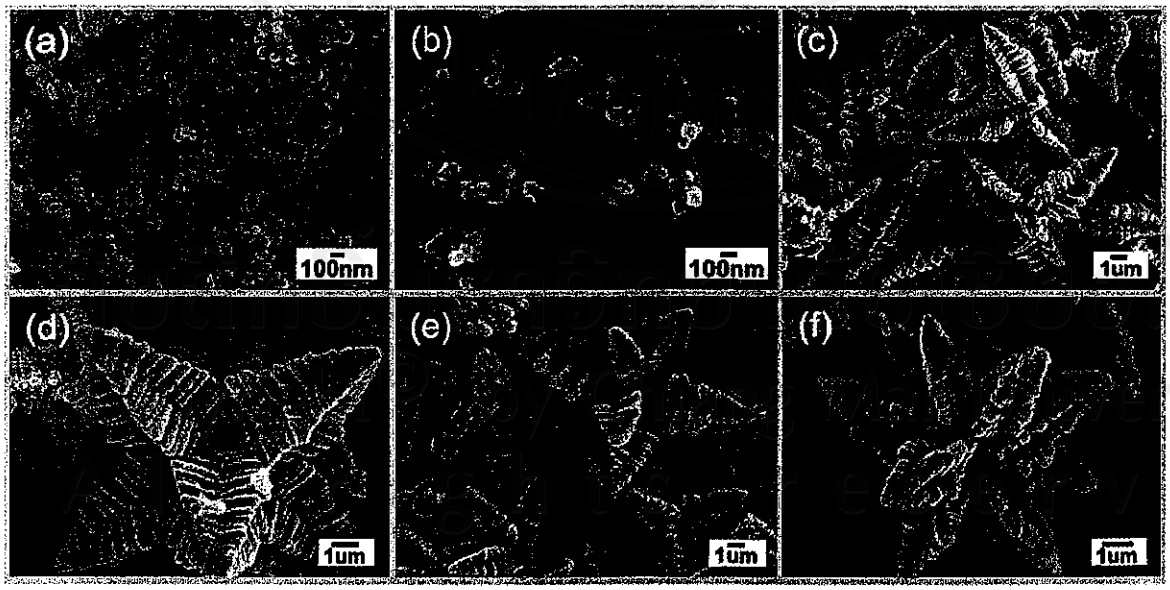

Fig 2. SEM images of the products synthesized in (a and b) the solutions with the pH of 7 and 11 for 12 h, and (c to f) the solutions with the pH of 2.36 for 8, 12, 24 and 48 h, respectively.

3.3 TEM and SAED

TEM images and SAED patterns (Fig 3) are used to specified morphologies and phases of the products. At the pH of 7 and 12 h, the product composes of a number of <10 nm particles in nano-sized clusters. The pattern was interpreted [16,17], and specified as cubic PbS [12]. For the present analysis, calculated electron beam [17] is in the $[\bar{1}1\bar{1}]$ direction. When the pH was increased to 11, the product

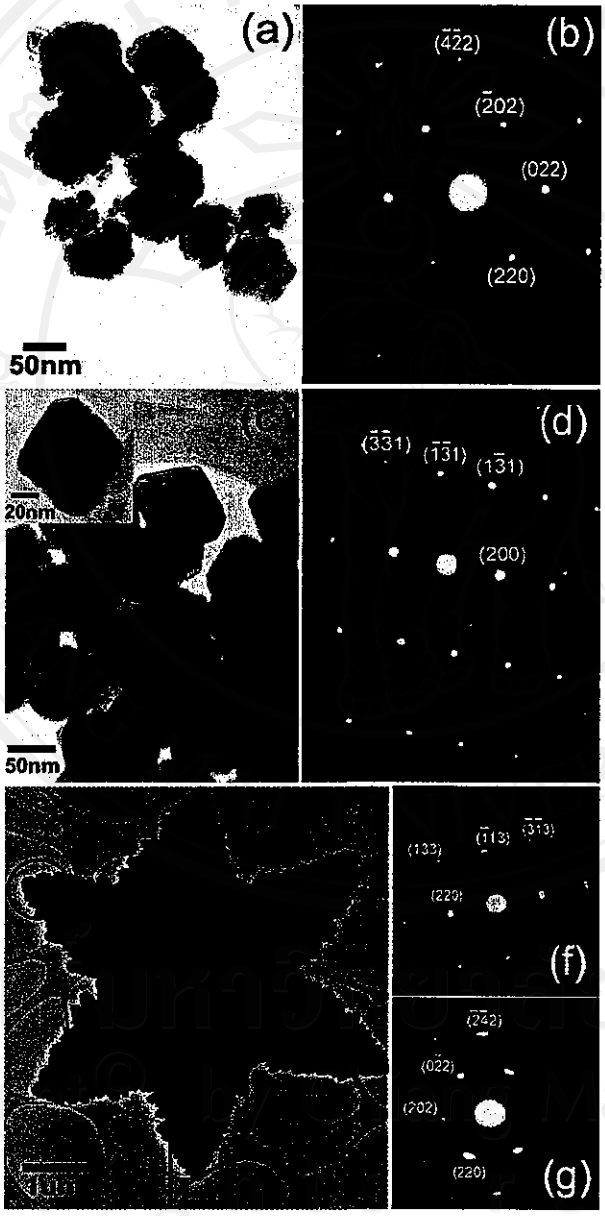

Fig 3. TEM images and SAED patterns of the products synthesized at different pH values and hydrothermal times. (a and b) pH7 and 12 h, (c and d) pH11 and 12 h, and (e, f and g) pH2.36 and 48 h [(f) and (g) were analyzed on the (e)-product marked with a circle and square, respectively].

composes of 75 nm truncated cubes. At lower magnification shown in the SEM image, it appears as granular. SAED pattern was analyzed using electron beam in the $[013]$ direction. It is in accord with cubic PbS as well. At the pH of 2.36 and 48 h, the product is flower-like and is cubic PbS phase. Calculated electron beams used for the product analysis at the circle and square are in the $[3\bar{3}2]$ and $[1\bar{1}1]$ directions, respectively.

For the present research, N-cetyl pyridinium chloride was used as a cationic surfactant. L-cysteine, a neutral and genetically coded amino acid, was used as a sulfur source and complexing agent. When $Pb(NO_3)_2$ reacted with L-cysteine to form complex followed by the production of PbS nuclei (very fine particles) in the solution with the pH of 2.36, the surfactant was selectively adsorbed onto their surfaces. Therefore, the crystals were modeled to grow into small plates composing the petals of micro-sized flowers. At the pH of 7 and 11, the solutions contain a greater number of OH^- ions than the acidic solution. The cationic surfactant became less efficient in adsorbing onto PbS nuclei, which were capable of growing into nano-sized particles in clusters or truncated cubes.

3.4 Raman analysis

Raman spectra (Fig 4) contain prominent bands whose peaks are at 135, 278, 436, 602 and 970 cm^{-1}. The peak below 150 cm^{-1} is tentatively attributable to the so-called plasma line of the excitation laser [5,18]. The 278 cm^{-1} peak corresponds to the phonon vibration mode [5]. Those at 436 and 602 cm^{-1} are specified as the first and second overtone modes, respectively [18]. The peak above 960 cm^{-1} is attributable to oxy-sulfates [5,18].

3.5 EDX

EDX spectra (Fig 5) reveal the presence of Pb and S. Cu of a copper stub was also detected. The detection of Pb and S using the EDX is in accord with the detection of PbS using the XRD and SAED.

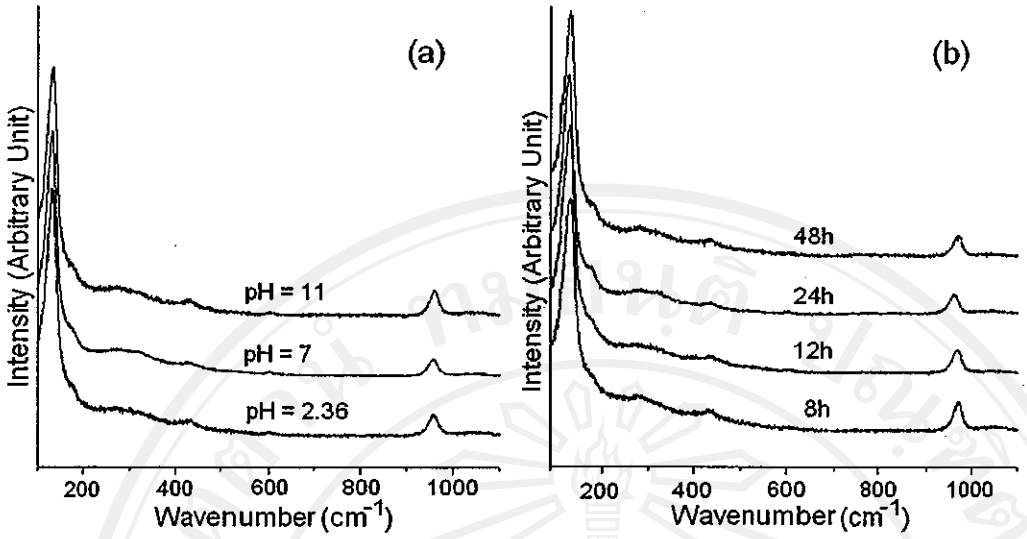

Fig 4. Raman spectra of the products synthesized in (a) the solutions with different pH values for 12 h, and (b) the solutions with the pH of 2.36 for different hydrothermal times.

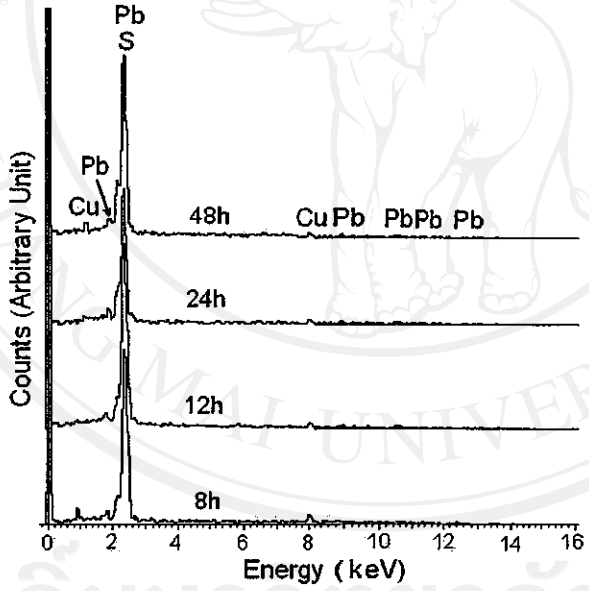

Fig 5. EDX spectra of the products synthesized in the solutions with the pH of 2.36 for different hydrothermal times.

3.6 Photoluminescence

Photoluminescence (PL) of the products (Fig 6) were analyzed using 250 nm exciting wavelength. The maximum PL intensities were detected at the same wavelength of 412 nm although their intensities are different. The intensities are sensitive to the morphologies but not for their emission wavelengths. They are increased with the increase in the acidities and hydrothermal times. At constant hydrothermal time and different pH values, PL intensity of the flower-like particles (pH 2.36, 12 h) is higher than those of the granules (pH 7, 12 h), and truncated cubes (pH 11, 12 h). When the hydrothermal times were prolonged to 48 h at constant pH value of 2.36, the flowers became the most complete and the intensity is the highest. In general, the intensities are very sensitive to the number of the electronic transfers and defects in the products [19].

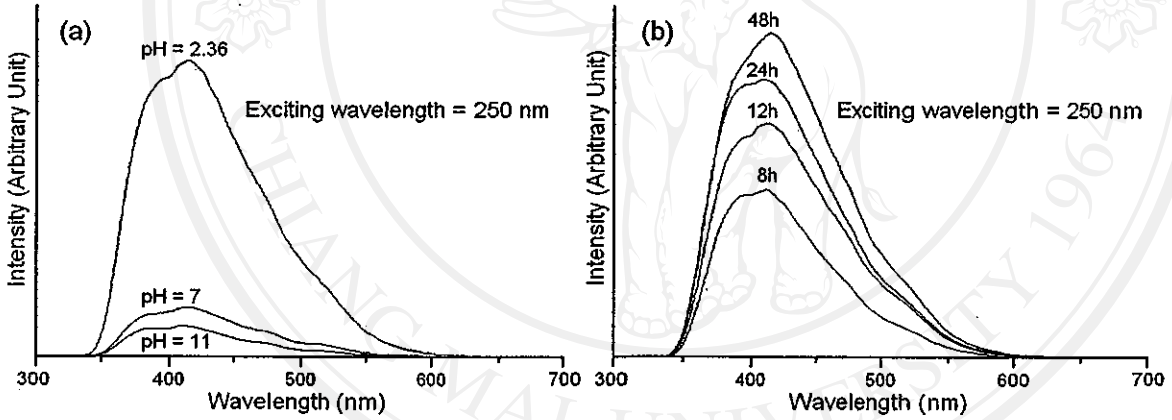

Fig 6. PL emission of the products synthesized in (a) the solutions with different pH values for 12 h, and (b) the solutions with the pH of 2.36 for different hydrothermal times.

4. Conclusions

Different shapes and sizes of PbS were hydrothermally synthesized using biomolecule (L-cysteine) and surfactant (N-cetyl pyridinium chloride) at 140 °C. The detection of PbS using XRD and SAED is in accord with the detection of Pb and S using EDX, and the first and second overtone modes using a Raman spectrometer. They are truncated cubes, granules and flower-like particles in the pH of 11, 7 and

2.36, respectively. At the pH of 2.36 and 48 h, the flowers composed of ten petals. Their emission wavelengths were detected at the same value of 412 nm.

References

1. H.F. Shao, Y.B. Zhang, X.F. Qian, J. Yin, Z.K. Zhu, Mater. Lett. 59 (2005) 3507.

2. L. Xu, W. Zhang, Y. Ding, W. Yu, J. Xing, F. Li, Y. Qian, J. Cryst. Growth 273 (2004) 213.

3. Y.C. Zhang, T. Qiao, X.Y. Hu, G.Y. Wang, X. Wu, J. Cryst. Growth 277 (2005) 518.

4. S. Wang, A. Pan, H. Yin, Y. He, Y. Lei, Z. Xu, B. Zou, Mater. Lett. 60 (2006) 1242.

5. A.M. Qin, Y.P. Fang, W.X. Zhao, H.Q. Liu, C.Y. Su, J. Cryst. Growth 283 (2005) 230.

6. S.F. Wang, F. Gu, M.K. Lü, D.Z. Wang, Z.S. Yang, H.P. Zhang, Y.Y. Zhou, A.Y. Zhang, Mater. Lett. 60 (2006) 2759.

7. G. Zhou, M. Lü, Z. Xiu, S. Wang, H. Zhang, Y. Zhou, S. Wang, J. Phys. Chem. B 110 (2006) 6543.

8. Y. Ni, F. Wang, H. Liu, G. Yin, J. Hong, X. Ma, Z. Xu, J. Cryst. Growth 262 (2004) 399.

9. L. Dong, Y. Chu, Y. Liu, M. Li, F. Yang, L. Li, J. Colloid Interf. Sci. 301 (2006) 503.

10. X. Chen, X. Zhang, Z. Wang, J. Wan, Y. Qian, Mater. Chem. Phys. 98 (2006) 419.

11. X. Chen, X. Zhang, C. Shi, X. Li, Y. Qian, Solid State Commun. 134 (2005) 613.

12. Powder Diffract. File, JCPDS Internat. Centre Diffract. Data, PA 19073-3273, U.S.A., 2001.

13. T. Thongtem, S. Thongtem, Ceram. Internat. 30 (2004) 1463.

14. T. Thongtem, S. Thongtem, Ceram. Internat. 31 (2005) 241.

15. T. Thongtem, S. Thongtem, Inorg. Mater. 42 (2006) 202.

16. K.W. Andrews, D.J. Dyson, S.R. Keown, Interpret. Electr. Diffract. Patter., 2nd ed, Plenum Press, NY, 1971.

17. B.D. Cullity, Elem. X-ray Diffract., 2nd ed., Addison-Wesley Publ. Co., MA, 1978.

18. G.D. Smith, S. Firth, R.J.H. Clark, M. Cardona, J. Appl. Phys., 92 (2002) 4375.

19. M. Alonso, E.J. Finn, Fundamental University Phys., Vol.3, Addison-Wesley Publ. Co., MA, 1968.

Output ที่ได้จากโครงการวิจัย ฯ

1. เผยแพร่ผลงานวิจัยในวารสารต่าง ๆ จำนวน 8 เรื่อง ดังนี้ คือ

[1] Titipun Thongtem, Anukorn Phuruangrat and Somchai Thongtem, Characterization of $MMoO_4$ (M = Ba, Sr and Ca) with different morphologies prepared using a cyclic microwave radiation, Materials Letters, 62 (2008) 454-457. (IF-2008 = 1.748)

[2] Titipun Thongtem, Anukorn Phuruangrat and Somchai Thongtem, Preparation and characterization of nanocrystalline $SrWO_4$ using cyclic microwave radiation, Current Applied Physics, 8 (2008) 189-197. (IF-2008 = 1.526)

[3] Titipun Thongtem, Sulawan Kaowphong and Somchai Thongtem, Sonochemical Preparation of $PbWO_4$ Crystals with Different Morphologies, Ceramics International, 35 (2009) 1103-1108. (IF-2008 = 1.369)

[4] Titipun Thongtem, Anukorn Phuruangrat and Somchai Thongtem, Free Surfactant Synthesis of Microcrystalline CdS by Solvothermal Reaction, Materials Letters, 61 (2007) 3235-3238. (IF-2008 = 1.748)

[5] Titipun Thongtem, Anukorn Phuruangrat and Somchai Thongtem, Synthesis and analysis of CuS with different morphologies using cyclic microwave irradiation, Journal of Materials Science, 42 (2007) 9316-9323. (IF-2008 = 1.181)

[6] Titipun Thongtem, Sulawan Kaowphong and Somchai Thongtem, Biomolecule and surfactant-assisted hydrothermal synthesis of PbS crystals, Ceramics International, 34 (2008) 1691-1695. (IF-2008 = 1.369)

[7] Titipun Thongtem, Anukorn Phuruangrat and Somchai Thongtem, Preparation of flower-like PbS nano-structures using cyclic microwave radiation, Journal of Ceramic Processing Research, 9 (2008) 335-337. (IF-2008 = 0.288)

[8] Titipun Thongtem, Anukorn Phuruangrat and Somchai Thongtem, Phase Transformation of Nanocrystalline CdS Synthesized by Solvothermal Reaction, Materials Science Forum, 544-545(2007)777-780.

2. ผลิตดุษฎีบัณฑิตได้จำนวน 2 คน
3. เสนอผลงานวิจัยในการประชุมต่าง ๆ ดังนี้ คือ

- Titipun Thongtem, Anukorn Phuruangrat and Somchai Thongtem, Characterization of CdS nanorods produced using solvothermal reaction, 15th International Symposium on Intercalation Compounds, May 11-15, 2009, Tsinghua University, Beijing, China, P134.

- Anukorn Phuruangrat, Titipun Thongtem and Somchai Thongtem, Effect of Cd and S sources on the aspect ratios of CdS synthesized by solvothermal reactions in mixed solvents, The 1st International Symposium on Hybrid Materials and Processing (HyMaP 2008), October 27-29, 2008, Grand Hotel, Busan, Korea, PD2-121.

- Titipun Thongtem, Anukorn Phuruangrat and Somchai Thongtem, Characterization of CdS nanowires produced using solvothermal reactions, 2nd International Conference on Advanced Nano Materials (ANM 2008), June 22-25, 2008, Aveiro, Portugal, Abstract Nos. 40 and 308.

- Titipun Thongtem, Sulawan Kaowphong and Somchai Thongtem, Carboxymethyl cellulose-assisted hydrothermal synthesis of PbS with nano and microcrystals, 2nd International Conference on Advanced Nano Materials (ANM 2008), June 22-25, 2008, Aveiro, Portugal, Abstract No. 41.

- Titipun Thongtem, Anukorn Phuruangrat and Somchai Thongtem, Sonochemical synthesis of $MMoO_4$ (M = Ca, Sr and Ba) nanocrystals, The 9th International Symposium on Eco-materials Processing and Design, 7-9 Jan 2008, Changwon, Korea, B-P-012.

- Titipun Thongtem, Anukorn Phuruangrat and Somchai Thongtem, Synthesis of $CaWO_4$, $SrWO_4$ and $BaWO_4$ with nanosized particles using a cyclic microwave radiation, The 9th International Symposium on Eco-materials Processing and Design, 7-9 Jan 2008, Changwon, Korea, B-P-013.

- Sulawan Kaowphong, Titipun Thongtem and Somchai Thongtem, Carboxymethyl cellulose-assisted hydrothermal synthesis of PbS with nano and microcrystals, The 9th International Conference on Atomically Controlled Surfaces, Interfaces and Nanostructures (ACSIN-9), November 11-15, 2007, Tokyo, Japan, PS1-54.

- Titipun Thongtem, Anukorn Phuruangrat and Somchai Thongtem, Characterization of MWO_4 (M = Ba, Sr and Ca) prepared using sonochemical process, The 9th International Conference on Atomically Controlled Surfaces, Interfaces and Nanostructures (ACSIN-9), November 11-15, 2007, Tokyo, Japan, PS3-74.

4. ตามหนังสือ ที่ ศธ 0542.07/98 วันที่ 6 มีนาคม 2552 ได้รับเชิญจาก ผู้ช่วยศาสตราจารย์ อนุรัตน์ สายทอง คณบดีคณะวิทยาศาสตร์และเทคโนโลยี มหาวิทยาลัยราชภัฏสกลนคร

ให้เป็นวิทยากรบรรยายพิเศษ ในการประชุมวิชาการด้านวิทยาศาสตร์และเทคโนโลยี ครั้งที่ 2 ในระหว่างวันที่ 9-10 กรกฎาคม 2552 ณ มหาวิทยาลัยราชภัฏสกลนคร

5. ได้รับเชิญจาก Professor Dr. Koichi Niihara (ICC3 President) ให้เป็น International Advisory Broad, 3 rd International Congress on Ceramics, Nov 14-18, 2010, Osaka, Japan
6. ตามหนังสือที่ นท.45.02.02/16/2551 วันที่ 20 พฤษภาคม 2551 ได้รับเชิญจาก ศาสตราจารย์ ดร. สุพจน์ หารหนองบัว ผู้อำนวยการศูนย์นวัตกรรมนาโนเทคโนโลยี จุฬาลงกรณ์มหาวิทยาลัย ให้เป็นผู้ทรงคุณวุฒิประเมินข้อเสนอโครงการวิจัย
7. ตามหนังสือที่ ศธ 57 53 00/1147 วันที่ 3 มีนาคม 2551 ได้รับเชิญจาก รองศาสตราจารย์ ดร. วัฒนพงศ์ เกิดทองมี คณบดีสำนักวิชาวิศวกรรมศาสตร์และทรัพยากร มหาวิทยาลัยวลัยลักษณ์ ให้เป็นประธานกรรมการสอบวิทยานิพนธ์ นักศึกษาหลักสูตรดุษฎีบัณฑิต สาขาวิชาวิทยาศาสตร์และวิศวกรรมวัสดุ
8. ตามบันทึก วันที่ 7 มกราคม 2551 ได้รับเชิญจาก รองศาสตราจารย์ ดร. ธรณินทร์ ไชยเรืองศรี หัวหน้าภาควิชาเคมีอุตสาหกรรม คณะวิทยาศาสตร์ ให้เป็นกรรมการผู้ทรงคุณวุฒิในการประเมินรายงานวิจัยฉบับสมบูรณ์
9. ตามหนังสือที่ คปก 075/2550 วันที่ 6 พฤศจิกายน 2550 ได้รับเชิญจาก ศาสตราจารย์ ดร. มนัส พรหมโคตร หัวหน้าผู้ประสานงานโครงการเครือข่าย คปก ให้เป็นผู้ประสานงานการจัดสัมมนา RGJ Seminar Series LX ครั้งที่ 60 ในวันที่ 28 มีนาคม 2551 ณ คณะวิทยาศาสตร์ มหาวิทยาลัยเชียงใหม่
10. ตามหนังสือที่ วท 5600/ว 052 วันที่ 6 สิงหาคม 2550 ได้รับเชิญจาก รองศาสตราจารย์ ดร. วีระพงษ์ แพสุวรรณ ผู้อำนวยการศูนย์ปฏิบัติการวิจัยเครื่องกำเนิดแสงซินโครตรอนแห่งชาติ ให้เป็นผู้ทรงคุณวุฒิประเมินโครงการวิจัยที่ขอรับทุนสนับสนุนจากศูนย์ ฯ
11. ตามหนังสือที่ นร 6808/791/2550 วันที่ 17 ธันวาคม 2550 ได้รับเชิญจาก ศาสตราจารย์ ดร. วิชัย บุญแสง ผู้อำนวนการฝ่ายวิชาการ สำนักงานกองทุนสนับสนุนการวิจัย ให้เป็นผู้ประเมินโครงการวิจัย

12. ตามประกาศสำนักงานกองทุนสนับสนุนการวิจัย ที่ ฝ 5/3//2550 วันที่ 1 พฤษภาคม 2550 ได้รับการแต่งตั้งจาก รองศาสตราจารย์ ดร. สุธีระ ประเสริฐสรรพ์ รองผู้อำนวยการสำนักงานกองทุนสนับสนุนการวิจัย ปฏิบัติราชการแทนผู้อำนวยการ ให้เป็นอนุกรรมการโครงการ "โครงงานอุตสาหกรรมและวิจัยสำหรับนักศึกษาปริญญาตรี"
13. ตามหนังสือที่ ศธ 0527.01/ว 9802 วันที่ 20 กันยายน 2550 ได้รับเชิญจาก ผู้ช่วยศาสตราจารย์ ดร. วิบูลย์ วัฒนาธร รองอธิการบดีฝ่ายวิจัยและประกันคุณภาพ มหาวิทยาลัยนเรศวร ให้เป็นผู้ทรงคุณวุฒิประเมินข้อเสนอการวิจัย
14. ตามบันทึกที่ ศธ 0515(019)/3771 วันที่ 30 ตุลาคม 2550 ได้รับเชิญจากผู้อำนวยการสถาบันวิจัยและพัฒนาวิทยาศาสตร์และเทคโนโลยี มหาวิทยาลัยเชียงใหม่ ให้เป็นผู้ทรงคุณวุฒิประเมินโครงการวิจัย ฯ
15. ตามบันทึกที่ ศธ 0542.07/222 วันที่ 2 สิงหาคม 2550 ได้รับเชิญจาก ผู้ช่วยศาสตราจารย์ อนุรัตน์ สายทอง คณบดีคณะวิทยาศาสตร์และเทคโนโลยี มหาวิทยาลัยราชภัฏสกลนคร ให้เป็นผู้ทรงคุณวุฒิวิพากษ์หลักสูตรวิทยาศาสตร์บัณฑิต สาขาวิชาฟิสิกส์ คณะวิทยาศาสตร์และเทคโนโลยี มหาวิทยาลัยราชภัฏสกลนคร
16. ได้รับเชิญจาก Professor Junichi Hojo, Professor Koichi Niihara, Professor Kozo Ishizaki, Professor Soo Wohn Lee and Professor Yubao Li ให้เป็น International Advisory Committee ใน Materials Science Forum, Vol 544-545, 2007 และในการประชุม 8th International Symposium on Eco-Materials Processing and Design (ISEPD 2007) 11-14 January 2007, Kitakyushu, Japan
17. ได้รับเชิญจาก Professor Soo Wohn Lee และ Professor Chan Won Lee ให้เป็น International Advisory Committee ในการประชุม 9th International Symposium on Eco-Materials Processing and Design (ISEPD 2008) 7-9 January 2008, Changwon, Korea
18. ได้รับเชิญจาก Professor J.F. Yang ให้เป็น International Advisory Committee ในการประชุม 10th International Symposium on Eco-Materials Processing and Design (ISEPD 2009) 13-15 January 2009, Xi'an, China

19. ได้รับเชิญจาก Professor H. Luo, และ Professor L. Gao ให้เป็น International Advisory Broad ในการประชุม The 3rd Asia-Oceania Ceramic Federation (AOCF-3) Conference, September 21-25, 2008, Yunnan, China
20. Committee Members, 16th International Conference on Composites/Nano-engineering (ICCE-16), July 20-26, 2008, China.
21. ได้รับการแต่งตั้ง ให้เป็นกรรมการวิชาการสาขาฟิสิกส์ เพื่อตรวจสอบบทคัดย่อสาขาวิชาฟิสิกส์ที่จะนำเสนอในการประชุม วทท 33 (ตุลาคม 2550)
22. ได้รับการแต่งตั้ง ให้เป็นกรรมการวิชาการสาขาฟิสิกส์ เพื่อตรวจสอบบทคัดย่อสาขาวิชาฟิสิกส์ที่จะนำเสนอในการประชุม วทท 34 (ตุลาคม 2551)
23. ได้รับเชิญให้เป็น reviewer เพื่อตรวจสอบ manuscript ที่จะตีพิมพ์ใน Materials Science and Engineering A, Materials Letters, Applied Surface Science, J. of Materials Processing Technology, J. of Ceramic Processing Research, Solid State Phenomena, Chiang Mai Journal of Science และอื่น ๆ
24. ได้รับรางวัลรองชนะเลิศอันดับหนึ่งที่มีผลงานวิจัยตีพิมพ์ในวารสารที่มี impact factor เป็นอันดับสอง จากอธิการบดี มช 2550

ผลงานวิจัยที่เผยแพร่ในวารสารต่าง ๆ

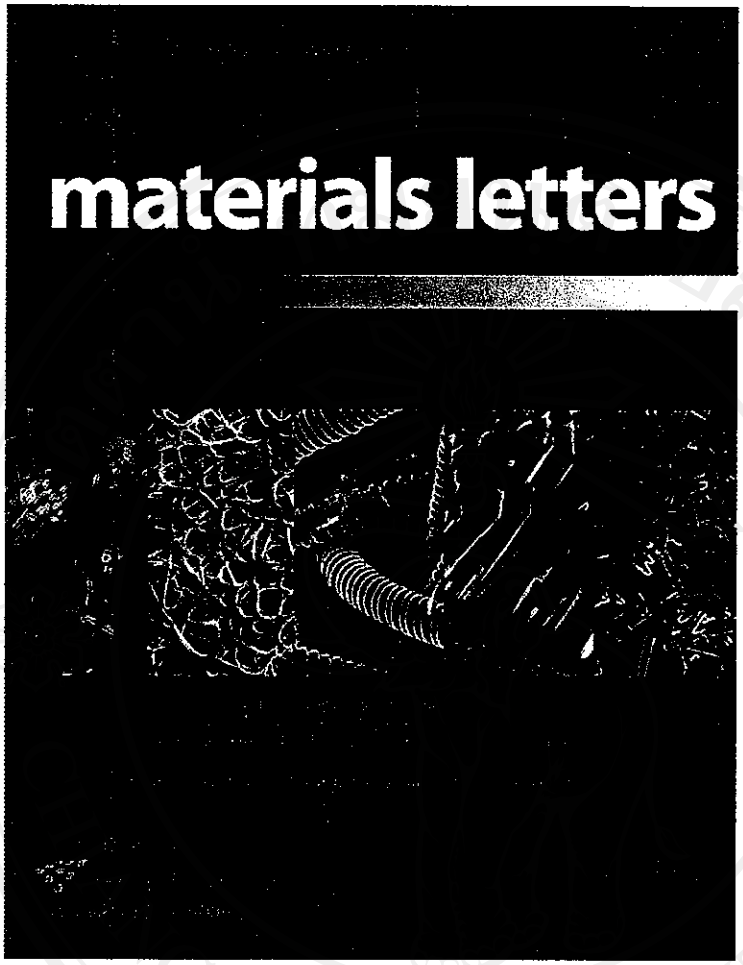

Available online at www.sciencedirect.com
ScienceDirect
Materials Letters 62 (2008) 454–457
materials letters
www.elsevier.com/locate/matlet

Characterization of $MMoO_4$ (M=Ba, Sr and Ca) with different morphologies prepared using a cyclic microwave radiation

Titipun Thongtem [a,*], Anukorn Phuruangrat [b], Somchai Thongtem [b]

[a] Department of Chemistry, Faculty of Science, Chiang Mai University, Chiang Mai 50200, Thailand
[b] Department of Physics, Faculty of Science, Chiang Mai University, Chiang Mai 50200, Thailand

Received 6 May 2007; accepted 22 May 2007
Available online 2 June 2007

Abstract

Scheelite molybdates ($MMoO_4$, M=Ba, Sr and Ca) were successfully prepared by the reactions of $M(NO_3)_2{\cdot}2H_2O$ and $Na_2MoO_4{\cdot}2H_2O$ in propylene glycol and NaOH using a microwave radiation. The phases were detected using XRD and SAED. TEM analysis revealed the presence of micro-sized bi-pyramids with a square base, nano-sized particles in clusters, and dispersed nano-sized particles for $BaMoO_4$, $SrMoO_4$ and $CaMoO_4$, respectively. Diffraction patterns of the bi-pyramids were simulated, and are in accord with the experimental results. Raman and FTIR spectra provide the evidence of scheelite structure with Mo–O stretching vibration in MoO_4^{2-} tetrahedrons at 742–901 cm^{-1}.

Keywords: Cyclic microwave radiation; Bi-pyramidal $BaMoO_4$; Nano-sized $SrMoO_4$; Nano-sized $CaMoO_4$

1. Introduction

The scheelite molybdates ($MMoO_4$, M=Ba, Sr and Ca) have C_{4h} point group with two formula units per primitive cell [1–3]. They have attracted particular interest in a variety of applications such as hosts for lanthanide activated lasers [4], luminescence materials [5,6], microwave applications [7] and catalysts [6,8]. The materials were prepared by different methods, such as mechanochemical process [9], solvothermal reaction [10] and microwave radiation with further calcination [4]. A conventional solvothermal process is a method used for growing crystalline materials in a solvent containing in a tightly closed autoclave (system) at high temperatures. Heat, generated from an electrical heater, is supplied to the system to raise its temperature. For a microwave-solvothermal process, the system is heated using a microwave radiation. It becomes hot by the vibration of charged particles with electric field intensity. The purpose of the research is to prepare $MMoO_4$ with different morphologies in basic solutions using a cyclic (on and off over a period of time, and happen in the same order) microwave radiation without the requirement of any further calcination. The reaction proceeded in an open system at atmospheric pressure. No other additives were used. The process is very simple, attractive and novel by focusing large amount of microwave radiation into the solutions to produce pure products.

2. Experiment

Each of 0.005 mol $M(NO_3)_2{\cdot}2H_2O$ (M=Ba, Sr and Ca) and $Na_2MoO_4{\cdot}2H_2O$ was dissolved in 20 ml propylene glycol containing 10 ml 3 M NaOH. The reactions cyclically proceeded

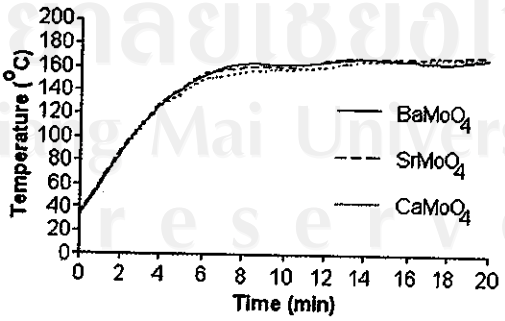

Fig. 1. Current temperatures of the system during processing.

* Corresponding author. Tel.: +66 53 941922; fax: +66 53 892277.
E-mail address: ttpthongtem@yahoo.com (T. Thongtem).

0167-577X/$ - see front matter © 2007 Elsevier B.V. All rights reserved.
doi:10.1016/j.matlet.2007.05.059

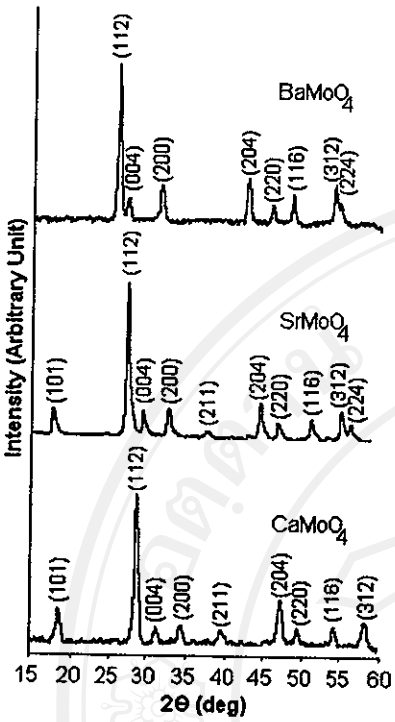

Fig. 2. XRD spectra of the products.

using a 600 W microwave for 20 min (10 cycles). One cycle is 2 min long and composes of irradiation and non-irradiation for 1 min each. Current temperatures of different solutions are shown in Fig. 1. They are increased with the increasing of the prolonged times within about the first 9 min and show very little oscillation around a constant value afterwards. The final products were washed with water and 95% ethanol, dried at 80 °C for 24 h, and intensively characterized.

3. Results and discussion

3.1. XRD

XRD spectra (Fig. 2) were compared with those of the JCPDS software (reference codes: 29-0193, 08-0482 and 85-0585) [2], and specified as $MMoO_4$ (M=Ba, Sr and Ca). They have scheelite structure with tetragonal crystal system and have $I4_1/a$ space-group symmetry [2,3,9,11]. Calculated lattice parameters [12] for $BaMoO_4$ ($a=b=0.5573$ and $c=1.2786$ nm), $SrMoO_4$ ($a=b=0.5406$ and $c=1.1988$ nm) and $CaMoO_4$ ($a=b=0.5212$ and $c=1.1438$ nm) are very close to those of the corresponding JCPDS software, and have the influence on their interplanar spaces. No other characteristic peaks of impurities were detected showing that the products are pure phase. Their strongest intensity peaks are at $2\theta=26.53$, 27.66 and 28.75 deg for $BaMoO_4$, $SrMoO_4$ and $CaMoO_4$, respectively. They diffracted from the same plane indexed by (112).

To produce $MMoO_4$, $M(NO_3)_2{\cdot}2H_2O$ reacted with $Na_2MoO_4{\cdot}2H_2O$ in propylene glycol under basic condition using a microwave radiation.

$$M(NO_3)_2 \cdot 2H_2O + Na_2MoO_4 \cdot 2H_2O \rightarrow MMoO_4 + 2NaNO_3 + 4H_2O$$

During the synthesis, vibrating electric field of a microwave applied a force on electric charged particles. They vibrated with the electric field strength. Vibrations of the reactants have the influence on the reaction to effectively proceed. Subsequently, pure product was produced.

3.2. Vibration spectra

Vibrations of $MMoO_4$ are classified into two types, the internal and external modes [13]. The first belongs to the vibration inside $[MoO_4]^{2-}$ molecular units of which the centers of mass are stationary. The second is called lattice phonon which corresponds to the motion of M^{2+} cations and the rigid molecular units. In free space, $[MoO_4]^{2-}$ tetrahedrons have T_d-symmetry [1,13]. Their vibrations compose of four internal modes ($\nu_1(A_1)$, $\nu_2(E)$, $\nu_3(F_2)$ and $\nu_4(F_2)$), one free rotation mode ($\nu_{f.r}(F_1)$), and

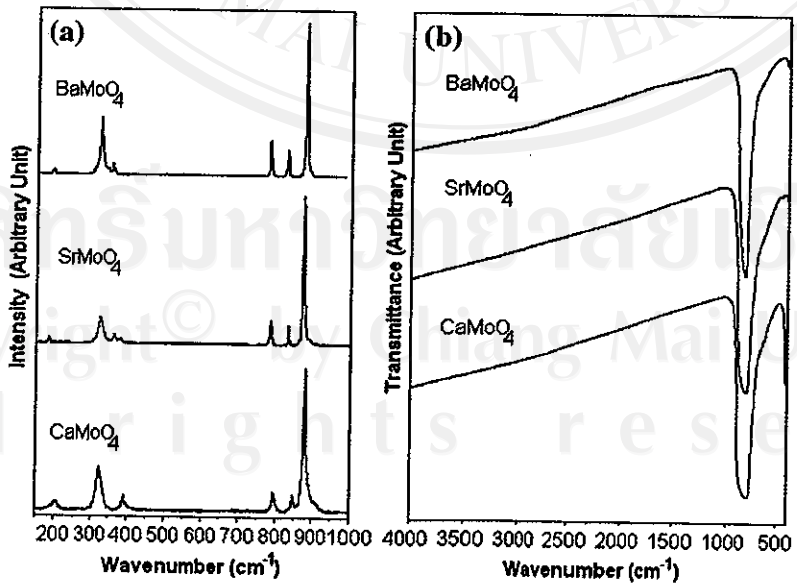

Fig. 3. (a) Raman and (b) FTIR spectra of the products.

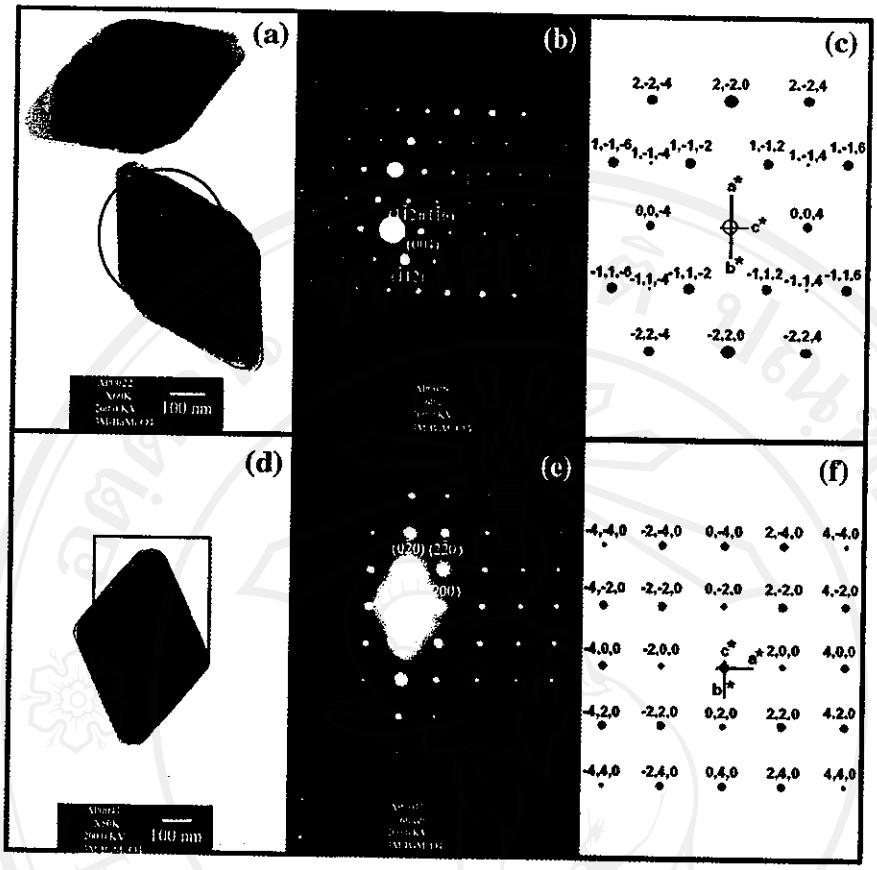

Fig. 4. TEM images, SAED and simulated patterns of $BaMoO_4$ [(b, c) and (e, f) are for a circle in (a) and a square in (d), respectively].

one translation mode (F_2) [13]. In lattice space, the symmetry is reduced to S_4. All degenerative vibrations are split [1,13] due to the crystal field effect and Davydov splitting [13]. For tetragonal scheelite primitive cell (wave vector, $k=0$) [13,14], there are 26 different vibrations ($\Gamma=3A_g+5A_u+5B_g+3B_u+5E_g+5E_u$) determined by group-theory calculation [1,13]. Among them, $3A_g$, $5B_g$ and $5E_g$ vibrations are Raman-active. Only $4A_u$ and $4E_u$ of the $5A_u$ and $5E_u$ vibrations are active in IR frequencies, and their remains ($1A_u$ and $1E_u$) are acoustic vibrations. The $3B_u$ vibrations are silent modes [1,13].

For the present research, six different vibrations were detected on Raman spectra (Fig. 3a). Among them, $\nu_1(A_g)$, $\nu_3(B_g)$, $\nu_3(E_g)$, $\nu_4(B_g)$, ν_2 (A_g) and $\nu_{f.r}(A_g)$ are at 872, 818, 776, 355, 320 and 188 cm^{-1} for $BaMoO_4$, 871, 829, 780, 362, 325 and 184 cm^{-1} for $SrMoO_4$, and 875, 843, 793, 391, 324 and 205 cm^{-1} for $CaMoO_4$, respectively. Each vibration mode is in accord with Raman vibrations analyzed by other researchers [1,13]. The spectra provide the evidence of scheelite structure for the three products [1,13]. In addition, FTIR spectra (Fig. 3b) were analyzed using a transmittance mode. For T_d-symmetry, $\nu_3(F_2)$ and ν_4 (F_2) are IR active and correspond to stretching and bending modes, respectively [3]. The spectra show a band of Mo–O stretching vibration in MoO_4^{2-} tetrahedrons [3] at 742–901 cm^{-1}. It is one of the internal modes specified as $\nu_3(F_2)$ antisymmetric stretching vibrations [3].

3.3. TEM and SAED

TEM images (Figs. 4a,d and 5) show different morphologies for different products although they were prepared using the same conditions. They consist of micro-sized bi-pyramids with a square base and their apexes of 651 nm apart for $BaMoO_4$, nano-sized particles in clusters for $SrMoO_4$, and dispersed nano-sized particles for $CaMoO_4$. A diffraction pattern (Fig. 4b) of $BaMoO_4$ at a circle in Fig. 4a was interpreted [12]. It appears as a periodic array of bright spots due to the diffraction of electron through crystallographic planes of the product. It shows that each of bi-pyramidal particles is single crystal. Both of the calculated angles between any pair of the directions belonging to these planes, and interplanar spaces determined from (hkl) are in accord with those of the diffraction pattern on the film. The pattern compose of a number of spots corresponding to (−112), (1−12), (004) and (1−16) planes of the crystalline particles, and was specified as $BaMoO_4$ [2]. The incident beam of electron might not be exactly perpendicular to the planes leading to the asymmetric diffraction pattern. Calculated zone axis [12] is in the [−1−10] direction which is parallel or nearly parallel to the electron beam. By using [−1−10] direction as zone axis, a diffraction pattern (Fig. 4c) for $BaMoO_4$ was simulated [15]. The pattern is symmetric and systematic. It is in good accord with the experimental result. Another diffraction pattern (Fig. 4e) at a square in Fig. 4d was also interpreted [12]. It corresponds to (0–20), (2–20) and (200) planes of the product which was specified as $BaMoO_4$ [2] with single crystal. Its zone axis is in the [001] direction. It is in good accord with the simulated pattern (Fig. 4f). In case of $SrMoO_4$ and $CaMoO_4$, the diffraction patterns (Fig. 5) show several concentric rings characterized as polycrystals. Each of them composes of a number of nano-sized crystals. They are so tiny that the analysis of a single crystal is not possible. Interplanar spaces were

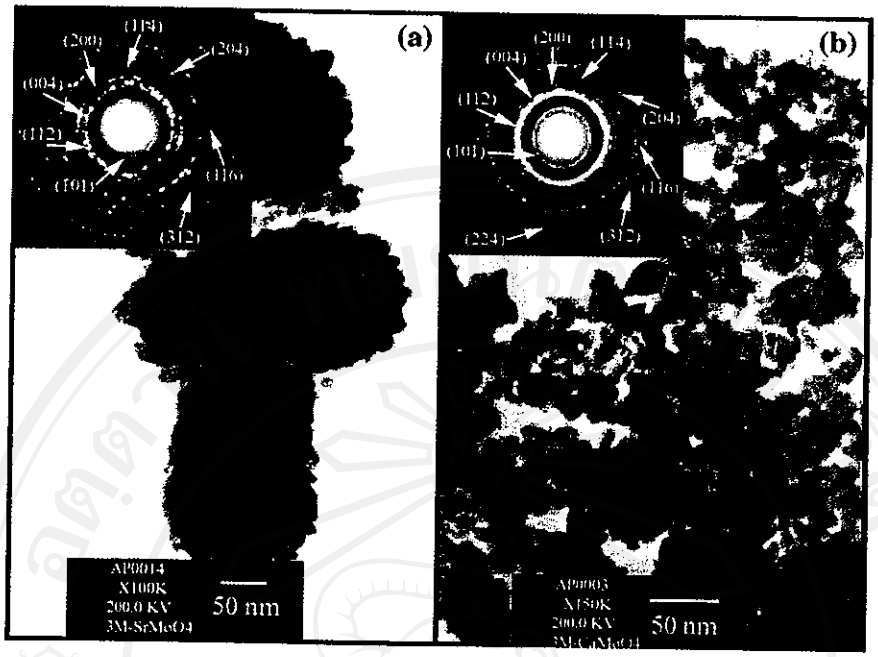

Fig. 5. TEM images and SAED patterns of (a) $SrMoO_4$ and (b) $CaMoO_4$.

calculated [16,17] using diameters of the diffraction rings, and compared with those of the JCPDS software [2]. Both patterns correspond to (101), (112), (004), (200), (114), (204), (116) and (312) planes. Additional (224) plane was detected in Fig. 5b. The patterns were specified as $SrMoO_4$ and $CaMoO_4$.

4. Conclusions

$MMoO_4$ (M=Ba, Sr and Ca) were successfully synthesized using a cyclic microwave radiation. Each of them is pure phase, and composes of micro-sized bi-pyramids with a square base for $BaMoO_4$, nano-sized particles in clusters for $SrMoO_4$, and dispersed nano-sized particles for $CaMoO_4$. The products provide the evidence of scheelite structure with Mo–O stretching vibration in MoO_4^{2-} tetrahedrons at 742–901 cm^{-1}.

Acknowledgement

The research was supported by the Thailand Research Fund, Bangkok, Thailand.

References

[1] S.P.S. Porto, J.F. Scott, Phys. Rev. 157 (1967) 716.
[2] Powder Diffract. File, JCPDS Internat. Centre Diffract. Data, PA 19073–3273, U.S.A. (2001).
[3] A.P. de Azevedo Marques, D.M.A. de Melo, C.A. Paskocimas, P.S. Pizani, M.R. Joya, E.R. Leite, E. Longo, J. Solid State Chem. 179 (2006) 671.
[4] J.H. Ryu, J.W. Yoon, C.S. Lim, K.B. Shim, Mater. Res. Bull. 40 (2005) 1468.
[5] Y. Wang, J. Ma, J. Tao, X. Zhu, J. Zhou, Z. Zhao, L. Xie, H. Tian, Ceram. Int. 33 (2007) 693.
[6] Y. Zhang, F. Yang, J. Yang, Y. Tang, P. Yuan, Solid State Commun. 133 (2005) 759.
[7] J.H. Ryu, J.W. Yoon, C.S. Lim, W.C. Oh, K.W. Shim, J. Alloys Comp. 390 (2005) 245.
[8] A. Sen, P. Pramanik, Mater. Lett. 50 (2001) 287.
[9] P. Parhi, S.S. Singh, A.R. Ray, A. Ramanan, Bull. Mater. Sci. 29 (2006) 115.
[10] C. Zhang, E. Shen, E. Wang, Z. Kang, L. Gao, C. Hu, L. Xu, Mater. Chem. Phys. 96 (2006) 240.
[11] V. Thangadurai, C. Knittlmayer, W. Weppner, Mater. Sci. Eng., B 106 (2004) 228.
[12] T. Thongtem, A. Phuruangrat, S. Thongtem, Mater. Lett. 61 (2007) 3235.
[13] T.T. Basiev, A.A. Sobol, Y.K. Voronko, P.G. Zverev, Optic. Mater. 15 (2000) 205.
[14] A. Golubović, R. Gajić, Z. Dohčević-Mitrović, S. Nikolić, J. Alloys Comp. 415 (2006) 16.
[15] C. Boudias, D. Monceau, CaRIne Crystallography 3.1, 17 rue du Moulin du Roy, F-60300 Senlis, France, (1989-1998).
[16] T. Thongtem, A. Phuruangrat, S. Thongtem, Mater. Lett. 60 (2006) 3776.
[17] T. Thongtem, S. Kaowphong, S. Thongtem, J. Mater. Sci. 42 (2007) 3923.

Available online at www.sciencedirect.com
ScienceDirect
Current Applied Physics 8 (2008) 189–197
Current Applied Physics
An official journal of the KPS
www.elsevier.com/locate/cap
www.kps.or.kr

Preparation and characterization of nanocrystalline $SrWO_4$ using cyclic microwave radiation

Titipun Thongtem [a,*], Anukorn Phuruangrat [b], Somchai Thongtem [b]

[a] Department of Chemistry, Faculty of Science, Chiang Mai University, Chiang Mai 50200, Thailand
[b] Department of Physics, Faculty of Science, Chiang Mai University, Chiang Mai 50200, Thailand

Received 29 April 2007; received in revised form 28 May 2007; accepted 3 August 2007
Available online 17 August 2007

Abstract

Nanocrystalline $SrWO_4$ was successfully prepared using $SrCl_2$ and Na_2WO_4 in ethylene glycol at different pH values, microwave powers and prolonged times. The phase was detected using XRD and SAED. TEM, HRTEM, SEM and particle size distribution revealed the presence of nano-sized crystals with their crystallographic planes aligning in systematic order. Raman and FTIR spectra provide the evidence of scheelite structure with W–O stretching vibration in WO_4^{2-} tetrahedrons at 781–912 cm^{-1}. PL emission of the products is considered to be from the $^1T_2 \rightarrow {}^1A_1$ transition of electrons within $[WO_4]^{2-}$ tetrahedrons at 420–428 nm (2.901–2.956 eV).

PACS: 81.16.Be; 81.07.Bc

Keywords: Cyclic microwave radiation; Nanocrystalline; $SrWO_4$

1. Introduction

Scheelite structured tungstates are specified as cubic close-packed array of M^{2+} cations and WO_4^{2-} anions. They belong to a body-centered tetragonal system and have C_{4h} point group with two formula units per primitive cell [1,2]. Typical scheelite structured tungstates are $CaWO_4$, $SrWO_4$, $BaWO_4$ and $PbWO_4$ [2–5]. They have attracted interest in a wide variety of applications such as laser host materials in quantum electronics and scintillators in medical devices [6], microwave applications [7], stimulated Raman scattering technique [8], humidity sensors [7] and catalysts [7]. They have luminescent property due to the electronic transition between oxygen and tungsten within tetrahedral WO_4^{2-} units [9]. $SrWO_4$ with different shapes and sizes was prepared by different methods, such as nano-particles, nano-peanuts, and nanorods with rough surface by a solvothermal – mediated microemulsion method [10], nanofilm on glass substrates by a reverse micelle system combined with dip-coating [11], hollow spheres by a precipitation reaction [12], and thin film on glass substrates by spray pyrolysis [2]. Other luminescent materials were $BaWO_4$ with olive-like, flake-like and whisker-like structures by hydrothermal process [3], nanocrystalline MWO_4 (M = Ca, Co, Ni, Cu and Zn) powders by evaporation of a polymer based metal-complex precursor solution [5], and nanocrystalline MWO_4 (M = Ca and Ni) by microwave-assisted synthesis with further calcination [7]. Sometimes, templates, surfactants and other additives were used to control the product morphologies.

Microwave radiation has very attractive attention used for preparing materials. It is able to reduce time scales of the reactions, and can rapidly lead to very high temperatures which have the influence to accelerate the reaction process. When microwave radiation is supplied to chemical solutions, one or more of the components dissolving in the solutions is capable of coupling with the radiation. It can lead to higher heating rate than that achieved by

* Corresponding author. Tel.: +66 (0) 53 943341; fax: +66 (0) 53 892277.
E-mail addresses: ttpthongtem@yahoo.com, ttpthongtem@hotmail.com (T. Thongtem).

1567-1739/$ - see front matter © 2007 Elsevier B.V. All rights reserved.
doi:10.1016/j.cap.2007.08.002

conventional method. Microwave radiation can solve the problems of temperature and concentration gradients. By focusing large amount of microwave radiation into the solutions, vibrating electric field applied a force on charged particles which vibrated accordingly. Vibrations of the reactants have the influence on the reaction to proceed with efficiency (shorter time and lower power). Subsequently, pure products were produced [13].

A polar solvent, which has permanent dipole moment, has relaxation process in microwave region. It is very good candidacy using in the process. Compounds with large permanent dipole moments also have large dielectric constants or relative permittivities [13], and are rapidly heated up by a microwave radiation [14]. When water (dielectric constant at 25 °C = 78.4 [15]) was used as a solvent, its temperature was about 110 °C by a microwave radiation within 1 min [14]. Ethylene glycol (dielectric constant at 25 °C = 40.3 [15] and T_b = 197 °C [16]) was heated up to about 120 °C within 3 min [16]. When relaxation time is one or two orders of magnitude different from that corresponding to the microwave frequency, the solvent is still to be an effective medium due to its large loss $\tan\delta$. The $90 - \delta$ is phase difference between electric field strength and current in the materials in which the loss energy develops as heat. For water (relaxation time = 9.04 ps) at 2.45 GHz microwave, $\tan\delta$ is only 0.1 [13]. It is good enough for using in the microwave process [13,17]. High boiling point solvents can prevent chemicals from overflowing. Therefore, solvents with $\tan\delta > 0.1$, such as ethylene glycol ($\tan\delta = 1.35$, relaxation time = 112.87 ps and T_b = 197 °C) is good choice for using in the microwave process [13,16].

For the present research, nanocrystalline $SrWO_4$ was prepared in ethylene glycol using different pH values, microwave powers and prolonged times without the requirement of any further calcination. No surfactants, complexing agents or other additives were used. The process is very simple, attractive and novel.

2. Experiment

Each of 0.005 mol $SrCl_2$ and Na_2WO_4 was dissolved in 30 ml ethylene glycol. The solution has a pH of 9.6 which was adjusted to the range of 3–13 using HCl or NaOH. The reactions cyclically proceeded at 180–600 W microwave powers for 20–80 min (10–40 cycles). One cycle is 2 min long and composes of irradiation and non-irradiation for 1 min each. Current temperatures at different microwave powers and prolonged times are shown in Fig. 1. At constant microwave power, the temperatures were increased with the increasing of the prolonged times. They tend to be constant after the first 10 min for 600, 450 and 300 W, and 20 min for 180 W.

To produce $SrWO_4$, $SrCl_2$ reacted with Na_2WO_4 dissolving in ethylene glycol by the use of a microwave radiation.

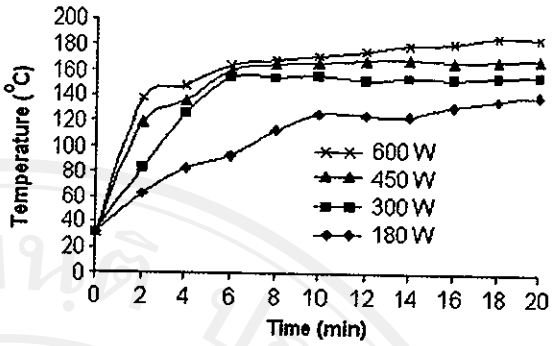

Fig. 1. Current temperatures at different microwave powers and prolonged times used for the present process.

$$SrCl_2 + Na_2WO_4 \xrightarrow[\text{microwave radiation}]{\text{ethylene glycol}} SrWO_4 + 2NaCl$$

The final products (precipitates) were washed with water and 95% ethanol, dried at 80 °C for 24 h, and characterized using XRD (SIEMENS D500) operated at 20 kV, 15 mA and using the Kα line from a Cu target, TEM (JEOL JEM-2010) and high resolution transmission electron microscopy (HRTEM) as well as the use of selected area electron diffraction (SAED) operated at 200 kV, SEM (JEOL JSM-6335 F) operated at 15 kV, Raman spectrometer (HORIBA JOBIN YVON T64000) using 50 mW Ar laser with $\lambda = 514.5$ nm, FTIR (BRUKER TENSOR27) with KBr as a diluting agent and operated in the range 400–4000 cm^{-1} and photoluminescence (PL) spectrometer (Perkin–Elmer LS50B) using a 270 nm exciting wavelength at room temperature.

3. Results and discussion

3.1. XRD

Comparing XRD spectra (Fig. 2) of the powdered products to that of the JCPDS software (reference code: 85-0587) [18]. They were specified as $SrWO_4$ with tetragonal crystal system and $I4_1/a$ space group. They have scheelite structure [2]. No other characteristic peaks of impurities were detected showing that the products prepared using a microwave radiation are pure phase. At 180 W for 20 min, no any product was produced using a solution with a pH of 3. The acidity seems to have the influence on the precipitation process. For the solutions with the pH of 5 and 7, broad spectra were detected showing that the products composed of very fine particles. The degree of crystalline products is low. The XRD peaks become sharper at higher pH values. At a pH of 9.6 for higher microwave powers and longer times, the spectra are very sharp showing that the products are very good crystals. Their strongest intensity peaks are at $2\theta = 27.6°$ and diffracted from (1 1 2) crystallographic planes.

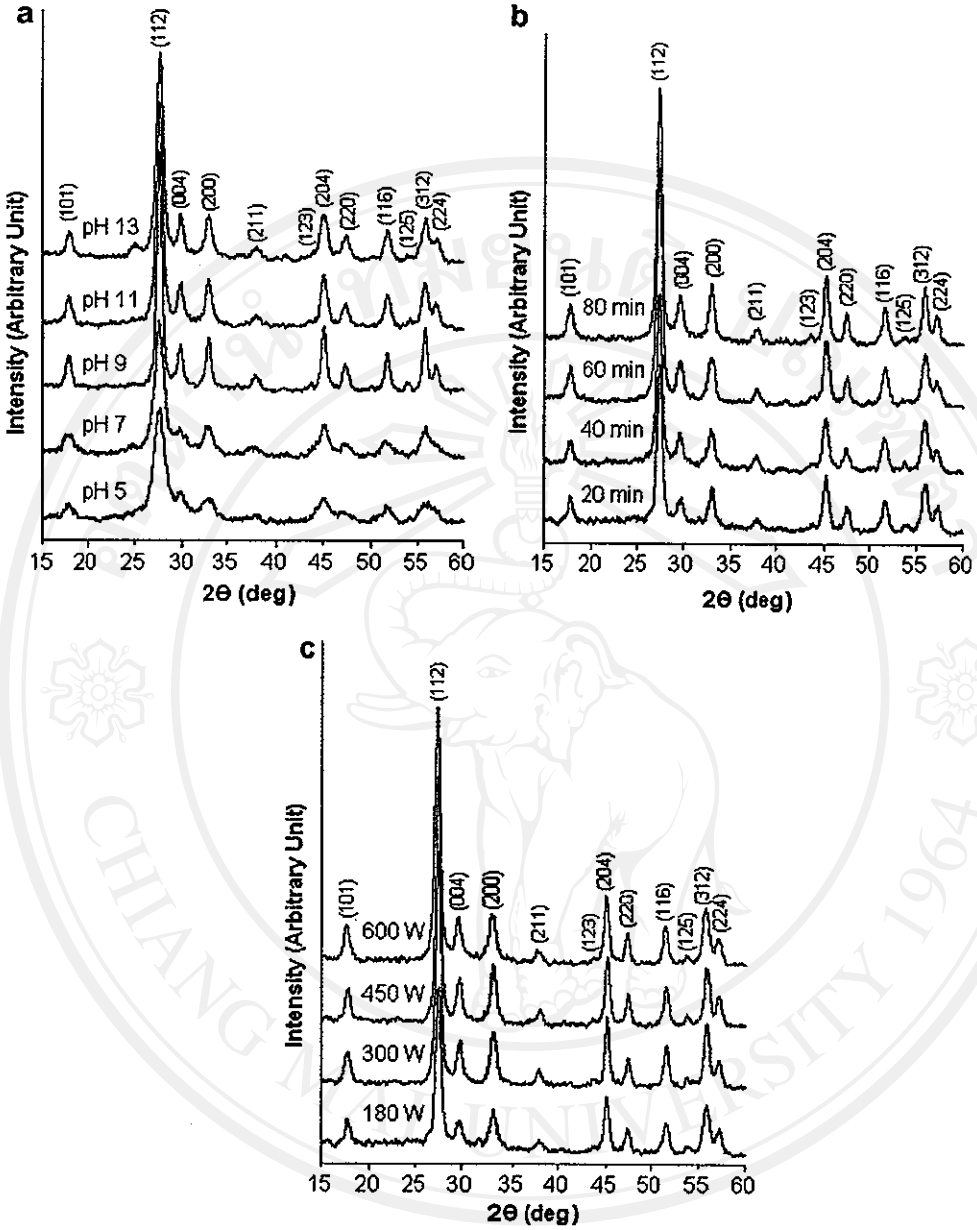

Fig. 2. XRD spectra of the products prepared using (a) 180 W for 20 min at different pH values, (b) 180 W at a pH of 9.6 for 20–80 min, and (c) a pH of 9.6 for 20 min at different microwave powers.

3.2. TEM, HRTEM, SEM and SAED

TEM images (Fig. 3) show nano-particles with different morphologies influenced by the microwave powers, prolonged times and pH values. At 180 W 20 min and pH 5, the product composes of <10 nm particles in clusters. Moiré fringes (e.g. marked with a square) were detected. They are the interference patterns between two crystallographic phases with slightly different lattice parameters [19]. Lattice planes (e.g. marked with a circle) were detected as well. They are crystallographic planes of the products. At 180 W 20 min and a pH of 9.6, the product composes of very fine particles in clusters. They appear as dark and grey contrast areas for the dense and less dense substances, respectively. When the pH was adjusted to 13, the product composes of nano-sized particles with oval shape in clusters. They are 219–381 nm long. Clearer morphology can be seen on SEM image (Fig. 4). These show that pH values play a role in the particle shapes and sizes.

In general, most polymeric anions formed in weekly acidic [20] and neutral solutions. Nucleation and growth rates of strontium tungstate particles were very low. Precipitates composing of very fine particles formed in small quantities. H^+ ions seemed to prevent the precipitation

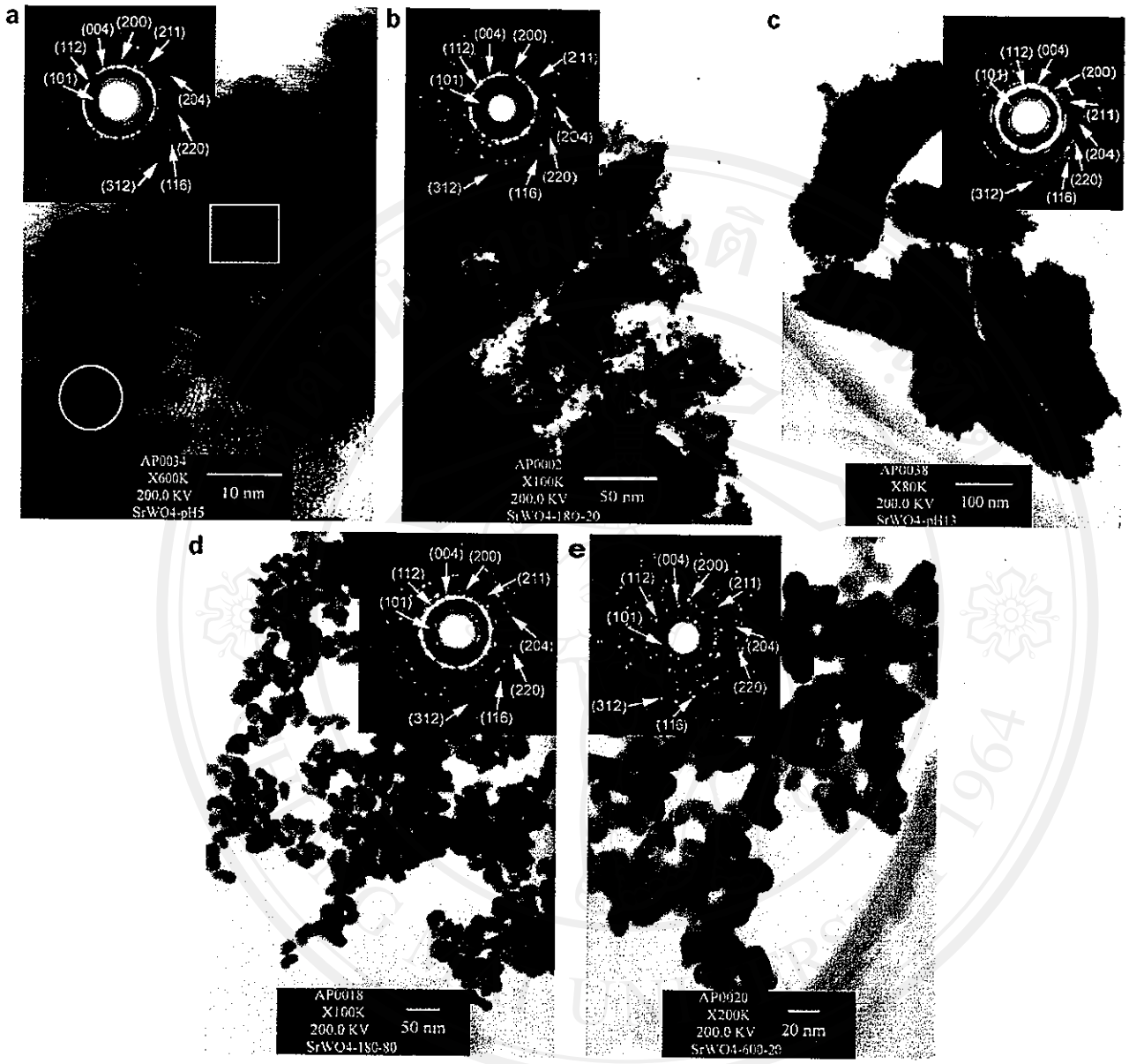

Fig. 3. TEM images and SAED patterns of the products prepared using (a) a pH of 5 at 180 W for 20 min, (b) a pH of 9.6 at 180 W for 20 min, (c) a pH of 13 at 180 W for 20 min, (d) a pH of 9.6 at 180 W for 80 min, and (e) a pH of 9.6 at 600 W for 20 min.

process. At higher pH values (weakly basic solutions), more precipitates were produced. The OH^- concentration was not sufficient to have the influence on growth directions. The particles became larger but were still nano-meter in size. In very strong basic solution, growth of the crystalline product was changed in such a way that different morphology formed. At the present stage, a number of OH^- ions selectively adsorbed on different crystallographic planes. The activities of the planes with sufficient OH^- ions were reduced, and growth rates in some certain directions were confined. These led to the anisotropic growth process. A number of nano-sized particles with oval shape formed. They were in clusters due to the attractive force among the different nano-sized particles.

For a pH of 9.6 and at 180 W microwave power, the particles became larger when the time was increased from 20 to 80 min. At pH 9.6 for 600 W and 20 min, the crystalline product became improved. The facets of the particles were detected. At a constant pH of 9.6, the particle sizes were measured along ten straight lines drawn in random directions. Their distributions are shown in Fig. 5. Average and standard deviation were then calculated. They were 3.39 ± 0.82, 18.42 ± 5.04 and 18.48 ± 4.32 nm for the products produced using 180 W 20 min, 180 W 80 min

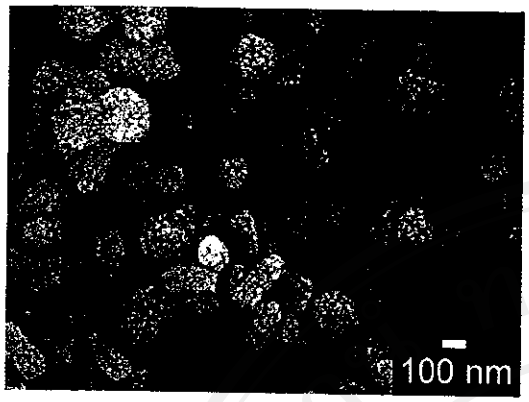

Fig. 4. SEM image of the product prepared in a solution with a pH of 13 using 180 W for 20 min.

and 600 W 20 min, respectively. Their particle sizes were increased with the increasing of the prolonged times and microwave powers.

HRTEM images of lattice planes (Fig. 6) for the products produced using different conditions were characterized. The images show that the crystallographic planes are aligned in systematic order although the products are not perfect crystals. They contain some defects. The (101), (112) and (004) planes were detected. Their interplanar spaces (d) were measured and are summarized in Table 1. The spaces are a little lower than those of the JCPDS software [18]. The differences are influenced by the temperature, stress, defects and others. SAED patterns (Fig. 3) show several concentric rings characterized as polycrystals. Interplanar spaces (d) were calculated [21,22] using their diffraction ring diameters, and compared with those of the JCPDS software [18]. They correspond to (101), (112), (004), (200), (211), (204), (220), (116) and (312) crystallographic planes of the products and were specified as $SrWO_4$. At 180 W for all the prolonged times and pH values, the inner rings are diffuse and continuous showing that the products compose of a number of nano-sized crystals. The degree of crystalline products is low. At 600 W, a clearer pattern was detected and composes of a number of bright spots arranged as discontinuous rings. At the present stage, the electron beam reflects and diffracts from polycrystals which become the largest at 600 W. Their coverage by the aperture is lesser in number leading to a greater degree of discontinuity in the diffraction rings. The present analyses show that the interpretations using XRD, SAED, TEM, HRTEM and SEM are in good accord.

3.3. Raman and FTIR spectra

Vibrations of $SrWO_4$ are classified into two types, the internal and external modes [23]. The first belongs to the

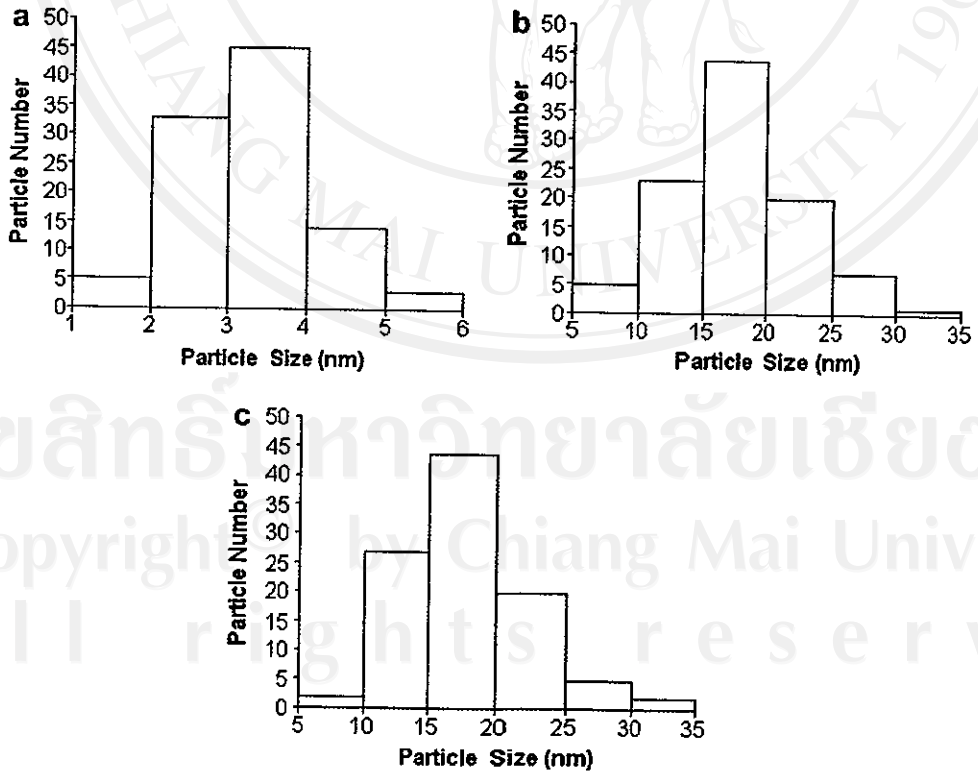

Fig. 5. Particle size distributions of the products prepared in a solution with a pH of 9.6 using (a) 180 W for 20 min, (b) 180 W for 80 min, and (c) 600 W for 20 min.

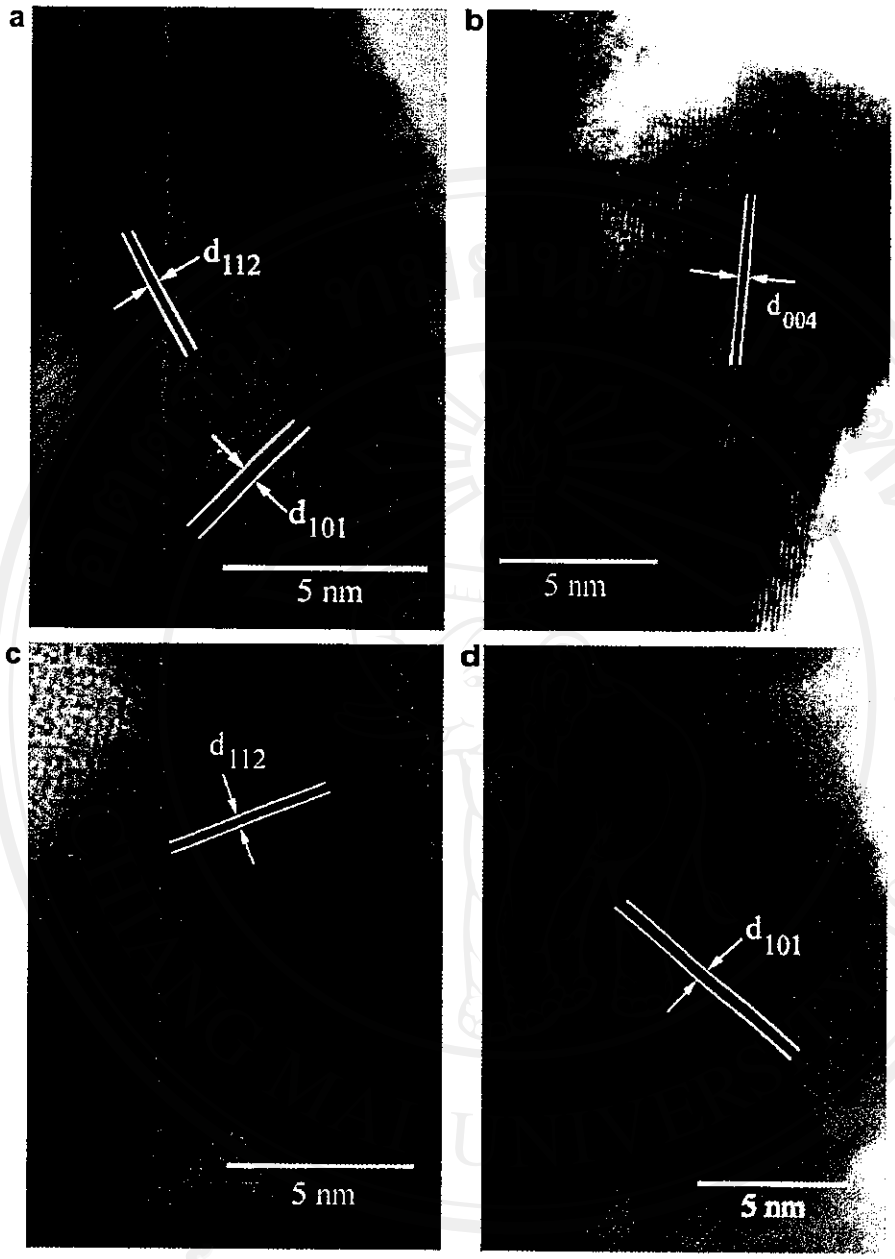

Fig. 6. HRTEM images of lattice planes for the products prepared using (a and b) a pH of 9 at 180 W for 20 min, (c) a pH of 9.6 at 180 W for 80 min, and (d) a pH of 9.6 at 600 W for 20 min.

vibration inside $[WO_4]^{2-}$ molecular units of which the centers of mass are stationary. The second is called lattice phonons which correspond to the motion of Sr^{2+} cations and the rigid molecular units. In free space, $[WO_4]^{2-}$ tetrahedrons have T_d-symmetry [23,24]. Their vibrations compose of four internal modes ($\nu_1(A_1)$, $\nu_2(E)$, ν_3 (F_2) and $\nu_4(F_2)$), one free rotation mode ($\nu_{f.r.}(F_1)$), and one translation mode (F_2) [23]. In lattice space, the symmetry is reduced to S_4. All degenerative vibrations are split [23,24] due to the crystal field effect and Davydov splitting [23]. For tetragonal scheelite primitive cell (wavevector, $\mathbf{k} = \mathbf{0}$) [1,23], there

Table 1
Interplanar spaces of the products prepared using different microwave powers, prolonged times and pH values

Preparation condition			Crystallographic plane	Interplanar space (nm)
Power (W)	Time (min)	pH		
600	20	9.6	101	0.4009
180	20	9	101	0.4255
	20	9	112	0.2837
	20	9	004	0.2727
	80	9.6	112	0.3030

are 26 different vibrations ($\Gamma = 3A_g + 5A_u + 5B_g + 3B_u + 5E_g + 5E_u$) determined by group-theory calculation [23,24]. Among them, $3A_g$, $5B_g$ and $5E_g$ vibrations are Raman-active. Only $4A_u$ and $4E_u$ of the $5A_u$ and $5E_u$ vibrations are active in infrared (IR) frequencies, and their remains ($1A_u$ and $1E_u$) are acoustic vibrations. The $3B_u$ vibrations are silent modes [1,23].

For the present research, six different vibrations were detected on Raman spectra (Fig. 7) of the products. Among them, $\nu_1(A_g)$, $\nu_3(B_g)$, $\nu_3(E_g)$, $\nu_4(B_g)$, $\nu_2(A_g)$ and $\nu_{f.r.}(A_g)$ are at 916.34, 832.48, 793.26, 371.01, 334.20 and 186.84 cm^{-1}, respectively. The vibration modes are very close to those for $SrWO_4$ with hollow spheres [12], $Sr_{1-x}Ca_xWO_4$ film [25] and $BaWO_4$ at 300 K [23]. The spectra provide the evidence of scheelite structure [12,23,25]. In addition, FTIR spectra (Fig. 8) of the products were analysed using a transmittance mode. For T_d-symmetry, $\nu_3(F_2)$ and $\nu_4(F_2)$ are IR active and correspond to stretching and bending modes, respectively [26,27]. The spectra show a band of W–O stretching vibration in WO_4^{2-} tetrahedrons [27] at 781–912 cm^{-1}. It is one of the internal modes specified as $\nu_3(F_2)$ antisymmetric stretching vibration [26]. The result is in accord with those of MWO_4 (M = Ca, Sr and Ba) [11,28]. Generally, vibration wavenumbers are influenced by atomic masses, force constant of lattice atoms, atomic bonding and others.

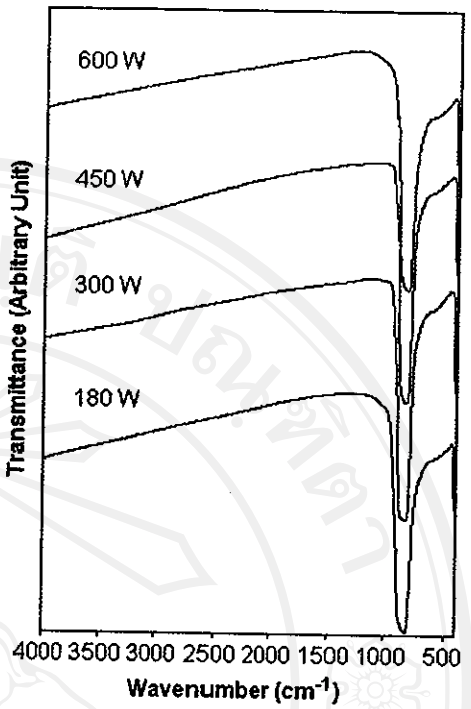

Fig. 8. FTIR spectra of the products prepared in a solution with a pH of 9.6 at different microwave powers for 20 min.

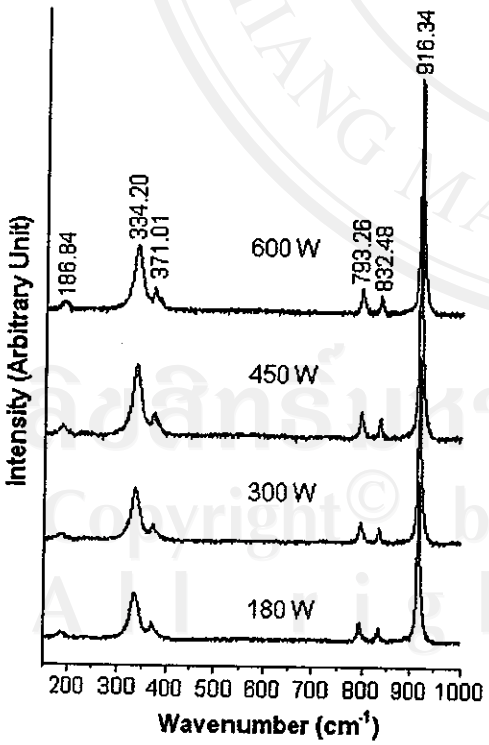

Fig. 7. Raman spectra of the products prepared in a solution with a pH of 9.6 at different microwave powers for 20 min.

3.4. PL spectra

The crystal-field splitting and hybridization of the molecular orbitals of $[WO_4]^{2-}$ tetrahedrons [4] are shown in Fig. 9. The W 5d(t_2) and W 5d(e) orbitals are hybridized with the O 2p(σ) and O 2p(π) ligand orbitals to form $[WO_4]^{2-}$ tetrahedrons. The four ligand p(σ) orbitals are compatible with the tetrahedral representation for a_1 and t_2 symmetries and the eight ligand p(π) orbitals are for t_1,

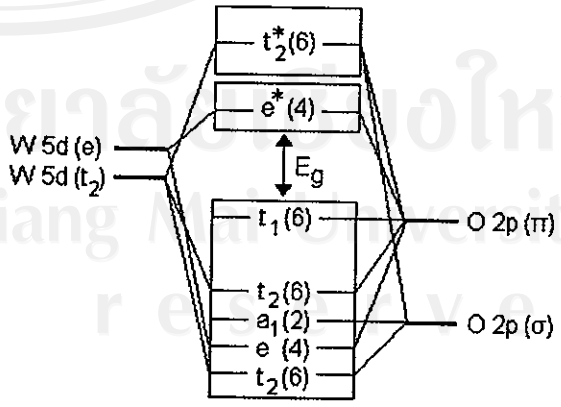

Fig. 9. Schematic diagram of the crystal-field splitting and hybridization of the molecular orbitals of $[WO_4]^{2-}$ tetrahedrons. [E_g = energy band gap, * = antibonding (unoccupied) states, and degeneracy of each cluster state is specified as the figures in brackets.]

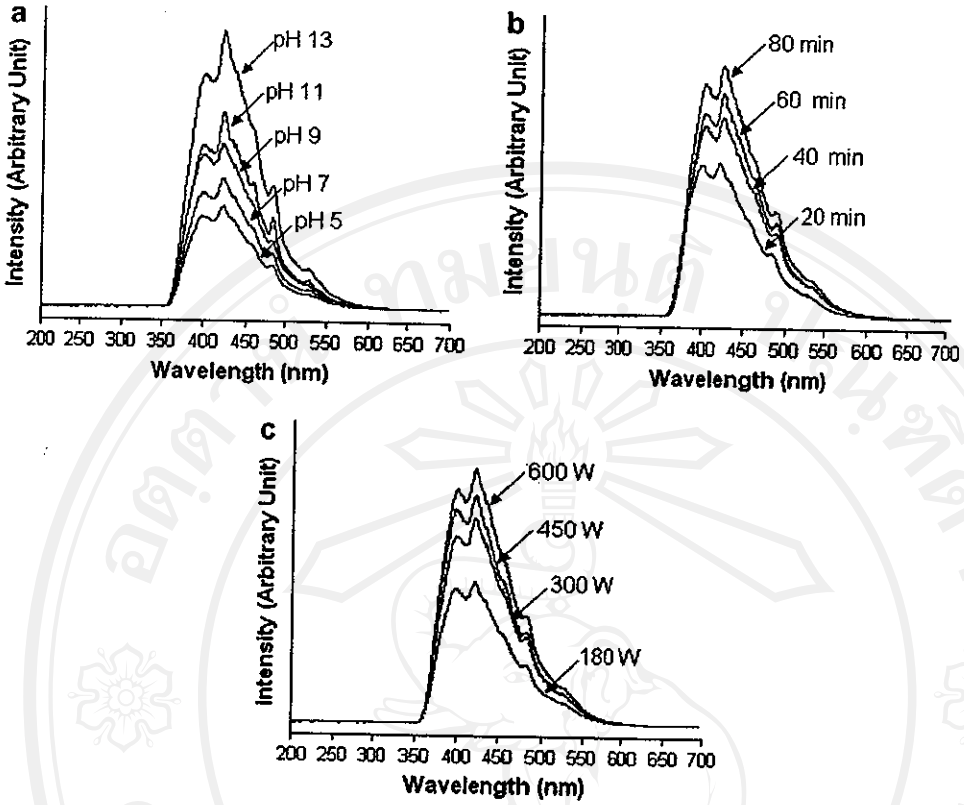

Fig. 10. PL spectra of the products prepared using (a) 180 W for 20 min at different pH values, (b) a pH of 9.6 at 180 W for different prolonged times, and (c) a pH of 9.6 for 20 min at different microwave powers.

t_2 and e symmetries. The top occupied state has t_1 symmetry formed from O 2p(π) states. The lowest unoccupied state has e symmetry formed from a combination of the W 5d(e) and O 2p(π) orbitals to give antibonding (*). The hybridization between the W 5d and O 2p orbitals is specified as covalent bonding between the ions. For ground state system, all one-electron states below band gap are filled to give a many-electron $^1A_1$ state. At the lowest excited state, there are one hole in t_1 (primarily O 2p(π)) state and one electron in e (primarily W 5d) state which give rise to many-electron $^1T_1$, $^3T_1$, $^1T_2$ and $^3T_2$ states. Among them, only $^1T_2 \rightarrow {}^1A_1$ transition is electric dipole allow [4,29].

By using a 270 nm exciting wavelength, PL spectra (Fig. 10) of the products were characterized. They show the narrow central peaks with their surrounding shoulders. The central (intrinsic) peaks are considered to be from the $^1T_2 \rightarrow {}^1A_1$ transition of electrons within $[WO_4]^{2-}$ anions [4,29,30]. The transition can be treated as an exciton [30]. The shoulders are from some defects and/or impurities, and interpreted as extrinsic transitions [30]. PL intensity is controlled by the number of charged transfers. For the present analysis, the emission peaks are in the blue spectral region at 420–428 nm (2.901–2.956 eV). Shapes, sizes, degree of crystal and other conditions can play a role in their emission peaks as well.

4. Conclusions

The advantages of microwave radiation are rapid, simple and efficient process used for producing nanocrystalline $SrWO_4$ in ethylene glycol at different microwave powers, prolonged times and pH values. All of the crystalline products are pure phase with scheelite structure and $I4_1/a$ space group. They compose of nano-sized particles and lattice planes in systematic array. The W–O stretching vibration in WO_4^{2-} tetrahedrons was detected at 781–912 cm^{-1}. Their emission peaks are due to the $^1T_2 \rightarrow {}^1A_1$ transition in WO_4^{2-} tetrahedrons at 420–428 nm (2.901–2.956 eV).

Acknowledgement

We would like to give thank to the Thailand Research Fund, Bangkok, for financial support.

References

[1] A. Golubović, R. Gajić, Z. Dohčević-Mitrović, S. Nikolić, J. Alloy. Compd. 415 (2006) 16–22.
[2] Z. Lou, M. Cocivera, Mater. Res. Bull. 37 (2002) 1573–1582.
[3] B. Xie, Y. Wu, Y. Jiang, F. Li, J. Wu, S. Yuan, W. Yu, Y. Qian, J. Cryst. Growth 235 (2002) 283–286.
[4] Y. Zhang, N.A.W. Holzwarth, R.T. Williams, Phys. Rev. B 57 (1998) 12738–12750.

[5] A. Sen, P. Pramanik, J. Eur. Ceram. Soc. 21 (2001) 745–750.
[6] B. Grobelna, B. Lipowska, A.M. Kłonkowski, J. Alloy. Compd. 419 (2006) 191–196.
[7] J.H. Ryu, J.W. Yoon, C.S. Lim, W.C. Oh, K.B. Shim, Ceram. Int. 31 (2005) 883–888.
[8] Z.C. Ling, H.R. Xia, D.G. Ran, F.Q. Liu, S.Q. Sun, J.D. Fan, H.J. Zhang, J.Y. Wang, L.L. Yu, Chem. Phys. Lett. 426 (2006) 85–90.
[9] V.B. Mikhailik, H. Kraus, D. Wahl, M. Itoh, M. Koike, I.K. Bailiff, Phys. Rev. B 69 (2004) 205110-1–205110-9.
[10] L. Sun, Q. Guo, X. Wu, S. Luo, W. Pan, K. Huang, J. Lu, L. Ren, M. Cao, C. Hu, J. Phys. Chem. C 111 (2007) 532–537.
[11] G. Zhang, R. Jia, Q. Wu, Mater. Sci. Eng. B 128 (2006) 254–259.
[12] X. Zhao, T.L.Y. Cheung, X. Zhang, D.H.L. Ng, J. Yu, J. Am. Ceram. Soc. 89 (2006) 2960–2963.
[13] C. Gabriel, S. Gabriel, E.H. Grant, B.S.J. Halstead, D.M.P. Mingos, Chem. Soc. Rev. 27 (1998) 213–223.
[14] R. He, X. Qian, J. Yin, Z. Zhu, J. Cryst. Growth 252 (2003) 505–510.
[15] S. Yin, M. Shinozaki, T. Sato, J. Lumin. 126 (2007) 427–433.
[16] J. Lu, Q. Han, X. Yang, L. Lu, X. Wang, Mater. Lett. 61 (2007) 2883–2886.
[17] J. Zhu, M. Zhou, J. Xu, X. Liao, Mater. Lett. 47 (2001) 25–29.
[18] Powder Diffract. File, JCPDS Internat. Centre Diffract. Data, PA 19073-3273, USA, 2001.
[19] K.I. Gnanasekar, H.A. Cathrino, J.C. Jiang, A.A. Mrse, G. Nagasubrahmanian, D.H. Doughty, B. Rambabu, Solid State Ion. 148 (2002) 299–309.
[20] F.A. Cotton, G. Wilkinson, C.A. Murillo, M. Bochmann, Advanced Inorganic Chemistry, 6th ed., John Wiley & Sons, New York, 1999, p. 925.
[21] T. Thongtem, A. Phuruangrat, S. Thongtem, Mater. Lett. 60 (2006) 3776–3781.
[22] A. Phuruangrat, T. Thongtem, S. Thongtem, Mater. Lett. 61 (2007) 3805–3808.
[23] T.T. Basiev, A.A. Sobol, Y.K. Voronko, P.G. Zverev, Opt. Mater. 15 (2000) 205–216.
[24] S.P.S. Porto, J.F. Scott, Phys. Rev. 157 (1967) 716–719.
[25] W.S. Cho, M. Yashima, M. Kakihana, A. Kudo, T. Sakata, M. Yoshimura, Appl. Phys. Lett. 68 (1996) 137–139.
[26] A.P. de Azevedo Marques, D.M.A. de Melo, C.A. Paskocimas, P.S. Pizani, M.R. Joya, E.R. Leite, E. Longo, J. Solid State Chem. 179 (2006) 671–678.
[27] G.M. Clark, W.P. Doyle, Spectrochim. Acta 22 (1966) 1441–1447.
[28] J.A. Gadsden, Infrared Spectra of Minerals and Related Inorganic Compounds, Butterworths, 1975, p. 152.
[29] M.J. Treadaway, R.C. Powell, J. Chem. Phys. 61 (1974) 4003–4011.
[30] V.B. Mikhailik, I.K. Bailiff, H. Kraus, P.A. Rodnyi, J. Ninkovic, Radiat. Measur. 38 (2004) 585–588.

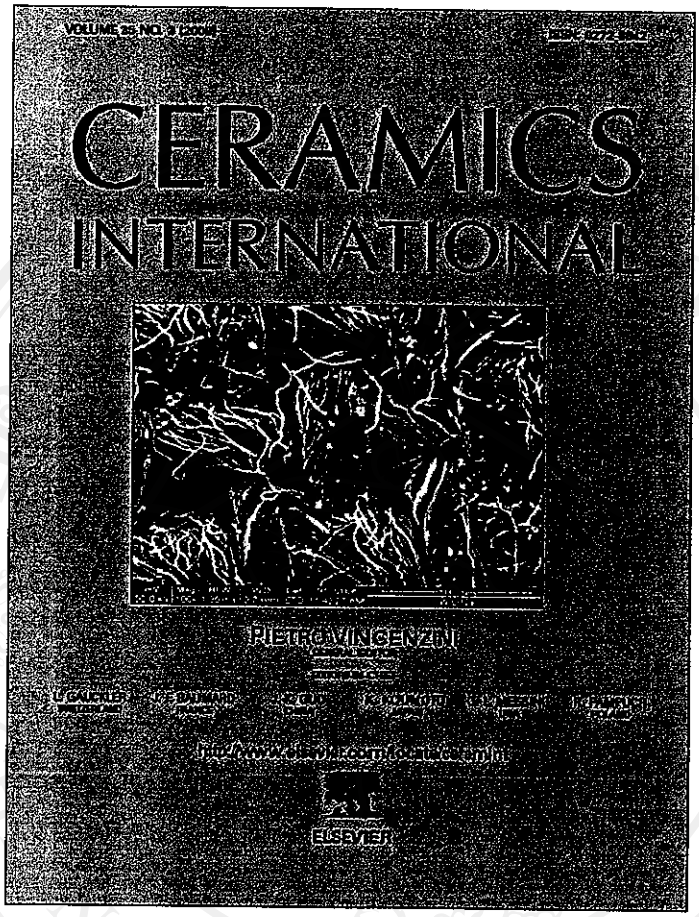

Available online at www.sciencedirect.com
ScienceDirect
Ceramics International 35 (2009) 1103–1108
CERAMICS INTERNATIONAL
www.elsevier.com/locate/ceramint

Sonochemical preparation of $PbWO_4$ crystals with different morphologies

Titipun Thongtem [a,*], Sulawan Kaowphong [b], Somchai Thongtem [b]

[a] Department of Chemistry, Faculty of Science, Chiang Mai University, Huay-Kaew Road, Chiang Mai 50200, Thailand
[b] Department of Physics, Faculty of Science, Chiang Mai University, Chiang Mai 50200, Thailand

Received 17 July 2007; received in revised form 15 February 2008; accepted 10 May 2008
Available online 19 July 2008

Abstract

$PbWO_4$ was prepared from $Na_2WO_4{\cdot}2H_2O$ and $Pb(OAc)_2{\cdot}3H_2O$ in a solution containing a cationic surfactant (*N*-cetyl pyridinium chloride) using the sonochemical process (ultrasonic irradiation). The product morphologies, characterized using scanning electron microscopy (SEM) and transmission electron microscopy (TEM), were controlled by the surfactant, pH values and ultrasonic irradiation times. X-ray diffraction (XRD) and selected area electron diffraction (SAED) studies revealed diffraction patterns in good agreement with the simulation model, along with Fourier transform infrared (FTIR) and Raman analyses showed a W–O stretching band consistent with tetragonal $PbWO_4$. Photoluminescent properties of the pine tree shaped products were also investigated.

Keywords: Lead tungstate; Sonochemical process; *N*-Cetyl pyridinium chloride; Pine tree shape

1. Introduction

$PbWO_4$ is one of the most interesting tungstates and it has found wide use in applications such as electromagnetic calorimetry, excitonic luminescence, thermoluminescence and stimulated Raman scattering behavior [1–3]. A variety of preparation processes have been used to produce different shapes and sizes which strongly affect the material's properties. These processes include synthesis with and without using organic additives, such as microemulsion-based synthesis [4,5], wet chemistry methods [3,6,7], microwave-assisted synthesis [8,9], sonochemical processes [2] and hydrothermal reactions [10]. Surfactants have been added in some of these processes and it is believed that they function as shape directors in product formations [6]. Other parameters, such as pH, temperature, prolonged reaction time and solvent system, can play a role in the formation of different shapes and sizes as well.

Several groups have reported the preparation of $PbWO_4$ using the sonochemical process that yields a variety of shapes: polyhedra, spindle-like and dot-shaped nanostructures [2], hollow spindle [11], and Sb(III)-doped single crystals [12]. The purpose of the present research was to sonochemically prepare $PbWO_4$ in a solution containing *N*-cetyl pyridinium chloride (a cationic surfactant) and classify and examine the resulting structures. The effects of pH and irradiation times on the morphologies have been investigated. An unusual pine tree shaped product, not previously reported from sonochemical studies, is a promising material that contains a number of defects having influence on the luminescent intensity [5].

2. Experiment

All chemicals were of reagent grade. Three solutions were prepared by separately dissolving 0.003 mol $Na_2WO_4{\cdot}2H_2O$, 0.005 mol *N*-cetyl pyridinium chloride (a cationic surfactant) and 0.003 mol $Pb(OAc)_2{\cdot}3H_2O$ in 20 ml de-ionized water each. The $Na_2WO_4{\cdot}2H_2O$ and *N*-cetyl pyridinium chloride solutions were mixed for 30 min under ultrasonic irradiation (sonochemical process). Then the $Pb(OAc)_2{\cdot}3H_2O$ solution was added and the pH was adjusted to be in the range of 3–11. Ultrasonic irradiation was carried out for 1–5 h, resulting in the gradual formation of white precipitates with different shapes and sizes. The crystals were washed with water and ethanol, and

* Corresponding author. Tel.: +66 53 941922x611; fax: +66 53 892277.
E-mail addresses: ttpthongtem@yahoo.com, ttpthongtem@hotmail.com (T. Thongtem).

0272-8842/$34.00
doi:10.1016/j.ceramint.2008.05.007

dried at 80 °C for 24 h for further analysis. The final products were analyzed using X-ray diffraction (XRD) operating at 20 kV, 15 mA, using the Kα line from a Cu target, transmission electron microscopy (TEM) as well as selected area electron diffraction (SAED) operated at 200 kV, scanning electron microscopy (SEM) operated at 15 kV, Fourier transform infrared (FTIR) with KBr as a diluting agent and operated in the range 400–4000 cm^{-1}, a Raman spectrometer using 50 mW Ar Laser with $\lambda = 514.5$ nm, and a luminescence spectrometer using a 300 nm exciting wavelength. In addition, diffraction patterns were simulated using CaRIne Crystallography 3.1 software [13] and compared with those interpreted from the experimental results.

3. Results and discussion

XRD spectra of all the products (Fig. 1) correspond to $PbWO_4$ with tetragonal stolzite structure [1,14]. Its space group is $I4_1/a$. The unit cell parameters are $a = b = 0.5445$ nm, $c = 1.2050$ nm, and $\alpha = \beta = \gamma = 90°$. The spectra diffracted from crystallographic planes of the products are (1 1 2), (0 0 4), (2 0 0), (1 2 1), (2 0 4), (2 2 0), (1 1 6), (3 1 2) and (2 2 4). The strongest intensity diffracted from (1 1 2) plane and is at $2\theta = 27.5°$. The spectra are very sharp showing that the product was composed of a number of crystals. No other characteristic peaks of impurities were detected showing that each product is a pure phase. By mixing $Na_2WO_4{\cdot}2H_2O$ and surfactant (positively charge), $(WO_4)^{2-}$ anions were possibly coordinated the surfactant molecules to form surfactant–tungstate complexes. The addition of $Pb(OAc)_2{\cdot}3H_2O$ into the solution containing the surfactant–tungstate complexes under the assistance of ultrasonic irradiation led to the substitution of the surfactant by Pb^{2+} cations. Once $PbWO_4$ nuclei (very fine particles) formed, they came together to form crystalline solids. The surfactant may have been selectively adsorbed onto the crystals [7] and possibly desorbed due to the ultrasonic irradiation, resulting in a particular shape from the anisotropic process.

SEM images of $PbWO_4$ are shown in Fig. 2. These are especially well-defined, complex and highly ordered. They are structurally similar to those prepared by wet chemical methods without sonication [15] but the current structures are more highly ordered. At the pH of 6.54 and for 1 h ultrasonic irradiation (Fig. 2a), the product is composed of six tree trunk like structures at right angle. Two pairs are in the same plane. One pair is shorter than the other. The third pair is at a right angle to the four-trunk structure. One trunk is on the top and the other is at the bottom. Sometimes the trunks were released by ultrasonic irradiation. The structure is complex, uniform and systematic. The trunks are in the shape of pine trees and have arrowhead-shaped tips. When the ultrasonic irradiation was prolonged (Fig. 2b–d), the trunks became longer. Some structures were broken and some side grains were released (marked with a circle in Fig. 2d). For the preparation without the use of a surfactant, the product (Fig. 2e) is in the shape of seaweed and resembles those of Liu et al. [15]. This demonstrates that *N*-cetyl pyridinium chloride plays the role in the product morphologies and functions as the shape director of the process. In addition, $PbWO_4$ crystals prepared using a variety of the pH values with 1 h irradiation (Fig. 2f–j) have different morphologies. They have corn-like shape for the pH of 3 and 5, pine tree structure for the pH 7, granular shape for the pH 9, and irregular shape and size particles in clusters for the pH 11. At the pH above 11, lead hydroxide complex instead of $PbWO_4$ is probably formed due to the high OH^- concentration. These results show that the pH value plays the role in the shape

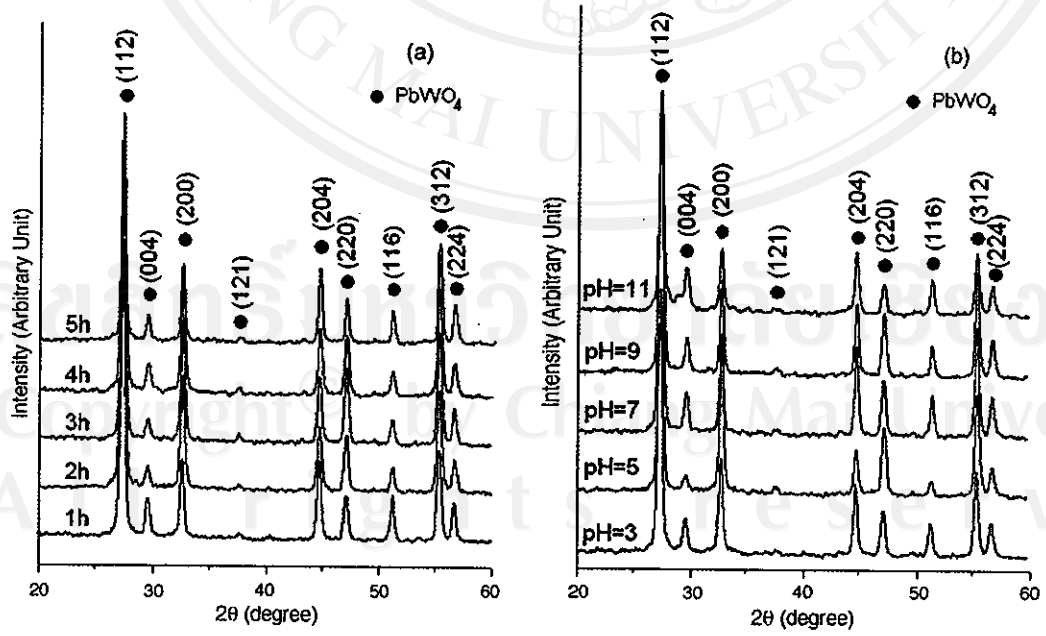

Fig. 1. XRD spectra of the products prepared in the solution containing *N*-cetyl pyridinium chloride using (a) the pH of 6.54 for different irradiation times and (b) the 1 h irradiation with different pH values.

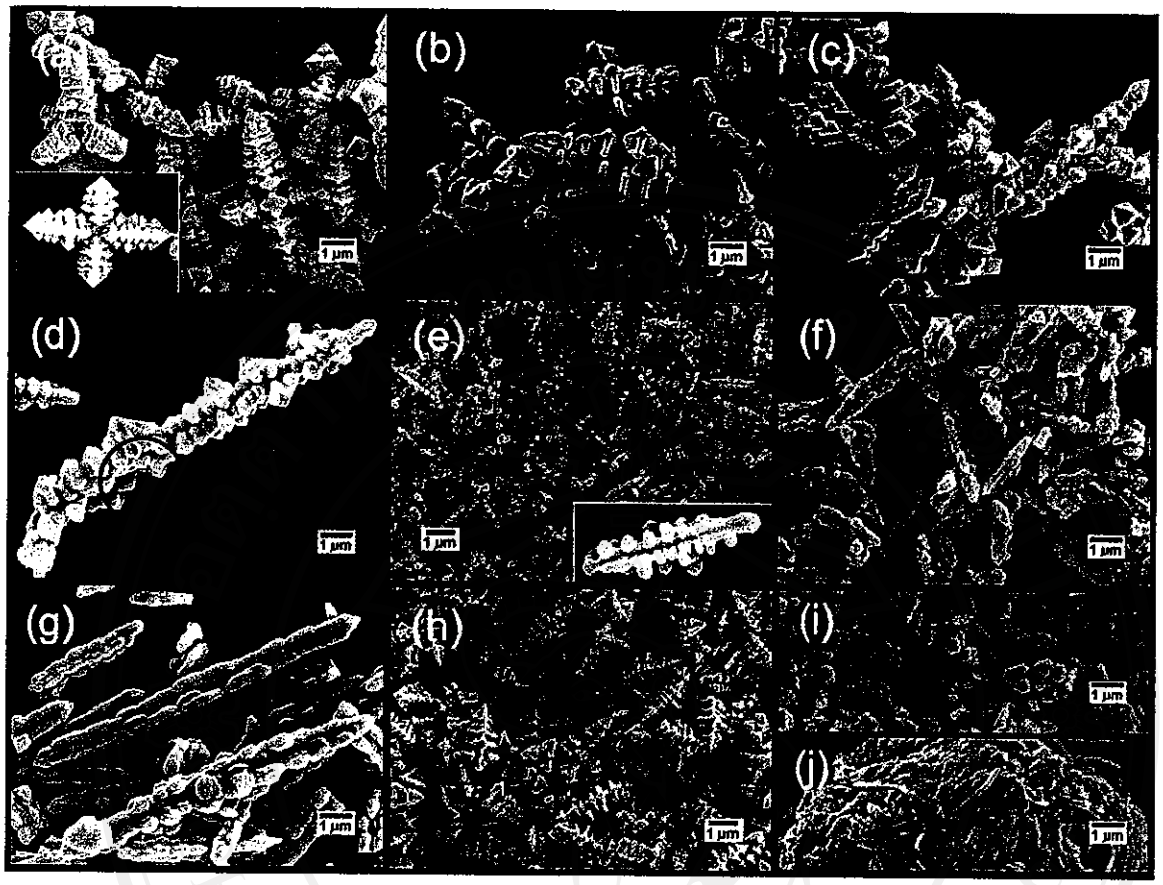

Fig. 2. SEM images of $PbWO_4$ prepared in (a–d) the solution containing *N*-cetyl pyridinium chloride (pH 6.54) with 1, 2, 3 and 5 h irradiations, (e) the surfactant-free solution (pH 6.26 and 1 h irradiation), and (f–j) the solution containing *N*-cetyl pyridinium chloride with the pH of 3, 5, 7, 9 and 11 (1 h irradiation), respectively.

and size of the products as well. At 1 h irradiation, the structures for the pH 6.54 (Fig. 2a) and 7 (Fig. 2h) are in the shape of a pine tree and are very similar.

Close examination of the TEM image of $PbWO_4$ prepared at pH 6.54 with 1 h of irradiation (Fig. 3a) shows the trunk of the product shaped like a pine tree which slopes up to a point. It has two halves that are the same in size and shape. SAED patterns (Fig. 3b and c) at two positions marked with a square and an ellipse on the product were interpreted [16–19]. The patterns correspond to $PbWO_4$ with tetragonal crystal system [14]. For the present research, zone axes [18–20] are in the [0 0 1] and [0 $\bar{1}$ 0] directions for the analyses at the square and ellipse, respectively. Each of them is parallel or nearly parallel to the electron beams. Diffraction patterns for $PbWO_4$ with [0 0 1] and [0 $\bar{1}$ 0] zone axes were simulated [13] and are shown in Fig. 3d and e. They are very symmetric and systematic. The a^*, b^* and c^* reciprocal lattice vectors for both patterns are in the [1 0 0], [0 1 0] and [0 0 1] directions, respectively. For one crystal structure, the corresponding lattice vectors are the same although their zone axes are different. Comparisons between the SAED and simulated patterns, they are in good accordance.

FTIR and Raman spectra of $PbWO_4$ with tetragonal stolzite structure are shown in Fig. 4. For the pH of 6.54 and different irradiation times (Fig. 4a), very strong W–O stretching bands of WO_4 tetrahedra were detected over the range 779–787 cm^{-1} [21–24]. O–H stretching and O–H bending bands of residual water were detected over the range 3302–3642 and 1654–1656 cm^{-1}, respectively. Comparisons to FTIR spectrum of *N*-cetyl pyridinium chloride (result not shown) reveal very weak bands of the surfactant at 2922 and 2852 cm^{-1}. At 1 h ultrasonic irradiation and different pH values (Fig. 4b), O–H stretching, O–H bending and W–O stretching bands were detected in the same way as the above. At the pH of 3, six vibrating bands of the surfactant were detected at 2922, 2852, 1631, 1486, 1175 and 478 cm^{-1}. The surfactant intensities decreased with the increase in the pH values. They were no longer detected at pH of 9 and 11. For pH 5, asymmetric and symmetric COO stretching bands of carboxylate group [25] were also detected at 1513 and 1410 cm^{-1}.

Raman spectra (Fig. 4c and d) revealed the presence of six vibrating bands over the range 100–1000 cm^{-1} although their morphologies are different. The $\nu_1(A_g)$, $\nu_3(B_g)$ and $\nu_3(E_g)$ specified as WO_4 stretching vibrations [2,22] were detected at 907.5, 768.5 and 752.7 cm^{-1}, respectively. The $\nu_1(A_g)$ has the strongest intensity. The $\nu_2(A_g)$ was detected as a strong band at 326.8 cm^{-1} with a weak band of $\nu_2(B_g)$ at 358.3 cm^{-1} [1,2]. They are the WO_4 bending vibrations [22,26]. The 176.9 cm^{-1} wavenumber is specified as a translational band of WO_4 groups

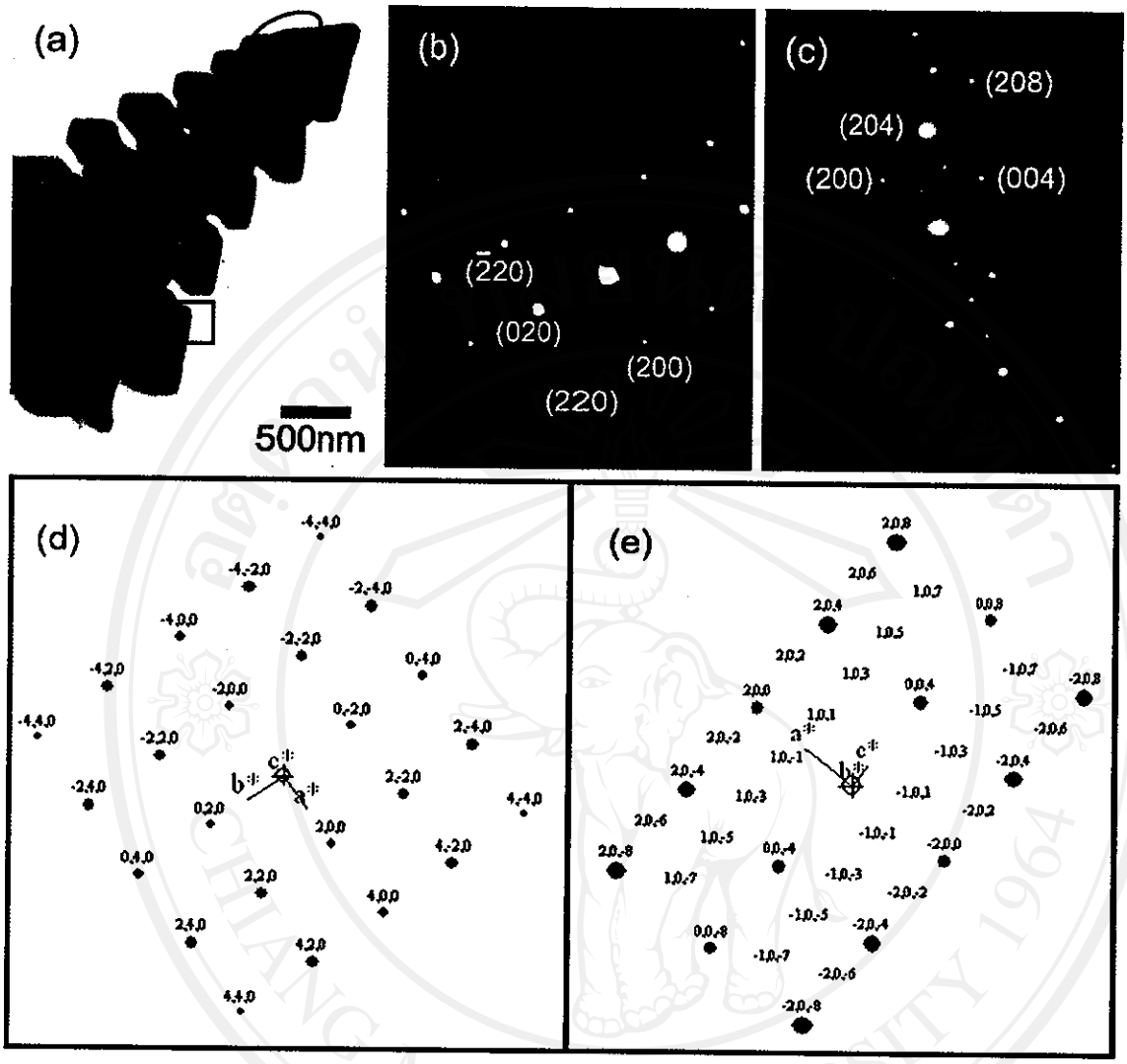

Fig. 3. (a) TEM image of $PbWO_4$ prepared in the solution containing *N*-cetyl pyridinium chloride (pH 6.54) with 1 h irradiation. (b–e) SAED and simulated patterns at the square and ellipse on the product, respectively.

[1,2]. There are some differences in the vibration frequencies, depending on the preparation processes and others.

The crystal-field splitting and hybridization of the molecular orbitals of $(WO_4)^{2-}$ tetrahedra [27] are shown in Fig. 5. The W 5d(t_2) and W 5d(e) orbitals are hybridized with the O 2p(σ) and O 2p(π) ligand orbitals to form $(WO_4)^{2-}$ tetrahedra. The four ligand p(σ) orbitals are compatible with the tetrahedral representation for a_1 and t_2 symmetries and the eight ligand p(π) orbitals are for t_1, t_2 and e symmetries. The top occupied state has t_1 symmetry formed from O 2p(π) states. The lowest unoccupied state has e symmetry formed from a combination of the W 5d(e) and O 2p(π) orbitals to give antibonding (*). The hybridization between the W 5d and O 2p orbitals is specified as covalent bonding between the ions. For ground state system, all one-electron states below band gap are filled to give a many-electron $^1A_1$ state. At the lowest excited state, there are one hole in t_1 (primarily O 2p(π)) state and one electron in e (primarily W 5d) state which give rise to many-electron $^1T_1$, $^3T_1$, $^1T_2$ and $^3T_2$ states. Among them, only $^1T_2 \rightarrow {}^1A_1$ transition is electric dipole allow [27,28].

For the present research, luminescence of the pine tree product is the strongest. Photoluminescent (PL) spectra of $PbWO_4$, the shape of a pine tree (Fig. 6), are very similar due to the similarity in the morphologies [5,8]. The PL emission is 415.5 nm wavelength due to the $^1T_2 \rightarrow {}^1A_1$ transition [27,28] of $(WO_4)^{2-}$ anions [8,9] in the blue range. The PL property is suitable for photoelectronic applications. Different morphologies can play the role in the difference of band gap and wavenumber. For instance, the emission wavenumbers of polyhedra, spindle-like and dot-shaped $PbWO_4$ nanostructures were detected at 493, 491 and 483 nm, respectively [2]. Dot-shaped $PbWO_4$ has the lowest wavenumber due to the smallest dimension. Crystallinity promotes PL intensity as well [2]. The polyhedral crystal is likely to contain the largest number of defects which lead to the highest PL intensity [2]. Comparing the macro- and nano-particles of $PbWO_4$, the first showed

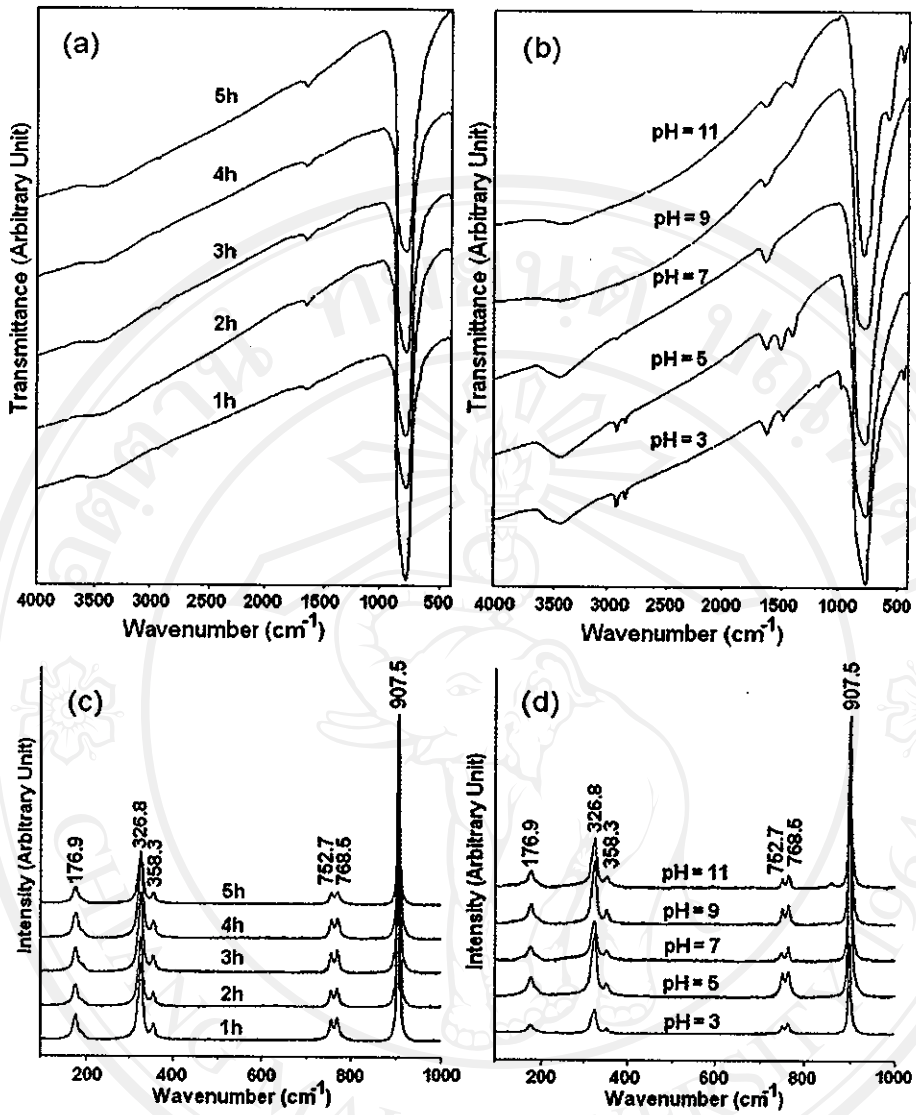

Fig. 4. (a and b) FTIR and (c and d) Raman spectra of $PbWO_4$ prepared in the solution containing *N*-cetyl pyridinium chloride using (a and c) the pH of 6.54 with 1–5 h irradiations, and (b and d) the 1 h irradiation with the pH of 3–11.

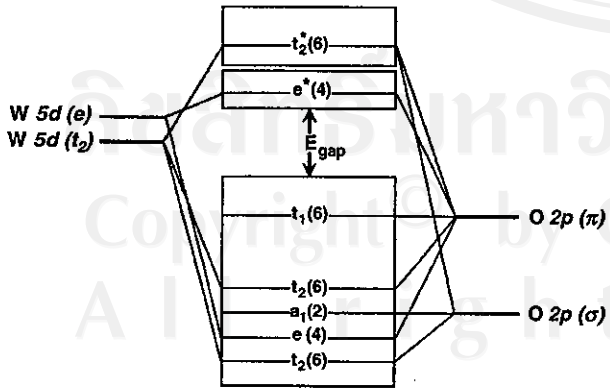

Fig. 5. Schematic diagram of the crystal-field splitting and hybridization of the molecular orbitals of $(WO_4)^{2-}$ tetrahedra. E_{gap} = energy band gap. *Antibonding (unoccupied) states. Degeneracy of each cluster state is specified as the figures in brackets [27].

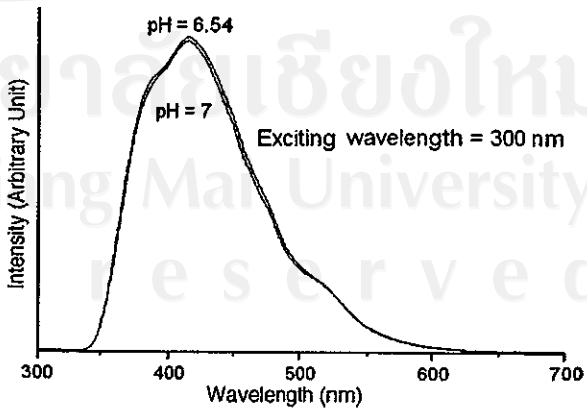

Fig. 6. PL spectra of $PbWO_4$ prepared in the solution containing *N*-cetyl pyridinium chloride using the pH of 6.54 and 7 with 1 h irradiation.

stronger blue emission than the second. The opposite is also true for the green emission [6]. The quantum sizes of particles influence their band gaps as well. For $CaWO_4$, band gap of bulk (2.95 eV, 421 nm) is smaller than that of nanofilm (3.03 eV, 409 nm) [21]. Photon energy emitted from the nanofilm is higher than that emitted from the bulk. It occurs a 12 nm blue-shift due to the quantum size effect [21].

4. Conclusions

$PbWO_4$ with different morphologies was successfully prepared from $Pb(OAc)_2{\cdot}3H_2O$, $Na_2WO_4{\cdot}2H_2O$ and *N*-cetyl pyridinium chloride by a sonochemical process. The final products, analyzed using XRD and SAED, were specified as pure $PbWO_4$ with tetragonal stolzite structure. SAED and simulated patterns are also in good agreement. The W–O stretching bands of WO_4 tetrahedra were detected by using FTIR at 779–787 cm^{-1} and Raman analysis at 907.5, 768.5 and 752.7 cm^{-1}. Their morphologies, characterized by SEM and TEM, were controlled by pH value, surfactant and irradiation times. They are corn-like, pine tree, granular and irregular in shape, depending on the reaction conditions. PL emission of the pine tree shaped products was detected at 415.5 nm due to the $^1T_2 \rightarrow {}^1A_1$ transition of $(WO_4)^{2-}$ tetrahedra.

Acknowledgements

We would like to give thank to the Thailand Research Fund (TRF), Commission on Higher Education (CHE), and Chiang Mai University (CMU) for financial support, and Dr. Richard Deming, Professor in Analytical Chemistry, Department of Chemistry and Biochemistry, California State University at Fullerton, California, U.S.A., for editorial assistance.

References

[1] J.Th. Kloprogge, M.L. Weier, L.V. Duong, R.L. Frost, Mater. Chem. Phys. 88 (2004) 438–443.
[2] J. Geng, J.J. Zhu, H.Y. Chen, Cryst. Growth Des. 6 (2006) 321–326.
[3] G. Zhou, M. L?, F. Gu, D. Xu, D. Yuan, J. Cryst. Growth 276 (2005) 577–582.
[4] L. Huo, Y. Chu, Mater. Lett. 60 (2006) 2675–2681.
[5] D. Chen, G. Shen, K. Tang, Zh. Liang, H. Zheng, J. Phys. Chem. B 108 (2004) 11280–11284.
[6] G. Zhou, M. L?, B. Su, F. Gu, Zh. Xiu, Sh. Wang, Opt. Mater. 28 (2006) 1385–1388.
[7] X.L. Hu, Y.J. Zhu, Langmuir 20 (2004) 1521–1523.
[8] J.H. Ryu, S.M. Koo, D.S. Chang, J.W. Yoon, Ch.S. Lim, Kw.B. Shim, Ceram. Int. 32 (2006) 647–652.
[9] J.H. Ryu, J.W. Yoon, Kw.B. Shim, Solid State Commun. 133 (2005) 657–661.
[10] Ch. An, K. Tang, G. Shen, Ch. Wang, Y. Qian, Mater. Lett. 57 (2002) 565–568.
[11] J. Geng, J.J. Zhu, D.J. Lu, H.Y. Chen, Inorg. Chem. 45 (2006) 8403–8407.
[12] J. Geng, D.J. Lu, J.J. Zhu, H.Y. Chen, J. Phys. Chem. B 110 (2006) 13777–13785.
[13] C. Boudias, D. Monceau, CaRIne Crystallography 3.1, 17 rue du Moulin du Roy, F-60300 Senlis, France, 1989–1998.
[14] JCPDS software, Powder Diffract. File, JCPDS Internat. Centre Diffract. Data, PA 19073-3273, U.S.A., reference code: 85-1857, 2001.
[15] B. Liu, S.H. Yu, L. Li, Q. Zhang, F. Zhang, K. Jiang, Angew. Chem. Int. Ed. 43 (2004) 4745–4750.
[16] K.W. Andrews, D.J. Dyson, S.R. Keown, Interpretation of Electron Diffraction Patterns, 2nd ed., Plenum Press, NY, 1971.
[17] B. Fultz, J. Howe, Transmission Electron Microscopy and Diffractometry of Materials, 2nd ed., Springer, 2002.
[18] T. Thongtem, A. Phuruangrat, S. Thongtem, Mater. Lett. 61 (2007) 3235–3238.
[19] T. Thongtem, A. Phuruangrat, S. Thongtem, Mater. Lett. 62 (2008) 454–457.
[20] B.D. Cullity, Elements of X-ray Diffraction, 2nd ed., Addison-Wesley Publ. Co., MA, 1978.
[21] G. Zhang, R. Jia, Q. Wu, Mater. Sci. Eng. B 128 (2006) 254–259.
[22] R.L. Frost, L. Duong, M. Weier, Spectrochim. Acta Part A 60 (2004) 1853–1859.
[23] J.A. Gadsden, Infrared Spectra of Minerals and Related Inorganic Compounds, Butterworths, England, 1975.
[24] G.M. Clark, W.P. Doyle, Spectrochim. Acta 22 (1966) 1441–1447.
[25] B. Smith, Infrared Spectral Interpretation, CRC Press, NY, 1999.
[26] Y. Huang, Hy.J. Seo, Q. Feng, Sh. Yuan, Mater. Sci. Eng. B 121 (2005) 103–107.
[27] Y. Zhang, N.A.W. Holzwarth, R.T. Williams, Phys. Rev. B 57 (1998) 12738–12750.
[28] M.J. Treadaway, R.C. Powell, J. Chem. Phys. 61 (1974) 4003–4011.

J Mater Sci (2007) 42:9316–9323
DOI 10.1007/s10853-007-1909-y

Synthesis and analysis of CuS with different morphologies using cyclic microwave irradiation

Titipun Thongtem · Anukorn Phuruangrat · Somchai Thongtem

Received: 10 March 2007 / Accepted: 31 May 2007 / Published online: 28 July 2007

Abstract Nano- and micro-sized CuS crystals were successfully synthesized from copper and sulfur sources ($CuCl_2 \cdot 2H_2O$, CuBr, $Cu(CH_3COO)_2 \cdot H_2O$, CH_3CSNH_2, $NH_2CSNHNH_2$ and NH_2CSNH_2) in ethylene glycol assisted by the cyclic irradiation of different microwave powers and prolonged times. By using XRD and SAED, CuS (hcp) was detected. The products characterized using SEM and TEM compose of assemblies of nano-flakes, clusters of nano-particles, nano-fibers, nano-rods and sponge-like structures influenced by the synthesized conditions. Their lattice vibrations are in the same Raman wavenumber at 474 cm^{-1}. Among the different products, the emission peaks are over the range 414–435 nm (2.85–2.99 ev). Reaction evidences of the sources were provided using FTIR. Phase and morphology formations are also proposed on according to the analytical results.

Introduction

Copper sulfides are the IB-VIA compounds. They have a wide varieties of compositions, ranging from S-rich (CuS_2) to Cu-rich (Cu_2S). CuS is an intermediate compound. It is very interesting due to its wide range of applications in optical and electrical devices, such as catalysts, solar cells and cathode materials in lithium rechargeable batteries [1]. It has metallic conduction property, and transforms into a superconductor below the 1.6 K [2]. Recently, copper sulfides with different morphologies have been synthesized. Among them are hollow spheres [1, 3], nanoparticles [4, 5], nanorods [6–8], nanoflakes [9], nanoplates [10], and nanocones and nanobelts [11]. There are different methods used for the synthesis, such as solid-state reaction [7], hydrothermal fabrication [2, 11], sonochemical synthesis [12], photochemical deposition [13] and microwave irradiation [4]. For the present research, nano- and micro-sized CuS crystals with different morphologies such as assemblies of nano-flakes, clusters of nano-sized particles, nano-fibers, nano-rods and sponge-like structures were successfully synthesized from different copper and sulfur sources in ethylene glycol by the cyclic exposure to microwave irradiation. No surfactants were used in the process, which is very simple and novelty.

Experiment

Each of 0.005 mole copper and sulfur sources was dissolved in 30 mL ethylene glycol and stirred for 30 min. The reactions cyclically proceeded using different microwave powers and prolonged times to produce products with different morphologies (Table 1). One cycle of 2 min prolonged time composes of irradiation and non-irradiation for 1 min each. Current temperatures at different microwave powers and prolonged times are shown in Fig. 1. At constant microwave power, the temperatures were increased with the increasing of the prolonged times within about the first 10 min. They tend to be constant afterwards. At the conclusion of the process, the final products were

T. Thongtem (✉)
Department of Chemistry, Faculty of Science, Chiang Mai University, Chiang Mai 50200, Thailand
e-mail: ttpthongtem@yahoo.com; ttpthongtem@hotmail.com

A. Phuruangrat · S. Thongtem
Department of Physics, Faculty of Science, Chiang Mai University, Chiang Mai 50200, Thailand

Table 1 Copper and sulfur sources, product codes and morphologies at different conditions

Copper and sulfur sources	Power (W)	Prolonged time (min)	Product codes	Morphologies
$CuCl_2 \cdot 2H_2O + CH_3CSNH_2$	180	10	CA1	Assemblies of nano-flakes (Micro-sized flowers)
	180	20	CA2	
	180	30	CA3	
	180	40	CA4	
	300	10	CA5	
	450	10	CA6	
	600	10	CA7	
$CuCl_2 \cdot 2H_2O + CH_3CSNH_2$	600	20	CA	Assemblies of nano-flakes (Micro-sized flowers)
$CuCl_2 \cdot 2H_2O + NH_2CSNHNH_2$	600	20	CC	
$CuCl_2 \cdot 2H_2O + NH_2CSNH_2$	600	20	CU	
$CuBr + CH_3CSNH_2$	600	20	BA	Clusters of nano-sized particles
$CuBr + NH_2CSNHNH_2$	600	20	BC	Nano-rods
$CuBr + NH_2CSNH_2$	600	20	BU	Sponge-like structures
$Cu(CH_3COO)_2 \cdot H_2O + CH_3CSNH_2$	600	20	AA	Assemblies of nano-flakes
$Cu(CH_3COO)_2 \cdot H_2O + NH_2CSNHNH_2$	600	20	AC	Nano-fibers
$Cu(CH_3COO)_2 \cdot H_2O + NH_2CSNH_2$	600	20	AU	Clusters of nano-sized particles

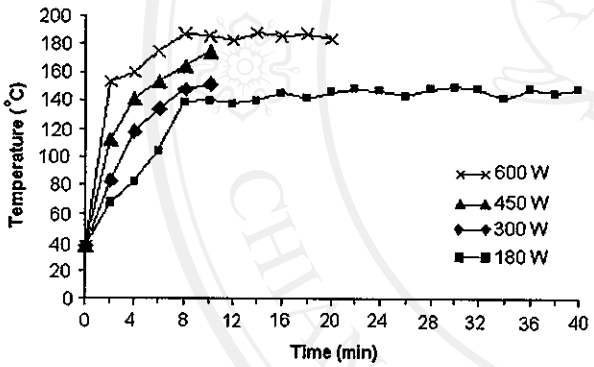

Fig. 1 Current temperatures at different microwave powers and prolonged times used for the present process

washed with water and ethanol, and dried at 80 °C for 12 h. Then, they were characterized using XRD operated at 20 kV, 15 mA and using the Kα line from a Cu target, SEM operated at 15 kV, TEM as well as the use of selected area electron diffraction (SAED) operated at 200 kV, FTIR with KBr as a diluting agent and operated in the range 400–4,000 cm^{-1}, Raman spectrometry using 50 mW Ar Laser with $\lambda = 514.5$ nm, and photoluminescence (PL) spectrometry using a 202 nm exciting wavelength.

Results and discussion

XRD

XRD spectra of the products (Fig. 2) synthesized using different conditions were analyzed and compared with that of the JCPDS software (reference code: 78–0876) [14]. When $CuCl_2 2H_2O$ and CH_3CSNH_2 were used as the starting agents, XRD spectra of the products synthesized at different prolonged times and microwave powers revealed the presence of pure CuS (hexagonal) with P63/mmc space group. No characteristic peaks arising from impurities such as CuO and Cu_2S were detected. The XRD peaks became higher and narrower with the increase in the prolonged times and microwave powers. These show that the crystalline products were improved. The prolonged times and microwave powers have the influence on the phase formation by assisting Cu and S atoms in violent vibrating and diffusing (higher amplitude) at longer time. The atoms have the better chance to reside in their normal lattices or in the periodic array. These lead to the increase in the degree or extent of the product crystalline. When one of the copper and sulfur sources were used at constant 20 min prolonged time and 600 W microwave power, pure CuS can be synthesized as well.

Phase formation

During the synthesis, $CuCl_2 2H_2O$ reacted with CH_3CSNH_2 in ethylene glycol for several steps and copper complex ($[Cu(CH_3CSNH_2)_2]^{2+}$) formed. Then, the complex was decomposed by microwave irradiation to produce CuS [4]. Due to the existence of crystal water in $CuCl_2 \cdot 2H_2O$ and trace water in ethylene glycol, CH_3CSNH_2 reacted with H_2O to form H_2S. Subsequently, H_2S was decomposed by the microwave irradiation [15, 16]. S^{2-} generated and further reacted with Cu^{2+} to produce CuS.

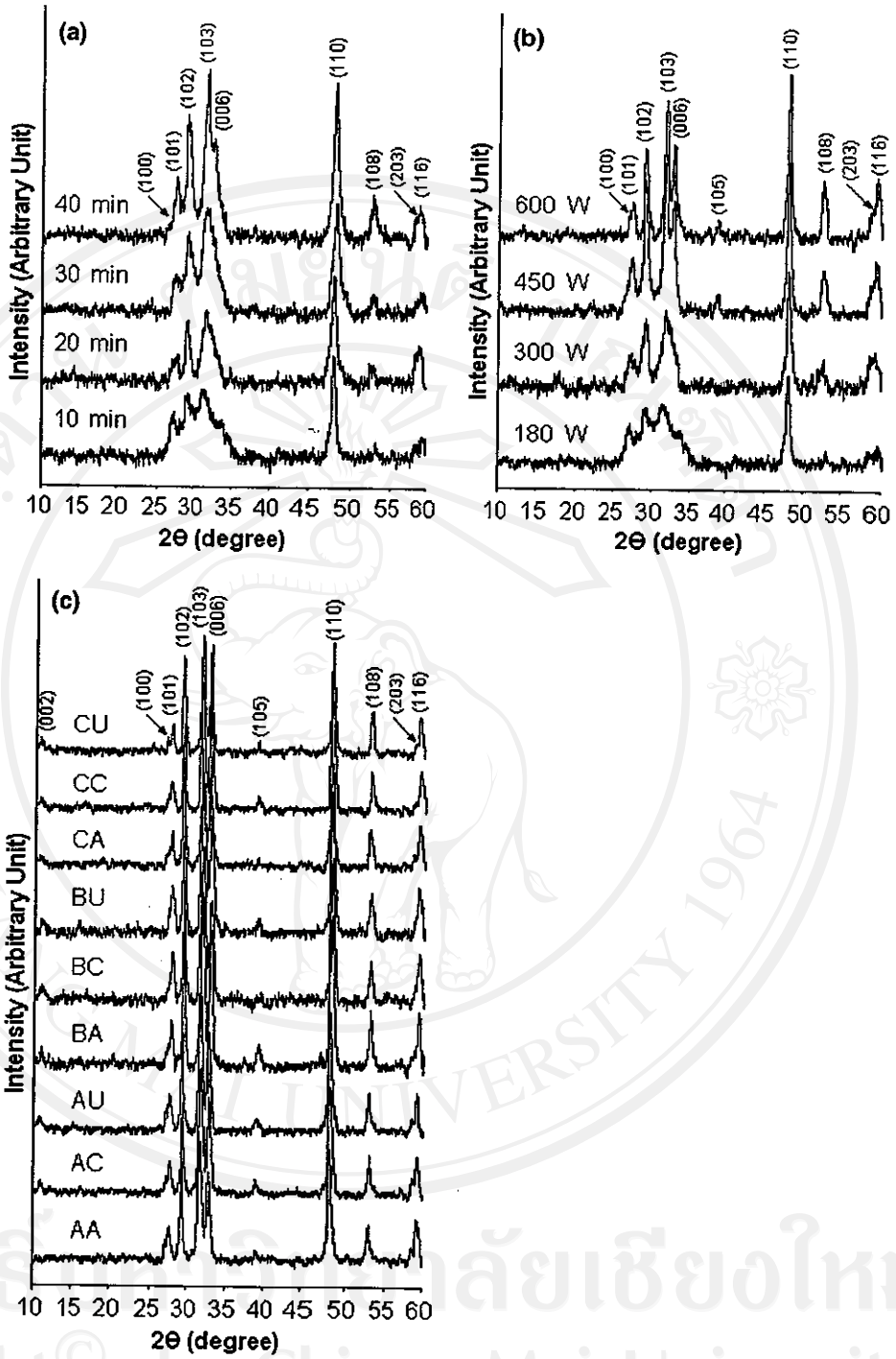

Fig. 2 XRD spectra of the products synthesized using different conditions (starting agents/microwave powers/ prolonged times). (a) $CuCl_2{\cdot}2H_2O$ and CH_3CSNH_2/ 180 W/10–40 min, (b) $CuCl_2{\cdot}2H_2O$ and CH_3CSNH_2/ 180-600 W/10 min, and (c) different starting agents/600 W/ 20 min

The reactions were similar to the above when $CuCl_2 \cdot 2H_2O$ was replaced by $Cu(CH_3COO)_2 \cdot H_2O$, and CH_3CSNH_2 by $NH_2CSNHNH_2$ or NH_2CSNH_2. In case of using CuBr as a copper source, Cu^{1+} is not stable in the solution. It can undergo disproportionation in which the oxidation state of Cu^{1+} is simultaneously raised and lowered [17].

$$2Cu^{1+} \longrightarrow Cu^{2+} + Cu^{0}$$

With the assistance of microwave irradiation, Cu^0 was further oxidized to Cu^{2+} by H_2S.

$$Cu^{0} \xrightarrow{\text{Microwave irradiation}} Cu^{2+} + 2e^{-}$$

Cu^{2+} combined with S^{2-} to produce CuS.

$$Cu^{2+} + S^{2-} \xrightarrow{\text{Microwave irradiation}} CuS$$

Reaction evidences between copper and sulfur sources were provided on according to the following. During the synthesizing process, copper and sulfur salts were separately dissolved in ethylene glycol and mixed. The precipitates (copper complexes) formed. Subsequently, they turned into black (CuS) in a microwave oven. In addition, pure thiourea (NH_2CSNH_2) and copper-thiourea complex were characterized using FTIR. Their spectra are shown in Fig. 3. For thiourea spectrum, bands of C = S and C–N stretching vibrations [18, 19], were detected at 735 and 1464 cm^{-1}, respectively. Corresponding bands of the complex were at 697 and 1494 cm^{-1}, respectively. Comparing to thiourea, the first vibration shows red-shift, which was caused by lowering in the wavenumber. It was characterized as the reduced double bond character of carbon and sulfur in the complex. The second is blue-shift due to the greater double bond character of carbon and nitrogen in the complex. It shows the presence of sulfur-copper coordination [19]. Three bands of NH_2 stretching vibrations of thiourea and the complex [19] were the same wavenumber at 3171, 3269 and 3373 cm^{-1}. Their NH_2 bending [18] is also the same wavenumber at 1600 cm^{-1}. The NH_2 stretching and bending vibrations are stationary. In the present case, no bonding between nitrogen and copper is present [18, 19]. Some difference in the intensity peak at 1104 cm^{-1} of thiourea and the complex was detected. When copper-thiourea complex was produced, the intensity peak in thiourea was diminished in the complex. It was influenced by a change in the nature of C = S and C–N bonds due to the complex formation [18].

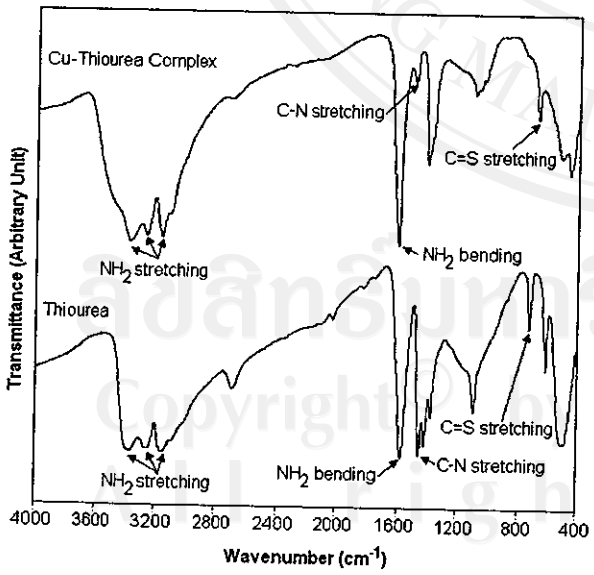

Fig. 3 FTIR spectra of thiourea and copper-thiourea complex

Microwave irradiation is at an advantage over other processes by solving the problems of concentration and temperature gradients in the solution. Its vibration frequency provides uniform condition for the nucleation and growth due to the rapid, uniform and effective heating process. It accelerates the reactions by assisting the decomposition of copper complexes and H_2S, the oxidation and reduction processes, and the formation of CuS.

SEM

Morphologies of the products synthesized using different prolonged times, microwave powers, and starting agents are summarized in Table 1, and SEM images of the selected products are shown in Fig. 4. For the synthesis process using $CuCl_2{\cdot}2H_2O$ and CH_3CSNH_2 as the starting agents at 180 W microwave powers for 10, 20, 30 and 40 min prolonged times, at 300, 450 and 600 W for 10 min, and at 600 W for 20 min, the products (CA1, CA2, CA3, CA4, CA5, CA6, CA7 and CA) are the assemblies of nano-flakes (micro-sized flowers). Both the flowers and flakes became larger at higher power and longer time. The flowers are 4.5 μm in diameters at 600 W and 20 min. A microwave oven supplies energy to the system, which was used to decompose the complexes and accelerate copper sulfide formation. Microwave powers and prolonged times did not have so strong influence on the product shapes as on the sizes.

At constant 600 W for 20 min with the same copper source ($CuCl_2 \cdot 2H_2O$) but different sulfur sources (CH_3CSNH_2, $NH_2CSNHNH_2$ and NH_2CSNH_2), the products (CA, CC and CU) are the assemblies of nano-flakes (micro-sized flowers) although the three sulfur sources are different. They compose of nano-flakes as the fundamental particles. It shows that $CuCl_2 \cdot 2H_2O$ dominated the sulfur sources. Product morphology was influenced by chloride ions in the system. Anions of the copper sources have the influence on growth of the particles. But for those synthesized using CuBr or $Cu(CH_3COO)_2 \cdot H_2O$ as copper sources with different sulfur sources, the products have a variety of morphologies. They are clusters of nano-sized particles, nanorods, sponge-like structures, assemblies of nano-flakes and

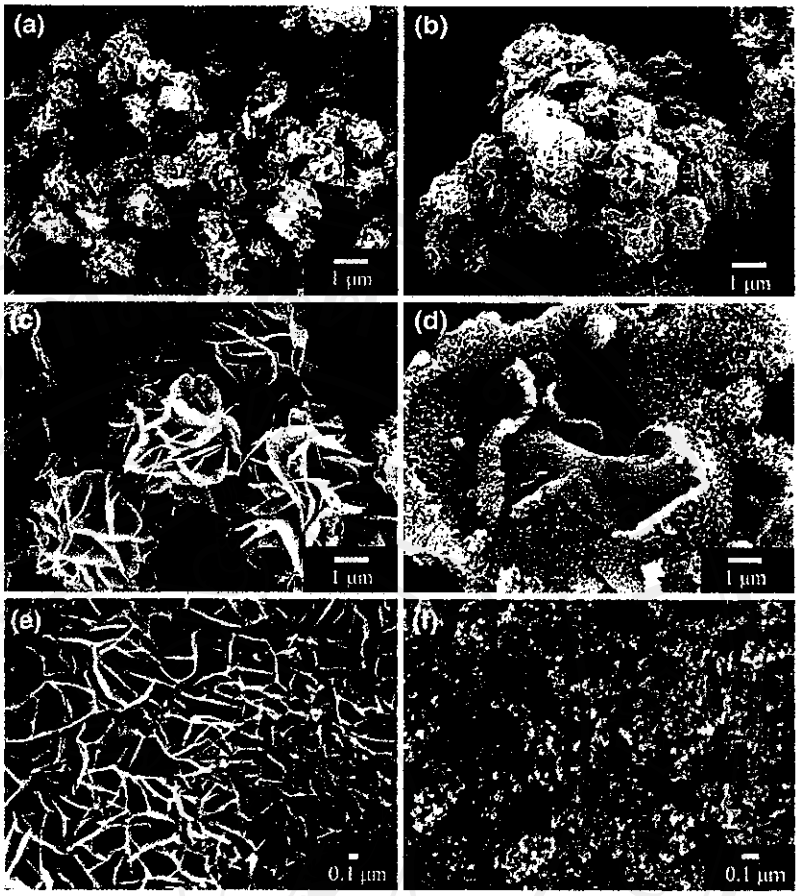

Fig. 4 SEM images of the products. (a–f) are CA1, CA7, CA, BU, AA and AU, respectively

nano-fibers for BA and AU, BC, BU, AA and AC, respectively. Different product morphologies were influenced by sulfur sources, which have different structure formulas. Nucleation and growth of the particles can play roles in the morphology. The crystal growth of some preferred structure or planes relates to the surface energy of the planes in the specified condition. It is described as the shape selective surface absorption process [20]. The amount of starting agents in the solution also has the influence on different orientation of the particles, which reflects nucleation and growth of the crystals. The orientation was increased with the increasing in the amount of starting agents [21]. Phase with the lowest free energy is thermodynamically stable, and has more chance to exist in the process [22]. This can reflect the product morphologies. Apart from the above, crystal growth is influenced by the solubility of the precursors in the particular solvent and synthesized temperature, which reflects the morphologies [20]. Polarities and boiling points of solvents [23], pH values of the solutions and others can play a role in the shapes and sizes due to the different rates of nucleation and growth.

Different starting agents play a significant role to produce the products with different shapes and sizes, which was influenced by nucleation and growth. They had more role than the microwave irradiation did.

During the formation of CuS, round particles were formed by the assemblage of hcp unit cells. Growths in the x-, y- and z- directions are almost at the same rates. Rod-shaped particles and fibers were formed by stacking up hcp unit cells. There were some unit cells stacked aside as well. To form rods and fibers, growth rate in the z-direction is the fastest. Flake-like particles were formed by the similar process as the rod/fiber formation but growth in the z-direction is the slowest.

The products may contain some imperfect round particles, curved rods/fibers and wavy flakes, due to the microwave vibration frequency, internal stress and others. Different morphologies have the influence on the luminescent property as well.

TEM and SAED

To show more details, the synthesized products were put into a beaker containing ethanol. After ultrasonic vibration,

the liquid was dropped on a copper grid and dried in ambient atmosphere. TEM images and SAED patterns (Fig. 5) of the selected products were characterized and analyzed. They compose of round nano-particles with <20 nm in diameter for BA and AU, nano-rods with <20 nm in diameter for BC, and nano-fibers with as long as 105 nm for AC.

SAED patterns show eight concentric rings corresponding to diffraction planes of the crystalline products. Diameters of the rings were measured from the diffraction patterns on the films. The values of d-spacing of the diffraction planes were calculated [24, 25] and compared with those of the JCPDS software [14]. The diffraction patterns show that the products compose of CuS with hexagonal structure. The analyses interpreted from SAED and XRD patterns are in good accord. The diffraction planes of the products are (100), (103), (006), (105), (110), (108), (203) and (116). The rings are diffuse and hollow showing that the products composed of very fine particles.

Raman analysis

Raman spectra of different products (Fig. 6) are very sharp showing that lattice atoms are arranged in the periodic array. Vibration modes of the crystalline products synthesized from different starting agents are in the same wavenumber at 474 cm^{-1} corresponding to the lattice vibrations. The present results are in accord with those of CuS thin films [26, 27]. Generally, vibration frequency is a parameter controlled by atomic masses, force constant of lattice atoms, atomic bonding and others.

PL spectra

PL emission of CuS dispersed in absolute ethanol (Fig. 7) was determined using a 202 nm (6.14 ev) exciting wavelength. PL spectra of all the products show the broad emission peaks in the range 414–435 nm (2.85–2.99 ev). For each of the copper sources, the spectra show the

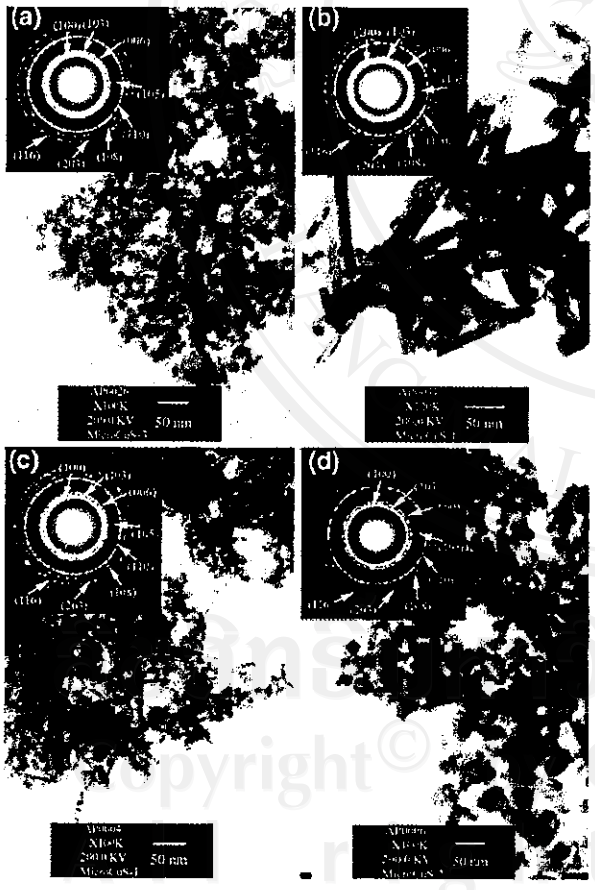

Fig. 5 TEM images and SAED patterns of the products synthesized at 600 W microwave power for 20 min prolonged time. (a–d) are BA, BC, AC and AU, respectively

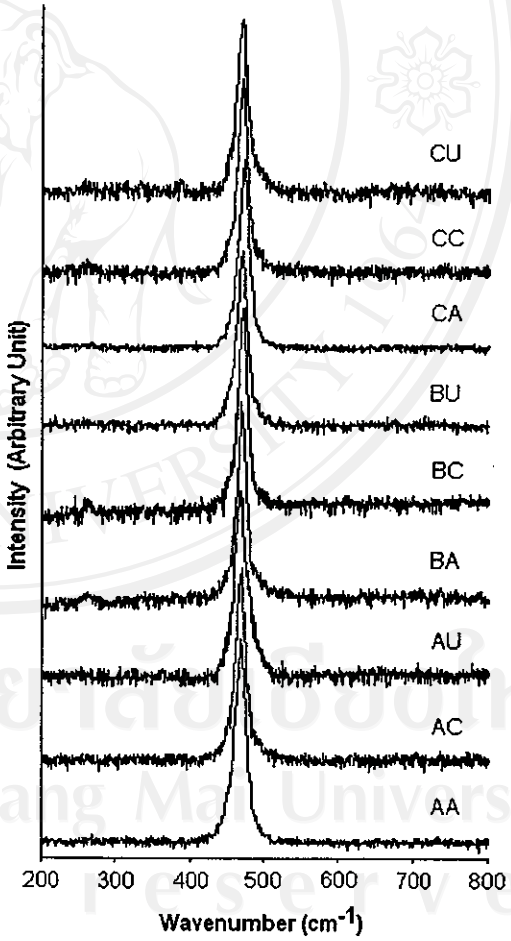

Fig. 6 Raman spectra of the products synthesized using different starting agents at 600 W microwave power for 20 min prolonged time

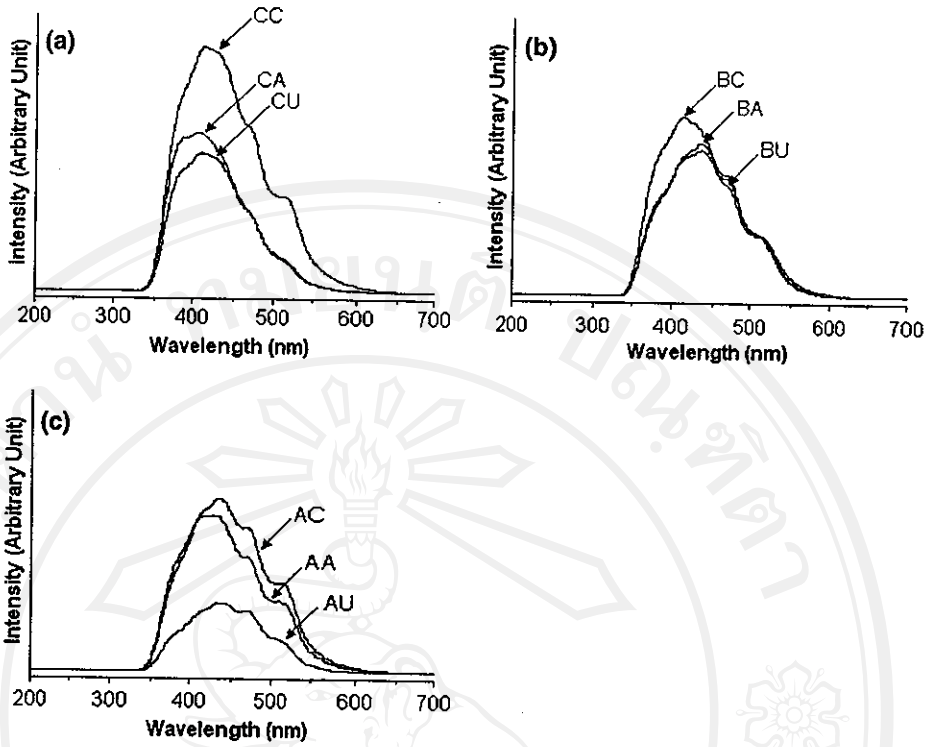

Fig. 7 PL spectra of different products synthesized at 600 W microwave power for 20 min prolonged time. (a) CA, CC and CU, (b) BA, BC and BU and (c) AA, AC and AU

highest intensities at 414 nm (2.99 ev), 414 nm (2.99 ev) and 434 nm (2.86 ev) for the CC, BC and AC products, respectively. The results are in accord with the emission peaks of CuS at 414 nm (2.995 ev) and 437.5 nm (2.834 ev) [28].

Conclusions

Nano- and micro-sized CuS crystals with different morphologies were successfully synthesized by the reactions of different copper and sulfur sources assisted by the cyclic microwave irradiation. The detections of CuS (hcp) phase using XRD and SAED, and of 474 cm^{-1} vibration wavenumber using the Raman spectrometer are in good accord. PL emission peaks of the products are at 414–435 nm (2.85–2.99 ev). Phase and morphology formations are proposed on according to the results characterized using XRD, FTIR, SAED, SEM and TEM.

Acknowledgement We would like to give thank to the Thailand Research Fund, Bangkok Thailand, for funding the research.

References

1. He Y, Yu X, Zhao X (2007) Mater Lett 61:3014
2. Tezuka K, Sheets WC, Kurihara R, Shan YJ, Imoto H, Marks TJ, Poeppelmeier KR (2007) Solid State Sci 9:95
3. Chen X, Wang Z, Wang X, Zhang R, Liu X, Lin W, Qian Y (2004) J Cryst Growth 263:570
4. Chen D, Tang K, Shen G, Sheng J, Fang Z, Liu X, Zheng H, Qian Y (2003) Mater Chem Phys 82:206
5. Ni Y, Liu H, Wang F, Yin G, Hong J, Ma X, Xu Z (2004) Appl Phys A 79:2007
6. Liao XH, Chen NY, Xu S, Yang SB, Zhu JJ (2003) J Cryst Growth 252:593
7. Wang X, Xu C, Zhang Z (2006) Mater Lett 60:345
8. Yang YJ, Xiang JW (2005) Appl Phys A 81:1351
9. Zhang HT, Wu G, Chen XH (2006) Mater Chem Phys 98:298
10. Xu H, Wang W, Zhu W (2006) Mater Lett 60:2203
11. Jiang C, Zhang W, Zou G, Xu L, Yu W, Qian Y (2005) Mater Lett 59:1008
12. Xu JZ, Xu S, Geng J, Li GX, Zhu JJ (2006) Ultrason Sonochem 13:451
13. Podder J, Kobayashi R, Ichimura M (2005) Thin Solid Films 472:71
14. Powder Diffract. File, JCPDS Internat. Centre Diffract. Data, PA 19073–3273, USA, (2001)
15. Huang NM, Kan CS, Khiew PS, Radiman S (2004) J Mater Sci 39:2411. DOI: 10.1023/B: JMSC.0000020003.51378.55
16. Li Y, Huang F, Zhang Q, Gu Z (2000) J Mater Sci 35:5933 DOI: 10.1023/A: 1026714004563
17. Shriver DF, Atkins PW, Overton TL, Rourke JP, Weller MT Armstrong FA (2006) Inorg. Chem, 4th ed., Oxford Univ. Press, p 151
18. Swaminathan K, Irving HMNH (1964) J Inorg Nucl Chem 26:1291
19. Yang J, Zeng JH, Yu SH, Yang L, Zhang YH, Qian YT (2000) Chem Mater 12:2924
20. Biswas S, Kar S, Chaudhuri S (2007) J Cryst Growth 299:94
21. Zhang YC, Hu XY, Qiao T (2004) Solid State Comm 132:779
22. Sopunna K, Thongtem T, McNallan M, Thongtem S (2006) J Mater Sci 41:4654. DOI: 10.1007/s 10853-006-0030-y

23. Lu J, Han Q, Yang X, Lu L, Wang X (2007) Mater Lett 61:2883
24. Thongtem T, Kaowphong S, Thongtem S (2007) J Mater Sci 42:3923
25. Phuruangrat A, Thongtem T, Thongtem S (2007) Mater Lett 61:3805
26. Wang SY, Wang W, Lu ZH (2003) Mater Sci Engin B 103:184
27. Minceva-Sukarova B, Najdoski M, Grozdanov I, Chunnilall CJ (1997) J Molec Struct 410–411:267
28. Ou S, Xie Q, Ma D, Liang J, Hu X, Yu W, Qian Y (2005) Mater Chem Phys 94:460

Available online at www.sciencedirect.com
ScienceDirect
Materials Letters 61 (2007) 3235–3238
materials letters
www.elsevier.com/locate/matlet

Free surfactant synthesis of microcrystalline CdS by solvothermal reaction

Titipun Thongtem *, Anukorn Phuruangrat, Somchai Thongtem

Faculty of Science, Chiang Mai University, Chiang Mai 50200, Thailand

Received 27 August 2006; accepted 8 November 2006
Available online 27 November 2006

Abstract

Microcrystalline CdS was solvothermally synthesized by free surfactant reaction at 200 °C in a variety of solvents [benzene (BZ), toluene (TL), *p*-xylene (XL), cyclohexane (CHX) and tetrahydrofuran (THF)]. An X-ray diffractometer (XRD), a selected area electron diffraction (SAED) technique and an energy dispersive X-ray (EDX) analyzer show that the products are CdS (hexagonal structure) composed of Cd and S. The SAED patterns are also in accord with a simulation model. Strong fundamental and weak overtone modes were detected using a Raman spectrometer at 297.0 and 597.1 cm^{-1}, respectively. By using a transmission electron microscope (TEM), those synthesized in BZ, TL and XL are the mixtures of hexagonal and triangular plates. They are hexagonal and rod shapes in CHX and THF, respectively. Photoluminescent (PL) energies at the maximum intensities were detected over the range of 3.10–3.16 eV (392–400 nm).

Keywords: Free surfactant synthesis; Solvothermal reaction; Microcrystalline CdS

1. Introduction

CdS is one of the IIB-VIA compounds that have novel optical and electrical properties [1]. Its band gap is 2.42 eV [2]. It has a wide variety of applications such as laser light emitting diodes, solar cells, and non-linear optical and electronic devices [3,4]. There are different methods used to synthesize nano- and microcrystalline CdS such as microwave-solvothermal synthesis [4], metal-oleylamine complex [5], hydrothermal route [6] and surfactant-ligand co-assisting solvothermal method [7]. Most of the products have different morphologies such as dendrites [2], flakes [8], spheres [9], nanorods [7,10], nanowires [11,12], triangular and hexagonal plates [13], flower-like shape [14] and sea-urchin-like shape [3]. The solvothermal process is simple and inexpensive; therefore, it is very attractive for use in the chemical synthesis of a substance. Among the required morphologies, different solvents in combination with organic additives were used. Presently, there are a few reports on the free surfactant synthesis of CdS by solvothermal reaction. The purpose of this research is to solvothermally synthesize microcrystalline CdS with different shapes and sizes by free surfactant reaction at low temperature in a variety of solvents.

2. Experiment

Each 0.005 mol of $CdCl_2{\cdot}2.5H_2O$ and $(NH_2)_2CS$ was dissolved in a variety of solvents [benzene (BZ), toluene (TL), *p*-xylene (XL), cyclohexane (CHX) and tetrahydrofuran (THF)]. They were mixed to occupy 65 vol.% of a 45 ml home-made stainless steel autoclaves. The free surfactant reaction proceeded at 200 °C for 10 h to form precipitates. By washing with water and ethanol, the precipitates were dried at 80 °C for 24 h. The final products were analyzed using an X-ray diffractometer (XRD) operated at 20 kV, 15 mA and using Cu K_α radiation in the 2θ angular range of 10–60°, a transmission electron microscope (TEM) as well as a selected area electron diffraction (SAED) technique operated at 200 kV, an energy dispersive X-ray (EDX) analyzer operated at 15 kV, a Raman spectrometer using 50 mW Ar Laser with λ=

* Corresponding author.
E-mail addresses: ttpthongtem@yahoo.com, ttpthongtem@hotmail.com (T. Thongtem).

0167-577X/$ - see front matter © 2006 Elsevier B.V. All rights reserved.
doi:10.1016/j.matlet.2006.11.040

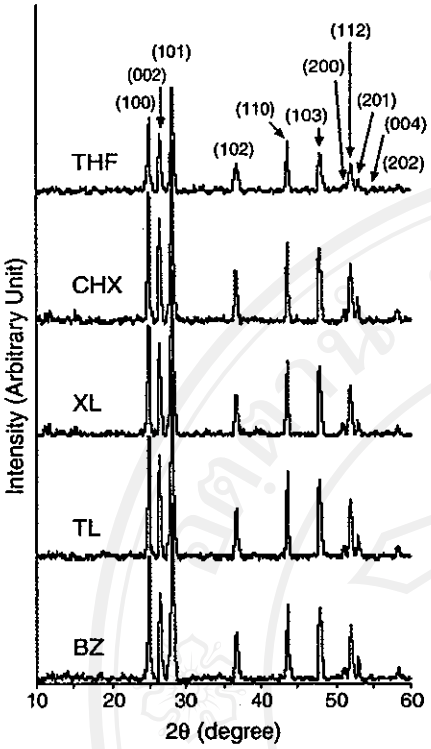

Fig. 1. XRD spectra of the products synthesized using a variety of solvents.

514.5 nm and a luminescence spectrometer using 225 nm exciting wavelength.

3. Results and discussion

3.1. XRD

XRD spectra (Fig. 1) are very sharp showing that the products are composed of crystals. Comparing the spectra to those of the JCPDS standard (PDF # 06-0314) [15], the products were identified as CdS with hexagonal structure. Generally, the hexagonal structure is more stable than the cubic one [16]. For the present research, no impurity peaks were detected showing that the products are pure phase. Calculated lattice parameters [17] are shown in Table 1. In general, the lattice parameters of crystals with the same structure are constant. For CdS synthesized using the solvents, a and c are 0.4135±0.0000 nm and 0.6717±0.0001 nm, respectively. They have zero and very little standard deviations, and are in accord with those of the JCPDS standard (a=0.4136 nm, c=0.6713 nm) [15].

Table 1
Calculated lattice parameters

Solvent	a (nm)	c (nm)
Benzene	0.4135	0.6716
Toluene	0.4135	0.6716
p-Xylene	0.4135	0.6718
Cyclohexane	0.4135	0.6716
Tetrahydrofuran	0.4135	0.6718
	0.4135±0.0000	0.6717±0.0001

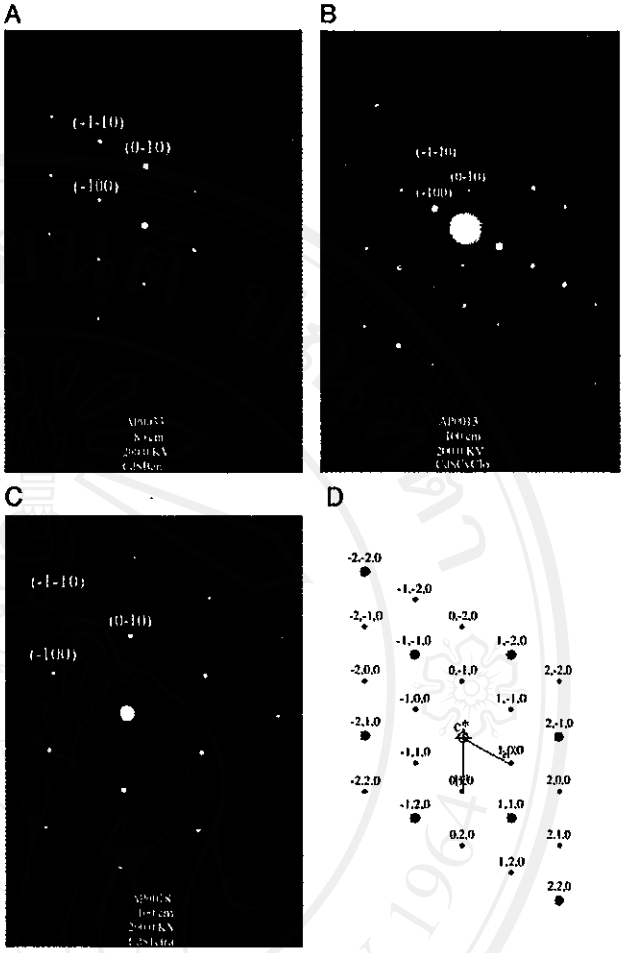

Fig. 2. SAED patterns of the products synthesized using (A) BZ, (B) CHX and (C) THF. (D) A simulation model of CdS.

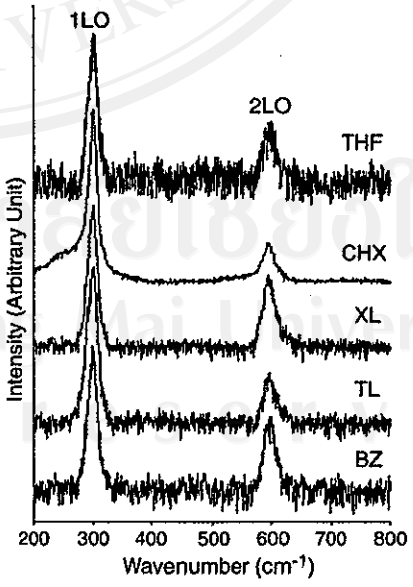

Fig. 3. Raman spectra of the products synthesized using a variety of solvents.

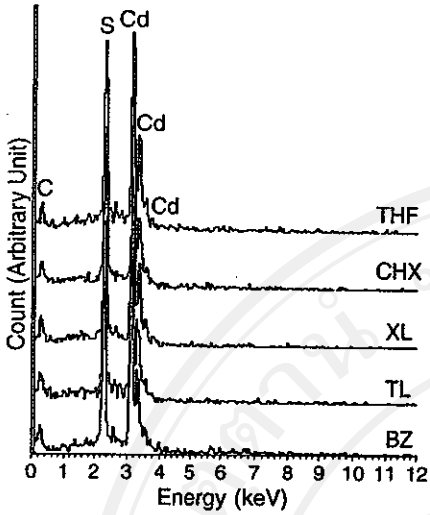

Fig. 4. EDX spectra of the products synthesized using a variety of solvents.

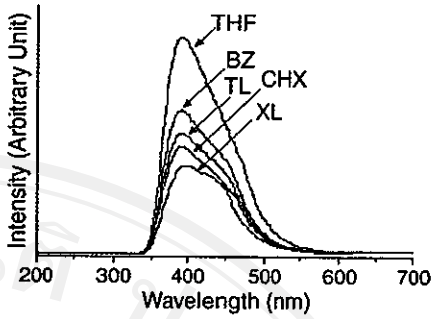

Fig. 6. PL spectra of the products synthesized using different solvents.

3.2. SAED

SAED patterns and a simulation model are shown in Fig. 2. The diffraction patterns were interpreted [18] and identified as CdS with hexagonal structure [15]. It shows that XRD and SAED analyses are in accord. Zone axis is in the [001] direction which is parallel or nearly parallel to the electron beam [18]. The SAED patterns are not exactly symmetric due to the deviation of electron beam from the zone axis. A diffraction pattern for CdS (hexagonal structure) using [001] as zone

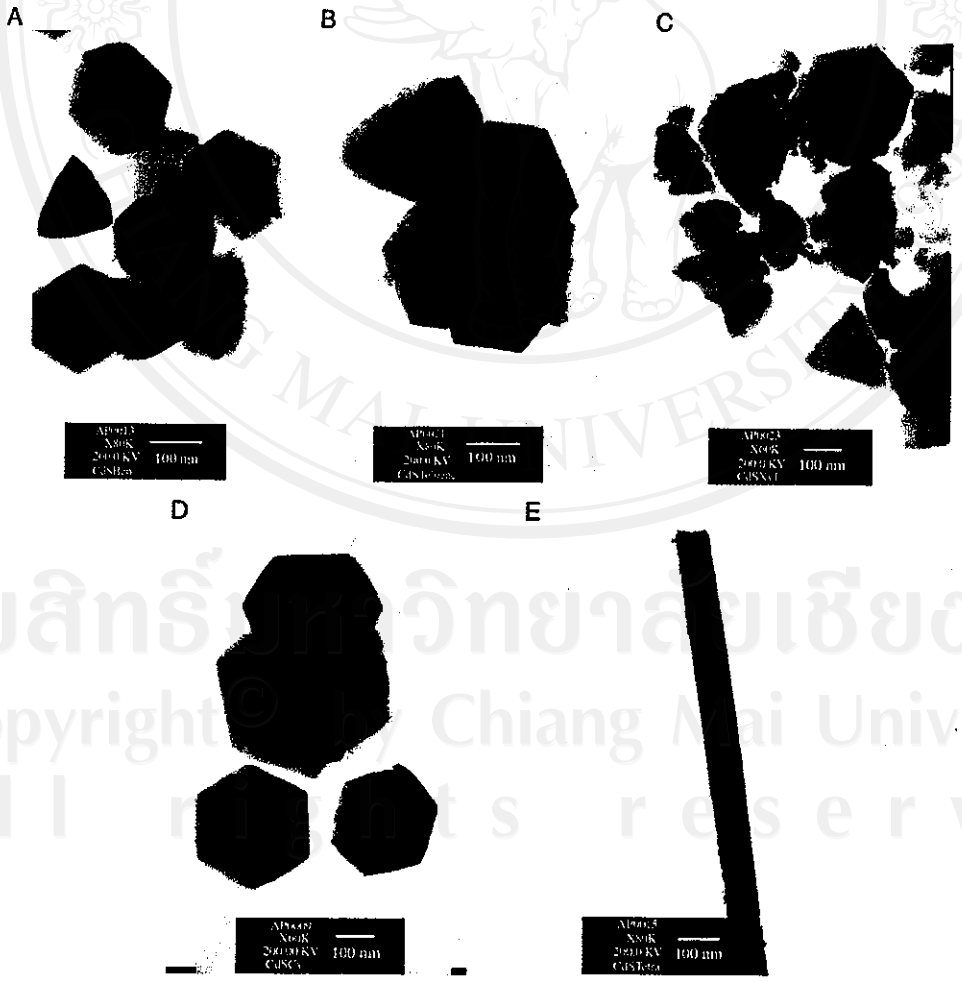

Fig. 5. TEM images of the products synthesized using (A) BZ, (B) TL, (C) XL, (D) CHX and (E) THF.

axis was simulated [19]. The pattern is symmetric and systematic. The results shown on the SAED patterns of the powders are in accord with that shown on the simulated pattern.

3.3. Raman spectra

Raman spectra of the products are shown in Fig. 3. Strong fundamental and weak overtone modes were detected at 297.0 and 597.1 cm^{-1}, respectively. The fundamental and overtone modes correspond to the 1LO (longitudinal optical) and 2LO peaks [16]. They are the results of phonon vibration [6,16]. For the present research, the spectra are very similar to that of CdS [6]. Compared to Ar Laser (λ=514.5 nm), a great deal of energy was lost during the inelastic scattering process. By using a Fourier transform infrared spectrometer (FTIR) (results not shown), no solvents were left in the products.

3.4. EDX

EDX spectra (Fig. 4) were interpreted [20]. They revealed the presence of three Cd peaks at 3.13, 3.32 and 3.53 keV which were identified as the L_{α}, $L_{\beta 1}$ and $L_{\beta 2}$ lines, respectively. S peak was detected at 2.31 keV identified as the $K_{\alpha 1,2}$ line. C of carbon tape was also detected at 0.28 keV ($K_{\alpha 1,2}$ line). EDX analysis shows that the atomic ratio of Cd:S is 1:1. The detection of Cd and S using the EDX, and CdS using the XRD and SAED are in accord.

3.5. TEM

TEM images (Fig. 5) show different morphologies controlled by a variety of solvents. The products are micro-sized particles. Some physical and chemical properties of the solvents seem to play a role in the shapes and sizes of the product particles [9], and the luminescent property [21]. For the present research, no surfactants were used. Relative polarities of BZ, TL, XL, CHX and THF are 0.111, 0.099, 0.074, 0.006 and 0.207, respectively [22]. The solvents are classified into three groups due to their polarities. CHX has the lowest value and THF at the highest. BZ, TL and XL have almost the same medium values. The particles shaped like the hexagon with 122–257 nm straight sides, and the rod with 81 nm in diameter when they were synthesized in CHX and THF, respectively. Those synthesized using one of the BZ, TL and XL solvents consist of both hexagons with 100–160 nm straight sides and triangles with 145–300 nm straight sides. The particles are hexagonal, a mixture of hexagonal and triangular, and rod shapes in the solvents with low, medium and high polarities, respectively. Structure formulae of the solvents, starting agents, temperature, time and others have an effect on their morphologies as well. Theoretically, it is possible to solvothermally synthesize nanocrystalline CdS using the present solvent at very high pressure. Under this condition, the crystallite size is then limited.

3.6. Photoluminescence

Photoluminescence (PL) of the products was analyzed using 225 nm exciting wavelength and are shown in Fig. 6. PL energies at the maximum intensities were detected over the range of 3.10–3.16 eV (392–400 nm). The intensity values and PL wavelengths are different and are controlled by their morphologies [23]. PL intensity of the rod-shaped crystal synthesized in THF is at the highest. Compared to the estimated band gap of bulk CdS (2.42 eV, 512 nm) [2], the PL energies are blue shifted. However, the band gap can be modified by high temperature treatment [24].

4. Conclusions

Microcrystalline CdS (hexagonal structure) with different morphologies was successfully synthesized by free surfactant reaction of $CdCl_2{\cdot}2.5H_2O$ and $(NH_2)_2CS$ in a home-made stainless steel autoclave at 200 °C. Solvent polarities seem to play a role in the shapes and sizes of the product particles. The calculated lattice parameters are very close to those of the JCPDS standard. The 1LO and 2LO peaks of CdS are at 297.0 and 597.1 cm^{-1}, respectively. PL energies of different products are blue shifted in comparison with the band gap of CdS (bulk).

Acknowledgements

We would like to give thanks to the Thailand Research Fund, Bangkok, and the Faculty of Science, Chiang Mai University, Chiang Mai, Thailand for funding the research.

References

[1] S.M. Zhou, Mater. Lett. 61 (2007) 119–122.
[2] A.M. Qin, Y.P. Fang, W.X. Zhao, H.Q. Liu, C.Y. Su, J. Cryst. Growth 283 (2005) 230–241.
[3] X. Liu, Mater. Chem. Phys. 91 (2005) 212–216.
[4] A.V. Murugan, R.S. Sonawane, B.B. Kale, S.K. Apte, A.V. Kulkarni, Mater. Chem. Phys. 71 (2001) 98–102.
[5] J. Joo, H.B. Na, T. Yu, J.H. Yu, Y.W. Kim, F. Wu, J.Z. Zhang, T. Hyeon, J. Am. Chem. Soc. 125 (2003) 11100–11105.
[6] C. Li, X. Yang, B. Yang, Y. Yan, Y. Qian, J. Cryst. Growth 291 (2006)45–51.
[7] C. Bao, M. Jin, R. Lu, P. Xue, Q. Zhang, D. Wang, Y. Zhao, J. Solid State Chem. 175 (2003) 322–327.
[8] N. Gao, F. Guo, Mater. Lett. 60 (2006) 3697–3700.
[9] F.H. Zhao, Q. Su, N.S. Xu, C.R. Ding, M.M. Wu, J. Mater. Sci. 41 (2006) 1449–1454.
[10] W. Qingqing, Z. Gaoling, H. Gaorong, Mater. Lett. 59 (2005) 2625–2629.
[11] C. Cheng, G. Xu, H. Zhang, H. Wang, J. Cao, H. Ji, Mater. Chem. Phys. 97 (2006) 448–451.
[12] X. Guo-yue, W. Han, C. Chuan-wei, Z. Hai-qian, C. Jie-ming, J. Guang-bin, Trans. Nonferrous Met. Soc. China 16 (2006) 105–109.
[13] M. Chen, L. Pan, J. Cao, H. Ji, G. Ji, X. Ma, Y. Zheng, Mater. Lett. 60 (2006) 3842–3845.
[14] L. Wang, L. Chen, T. Luo, Y. Qian, Mater. Lett. 60 (2006) 3627–3630.
[15] Powder Diffract. File, JCPDS Internat. Centre Diffract. Data, PA 19073-3273, U.S.A., (2001).
[16] J. Lee, Thin Solid Films 451–452 (2004) 170–174.
[17] B.D. Cullity, Elem. X-ray Diffract, 2nd ed., Addison-Wesley Publ. Co., MA, 1978.
[18] K.W. Andrews, D.J. Dyson, S.R. Keown, Interpret. Electr. Diffract. Patter, 2nd ed, Plenum Press, NY, 1971.
[19] C. Boudias, D. Monceau, CaRIne Crystallography 3.1, 17 rue du Moulin du Roy, F-60300 Senlis, France, (1989–1998).
[20] X-ray Absorp. Emiss. Energ., Oxford Instrum. Analyt., Halifax Rd., High Wycombe Bucks HP12 3SE, U.K.
[21] K.S. Babu, C. Vijayan, P. Haridoss, Mater. Lett. 60 (2006) 124–128.
[22] http://virtual.yosemite.cc.ca.us/smurov/orgsoltab.htm (Aug. 2006).
[23] G. Zhou, M. Lü, Z. Xiu, S. Wang, H. Zhang, Y. Zhou, S. Wang, J. Phys. Chem., B 110 (2006) 6543–6548.
[24] O. de Melo, L. Hernández, O. Zelaya-Angel, R. Lozada-Morales, M. Becerril, E. Vasco, Appl. Phys. Lett. 65 (1994) 1278–1280.

online at http://www.scientific.net

Phase Transformation of Nanocrystalline CdS Synthesized by Solvothermal Reaction

Titipun Thongtem*, Anukorn Phuruangrat and Somchai Thongtem
Faculty of Science, Chiang Mai University, Chiang Mai 50200, Thailand
* : Corresponding Author, ttpthongtem@yahoo.com and ttpthongtem@hotmail.com

Keywords : Phase Transformation, Nanocrystalline CdS, Solvothermal reaction

Abstract. CdS was synthesized by solvothermal reaction of $CdCl_2.2.5H_2O$ and $(NH_2)_2CS$ in ammonia solution at 200 °C for 10 h. XRD, TEM and SAED show that the products are nanocrystalline CdS. The phase is 100 % hexagonal (hcp) in pure water, gradually transformed into cubic with the increase of NH_3 concentration, and 100 % cubic in 25 % NH_3 solution. By using FTIR, no solvents were detected in the products. Raman analysis revealed the presence of 1LO (longitudinal optical) and 2LO phonon peaks at 297.0 and 597.1 cm^{-1} for CdS (hcp), and 295.9 and 596.9 cm^{-1} for CdS (cubic), respectively. Strong peaks of the photoluminescent (PL) spectra were detected at 450 nm for hcp, and 519 nm for cubic.

Introduction

Among group II-VI compounds, CdS has received significant attention due to its outstanding potential applications [1] such as solar cells [2], light emitting diodes [1] and photocatalysts [1]. Recently, nanocrystallines have been increasingly important due to their novel properties controlled by the shapes and sizes [3]. Therefore, nanocrystalline has been the subject to investigate. There are a variety of methods used to synthesize the compound such as polyol route [1], hot-wall epitaxy [4] and hydrothermal [5]. For the present research, nanocrystalline CdS was synthesized using a home-made stainless steel autoclave. Phase transformation, luminescent property and morphology were then studied and explained.

Experiment

Each 0.005 mol of $CdCl_2.2.5H_2O$ and $(NH_2)_2CS$ dissolving in 0 – 25 % NH_3 solution were mixed to occupy 65 vol % of a home-made stainless steel autoclave. The reaction proceeded at 200 °C for 10 h to form precipitate. By washing with water and ethanol, the precipitate was dried at 80 °C for 24 h. The final products were analyzed to determine their characters and properties.

Results and Discussion

Comparing XRD spectra (Fig 1) to those of the JCPDS standard (Reference codes : 06-0314 for CdS (hcp) and 89-0440 for CdS (cubic)) [6], the products synthesized using pure water (0 % NH_3) and 25 % NH_3 were specified as CdS (hcp) and CdS (cubic), respectively. The diffraction peaks of hcp correspond to (100), (002), (101), (102), (110), (103), (200), (112), (201), (004) and (202) planes of the product. The (101) peak is the highest. For cubic, they correspond to (111), (200), (220) and (311) planes and the first peak is the highest. All peaks of hcp were decreased with the increase of the NH_3 concentration. Those of cubic showed the opposite effect. The products are the mixture (solid solution) of hcp and cubic phases in 5, 10, 15 and 20 % NH_3 solutions. Two different calculated phases [7] using (101) hcp and (200) cubic peaks are shown (Fig 2), hcp on the left extremity and cubic on the right. Mixture of the phases is between the two ends. These show that NH_3 concentration plays the role in the phase formation. Calculated lattice parameters (a = 41.360 and c = 67.182 nm for hcp, and a = 58.311 nm for cubic) [7] are very close to those of the JCPDS standard (a = 41.360 and c = 67.130 nm for hcp, and a = 58.304 nm for cubic) [6].

TEM images and SAED patterns are shown (Fig 3). The products compose of rather round particles of which the sizes were measured (Fig 4). They are 62.1 ± 20.1 nm for the product synthesizing in pure water, and 37.2 ± 13.7 nm in 25 % NH_3 solution. The first composes of larger particles and size distributions than the second does. The solvent is likely to play the role in the particle sizes and size distributions. SAED patterns compose of a number of bright spots of concentric rings. The diffraction rings of the product in 25 % NH_3 are not sharp resulting from the effect of fine particles. The diameter of each ring was measured and the interplanar space (d) was calculated [8]. Comparing to the JCPDS standard [6], the products synthesized in pure water and 25 % NH_3 correspond to CdS (hcp) and CdS (cubic), respectively. SAED and XRD planes of both products are in accord.

Raman spectra of hcp and cubic phases (Fig 5) are almost identical to each other. Two peaks were detected on both spectra. The products are nanocrystalline CdS; therefore, their spectra are rather broad [9]. The strong 1LO (longitudinal optical) and weak 2LO phonon peaks corresponding to the fundamental and overtone modes [5] are at 297.0 and 597.1 cm^{-1} for CdS (hcp), and 295.9 and 596.9 cm^{-1} for CdS (cubic), respectively. The Raman shift values of CdS (hcp) and CdS (cubic) are in accord with those of the undoped CdS (hcp) [2] and CdS (mixture of hcp and cubic phases) [10] films. The explanation clearly shows that Raman shift values for both phases are very close to each other. The values of full width at half maximum (FWHM) of 1LO and 2LO peaks are 18.2 and 27.6 cm^{-1} for CdS (hcp), and 15.8 and 26.1 cm^{-1} for CdS (cubic), respectively. CdS (hcp) is the stable phase. FWHM of the dominant 1LO agrees very well with that of the undoped CdS film [2] reflecting the quality of the synthesized product. By using FTIR (results not shown), no solvents were left in the products.

Photoluminescent (PL) spectra of hcp and cubic phases were analyzed using exciting wavelength (λ_{ex}) of 231 and 282 nm, respectively (Fig 6). The strong peaks were detected at 450 nm (2.755 ev) for hcp, and 519 nm (2.389 ev) for cubic. The radiation of longer wavelength than λ_{ex} was emitted due to some energy loss and others. The PL property was controlled by the crystal sizes and shapes [3]. Comparing to band gaps of 2.42 ev (512 nm) for bulk CdS (hcp) [11] and 2.366 ev (524 nm) for CdS (cubic) film [4], the strong peaks of the synthesized products are blue shift. It is the result of the quantum size effect [11] which is increasing in the extent as the particle size decreases and the surface-to-volume ratio increases. Band gap can be modified by heating the products at high temperatures [12], and the synthesized processes as well. An electron in valence band was excited into conduction band, and hole was left in the valence band. Generally, the solid has some defects introducing energy levels in the forbidden region. The excited state is not stable. The electron in conduction band recombined with the hole in valence band via the energy levels of the defects [13]. Therefore, band gaps for the synthesized products are no less than 2.755 ev for CdS (hcp) and 2.389 ev for CdS (cubic).

Summary

Nanocrystalline CdS was successfully synthesized by 200 °C solvothermal reaction in 0-25 % NH_3 solution. The phase is hcp using pure water, transformed into cubic by the increase of the NH_3 concentration, and cubic in 25 % NH_3 solution. Raman spectra of hcp and cubic phases are almost identical with the presence of 1LO and 2 LO peaks. Their strong luminescent peaks were detected at 450 nm (2.755 ev) and 519 nm (2.389 ev), respectively.

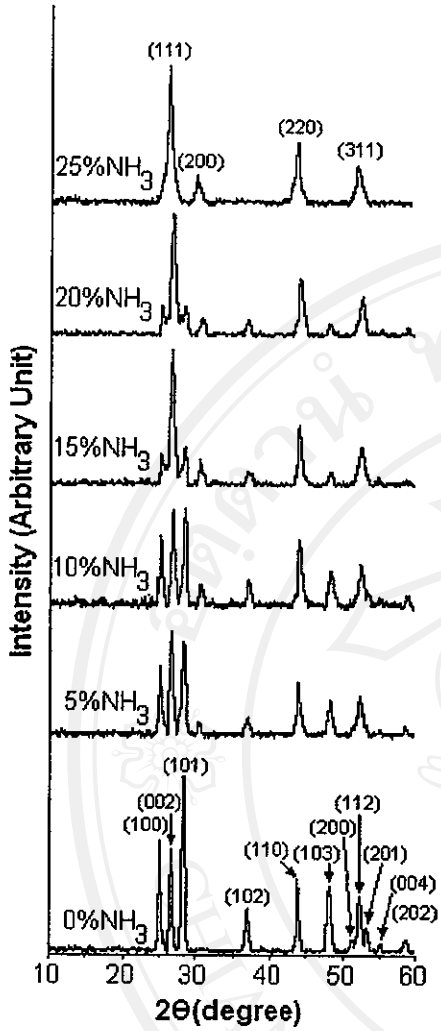

Fig 1. XRD spectra of CdS synthesized using different percentages of NH_3 solution.

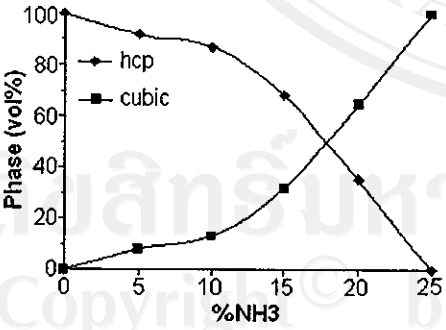

Fig 2. CdS phases synthesized using different percentages of NH_3 solution.

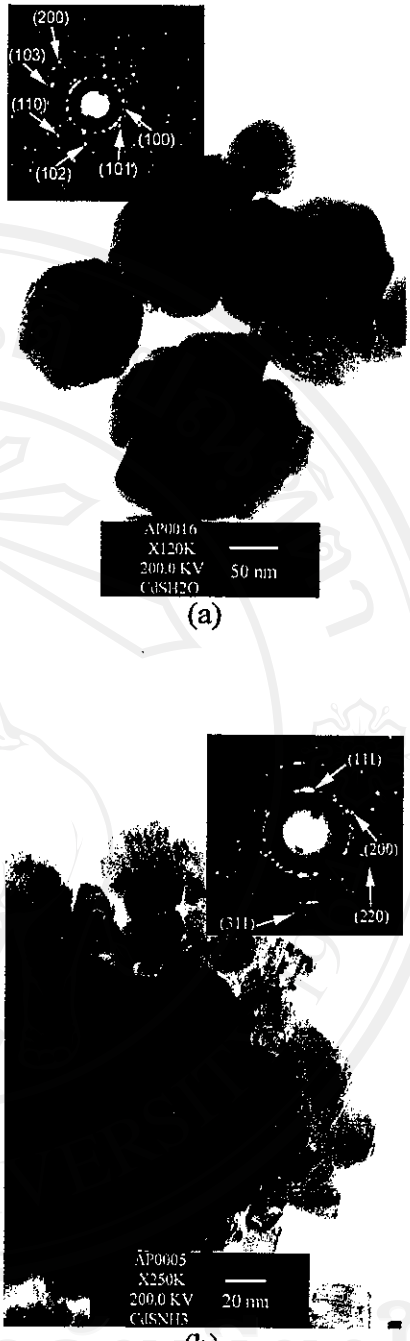

Fig 3. TEM images and SAED patterns of CdS synthesized using (a) pure water and (b) 25 % NH_3 solution.

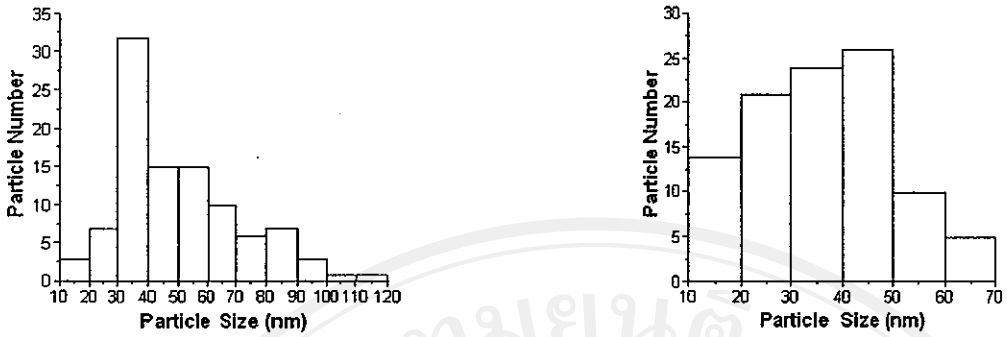

Fig 4. Particle size distributions of CdS synthesized using (a) pure water and (b) 25 % NH_3 solution.

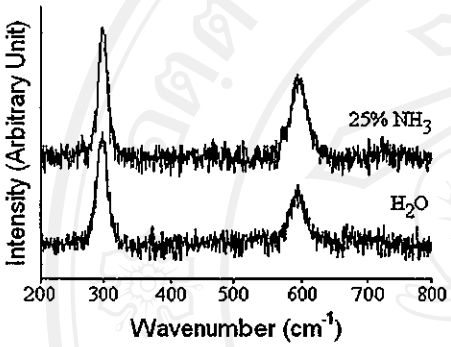

Fig 5. Raman spectra of CdS synthesized using pure water and 25 % NH_3 solution.

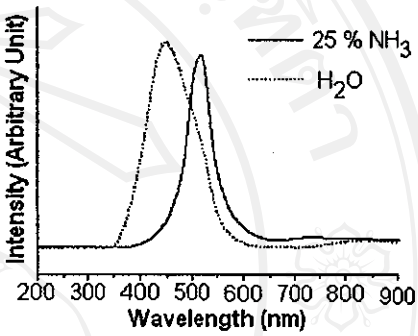

Fig 6. PL spectra of CdS synthesized using pure water and 25 % NH_3 solution.

Acknowledgements : We would like to give thank to the Commission on Higher Education, and Thailand Research Fund, Bangkok, Thailand, for funding the research.

References

[1] Y.J. Yang, Coll. Surf. A, 276(2006)192-196
[2] J. Lee, Thin Solid Film., 451-452(2004)170-174
[3] Q. Wang, D. Pan, S. Jiang, X. Ji, L. An, B. Jiang, J. Cryst. Growth, 286(2006)83-90
[4] Y.M. Yu, K. Kim, B. O., K.S. Lee, Y.D. Choi, P.Y. Yu, J. Appl. Phys., 92(2002)1162-1164
[5] C. Li, X. Yang, B. Yang, Y. Yan, Y. Qian, J. Cryst. Growth, 291(2006)45-51
[6] Powder Diffract. File, JCPDS Internat. Centre Diffract. Data, PA 19073-3273,U.S.A.,(2001)
[7] B.D. Cullity, (Elem. X-ray Diffract., Addison-Wesley Publ. Co., MA, 1967)
[8] K.W. Andrews, D.J. Dyson, S.R. Keown, (Interpret. Electr. Diffract. Patter., 2nd ed, Plenum Press, NY, 1971)
[9] K.K. Nanda, S.N. Sahu, Appl. Surf. Sci., 119(1997)50-54
[10] O. Trujillo, R. Moss, K.D. Vuong, D.H. Lee, R. Noble, D. Finnigan, S. Orloff, E. Tenpas, C. Park, J. Fagan, X.W. Wang, Thin Solid Film., 290-291(1996)13-17
[11] X. Guo-yue, W. Han, C. Chuan-wei, Z. Hai-qian, C. Jie-ming, J. Guang-bin, Trans. Nonferrous Met. Soc. China, 16(2006)105-109
[12] O. de Melo, L. Hernández, O. Zelaya-Angel, R. Lozada-Morales, M. Becerril, E. Vasco, Appl. Phys. Lett. 65(1994)1278-1280
[13] M. Alonso, E.J. Finn, (Fundamental University Phys., Vol.3, Addison-Wesley Publ. Co., MA, 1968)

Journal of Ceramic Processing Research. Vol. 9, No. 4, pp. 335~337 (2008)

J O U R N A L O F
Ceramic Processing Research

Preparation of flower-like PbS nano-structures using cyclic microwave radiation

Titipun Thongtem[a,*], Anukorn Phuruangrat[b] and Somchai Thongtem[b]
[a]*Department of Chemistry, Faculty of Science, Chiang Mai University, Chiang Mai 50200, Thailand*
[b]*Department of Physics, Faculty of Science, Chiang Mai University, Chiang Mai 50200, Thailand*

Flower-like PbS nano-structures were successfully prepared from different mole ratios of $Pb(NO_3)_2$ to CH_5N_3S in propylene glycol, using the cyclic process of 600 W microwave power for 15 minutes. PbS (cubic) was detected using X-ray diffraction (XRD) and selected area electron diffraction (SAED). The experimental and simulated patterns are in good accord. A Raman spectrometer revealed the presence of vibrations at 134, 275 and 431 cm^{-1}. Flower-like PbS nano-structures were also characterized using a scanning electron microscope (SEM) and a transmission electron microscope (TEM), although the products were prepared using different mole ratios of the starting agents.

Key words: Cyclic microwave radiation, Flower-like PbS nano-structures.

Introduction

Generally, different morphologies of luminescent materials have an influence on their properties [1]. Preparation of such materials is now increasingly important. PbS is a material which has a small band gap (0.41 eV) and large exciton Bohr radius (18 nm) [2-4]. It has novel semiconducting and optical properties [5], which are very sensitive to a quantum-size effect [2, 3]. There are different nano- and micro-structures of PbS that have an influence on its properties. Among them are nanocubes [6], nanoparticles [7], dendrites [6, 8], star-shapes [9], flower-like crystals [10], nanotubes [11] and nanorods [11, 12]. They can be prepared by different methods, such as microwave radiation [10], a hydrothermal process [4], solvothermal synthesis [6], electroless chemical deposition [13] and a sonochemical process [11].

Microwave radiation [14] is a very attractive method used for preparing materials. It is able to reduce time scales of the reactions, and accelerate the reaction process. When microwave radiation is supplied to chemicals, one or more of them is capable of coupling with the radiation. This can lead to a high temperature faster than that achieved by a conventional method. Microwave radiation can solve the problems of temperature and concentration gradients. By focusing large amounts of microwave radiation into solutions, the vibrating electric field applies a force on charged particles which vibrate accordingly. Vibrations of the reactants have an influence on the reaction to proceed with efficiency. Subsequently, pure product is produced.

At present, there are a few reports on the preparation of flower-like PbS using microwave radiation. For the present research, flower-like PbS nano-structures were prepared from different mole ratios of Pb and S sources, using a cyclic microwave radiation. The final products were then analyzed for further discussion.

*Corresponding author:
Tel : +66 (0)53 941922-24
Fax: +66 (0)53 892 277
E-mail: ttpthongtem@yahoo.com; ttpthongtem@hotmail.com

Experiment

Flower-like PbS particles were prepared from 1 : 4, 1 : 1 and 4 : 1 mole ratios of $Pb(NO_3)_2$ to CH_5N_3S in propylene glycol, using 600 W microwave power for 15 minutes. The process was repeated many times and always happened in the same order. For every 100 s, microwave radiation was on for 30 s and off for 70 s. At the conclusion of the test, the products were washed with water and ethanol, and dried at 80 °C for 12 h. The final products were characterized using an X-ray diffractometer (XRD) operated at 20 kV, 15 mA and using Cu K_α radiation in the 2θ angular range of 15-60 degrees, a Raman spectrometer using a 50 mW Ar laser with $\lambda = 514.5$ nm at room temperature, a scanning electron microscope (SEM) operated at 15 kV and a transmission electron microscope (TEM) as well as the use of the selected area electron diffraction (SAED) technique operated at 200 kV. The electron diffraction pattern was simulated [15] and compared with that obtained experimentally [16].

Results and Discussion

XRD

XRD spectra Fig. 1(a) were indexed using Bragg's law for X-ray diffraction and compared with that of the JCPDS software (reference code : 05-0592) [17]. They were specified that the products were cubic PbS ($a = b = c$, $\alpha = \beta = \gamma = 90$ degrees) with the Fm-3 m space

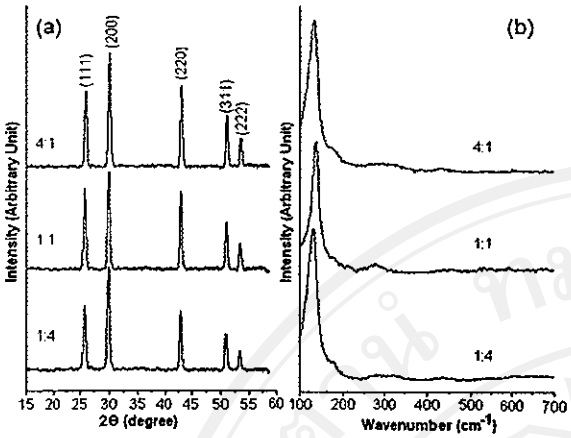

Fig. 1. (a) XRD and (b) Raman spectra of the products prepared using different mole ratios of $Pb(NO_3)_2$ to CH_5N_3S.

Table 1. Calculated lattice parameters of PbS (cubic) prepared using different mole ratios of $Pb(NO_3)_2$ to CH_5N_3S

Plane	Lattice parameter (Å)		
	1 : 4	1 : 1	4 : 1
(111)	5.9670	5.9611	5.9675
(200)	5.9456	5.9531	5.9620
(220)	5.9447	5.9436	5.9476
(311)	5.9391	5.9380	5.9415
(222)	5.9416	5.9405	5.9422
	5.9476 ± 0.0111	5.9473 ± 0.0096	5.9522 ± 0.0119

group. The strongest intensity is at $2\theta = 30.1$ degrees and diffracted from the (200) planes of the crystalline products. The spectra are very sharp showing that well-crystallized crystals were successfully synthesized [18, 19]. The products are composed of a number of atoms aligning in a periodic lattice. No characteristic peaks of impurities were detected showing that each of the products is a pure phase. Atoms were involved in violent vibration with the microwave frequency. They aligned in a systematic and symmetric order, which led to high intensities. Their lattice parameters were calculated form the equation of plane spacing for the cubic crystal system and Bragg's law for diffraction [20]. The parameters corresponding to different crystallographic planes of the products are summarized in Table 1. The averages and standard deviations are 5.9476 ± 0.0111, 5.9473 ± 0.0096 and 5.9522 ± 0.0119 Å for the products prepared using 1 : 4, 1 : 1 and 4 : 1 mole ratios of $Pb(NO_3)_2$ to CH_5N_3S, respectively. They are very close to those of the JCPDS software [17].

To form PbS (cubic), the reaction [21] proceeded according to the following :

$$Pb(NO_3)_2 + CH_5N_3S \rightarrow PbS + CH_5N_3(NO_3)_2 \quad (1)$$

Theoretically, 1 mol $Pb(NO_3)_2$ and 1 mol CH_5N_3S were used to produce 1 mol PbS and 1 mol $CH_5N_3(NO_3)_2$. For the present research, PbS was able to be produced even when either of the reactants was in excess.

Raman analysis

A definite existence of PbS (cubic) was analyzed using a Raman spectrometer. These test specimens are not destructed and are able to be re-used for other purposes. Their Raman spectra Fig. 1(b) contain prominent bands at the same wavenumbers. They are influenced by some parameters, such as atomic masses of Pb and S, and vibration constant of bonding between Pb and S atoms residing in the lattice. Among the different spectra, their peaks are at 134, 275 and 431 cm^{-1}. The peak below 150 cm^{-1} is tentatively attributable to the so-called plasma line of the excitation laser [5, 22]. The 275 cm^{-1} peak corresponds to two-phonon process [5]. The peak at 431 cm^{-1} is allowed in the rock-salt structure [23]. It is specified as the first overtone mode [22], which involves two phonons with equal but opposite wave vectors (**k**) [23]. The fundamental longitudinal optical (LO) mode of the rock-salt structure at approximately 215.5 cm^{-1} was unable to be detected due to the rising in intensity of baseline (disorder in PbS lattice) at low wavenumbers. The baseline intensity covered the fundamental LO mode, which was forbidden [22, 23].

SEM

SEM images Fig. 2 show that the products are micro-sized flowers over the whole range of $Pb(NO_3)_2$ and CH_5N_3S mole ratios. Flower-like PbS nano-structures were able to be produced even when either of the reactants was in excess. The flower-like products are made up of several petals, which slope up to a point. They have two halves that are the same in size and shape. Each of the petals is composed of a number of small plates arranged in a systematic order. The distance between two apices of the two petals across the center of the flower is 1.7-5.8 micrometers long. The micro-flower is the most complete at 1 : 4 mole ratio.

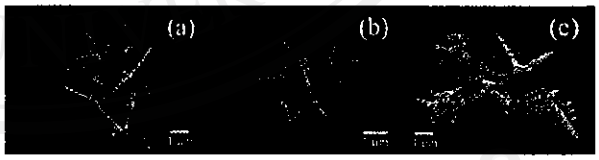

Fig. 2. SEM images of the products prepared using (a) 1 : 4, (b) 1 : 1, and (c) 4 : 1 mole ratios of $Pb(NO_3)_2$ to CH_5N_3S, respectively.

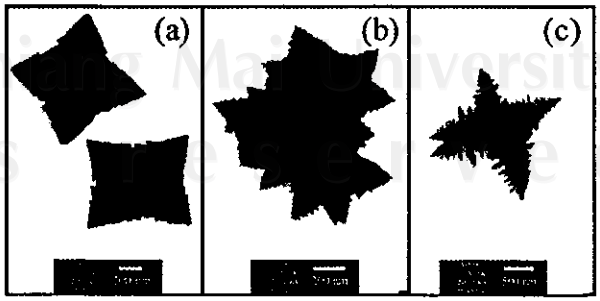

Fig. 3. TEM images of the products prepared using (a) 1 : 4, (b) 1 : 1, and (c) 4 : 1 mole ratios of $Pb(NO_3)_2$ to CH_5N_3S, respectively.

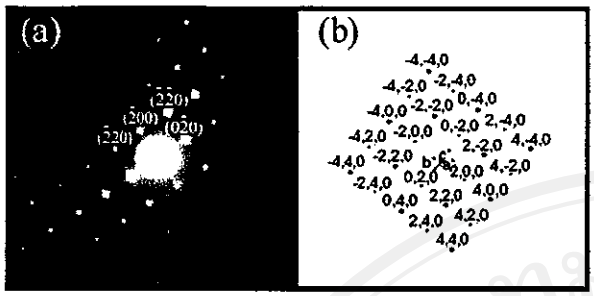

Fig. 4. (a) SAED and (b) simulated patterns of the product prepared using 4 : 1 mole ratio of $Pb(NO_3)_2$ to CH_5N_3S.

TEM, SAED and simulation

TEM images Fig. 3. were used to specify the morphologies of the products. They have a flat shape with four or more acute angles. The results characterized using TEM are in accord with those characterized using SEM. A SAED pattern Fig. 4(a) of the product prepared using a 4 : 1 mole ratio of $Pb(NO_3)_2$ to CH_5N_3S appears as a symmetric and systematic array of bright spots showing that a number of atoms are arranged on their crystal lattices. The pattern was interpreted [16], and specified as cubic PbS [17]. The calculated electron beam used for the analysis is in the [001] direction. A diffraction pattern of the product with the electron beam in the [001] direction was simulated by respective use of a*, b* and c* lattice vectors in [100], [010] and [001] directions [15]. The simulated pattern Fig. 4(b) is composed of systematic and symmetric bright spots, and is in good accord with the experimental pattern. Additional concentric rings were also detected in the experimental pattern. They were caused by the C supporting grid in the TEM chamber.

Conclusions

Flower-like PbS nano-structures were successfully prepared from 1 : 4, 1 : 1 and 4 : 1 mole ratios of $Pb(NO_3)_2$ to CH_5N_3S in propylene glycol, using cyclic microwave radiation. XRD and SAED analyses revealed the presence of PbS with a cubic structure. For the present analysis, the experimental and simulated patterns are in good accord. Calculated lattice parameters are 5.9476 ± 0.0111, 5.9473 ± 0.0096 and 5.9522 ± 0.0119 Å for the products prepared using 1 : 4, 1 : 1 and 4 : 1 mole ratios of $Pb(NO_3)_2$ to CH_5N_3S. Both SEM and TEM analyses revealed the presence of flower-like PbS nano-structures which were prepared using different mole ratios of Pb and S sources. The 431 cm^{-1} first overtone mode was detected using a Raman spectrometer, but the fundamental one was forbidden.

Acknowledgements

The research was supported by the Thailand Research Fund and National Research Council of Thailand.

References

1. H.F. Shao, Y.B. Zhang, X.F. Qian, J. Yin, and Z.K. Zhu, Mater. Lett. 59 (2005) 3507-3513.
2. L. Xu, W. Zhang, Y. Ding, W. Yu, J. Xing, F. Li, and Y. Qian, J. Cryst. Growth 273 (2004) 213-219.
3. Y.C. Zhang, T. Qiao, X.Y. Hu, G.Y. Wang, and X. Wu, J. Cryst. Growth 277 (2005) 518-523.
4. S. Wang, A. Pan, H. Yin, Y. He, Y. Lei, Z. Xu, and B. Zou, Mater. Lett. 60 (2006) 1242-1246.
5. A.M. Qin, Y.P. Fang, W.X. Zhao, H.Q. Liu, and C.Y. Su, J. Cryst. Growth 283 (2005) 230-241.
6. W. Zhang, Q. Yang, L. Xu, W. Yu, and Y. Qian, Mater. Lett. 59 (2005) 3383-3388.
7. U.K. Gautam and R. Seshadri, Mater. Res. Bull. 39 (2004) 669-676.
8. Z. Zhang, S.H. Lee, J. Vittal, and W.S. Chin, J. Phys. Chem. B 110 (2006) 6649-6654.
9. G. Zhou, M. Lü, Z. Xiu, S. Wang, H. Zhang, Y. Zhou, and S. Wang, J. Phys. Chem. B 110 (2006) 6543-6548.
10. Y. Ni, F. Wang, H. Liu, G. Yin, J. Hong, X. Ma, and Z. Xu, J. Cryst. Growth 262 (2004) 399-402.
11. S.F. Wang, F. Gu, M.K. Lü, G.J. Zhou, and A.Y. Zhang, J. Cryst. Growth 289 (2006) 621-625.
12. T. Saraidarov, R. Reisfeld, A. Sashchiuk, and E. Lifshitz, Physica E 37 (2007) 173-177.
13. B. Minceva-Sukarova, M. Najdoski, I. Grozdanov, and C.J. Chunnilall, J. Molec. Struct. 410-411 (1997) 267-270.
14. C. Gabriel, S. Gabriel, E.H. Grant, B.S.J. Halstead, and D.M.P. Mingos, Chem. Soc. Rev. 27 (1998) 213-223.
15. C. Boudias and D. Monceau, CaRIne Crystallography 3.1, 17 rue du Moulin du Roy, F-60300 Senlis, France (1989-1998).
16. T. Thongtem, A. Phuruangrat, and S. Thongtem, Mater. Lett. 61 (2007) 3235-3238.
17. Powder Diffract. File, JCPDS Internat. Centre Diffract. Data, PA 19073-3273, U.S.A. (2001).
18. T. Thongtem and S. Thongtem, Ceram. Internat. 30 (2004) 1463-1470.
19. T. Thongtem and S. Thongtem, Ceram. Internat. 31 (2005) 241-247.
20. C. Suryanarayana and M.G. Norton, X-ray Diffract, A Practical Approach, Plenum Press, New York (1998).
21. L. Xu, W. Zhang, Y. Ding, W. Yu, J. Xing, F. Li, and Y. Qian, J. Cryst. Growth 273 (2004) 213-219.
22. G.D. Smith, S. Firth, R.J.H. Clark, and M. Cardona, J. Appl. Phys. 92 (2002) 4375-4380.
23. R. Sherwin, R.J.H. Clark, R. Lauck, and M. Cardona, Solid State Comm. 134 (2005) 565-570.

Available online at www.sciencedirect.com
ScienceDirect
Ceramics International 34 (2008) 1691–1695
CERAMICS INTERNATIONAL
www.elsevier.com/locate/ceramint

Biomolecule and surfactant-assisted hydrothermal synthesis of PbS crystals

Titipun Thongtem [a,*], Sulawan Kaowphong [b], Somchai Thongtem [b]

[a] Department of Chemistry, Faculty of Science, Chiang Mai University, Chiang Mai 50200, Thailand
[b] Department of Physics, Faculty of Science, Chiang Mai University, Chiang Mai 50200, Thailand

Received 17 January 2007; received in revised form 13 April 2007; accepted 14 May 2007
Available online 10 August 2007

Abstract

PbS crystals were hydrothermally synthesized using $Pb(NO_3)_2$, L-cysteine, and *N*-cetyl pyridinium chloride in solutions with different pH values at 140 °C. Flower-like, granular and truncated cubic PbS crystals composing of Pb and S were detected using an X-ray diffractometer (XRD), a scanning electron microscope (SEM), a transmission electron microscope (TEM), a selected area electron diffraction (SAED) technique and an energy dispersive X-ray (EDX) analyzer. In addition, a Raman spectrometer revealed the presence of the first and second overtone modes at 436 and 602 cm^{-1}, respectively. Emission spectra of the products were detected at 412 nm using a photoluminescence (PL) spectrometer.

Keywords: Hydrothermal synthesis; L-Cysteine; *N*-Cetyl pyridinium chloride; PbS crystals

1. Introduction

It is generally known that luminescence of materials are influenced by their different shapes and sizes [1]. Therefore, the synthesis of nano- and micro-crystals has become increasingly attractive. One of the materials is PbS which has a small band gap (0.41 eV) and a large exciton Bohr radius (18 nm) [2–4]. It has novel semiconducting and optical properties [5], which are very sensitive to the quantum-size effect [2,3]. There are a variety of shapes and sizes that play a role in determining their properties. Among them are cross shaped [6], star-like [3,7], fish bone-like [3], flower-like [3,8], nano-cubic [7], nano-rod [9], nano-belt [9], and nano-dendrite [9]. Biomolecules were used as a sulfur source and complexing agent for the synthetic processes [10,11]. A surfactant was used as the directing molecule to control the shapes and sizes of the crystals [1,4,9]. Currently, there are no reports on the use of both bio- and surfactant-molecules in a reaction process. For the present research, nano- and micro-crystalline PbS was hydrothermally synthesized using L-cysteine and *N*-cetyl pyridinium chloride at different pH values and at prolonged times. The final products were then analyzed for further discussion.

2. Experiment

Different shapes and sizes of PbS crystals were synthesized in home-made stainless steel autoclaves using 0.003 mol $Pb(NO_3)_2$, 0.003 mol L-cysteine ($C_3H_7NO_2S$) and 0.0005 mol *N*-cetyl pyridinium chloride ($C_{21}H_{38}NCl$) in 40 ml deionized water at 140 °C. After washing with water and 95% ethanol, and drying at 80 °C for 24 h, the final products were analyzed using an X-ray diffractometer (XRD) operated at 20 kV, 15 mA and using Cu Kα radiation in the 2θ angular range of 15–60°, transmission electron microscope (TEM) as well as the use of the selected area electron diffraction (SAED) technique operated at 200 kV, a scanning electron microscope (SEM) and an energy dispersive X-ray (EDX) analyzer operated at 15 kV, a Raman spectrometer using 50 mW Ar Laser with $\lambda = 514.5$ nm, and a luminescence spectrometer using 250 nm exciting wavelength.

* Corresponding author.
E-mail addresses: ttpthongtem@yahoo.com, ttpthongtem@hotmail.com (T. Thongtem).

0272-8842/$34.00
doi:10.1016/j.ceramint.2007.05.007

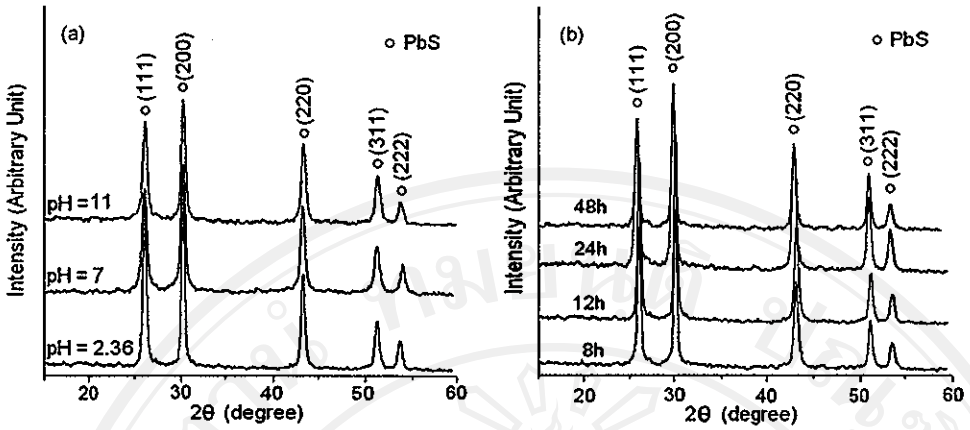

Fig. 1. XRD spectra of the products synthesized in (a) the solutions with different pH values for 12 h and (b) the solutions with the pH of 2.36 for different hydrothermal times.

3. Results and discussion

XRD spectra (Fig. 1) were indexed using Bragg's law for X-ray diffraction and compared with those of the JCPDS software (reference code: 05-0592) [12]. They were specified as cubic PbS with Fm-3m space group. The spectra are very sharp showing that well-crystallized PbS was successfully synthesized [13–15]. The products compose of a number of atoms aligning in a periodic lattice. The strongest intensity is at $2\theta = 30.08°$ and diffracted from (2 0 0) plane of the crystalline products. For the present analysis, no characteristic peaks of impurities were detected showing that the products are pure phase.

Morphologies of the products were analyzed using SEM. Their images (Fig. 2) show that the products were successfully synthesized in a variety of shapes and sizes which were influenced by the pH values, cationic surfactant and hydrothermal times. At a pH of 7 and 11 for 12 h hydrothermal reaction, the products compose of a number of nano-sized granules. At a pH of 2.36 and 8–48 h prolonged times, the products become micro-sized flowers. At 8 h hydrothermal reaction, the flower-like product is made up of three to four petals and is not complete. At 12 h reaction, the product is made up of several petals. A distance between two apices of the two petals across the center of the flower is approximately fourteen microns long. Each of the petals is composed of a number of small plates arranged in systematic order. The products are more complete and contain a greater number of petals when the hydrothermal times were prolonged. There are ten petals at 48 h reaction. The products are very beautiful and attractive. They have never been synthesized using the biomolecule and surfactant in the hydrothermal reaction.

In addition to these, TEM images and SAED patterns (Fig. 3) are used to specify the morphologies and phases of the products. At a pH of 7 and 12 h, the product is composed of a number of <10 nm particles in nano-sized clusters. SAED

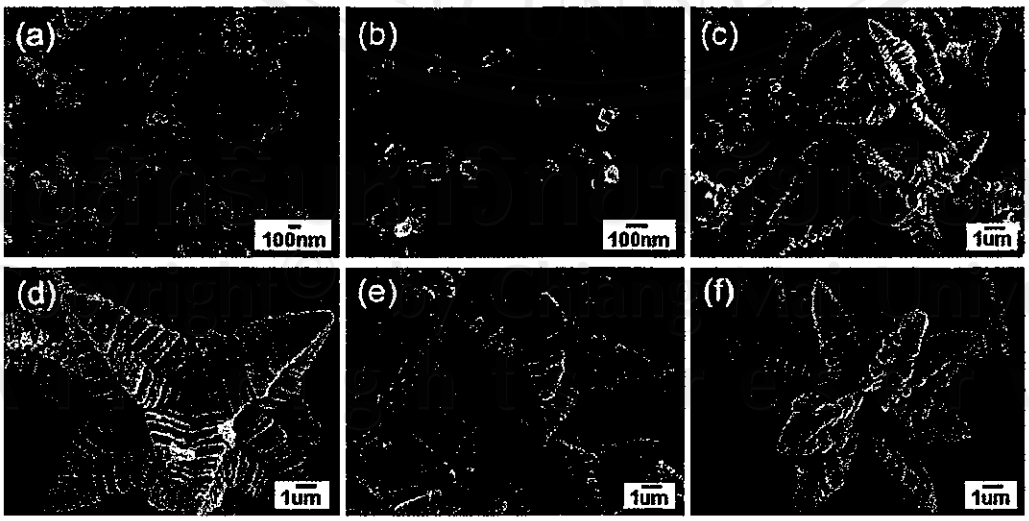

Fig. 2. SEM images of the products synthesized in (a and b) the solutions with the pH of 7 and 11 for 12 h and (c–f) the solutions with the pH of 2.36 for 8, 12, 24 and 48 h, respectively.

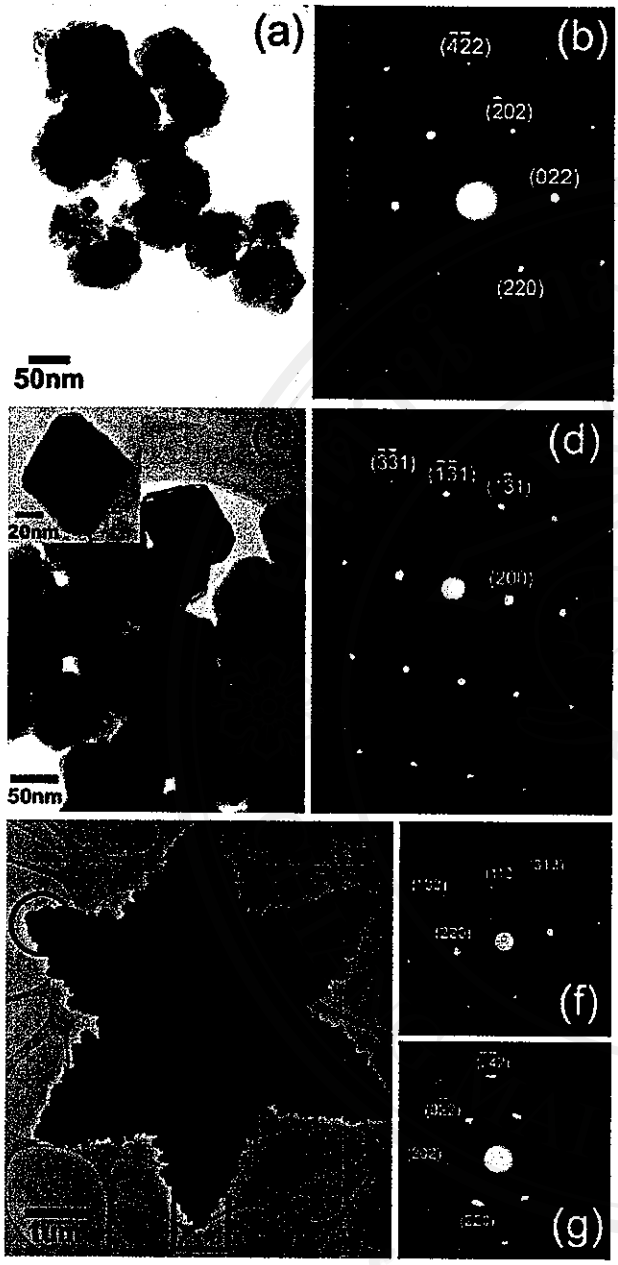

Fig. 3. TEM images and SAED patterns of the products synthesized at different pH values and hydrothermal times. (a and b) pH 7 and 12 h; (c and d) pH 11 and 12 h, and (e, f and g) pH 2.36 and 48 h. [(f and g) were analyzed on the (e)-product marked with a circle and square, respectively].

pattern of the product appears as systematic array of bright spots showing that a number of atoms are aligned in their normal lattice. The pattern was interpreted [16,17], and specified as cubic PbS crystal [12]. For the present analysis, the calculated electron beam [17] is in the $[\bar{1}\,1\,\bar{1}]$ direction. It is the direction that a beam of electrons was sent to the face of a crystal. When the pH was increased to 11, the product was composed of 75 nm truncated cubes. At lower magnification shown in the SEM image, it appears as granular. The SAED pattern was analyzed using an electron beam in the [0 1 3]

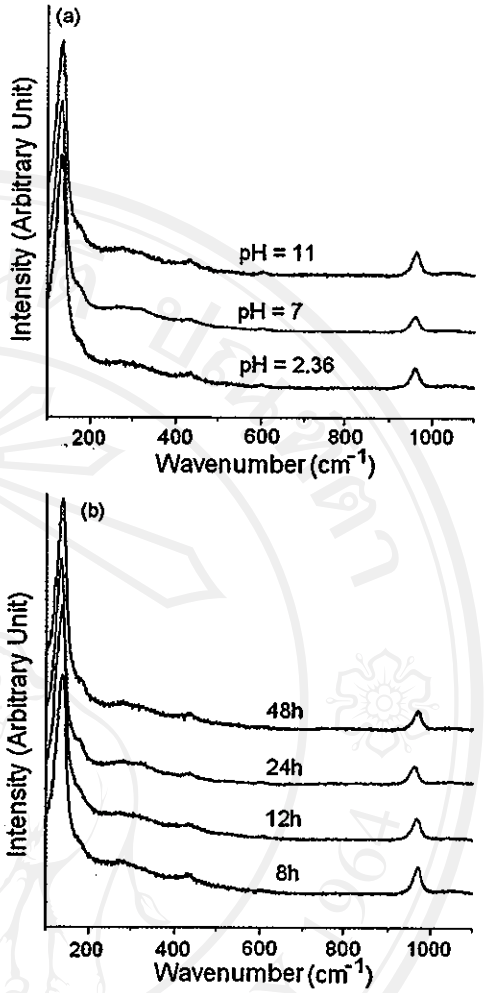

Fig. 4. Raman spectra of the products synthesized in (a) the solutions with different pH values for 12 h, and (b) the solutions with the pH of 2.36 for different hydrothermal times.

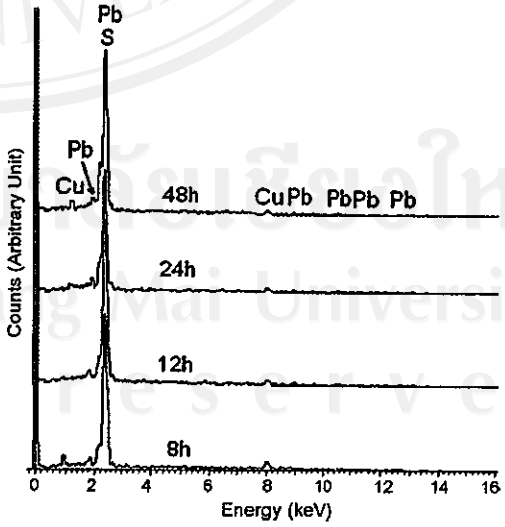

Fig. 5. EDX spectra of the products synthesized in the solutions with the pH of 2.36 for different hydrothermal times.

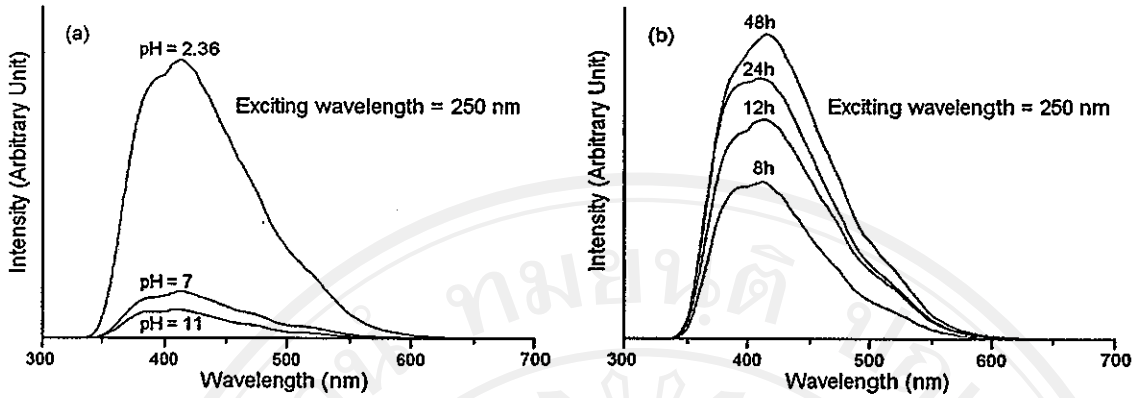

Fig. 6. PL emission of the products synthesized in (a) the solutions with different pH values for 12 h, and (b) the solutions with the pH of 2.36 for different hydrothermal times.

direction and specified as cubic PbS as well. At a pH of 2.36 and 48 h, the product is flower-like and specified as cubic PbS phase. Calculated electron beams used for the product analysis at a circle and square of the corresponding TEM image are in $[3\bar{3}2]$ and $[1\bar{1}\bar{1}]$ directions, respectively.

For the present research, *N*-cetyl pyridinium chloride was used as a cationic surfactant. L-Cysteine, a neutral and genetically coded amino acid, was used as a sulfur source and complexing agent. When $Pb(NO_3)_2$ reacted with L-cysteine to form a complex followed by the production of PbS nuclei (very fine particles) in the solution with the pH of 2.36, the surfactant was selectively adsorbed onto their surfaces. Therefore, the crystals were modeled to grow into small plates which compose the petals of micro-sized flowers. At a pH of 7 and 11, the solutions contain a greater number of OH^- ions than the acidic solution does. The cationic surfactant became less efficient in adsorbing onto PbS nuclei, which were capable of growing into the nano-sized particles in clusters and truncated cubes at the pH of 7 and 11, respectively.

A definite existence of the products was analyzed using a Raman spectrometer. The spectra (Fig. 4) contain prominent bands at the same wavenumbers although the products were synthesized using different conditions. Among the different spectra, their peaks are at 135, 278, 436, 602 and 970 cm^{-1}. The peak below 150 cm^{-1} is tentatively attributable to the so-called plasma line of the excitation laser [5,18]. The 278 cm^{-1} peak corresponds to two phonon process [5]. Those at 436 and 602 cm^{-1} are specified as the first and second overtone modes, respectively [18]. The peak above 960 cm^{-1} is attributable to oxy-sulfates [5,18]. Their constituents were characterized using EDX. The spectra (Fig. 5) reveal the presence of Pb and S. Cu of a copper stub was also detected. The detection of Pb and S using the EDX is in accord with the detection of PbS using the XRD and SAED.

Photoluminescence (PL) property of the products was characterized using a 250 nm exciting wavelength. Their PL spectra are shown in Fig. 6. The maximum intensities were detected at the same wavelength of 412 nm although their intensities are different. The intensities are sensitive to the morphologies. They increased with the increase in the acidities and hydrothermal times. At a constant hydrothermal time and different pH values, the PL intensity of the flower-like particles (pH 2.36, 12 h) is higher than those of the granules (pH 7, 12 h), and truncated cubes (pH 11, 12 h). At a constant pH value of 2.36, the flowers became the most complete at 48 h. At the present stage, the PL intensity was the highest. In general, the intensities are very sensitive to the number of electronic transfers and defects in the products as well [19].

4. Conclusions

Different shapes and sizes of PbS crystals were hydrothermally synthesized using biomolecule (L-cysteine) and surfactant (*N*-cetyl pyridinium chloride) at 140 °C. The detection of PbS phase, Pb and S constituents, and the first and second overtone modes are in good accord. These shapes are truncated cubes, granules and flower-like particles at a pH of 11, 7 and 2.36, respectively. At a pH of 2.36 and 48 h, the flowers were composed of ten petals. Their emission wavelengths were detected at the same value of 412 nm.

Acknowledgement

We would like to give thank to the Thailand Research Fund (TRF), Bangkok Thailand, for funding the research.

References

[1] H.F. Shao, Y.B. Zhang, X.F. Qian, J. Yin, Z.K. Zhu, Preparation of rod-shape $PbSO_4$ nanocrystal and its phase transition to PbS, Mater. Lett. 59 (2005) 3507–3513.
[2] L. Xu, W. Zhang, Y. Ding, W. Yu, J. Xing, F. Li, Y. Qian, Shape-controlled synthesis of PbS microcrystals in large yields via a solvothermal process, J. Cryst. Growth 273 (2004) 213–219.
[3] Y.C. Zhang, T. Qiao, X.Y. Hu, G.Y. Wang, X. Wu, Shape-controlled synthesis of PbS microcrystallites by mild solvothermal decomposition of a single-source molecular precursor, J. Cryst. Growth 277 (2005) 518–523.
[4] S. Wang, A. Pan, H. Yin, Y. He, Y. Lei, Z. Xu, B. Zou, Synthesis of PbS microcrystals via a hydrothermal process, Mater. Lett. 60 (2006) 1242–1246.

[5] A.M. Qin, Y.P. Fang, W.X. Zhao, H.Q. Liu, C.Y. Su, Directionally dendritic growth of metal chalcogenide crystals via mild template-free solvothermal method, J. Cryst. Growth 283 (2005) 230–241.
[6] S.F. Wang, F. Gu, M.K. Lü, D.Z. Wang, Z.S. Yang, H.P. Zhang, Y.Y. Zhou, A.Y. Zhang, Synthesis of cross-shaped PbS nanostructures by a surfactant-assisted reflux process, Mater. Lett. 60 (2006) 2759–2763.
[7] G.Z. Zhou, M. Lü, Z. Xiu, S. Wang, H. Zhang, Y. Zhou, S. Wang, Controlled synthesis of high-quality PbS star-shaped dendrites, multipods, truncated nanocubes, and nanocubes and their shape evolution process, J. Phys. Chem. B 110 (2006) 6543–6548.
[8] Y. Ni, F. Wang, H. Liu, G. Yin, J. Hong, X. Ma, Z. Xu, A novel aqueous-phase route to prepare flower-shaped PbS micron crystals, J. Cryst. Growth 262 (2004) 399–402.
[9] L. Dong, Y. Chu, Y. Liu, M. Li, F. Yang, L. Li, Surfactant-assisted fabrication PbS nanorods, nanobelts, nanovelvet-flowers and dendritic nanostructures at lower temperature in aqueous solution, J. Colloid Interf. Sci. 301 (2006) 503–510.
[10] X. Chen, X. Zhang, Z. Wang, J. Wan, Y. Qian, Biomolecule-assisted hydrothermal synthesis and one-dimensional self-assembly of copper sulfide nanocrystallites, Mater. Chem. Phys. 98 (2006) 419–421.
[11] X. Chen, X. Zhang, C. Shi, X. Li, Y. Qian, A simple biomolecule-assisted hydrothermal approach to antimony sulfide nanowires, Solid State Commun. 134 (2005) 613–615.
[12] Powder Diffract. File, JCPDS Int. Centre Diffract. Data, PA 19073-3273, USA, 2001.
[13] T. Thongtem, S. Thongtem, Characterization of $Bi_4Ti_3O_{12}$ powder prepared by the citrate and oxalate coprecipitation processes, Ceram. Int. 30 (2004) 1463–1470.
[14] T. Thongtem, S. Thongtem, Synthesis of $Li_{1-x}Ni_{1+x}O_2$ using malonic acid as a chelating agent, Ceram. Int. 31 (2005) 241–247.
[15] T. Thongtem, S. Thongtem, Characterization of $Li_{1-x}Ni_{1+x}O_2$ prepared using succinic acid as a complexing agent, Inorg. Mater. 42 (2006) 202–209.
[16] K.W. Andrews, D.J. Dyson, S.R. Keown, Interpretation of Electron Diffraction Patterns, second ed., Plenum Press, NY, 1971.
[17] B.D. Cullity, Elements of X-ray Diffraction, second ed., Addison-Wesley Publ. Co., MA, 1978.
[18] G.D. Smith, S. Firth, R.J.H. Clark, M. Cardona, First- and second-order Raman spectra of galena (PbS), J. Appl. Phys. 92 (2002) 4375–4380.
[19] M. Alonso, E.J. Finn, Fundamental University Physics, vol. 3, Addison-Wesley Publ. Co., MA, 1968.